# Analysis of function and signaling pathway of guanine nucleotide exchange factor DOCK1 in acute myeloid leukemia

**Dissertation**

Zur Erlangung des Doktorgrades der Naturwissenschaften (Dr. rer. nat.)

an der Fakultät für Mathematik, Informatik und Naturwissenschaften

Fachbereich Biologie

der Universität Hamburg

vorgelegt von

**Frauke Fuchs**

Hamburg 2020

Tag der Disputation: 04. September 2020

Gutachter der Dissertation:

Professor Dr. med. Walter Fiedler

Universitätsklinikum Hamburg-Eppendorf, Zentrum für Onkologie, II. Medizinische Klinik und Poliklinik

Professor Dr. rer. nat. Julia Kehr

Universität Hamburg, Fakultät für Mathematik, Informatik und Naturwissenschaften, Fachbereich Biologie, Molekulare Pflanzengenetik

DEPARTMENT OF PHARMACOLOGY

Mansfield Road, Oxford, OX1 3QT
Tel: +44(0)1865 271856 Fax: +44(0)1865 281131

UNIVERSITY OF OXFORD

24th June 2020

Frauke Fuchs: PhD Thesis

To whom it may concern.

We are very pleased to write in support of the PhD thesis written by the candidate, Frauke Fuchs. We have both read the thesis and can confirm that it is written in a very clear and precise style. Use of English language and grammar is correct and appropriate throughout. Indeed, it is written to a very high standard that is comparable, if not greater than that produced by a native speaker. We wish to add our compliments to the author. Frauke spent a very successful six months with us in our laboratory in Oxford during her undergraduate studies and it was a delight to get to know her.

Yours sincerely

Dr Nick Platt
Senior research fellow

Professor Frances Platt
Professor of Pharmacology and Biochemistry
Head of Department.

# TABLE OF CONTENTS

# LIST OF ABBREVIATIONS

| | |
|---|---|
| °C | degree Celsius |
| µg | microgram |
| µL | microliter |
| µm | micrometer |
| µM | micromolar |
| A | ampere |
| ACF7 | actin cross-linking family 7 |
| Allo-HSCT | allogeneic hematopoietic stem cell transplantation |
| AML | acute myeloid leukemia |
| Ang-1 | angiopoietin-1 |
| ANKRD26 | ankyrin repeat domain-containing protein 26 |
| ANKRD28 | ankyrin domain repeat protein 28 |
| APC | allophycocyanin |
| APC/Cy7 | allophycocyanin/cyanine 7 |
| APS | ammonium persulfate |
| ARM | armadillo |
| ARPC1A | actin-related protein 2/3 complex subunit 1A |
| ASXL1 | ASXL transcriptional regulator 1 |
| ATCC | American Type Culture Collection |
| BCL-2 | B-cell Lymphoma 2 |
| bp | base pair |
| BM | bone marrow |
| BSA | bovine serum albumin |
| c | concentration |
| $CaCl_2$ | calcium chloride |
| CAF | cancer-associated fibroblasts |
| CAR cells | CXCL12-abundant reticular cells |
| cDNA | complementary deoxyribonucleic acid |
| CEBPA | CCAAT enhancer binding protein alpha |
| CFG MFM | Core Facility Genomics of the Medical Faculty Münster |
| cKit | tyrosine-protein kinase KIT |
| cm | centimeter |
| $cm^2$ | square centimeter |
| $CO_2$ | carbon dioxid |
| CPYPP | 4-[3-(2-Chlorophenyl)-2-propen-1-ylidene]-1-phenyl-3,5-pyrazolidinedione |
| CR | complete remission |
| $CR_i$ | CR with incomplete hematologic recovery |
| ctrl | control |
| CXCR4 | C-X-C Motif Chemokine Receptor 4 |
| 3D | three dimensional |
| DAPI | 4’,6-diamidino-2-phenylindole |
| $ddH_2O$ | ultra-pure double-distilled water |
| DEPC | diethyl pyrocarbonate |
| DH | Dbl-homology |
| DHR | DOCK homology region |
| dkd | double-knockdown |
| DMEM | Dubecco's Modified Eagle Medium |
| DMSO | dimethyl sulfoxide |
| DNA | deoxyribonucleic acid |
| DNMT | DNA methyltransferase |
| DNMT3A | DNA methyltransferase 3 alpha |
| dNTP | deoxyribonucleotide |
| DOCK | dedicator of cytokinesis |
| dsDNA | double-stranded deoxyribonucleic acid |
| DSMZ | Deutsche Sammlung von Mikroorganismen und Zellkulturen GmbH |
| Dyn | dyne |
| E. coli | *Escherichia coli* |
| EDTA | ethylenediaminetetraacetic acid |
| *e.g.* | *exempli gratia* |
| EGF | epidermal growth factor |
| EGFRvIII | epidermal growth factor receptor mutant |
| eGFP | enhanced green fluorescent protein |
| ELMO | engulfment and cell motility protein |
| ELN | European LeukemiaNet |
| EMT | epithelial-mesenchymal transition |
| $E_S$ | selection efficiency |
| $E_T$ | transduction efficiency |
| EU | European Union |

| | |
|---|---|
| F | F-value |
| f, fw | forward |
| FAB | French-American-British |
| FACS | fluorescence activated cell sorting |
| FBS | fetal bovine serum |
| FC | fold change |
| FDA | U.S. Food and Drug Administration |
| FDR | false discovery rate |
| FLT3 | fms related receptor tyrosine kinase 3 |
| FITC | fluorescein isothiocyanate |
| FMO | fluorescence minus one |
| FOXO | forkhead box O |
| FSC | forward scatter |
| g | gram, gravitational force (g-force) |
| GAP | GTPase-activating protein |
| GAPDH | glyceraldehyde 3-phosphate dehydrogenase |
| GBM | glioblastoma multiforme |
| GDI | guanine nucleotide-dissociation inhibitor |
| GDP | guanosine diphosphate |
| GEF | guanine nucleotide exchange factor |
| GM | granulocyte-macrophage |
| GM-CSF | granulocyte-macrophage colony-stimulating factor |
| GMP | granulocyte-macrophage progenitor |
| GTP | guanosine triphosphate |
| HBS | HEPES-buffered saline |
| HCl | hydrochloric acid |
| HDBEC | human dermal blood endothelial cells |
| HEPES | 2-[4-(2-hydroxyethyl)piperazin-1-yl]ethanesulfonic acid |
| HGF | hepatocyte growth factor |
| HIF | hypoxia-inducible factor |
| HMA | DNA-hypomethylating agents |
| hnRNP A2/B1 | heterogeneous nuclear ribonucleoproteins A2/B1 |
| hr | hour |
| HRP | horseradish peroxidase |
| HSCs | hematopoietic stem cells |
| HSPCs | hematopoietic stem and progenitor cells |
| HUVEC | human umbilical vein endothelial cells |
| IDH | isocitrate dehydrogenase (NADP(+)) |
| IgG | immunoglobulin G |
| ITD | internal tandem duplication |
| IVC | individually ventilated cages |
| JAK | janus kinase |
| JAK2 | janus kinase 2 |
| kb | kilobase |
| kd | knockdown |
| kDa | kilodalton |
| KMT2A | lysine methyltransferase 2A |
| L | liter |
| L-15 | Leibovitz's L-15 medium |
| LeGO | lentiviral gene ontology |
| LMPP | lymphoid-primed multipotent progenitor |
| LSCs | leukemic stem cells |
| M | molar (= mol/L) |
| MALDI | matrix assisted laser desorption ionization |
| MAPK | mitogen-activated protein kinase |
| min | minute |
| miR | microRNA |
| mL | milliliter |
| MMP-2 | matrix metalloproteinase 2 |
| MPN | myeloproliferative neoplasms |
| MPP | multipotent progenitor |
| MPP4 | MAGUK p55 subfamily member 4 |
| mRNA | messenger RNA |
| MS | mass spectrometry |
| MSC | mesenchymal stem cell |
| mTOR | mammalian target of rapamycin |
| neg. | negative |
| NF-κB | nuclear factor-κB |
| ng | nanogram |
| NK cells | natural killer cells |
| nM | nanomolar |
| NOS | not otherwise specified |
| NPM1 | nucleophosmin 1 |
| OPN | osteopontin |
| ORR | overall response rate |
| OS | overall survival |
| pAML | primary AML |

| | |
|---|---|
| PAGE | polyacrylamide gel electrophoresis |
| PB | peripheral blood |
| PBS | phosphate buffered saline |
| PCR | polymerase chain reaction |
| PDGF | platelet-derived growth factor |
| PDGFRα | platelet-derived growth factor receptor α |
| PE/Cy7 | phycoerythrin/cyanine 7 |
| PerCP/Cy5-5 | peridinin-chlorophyll-protein/cyanin 5.5 |
| pH | potential hydrogen |
| PH | pleckstrin-homology |
| PI3K | phosphatidylinositol-3-kinase |
| PI3P | phosphatidylinositol-3-phosphate |
| $PIP_3$ | phosphatidylinositol (3,4,5)-triphosphate |
| PKA | protein kinase A |
| PLP | periodate-lysine-paraformaldehyde |
| PMF | peptide mass fingerprinting |
| pos. | positive |
| Pten | phosphatase and tensin homolog |
| r, rev, rv | reverse |
| RH | relative humidity |
| RNA | ribonucleic acid |
| RNase | ribonuclease |
| RNA-Seq | RNA-Sequencing |
| rpm | rounds per minute |
| RPMI | Rooswell Park Memorial Institut Medium 1640 |
| R/R | relapsed/refractory |
| RRP1B | ribosomal RNA processing protein 1B (RRP1B) |
| RS | relative survival |
| RT-qPCR | reverse transcription quantitative real-time polymerase chain reaction |
| RUNX1 | RUNX family transcription factor 1 |
| s | second |
| Sca1 | stem cell antigen-1 |
| SCF | stem cell factor |
| scr | scrambled |
| SD | standard deviation |
| SDF-1α | stromal cell-derived factor 1α (also known as CXCL12) |
| SDS | sodium dodecyl sulfate |
| shRNA | short hairpin RNA |
| SSC | side scatter |
| STAT | signal transducer and activator of transcription |
| T | transduction number |
| TAE | tris-acetate- EDTA |
| TBOPP | 1-(2-(3´-(trifluoromethyl)-[1,1´-biphenyl]-4-yl)-2-oxoethyl)-5-pyrrolidinylsulfonyl-2(1H)-pyridone |
| TBS | tris-buffered saline |
| TBS-T | tris-buffered saline with |
| TEMED | tetramethylethylenediamine |
| TET2 | tet methylcytosine dioxygenase 2 |
| TGF- β | transforming growth factor-β |
| TKD | tyrosine kinase domain |
| TNF-α | tumor necrosis factor-α |
| TOF | time of flight |
| TP53 | tumor protein p53 |
| TPO | thrombopoietin |
| Tregs | regulatory T cells |
| TRM | treatment-related mortality |
| UKE | Universitätsklinikum Hamburg-Eppendorf |
| UV | ultraviolet |
| V | volt |
| VCAM-1 | vascular cell adhesion molecule 1 |
| VEGF | vascular endothelial growth factor |
| VLA-4 | very late antigen-4 |
| v/v | volume per volume |
| WDFY3 | WD repeat and FYVE domain-containing protein 3 |
| WHO | World Health Organization |
| wt | wildtype |
| w/v | weight per volume |
| Zir | zizimin related |
| Ziz | zizimi |

# LIST OF FIGURES

# LIST OF TABLES

# LIST OF SUPPLEMENTARY TABLES AND FIGURES

# ABSTRACT

Acute myeloid leukemia (AML) is a malignant disease of the hematopoietic system and is characterized by immature myeloid cell proliferation, leading to bone marrow failure. Despite intensive chemotherapy, prognosis for patients remains unsatisfactory and new therapeutic approaches are needed. The bone marrow niche is a key player in the pathogenesis of AML and home of the leukemic stem cells (LSCs), which are believed to be responsible for leukemic relapse due to their resistance to chemotherapy.

Microarray-based gene expression analysis of co-cultured primary AML blasts with endothelial cells revealed the Rac Guanine nucleotide exchange factor (GEF) DOCK1 (Dedicator of cytokinesis 1) as a possible component in the interaction between the bone marrow niche and AML cells. As a GEF, DOCK1 has a critical role in various cellular processes such as phagocytosis, cell migration and invasion. Further analysis of published gene expression data of a large cohort of AML patients (n = 290) identified DOCK1 as an independent prognostic marker, since high DOCK1 expression was associated with poor overall survival as well as poor event-free survival. These findings are in line with a recently published study by Lee *et al*.[1]. Aim of this project was to evaluate the influence of DOCK1 to the pathophysiology of AML and to identify potential members of the DOCK1-signaling pathway.

The antileukemic effect of DOCK1 inhibition or downregulation was assessed in *in vitro* assays. Furthermore, the overexpression of *DOCK1* as well as the downregulation of DOCK1 binding partner engulfment and cell motility protein 1 (ELMO1) was evaluated. To investigate the antileukemic effect of DOCK-inhibition with small molecule inhibitors TBOPP and CPYPP, proliferation and colony formation assays, using the *DOCK1* expressing AML cell lines TF-1 and UKE-1 were performed. Functional and stable *DOCK1* and *ELMO1* knockdown in TF-1 and UKE-1 cells were generated by using specific shRNAs in a lentiviral vector system, which additionally allows a fluorescent labeling of the cells. Following knockdown confirmation by RT-qPCR and Western Blot, functional assays to analyze the proliferation, colony formation and adhesion properties were performed. Assessment of proliferative and clonogenic properties demonstrated an antileukemic effect in AML cells only for the treatment with the DOCK-inhibitors TBOPP and CPYPP. The decreased proliferation and colony formation could not be reproduced by shRNA-based knockdown of *DOCK1* or its binding partner *ELMO1*,

indicating that other DOCK variants may be additionally involved in the antileukemic effect of the small molecule inhibitors. Furthermore, functional assays with *DOCK1*-overexpressing cells underlined the assumption that *DOCK1*-expression is not essential for the functional properties of malignant cells in AML *in vitro*.

Based on preliminary data, a role of DOCK1 for the homing and retention of AML cells within the bone marrow niche can be assumed. To investigate the effect of the *DOCK1* knockdown or overexpression *in vivo*, transduced cells were transplanted intravenously into immunodeficient NSG or NSGS mice. Although murine xenograft models confirmed the *in vitro* findings by showing no survival benefit for *DOCK1* deficient AML, it was clearly demonstrated that there is a relevance of DOCK1 *in vivo*, since distinct differences between *DOCK1*-expressing cells and *DOCK1*-deficient cells were revealed. *DOCK1* expression in AML cells led to a greater promotion of splenomegaly and a higher early leukemic infiltration as well as hematopoietic stem and progenitor cell (HSPC) egress from the bone marrow. The underlying mechanisms and the consequences for the course of the disease remain still unknown. Possibly certain genes or proteins, which have been identified by RNA-sequencing or mass spectrometric analysis, might be involved in the DOCK1-mediated effects. Further detailed investigations are necessary to understand the impact and relevance of the DOCK1-induced phenomena.

# ZUSAMMENFASSUNG

Die akute myeloische Leukämie (AML) ist eine maligne Erkrankung des hämatopoetischen Systems, die durch die Zellproliferation von unreifen myeloischen Vorläuferzellen und letztlich die Verdrängung der normalen Hämatopoese charakterisiert ist. Trotz intensiver Chemotherapie ist die Prognose für die Patienten nach wie vor unbefriedigend und neue Therapieansätze sind dringend erforderlich. Die Knochenmarknische nimmt eine Schlüsselrolle in der Pathogenese der AML ein und ist Ort der Ansiedelung für leukämische Stammzellen (LSCs), welche aufgrund ihrer Chemotherapie-Resistenz für das Auftreten von Rezidiven verantwortlich gemacht werden.

Microarray-basierte Genexpressions-Analysen von co-kultivierten AML Blasten mit Endothelzellen haben das Gen *DOCK1* (*Dedicator of cytokinesis 1*), welches für den Rac *Guanine nucleotide exchange factor* (GEF) DOCK1 kodiert, als möglichen Bestandteil in der Interaktion zwischen Zellen der Knochenmarknische und den AML-Zellen identifizieren. Als GEF spielt DOCK1 bei vielen verschiedenen zellulären Prozessen, wie der Phagozytose, der Zellmigration sowie Invasion, eine wichtige Rolle. Weiterhin hat die Analyse von publizierten Genexpressions-Daten einer großen Kohorte von AML-Patienten (n = 290) DOCK1 als unabhängigen prognostischen Marker identifiziert, da eine hohe DOCK1-Expression sowohl mit einem schlechten Gesamtüberleben als auch mit einem schlechten ereignisfreien Überleben assoziiert war. Diese Schlussfolgerung entspricht den Ergebnissen einer kürzlich veröffentlichten Studie von Lee *et al*.[1]. Ziel dieser Arbeit war es, die Bedeutung von DOCK1 in der Pathophysiologie der AML zu evaluieren sowie mögliche Mitglieder der DOCK1-Signalkaskade zu identifizieren.

In *in vitro*-Assays wurde die anti-leukämische Wirkung der Inhibition oder der genetischen Herunterregulierung von DOCK1 untersucht. Weiterhin wurde die Überexpression von DOCK1 sowie der *Knockdown* von ELMO1, dem Bindungspartner von DOCK1, betrachtet. Um die anti-leukämische Wirkung der DOCK-Inhibition mit den kleinmolekularen Inhibitoren TBOPP und CPYPP zu untersuchen, wurden Proliferations- sowie Koloniebildungsassays mit den DOCK1-exprimierenden AML-Zelllinien TF-1 und UKE-1 durchgeführt. Um einen funktionellen und stabilen *DOCK1*- sowie *ELMO1-Knockdown* in TF-1- und UKE-1-Zellen zu erzeugen, wurden

spezifische shRNAs in einem lentiviralen Vektorsystem, das zusätzlich eine Fluoreszenzmarkierung der Zellen erlaubt, verwendet. Nach der Verifizierung des *Knockdowns* durch RT-qPCR und Western Blot wurden funktionelle Assays zur Analyse der Proliferations-, Koloniebildungs- und Adhäsionseigenschaften durchgeführt. Die Bestimmung der proliferativen und klonogenen Eigenschaften zeigte eine anti-leukämische Wirkung in AML-Zellen nur für die Behandlung mit den DOCK-Inhibitoren TBOPP und CPYPP. Die verminderte Proliferation sowie Koloniebildung konnte durch den shRNA-vermittelten *Knockdown* von *DOCK1* oder seinem Bindungspartner *ELMO1* nicht reproduziert werden, woraus sich schließen lässt, dass andere DOCK-Varianten zusätzlich an der anti-leukämischen Wirkung der kleinmolekularen Inhibitoren beteiligt sein könnten. Darüber hinaus bekräftigten funktionelle Assays mit *DOCK1*-Überexpressions-Zellen die Annahme, dass die *DOCK1*-Expression für die funktionellen Eigenschaften maligner Zellen bei der AML *in vitro* nicht essentiell ist.

Auf der Grundlage vorläufiger Daten, kann eine Funktion für DOCK1 bei dem *Homing* und die Retention von AML-Zellen innerhalb der Knochenmarknische angenommen werden. Um den Effekt eines *DOCK1-Knockdowns* oder einer -Überexpression *in vivo* zu untersuchen, wurden transduzierte Zellen intravenös in NSG- oder NSGS-Mäuse transplantiert. Obwohl die murinen Xenotransplantat-Modelle die *in vitro*-Daten bestätigten, indem sie keinen Überlebensvorteil für eine DOCK1-defiziente AML zeigten, konnte eindeutig demonstriert werden, dass DOCK1 eine Relevanz *in vivo* besitzt, da deutliche Unterschiede zwischen *DOCK1*-exprimierenden und *DOCK1*-defizienten Zellen nachgewiesen werden konnten. Die *DOCK1*-Expression in AML-Zellen führte zu einer verstärkten Splenomegalie, einer höheren frühen Infiltration des Knochenmarks durch AML-Zellen sowie einem stärkeren Austritt von hämatopoetischen Stamm- und Vorläuferzellen (HSPCs) aus dem Knochenmark. Die zugrundeliegenden Mechanismen und die Folgen für den Krankheitsverlauf sind nach wie vor unbekannt. Möglicherweise könnten bestimmte Gene oder Proteine, die im Rahmen dieser Arbeit durch RNA-Sequenzierung oder massenspektrometrischer Analyse identifiziert wurden, an den DOCK1-vermittelten Effekten beteiligt sein. Weitere detaillierte Untersuchungen sind notwendig, um die Auswirkungen und die Relevanz der DOCK1-induzierten Phänomene zu verstehen.

# I. INTRODUCTION

## 1.1 Acute myeloid leukemia (AML)

Acute myeloid leukemia is a malignant disease of the hematopoietic system and is characterized by a clonal expansion of myeloid progenitor cells, leading to impaired hematopoiesis and cytopenia[2,3]. AML is a heterogeneous group of diseases, with biologically and prognostically different subgroups[4].

With an age-standardized incidence rate of 3.1 per 100 000, AML is considered a rare disease[5]. It is the most common type of acute leukemia in adults, with 80% of the respective cases[6]. Approximately 4 100 cases of AML are registered annually in Germany, with an increasing incidence with age[6]. From 2011-2013, the median age of disease onset in Germany was 72[6]. Independent of age, the incidence of AML is slightly greater in men than in women[6,7]. Due to its aggressiveness, AML rapidly progresses, if left untreated. Despite the overall survival (OS) of adult patients with AML improved, due to progress in treatment and supportive care, the prognosis still remains unsatisfactory[8,9]. Especially for younger patients (< 60 years), the outcome improved significantly, while for elderly patients (≥ 60 years) the prognosis remains poor[9–11]. The 5-year relative survival (RS) rate in Germany was only 23.7% (2009-2013), with significant decrease in survival with increasing age at disease onset[6]. For 15-34-year-old patients, the 5-year RS was 60%, but decreased to only 5% for patients age 75 and older[6,12].

### 1.1.1 Pathophysiology and genomic landscape of AML

AML can arise as a *de novo* malignancy in previously healthy patients (primary AML) or result as a secondary AML in patients with underlying hematological diseases or prior cytotoxic therapy, like radiation or treatment with topoisomerase II-inhibitors, alkylating agents or antimetabolites[13]. Secondary AML accounts for 10-30% of all AML cases and is associated with a poor outcome, especially in younger patients (< 60 years)[14,15].

AML is characterized by an uncontrolled proliferation of myeloid progenitor cells, the leukemic blasts, resulting from chromosomal abnormalities as well as from gene mutations[4]. In 97% of all cases, gene mutations are identified[16]. In general, cancer develops from somatic mutations, which enables the respective clone with a selection benefit in terms of improved

survival or proliferation[17]. Such mutations, known as driver-mutations, account for the complexity of the disease. AML is a genetically complex and dynamic disease, with patients typically having more than one driver-mutation and multiple malignant subclones can co-exist next to the founding clone[18]. The clonal heterogeneity can change during the different stages of the disease due to clonal or subclonal evolution[19]. With whole-genome and whole-exome sequencing of 200 AML patient samples, the Cancer Genome Atlas Research Network organized commonly mutated genes in nine functional categories[18]. The majority of gene mutations occur in genes involved in signaling pathways (59% of cases), such as the fms related receptor tyrosine kinase 3 (*FLT3*), leading to a benefit in proliferation[3,18]. Mutations in genes related to deoxyribonucleic acid (DNA)-methylation, such as DNA methyltransferase 3 alpha (*DNMT3A*), tet methylcytosine dioxygenase 2 (*TET2*), isocitrate dehydrogenase (NADP(+)) 1 and 2 (*IDH1*, *IDH2*), account for 44% of cases and can lead to deregulation of DNA methylation[3,18]. Chromatin-modifying genes were mutated in 30% of cases and genes like ASXL transcriptional regulator 1 (*ASXL1*) or lysine methyltransferase 2A (*KMT2A*) were categorized in this group[3,18]. The gene nucleophosmin 1 (*NPM1*) was mutated in 27% of cases, leading to aberrant localization of NPM1 and NPM1-interacting proteins[3,18]. The fifth category includes genes for myeloid transcription factors, like RUNX family transcription factor 1 (*RUNX1*) or CCAAT enhancer binding protein alpha (*CEBPA*) and occur in 22% of cases[3,18]. Transcription factor-fusions, such as *RUNX1-RUNX1T1* or *PML-RARA*, account for 18% of cases[18]. Both, mutations in myeloid transcription factors and transcription factor-fusions result in transcriptional deregulation[3]. In 16% of cases, mutations in tumor-suppressor genes, such as tumor protein p53 (*TP53*), occur and 14% of cases account for mutations of the spliceosome-complex genes, which are involved in RNA processing, whereas 13% of cases occur in genes of the cohesion-complex[3,18].

### 1.1.2 Pathogenesis, diagnosis and classification of AML

Clinical presentation of AML is mainly determined by the accumulation of immature leukemic blasts and reduced hematopoiesis[2,3]. Blast infiltration originates in the bone marrow and can pass into the peripheral blood and other tissue, like spleen, liver or lymph nodes[3]. Displacement of normal hematopoiesis is causing the clinical manifestation in life-threatening condition of leukocytosis and signs of bone marrow failure, like anemia, thrombocytopenia

and neutropenia, leading to symptoms such as fatigue, anorexia, weight loss, hemorrhage and infections[4,20].

Diagnosis of AML is based on the analysis of bone marrow (BM) and peripheral blood (PB), with a leukemic blast count of ≥ 20%, except for AML with t(8;21), inv(16) or t(15;17), which are diagnosed regardless of the blast count[21]. To further diagnose AML, the myeloid origin is assessed by immunophenotyping[22]. With cytogenetic analysis and screening for genetic mutations in *NPM1*, *CEBPA*, *RUNX1*, *FLT3*, *TP53* and *ASXL1*, the suspected AML is evaluated and classified[21].

Based on morphological and cytochemical characterization of the leukemic blasts, a first classification system for AML was implemented in 1976 by the French-American-British (FAB) Cooperative Group with eight subtypes M0-M7[23–27]. To reflect progress in the diagnostics of myeloid neoplasms and acute leukemia, a new classification system was introduced by the World Health Organization (WHO) in collaboration with the Society for Hematopathology and the European Association for Haematopathology in 2001[28]. The last update of the *WHO Classification of Tumours of Haematopoietic and Lymphoid Tissues* took place in 2016[29]. The new classification is based on genetic findings as well as morphologic, immunophenotypic, cytochemical assessment and clinical information[28,29]. For AML and related neoplasms, the WHO is distinguishing six subtypes, mainly based on cytogenetic and molecular genetic properties[29]. Table 1 is showing AML disease entities according to the WHO classification. The AML not otherwise specified (NOS) subtype is further divided into subgroups, based on morphological properties mainly defined by former FAB classification[30].

**Table 1: WHO classification of AML and related neoplasms** (adapted from Arber *et al*.)[29]

| Subtype | Specification (further subgroups) |
|---|---|
| AML with recurrent genetic abnormalities | AML with t(8:21)(q22;q22); *RUNX1-RUNX1T1*<br>AML with inv(16)(p13.1q22) or t(16;16)(p13.1;q22); *CBFB-MYH11*<br>APL (acute promyelocytic leukemia) with *PML-RARA*<br>AML with t(9;11)(p21.3;q23.3); *MLLT3-KMT2A*<br>AML with t(6;9)(p23;q34.1); *DEK-NUP214*<br>AML with inv(3)(q21.3q26.2) or t(3;3)(q21.3;q26.2); *GATA2, MECOM*<br>AML (megakaryoblastic) with t(1;22)(p13.3;q13.3); *RBM15-MKL1*<br>Provisional entity: AML with *BCR-ABL1*<br>AML with mutated *NPM1*<br>AML with biallelic mutations of *CEBPA*<br>Provisional entity: AML with mutated *RUNX1* |
| AML with myelodysplasia-related changes | |
| Therapy-related myeloid neoplasms | |
| AML not otherwise specified (NOS) | AML with minimal differentiation<br>AML without maturation<br>AML with maturation<br>Acute myelomonocytic leukemia<br>Acute monoblastic/monocytic leukemia<br>Pure erythroid leukemia<br>Acute megakaryoblastic leukemia<br>Acute basophilic leukemia<br>Acute panmyelosis with myelofibrosis |
| Myeloid sarcoma | |
| Myeloid proliferations related to Down syndrome Transient | Transient abnormal myelopoiesis (TAM)<br>Myeloid leukemia associated with Down syndrome |

### 1.1.3 Prognosis

Detailed assessment of prognostic factors in patients is crucial for the appropriate treatment of AML. Based on prognostic factors, patients can be stratified for their risk of treatment resistance or treatment-related mortality (TRM)[4]. In general, prognostic factors can be divided into patient-associated and disease-related factors[3]. Unfavorable patient-associated factors, which can predict the risk of TRM, are increasing age and poor performance status[3]. Both are associated with lower complete remission (CR) rates and decreased overall survival (OS)[8,31]. Disease-related factors, such as leukocyte count, mutational status and previous bone marrow disorders or previous cytotoxic therapy, can be indicators of resistance to standard treatment[3]. Secondary AML (previous hematological malignancy or therapy-related AML) is associated with poor prognosis independent of other risk factors, with significant prognostic impact in younger patients[32]. The most important factor for risk stratification is the

cytogenetic status[33]. According to the European LeukemiaNet (ELN) recommendations, patients can be stratified into three risk groups based on their cytogenetic profile under consideration of genetic mutational status: favorable, intermediate and adverse[21]. Table 2 is showing the prognostic risk groups by genetic abnormalities. Important to note is that the prognostic impact of many markers depends on the presence or absence of other mutations as well as on the treatment itself[21,34].

**Table 2: Prognostic risk groups based on genetic profile** (adapted from Döhner *et al*.)[21]

| Risk group | Genetic abnormality |
|---|---|
| Favorable | t(8;21)(q22;q22.1); *RUNX1-RUNX1T1*<br>inv(16)(p13.1q22) or t(16;16)(p13.1;q22); *CBFB-MYH11*<br>Mutated *NPM1* without *FLT3*-ITD or with *FLT3*-ITD$^{low}$*<br>Biallelic mutated *CEBPA* |
| Intermediate | Mutated *NPM1* and *FLT3*-ITD$^{high}$*<br>Wild-type *NPM1* without *FLT3*-ITD or with *FLT3*-ITD$^{low}$* (without adverse-risk genetic lesions)<br>t(9;11)(p21.3;q23.3); *MLLT3-KMT2A*<br>Cytogenetic abnormalities not classified as favorable or adverse |
| Adverse | t(6;9)(p23;q34.1); *DEK-NUP214*<br>t(v;11q23.3); *KMT2A* rearranged<br>t(9;22)(q34.1;q11.2); *BCR-ABL1*<br>inv(3)(q21.3q26.2) or t(3;3)(q21.3;q26.2); *GATA2*,*MECOM(EVI1)* -5 or del(5q); -7; -17/abn(17p)<br>Complex karyotype, monosomal karyotype<br>Wild-type *NPM1* and *FLT3*-ITD$^{high}$*<br>Mutated *RUNX1***<br>Mutated *ASXL1***<br>Mutated *TP53* |

* Low = low allelic ratio (< 0.5); high = high allelic ratio (≥ 0.5); semiquantitative assessment of *FLT3*-ITD allelic ratio by DNA fragment analysis.

** If these markers co-occur with favorable markers, they should not be used as adverse prognostic markers.

### 1.1.4 Treatment of AML

Although the prognosis for patients improved over the last decades, the general strategy for therapy has not changed[21]. Conventional treatment of AML patients consists of initial induction therapy followed by consolidation therapy[20,21]. The patient status is evaluated to assess whether they are eligible for intensive induction chemotherapy. The backbone of induction therapy is the well-known "3+7"-chemotherapy regime, with anthracycline, mostly daunorubicin (at least 60 mg/m$^2$), for 3 days and continuous infusion of cytarabine (100-200 mg/m$^2$) for 7 days, to achieve complete remission (CR)[20,21]. CR is defined as a bone marrow blast count < 5%, with the absence of circulating blasts and extramedullary disease as

well as hematologic recovery (neutrophil count ≥ 1000/µL, platelet count ≥ 100 000/µL)[21]. In 60-80% of younger patients (≤ 60 years) and 40-60% of elderly patients, CR is achieved after intensive induction therapy[3]. Following the induction, consolidation therapy is mandatory to eliminate minimal residual disease and achieve long term remission[20]. Without consolidation therapy, relapse is inevitable[4]. For consolidation, different treatment options are available, depending on patients' risk stratification. First-line consolidation treatment for patients with favorable prognosis is intensive chemotherapy, with intermediate-dose cytarabine (two to four cycles with up to six dosages of 1000-1500 mg/m$^2$ cytarabine), leading to 60-70% cure rates[3,4,21]. For intermediate-risk and adverse-risk patients, the treatment decision is not so clear and depends on benefit-risk assessment[4,21]. For eligible patients, allogeneic hematopoietic stem cell transplantation (allo-HSCT) is recommended[4,21]. Allo-HSCT is considered as the strongest antineoplastic therapy, due to intensive preparative regime of chemotherapy or radiation prior transplantation and mainly due to the immunologic graft-versus-leukemia effect, but is also associated with high risk of severe complications, such as graft-versus-host disease and relapse[3,35].

Despite intensive care and treatment of patients suffering of AML, high rates of relapse occur and the outcome, especially of elderly patients, remains poor[5,6,8–12]. Therefore, novel treatments are urgently needed. In the last decade, several new pharmacological approaches for the treatment of AML were approved by the U.S. Food and Drug Administration (FDA)[36]. An overview of the most important novel therapeutic approaches, leading to FDA approved treatment options, will be presented hereafter.

### *FLT3-Inhibitors*

Mutations in receptor tyrosine kinase genes, such as *FLT3* or *KIT*, occur frequently in AML patients, leading to enhanced proliferation and cell survival through activation of various signaling pathways[18,37]. Especially the internal tandem duplication in *FLT3* (FLT3-ITD) has an important prognostic impact and is present in about 30% of AML patients[2]. Next to the ITD form, point mutations in the tyrosine kinase domain (TKD) of *FLT3* occur in approximately 5% of AML cases[37]. Therefore, FLT3-inhibitors were developed. First-generation inhibitors (midostaurin, sorafenib, sunitinib) are unselective for a variety of tyrosine kinases, like FLT3, proto-oncogene c-KIT, platelet-derived growth factor (PDGF) as well as vascular endothelial growth factor (VEGF), and second-generation inhibitors (quizartinib, crenolanib, gilteritinib)

have a higher specificity for FLT3[36]. FLT3-inhibitors are further classified by their targeted conformation of the kinase. Type I inhibitors bind to the active and inactive conformation, whereas type II only binds to the inactive state[38]. Therefore, type I inhibitors are active for both mutant *FLT3* clones (ITD and TKD) and type II inhibitors only for FLT3-ITD[38].

Midostaurin was the first FDA approved first-generation FLT3-inhibitor and it is used in *FLT3*-mutated patients in addition to the conventional induction and consolidation chemotherapy regime[39]. The RATIFY study showed a benefit in OS and event-free survival after the addition of midostaurin to the conventional chemotherapy, which was leading to the FDA approval[40]. Gilteritinib is a second-generation FLT3-inhibitor and was recently approved by the FDA for the treatment of relapsed/refractory (R/R) FLT3-mutated AML, based on the ADMIRAL study[41,42]. FLT3-inhibitors lead to a marked blast reduction, especially a reduction within the peripheral blood, but often evoke resistance to treatment, leading to patient relapse[36].

*IDH-Inhibitors*

The genes *IDH1* and *IDH2* for metabolic enzymes are frequently mutated in AML (*IDH1*: 6-16%, *IDH2*: 8-19%), mostly in cytogenetically normal AML, interfering with DNA methylation and mitochondrial function[43]. Ivosidenib, a recently FDA-approved IDH1-inhibitor, is indicated for R/R *IDH1*-mutated AML[44]. DiNardo *et al*. could show favorable outcome with an overall response rate (ORR) of 41% and 21% CR in R/R AML-patients, orally treated with 500 mg ivosidenib[45]. Enasidenib is an IDH2-inhibitor, approved for patients with R/R *IDH2*-mutated AML[46]. Stein *et al*. could show a promising outcome with 40% ORR and 19% CR in patients, orally treated with 100 mg enasidenib[47]. Both inhibitors display similar pharmacological effects by promoting the differentiation of leukemic blasts into mature cells[48,49]. Serious treatment-related adverse events, such as differentiation syndrome or leukocytosis, occur with both compounds, but with a low frequency[45,47]. Different resistance mechanisms, such as isoform-switch between IDH1 and IDH2, were described[50].

*B-cell Lymphoma 2 (BCL-2) Pathway Inhibitors*

BCL-2 is part of the intrinsic mitochondrial pathway and is involved in the survival and maintenance of AML[36]. So far, no mutations for *BCL-2* have been found in AML, but its expression is often deregulated, without affecting the prognosis[51]. Especially in leukemic stem cells (LSCs), *BCL-2* expression can be upregulated[52]. LSCs have been found to be highly

resistant to conventional therapy[53] (further details in section 1.2). Venetoclax, a potent and selective BCL-2-inhibitor, was recently approved by the FDA for the treatment of newly diagnosed AML in elderly patients (≥ 75 years) or in patients with comorbidities that preclude the use of intensive induction therapy, in combination with azacytidine, decitabine or low-dose cytarabine, based on two open-label non-randomized trials[54]. DiNardo *et al*. could show that venetoclax in combination with azacytidine or decitabine is a well-tolerated and effective treatment option for elderly patients, with an achieved CR + $CR_i$ (CR with incomplete hematologic recovery) of 67%[55]. Further clinical studies of venetoclax in other treatment combinations and patient conditions are ongoing.

*Hedgehog Pathway Inhibitors*

A pathological role of the hedgehog pathway, an essential signaling pathway in embryonic development and early hematopoiesis, has been revealed in various cancer entities, including hematologic malignancies[56]. The hedgehog signaling pathway may be important for leukemic stem cell maintenance and chemotherapy resistance[56]. Wellbrock *et al*. could find expression of several members of the hedgehog signaling pathway in AML patients, including the transcription factors *GLI1*, *GLI2* and *GLI3*[57]. For *GLI*-expression, a negative prognostic impact was demonstrated[57]. The recently approved hedgehog pathway inhibitor glasdegib is binding to, and therefore inhibiting, the transmembrane protein Smoothened, leading to an enhanced sensitivity to chemotherapy in leukemic blasts[58]. Glasdegib is approved for the combined treatment with low-dose cytarabine in newly diagnosed elderly patients (≥ 75 years) or in patients who are not eligible for intensive induction chemotherapy[59]. The study BRIGHT AML 1003, which lead to the FDA approval, showed a significant reduction in mortality compared to the low-dose cytarabine treatment alone with an OS of 8.3 month and 18.2% CR for the combination and 4.3 month OS and 2.6% CR for the low-dose cytarabine treatment[60].

*DNA-Hypomethylating Agents (HMAs)*

Mutations in genes encoding for DNA-methyltransferases, such as *DMNT3A*, frequently occur in AML patients, leading to alterations in function and influencing epigenetic processes[18]. FDA approved drugs azacitidine and decitabine belong to the class of HMAs. They are irreversible inhibitors for DNA-methyltransferases, causing their proteasomal degradation[61]. Although both drugs are routinely used, the response rate is not satisfactory[36]. Several other drugs

targeting the epigenetic regulation as well as combination strategies are under investigation, aiming to optimize the pharmacological treatment.

Despite great progress in treatment that has been made in the last decades, further research on novel therapeutic approaches is still urgently needed. Not only the here mentioned targets are an active field of research, other approaches such as immunotherapy, TP53 pathway inhibitors and further epigenetic therapy are intensely investigated, with several novel compounds in the line, some already in clinical studies.

## 1.2 Leukemic stem cells (LSCs)

Leukemic stem cells (LSCs) are described as a rare population of leukemic cells, which display capacity of self-renewal, proliferation and differentiation into leukemic blasts[62]. Biological properties of LSCs further include resistance to chemotoxic compounds and apoptosis as well as cell cycle quiescence[53]. They are defined by their ability to initiate leukemia in xenotransplantation models with immunodeficient mice[63]. AML cells are characterized by their clonal heterogeneity[19]. Bonnet and Dick were the first to describe a hierarchical organization of the leukemic cell clones, similar to the normal hematopoiesis, with LSCs at the origin, maintaining the disease[64]. It is still controversial, whether LSCs arise from normal hematopoietic stem cells (HSCs) or from more mature progenitor cells by mutational changes, gaining stem cell characteristics[65–67]. Initiating driver-mutations, often acquired in epigenetic regulators, result in preleukemic hematopoietic stem cells with a clonal advantage, but still able to differentiate normally and yet unable to induce leukemia[65,66,68]. Further genetic lesions, leading to LSCs, are required to initiate leukemic onset[68,69]. This cancer stem cell model is well established and provides an explanation for the poor outcome in AML, due to chemotherapy resistance and disease relapse. In order to cure the disease, it is now common consensus that LSCs have to be eliminated[53,62].

### 1.2.1 Immunophenotype of LSCs

The assessment of the immunophenotype of LSCs is of great interest for development of potential LSC-targeted treatment. The population of LSCs was found to be highly heterogeneous in terms of their cell surface marker expression, as reviewed by Thomas and

Majeti[53]. Some of the expressed makers are also present on normal hematopoietic stem or progenitor cells (HSPCs), whereas others are shared with bulk leukemic blasts[53]. So far, no universal LSC-marker for all AML patients could be identified, even though several unique surface markers for LSCs were described.

*$CD34^+$ AML*

Initially, LSCs were defined as a $CD34^+$ $CD38^-$ cell population, but further studies demonstrated that LSCs are also present in other subpopulations[53,63,64]. Most of the studies were performed with $CD34^+$ AML samples, which are defined by positive CD34 expression on more than 10% of leukemic blasts[53]. For $CD34^+$ AML it was shown that LSCs are predominantly present within the $CD34^+$ $CD38^-$ subpopulation, but can be also present in the $CD34^+$ $CD38^+$ or $CD34^-$ fraction[70,71]. Goardon *et al*. could show a more specified classification of LSCs in $CD34^+$ AML, by detailed immunophenotyping[67]. The majority of AML samples (approximately 80%) displayed a dominant $CD34^+$ $CD45RA^+$ phenotype, whereas only 14% of samples had a dominant $Lin^-$ $CD34^+$ $CD38^-$ $CD90^-$ $CD45RA^-$ population, which was named MPP-like, due to the corresponding multipotent progenitor (MPP)-phenotype in normal hematopoiesis[67]. The $CD34^+$ $CD45RA^+$ population mainly consisted of two subpopulations, the $Lin^-$ $CD34^+$ $CD38^-$ $CD90^-$ $CD45RA^+$ subgroup named LMPP-like LSCs and the $Lin^-$ $CD34^+$ $CD38^+$ $CD123^+$ $CD45RA^+$ subgroup named GMP-like LSCs[67]. The groups were named according to the similar phenotype of lymphoid-primed multipotent progenitors (LMPP) and granulocyte-macrophage progenitors (GMP), respectively. It could be shown that the LMPP-like LSCs and GMP-like LSCs co-existed in 80% of cases, and they were hierarchically ordered[67]. The immature LMPP-like LSCs give rise to the more mature GMP-like LSCs, but not the converse[67]. Furthermore, it was demonstrated that the $CD34^+$ $CD38^-$ population had a higher frequency of LSCs compared to the $CD34^+$ $CD38^+$ population, consistent with a higher potential for self-renewal[67,72].

So far, no universal surface marker for $CD34^+$ $CD38^-$ LSCs expressed in all AML patients could be identified due to the high heterogeneity of the disease. Nevertheless, several markers, which can be upregulated in $CD34^+$ $CD38^-$ LSCs compared to normal $CD34^+$ $CD38^-$ HSPCs, are described. Many of those unique markers, such as CD123[73], CD47[74,75] and IL1RAP[76], are under investigation for targeted therapy[53].

*CD34⁻ AML*

CD34⁻ AML is defined by CD34 expression on less than 10% of leukemic blasts[53]. Therefore, only a small population of CD34⁺ cells is present. In CD34⁻ AML samples, LSCs could be identified within both fractions, the CD34⁻ and CD34⁺, not hierarchically arranged[69]. Quek *et al*. identified a precursor granulocyte-macrophage (GM)-like subpopulation (CD34⁻ CD117⁺ CD244⁻/⁺) as the main reservoir for LSCs within CD34⁻ AML[69].

### 1.2.2 Functional properties and regulation of LSCs

Main characteristics of LSCs are self-renewal, proliferation and differentiation into leukemic blasts, as well as resistance to chemotherapy and cell cycle quiescence[53,62]. These properties are influenced by a variety of signaling pathways and cellular processes, often shared with normal HSPCs[62]. Signaling pathways, which are tightly regulated in normal HSPCs, such as Wnt/β-catenin, Notch, JAK/STAT and PI3K/AKT were found aberrantly regulated in LSCs.

- The **Wnt/β-catenin signaling pathway** is well known to be important for HSC self-renewal and maintenance[77]. Moreover, it was found to play a critical role in self-renewal for LSCs that are derived from either HSCs or granulocyte macrophage progenitors (GMPs)[78]. The majority of AML cases display aberrant regulation of the Wnt/β-catenin signaling pathway and it was demonstrated that Wnt/β-catenin signaling pathway is constitutively activated in LSCs[79].
- The **Janus kinase (JAK)/signal transducer and activator of transcription (STAT) signaling pathway**, which is important for cell proliferation and survival, was found to be involved in LSC survival[80]. Cook *et al*. demonstrated an increased and constitutive JAK/STAT signaling in LSCs, particularly in LSCs from high-risk AML patients[80]. Furthermore, they showed that LSCs were sensitive to Janus kinase 2 (JAK2) inhibition, while normal HSCs remained unaffected[80].
- A main signaling pathway for hematopoietic growth factors and cytokines is the **Phosphatidylinositol 3-kinase (PI3K)/AKT pathway**[81]. Multiple AKT effectors, including mammalian target of rapamycin (mTOR) and forkhead box O (FOXO), regulate several biological processes such as cell survival, proliferation and cell cycle regulation[82]. In normal HSPCs, PI3K/AKT pathway is tightly regulated to maintain stem cell properties[81]. In AML, this pathway is often found to be constitutively activated[83].

Different *in vivo* mouse models revealed the critical role of the PI3K/AKT pathway in HSCs and LSCs. Targeted deletion of the negative regulator phosphatase and tensin homolog (Pten) or a constitutively active form of AKT led to HSC exhaustion and leukemogenesis[84,85]. Yilmaz *et al*. could demonstrate with their *Pten* deletion model that HSCs, in contrast to LSCs, were unable to maintain their stem cell function upon *Pten* deletion[85]. Furthermore, inhibition of mTOR with rapamycin led to LSC depletion as well as restored HSC function[85].

- Adult HSCs are stimulated by **Notch signaling**, which was demonstrated to promote HSPC expansion[81,86]. The role of Notch signaling in LSCs however, remains controversial. In myeloid linage context, Notch signaling has been reported to play a tumor suppressor role in LSCs[81]. Several groups could demonstrate that downregulation of Notch signaling promotes leukemogenesis or that induced activation of the signaling pathway lead to decreased AML cell proliferation[87–91]. On the contrary, certain authors also suggested an oncogenic role for activated Notch signaling in myeloid LSCs by promoting leukemogenesis, especially in context with the bone marrow microenvironment (refer 1.3)[92,93].

- A possible mechanism to evade apoptosis might be the up-regulation of **nuclear factor-κB** (NF-κB) in LSCs[94]. Guzman *et al*. demonstrated a constitutive activation of NF-κB in AML stem cells and showed that inhibition of NF-κB led to rapid cell death in leukemic cells, but not in normal $CD34^+$ cells[94].

- Important regulators for HSCs and LSCs are specific **microRNAs** (miR) by functioning as gene expression modulators[95]. Han *et al*. suggested that miR-29a initiates AML by converting non-self-renewing myeloid progenitors into LSCs[96]. They demonstrated that AML cells as well as HSCs display a high expression of miR-29a, whereas the expression in myeloid progenitors is downregulated[96]. Similarly, miR-99 was shown to regulate self-renewal in normal HSCs as well as in LSCs by inhibiting differentiation[97]. Lechman *et al*. identified miR-126 as a critical regulator of LSC maintenance[98]. They could show that miR-126 targeted members of the PI3K/AKT/mTOR signaling pathway and by that preserved cell cycle quiescence as well as self-renewal and promoted chemotherapy resistance of LSCs[98]. A reduction in miR-126 level led to opposing effects in HSCs and LSCs. While LSC maintenance was impaired, HSCs were expanded[98].

## 1.3 The bone marrow microenvironment

The bone marrow is the site of hematopoiesis and therefore important for stem cell homing and maintenance of HSC function[99]. The HSCs reside in local microenvironments within the bone marrow, the HSC niches[100]. A complex interaction network enables cross-communication between HSCs and bone marrow microenvironment[100]. This is highly regulated and thus contributes to the maintenance and retention of HSC[100]. The bone marrow microenvironment is considered to contribute to the development and maintenance of LSCs[101]. In AML, LSCs reside in the HSC niches, which provide conditions to promote LSC survival, quiescence, chemotherapy resistance as well as proliferation and differentiation[99,101]. It is thought that leukemic cells hijack HSC niches and remodel them into malignant niches, which are favorable for LSCs at the expense of normal HSPCs[102]. The bone marrow microenvironment is therefore playing a key role in AML pathogenesis[103].

### 1.3.1 Physiological bone marrow microenvironment

The bone marrow is a complex organ that is comprised of several hematopoietic and non-hematopoietic cell types within the cavities of bones[100]. It is highly vascularized and innervated[100]. Primary function of the BM is the hematopoiesis mediated by HSCs[103]. Non-hematopoietic cells, together with extracellular components, are responsible for building a microenvironment that supports hematopoiesis, the HSC niches (Figure 1)[100,104]. The concept of HSC niches was first described by R. Schofield in 1978 and until today the understanding of components and interaction networks within the BM microenvironment increased greatly[105]. Cellular and molecular components such as mesenchymal stem cells (MSC), endothelial cells, osteoblasts, adipocytes, non-myelinating Schwann cells and sympathetic neurons are involved in HSC homing and retention[100,106–111]. There are two types of HSC niches described: the endosteal niche and the perivascular niche[99,112]. The role of the distinct niches in regard of HSC homing is controversially discussed, even though both niches are tightly linked in location and function and a clear separation is difficult[99].

- The endosteum is defined as a thin layer of endosteal cells, mainly osteoblasts and osteoclasts, at the inner surface of bone cavities and the outer surface of trabeculae bone spicules within the cavities[100]. The **endosteal niche** is located in close proximity to the endosteum and is thought to facilitate mainly HSC quiescence[104,113]. Key

regulators within the endosteal niche are the osteoblasts, osteoclasts, osteal macrophages and CXCL12-abundant reticular (CAR) cells[104,113].

- The **perivascular niche** is associated with vascular endothelium and its surrounding stromal cells[107]. They are mainly located in vicinity to sinusoids within the trabecular bone[101]. Several types of cells compose this niche, including endothelial cells, MSCs, CAR cells, megakaryocytes and adipocytes[104]. The function of the perivascular niche was initially considered to support HSC proliferation and differentiation rather than cell cycle quiescence, but recent studies indicate a critical role of the perivascular niche also in HSC quiescence[104,107,114].

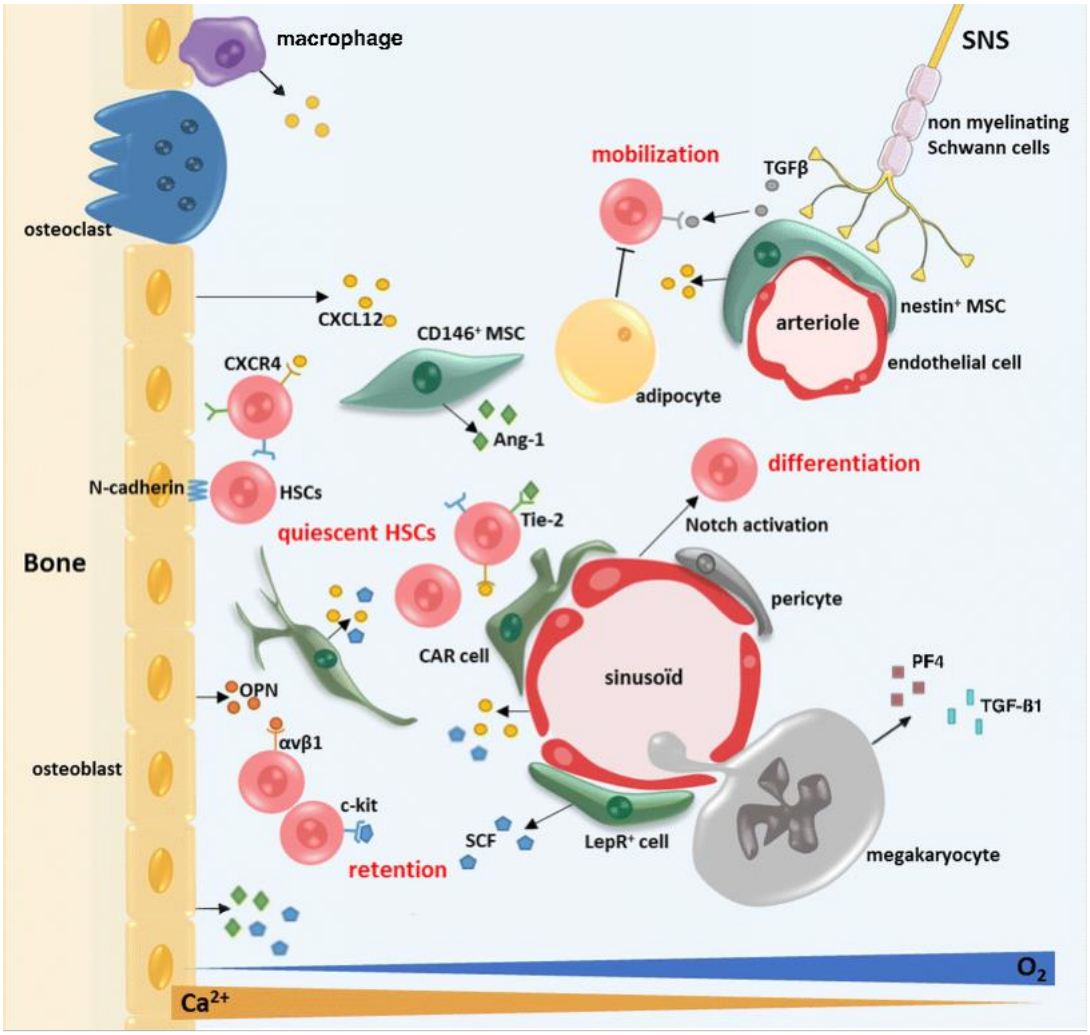


**Figure 1: Bone marrow microenvironment.** Non-hematopoietic cells together with extracellular components assemble niches, which regulate HSC fate. The perivascular niche is associated with vascular endothelium and its surrounding stromal cells, whereas the endosteal niche is located in close proximity to the endosteum. Ang-1, angiopoietin-1; CAR cells, CXCL12-abundant reticular cells; CXCL12, stromal cell-derived factor 1α; CXCR4, C-X-C Motif Chemokine Receptor 4; HSCs, hematopoietic stem cells; LepR, leptin receptor; MSC, mesenchymal stem cells; OPN, osteopontin; PF4, platelet factor 4; SCF, stem cell factor; SNS, sympathetic nervous system; TGF-β, transforming growth factor-β. (Figure and text modified from Goulard *et al.*)[104]

### 1.3.2 Cellular and molecular components

As reviewed by Goulard *et al*. and Hira *et al*. a variety of cellular components play an important role in the composition of HSC niches as mediators of extrinsic signals[104,113]. Molecular components, such as adhesion molecules, cytokines and their cytokine receptors, are critical for the cross-communication between HSCs and their microenvironment[104]. They support maintenance of normal hematopoiesis by regulating HSC fate and holding the balance between homing and migration[104,115]. An important regulator for HSC maintenance is hypoxia through induction of hypoxia-inducible factor (HIF)-2α[116].

*Mesenchymal stem cells (MSCs)*

MSCs are a heterogeneous group of cells defined by their specific phenotype ($CD105^+$, $CD73^+$, $CD90^+$, $CD34^-$, $CD45^-$, $CD14^-$ or $CD11b^-$, $CD19^-$ or $CD79\alpha^-$, $HLA\text{-}DR^-$) and their capacity to differentiate into a number of cell types, including adipocytes, osteoblasts and chondroblasts[117]. They play an important role in HSC niches, despite their rare occurrence within the BM[104]. Especially the subtypes CAR cells and $nestin^+$ cells are of significant importance[104]. $Nestin^+$ cells are mainly located in the perivascular niche and they express a variety of molecules, including stromal cell-derived factor 1α (SDF-1α, also known as CXCL12), stem cell factor (SCF), angiopoietin-1 (Ang-1), IL-7, vascular cell adhesion molecule 1 (VCAM-1) and osteopontin (OPN), to support HSC homing and quiescence[104,106,118]. Furthermore, they are associated with sympathetic neurons and in close proximity to HSCs[106]. The activity of $nestin^+$ cells can be downregulated by β-adrenergic signaling, resulting in HSC mobilization due to a decreased expression of HSC maintenance genes, such as *CXCL12*[106]. HSCs mobilization is following a circadian oscillating rhythm and it could be demonstrated with murine models that this rhythm is controlled by circadian noradrenalin signaling and therefore circadian secretion of CXCL12 within the HSC niche[119]. CAR cells are components of the endosteal niche and of the perivascular niche, where they form network-like structures[120]. Due to high expression of CXCL12 as well as SCF they regulate the quiescence and self-renewing of HSCs[120,121]. It was demonstrated that CAR cells are the main producers of CXCL12 and SCF within the bone marrow[121].

*Endothelial cells*

Trafficking and homing of HSPC in the perivascular niche is mainly regulated by endothelial cells[122]. Important for HSC retention in the perivascular niche is their expression of adhesion molecules such as VCAM-1, which interacts with its ligand very late antigen-4 (VLA-4) on the surface of HSCs, or E-selectin, which interacts with CD44[113,123,124]. Downregulation of VCAM-1 expression leads to HSC migration out of the niche[113]. Endothelial cells also contribute to the regulation of HSC quiescence and self-renewal by expressing CXCL12 and SCF[113,123].

*Osteoblasts and Osteoclasts*

Osteoblasts are the main cell type within the endosteum and important mediators of extrinsic signals for HSC within the endosteal niche[113]. Through several mechanisms, the fate of HSCs is determined by osteoblasts. They promote homing of HSCs to endosteal niches by secreting OPN, which binds mainly to integrins and CD44 at HSCs[115,125]. Osteoblasts are also expressing the factors CXCL12, SCF and Ang-1, which mediate HSC retention and quiescence[104,108,126,127]. Secretion of thrombopoietin (TPO) by osteoblasts supports HSC self-renewal and survival by activating several signaling pathways in HSCs, including JAK/STAT, PI3K/AKT and mitogen-activated protein kinase (MAPK)[128,129]. Notch signaling is activated in HSCs through osteoblastic factor Jagged-1 and plays an important role in HSC maintenance[108]. Furthermore, osteoblasts secrete transforming growth factor-β (TGF-β), which also supports HSC maintenance[130].

Osteoclasts play a contradictory role within the endosteal niche[113]. They support HSC retention and maintenance through $Ca^{2+}$-release during bone resorption and through activation of TGF-β[131,132]. On the contrary, they can contribute to the mobilization of HSCs through various mechanisms. During hematopoietic stress, osteoclasts can secrete proteases, which downregulate the signal for HSC retention by degrading CXCL12, SCF and OPN[133].

*Additional cellular components*

As previously described, sympathetic neurons within the bone marrow regulate HSC retention by β-adrenergic signaling[106]. Furthermore, the neuron-sheathing non-myelinating Schwann cells regulate HSC maintenance by activating TGF-β/Smad signaling[110]. Besides β-adrenergic neurons, also macrophages are able to influence the CXCL12 expression of MSCs, and therefore the retention of HSCs[134]. Moreover, they are able to express CXCL12

themselves[104,135]. By expressing osteocalcin, macrophages support the survival of osteoblasts[104,135]. Important for HSC quiescence in the niche are megakaryocytes by expressing platelet factor 4 (PF4) and by the secretion of TGF-β1[136,137]. Adipocytes were reported to support HSC proliferation while maintaining their immaturity by expressing adiponectin[138]. Furthermore, Zhou *et al*. showed that bone marrow adipocytes express SDF, which promotes HSC regeneration[139]. However, their overall role in HSC niches is still mainly unknown and controversial, as reviewed by Cuminetti and Arranz[109].

### 1.3.3 AML cells and the bone marrow microenvironment

AML cells have the ability to infiltrate HSC niches and to exploit the supporting systems for HSC[102]. As LSCs, they reside within the bone marrow microenvironment and studies indicate that due to the presence of LSCs, the niches can be reshaped into LSC promoting microenvironments, leading to a depletion of normal HSCs[102]. Several interactions and pathways within the HSC niche can influence leukemic initiation and propagation in AML, as reviewed by Behrmann *et al*.[99]. A number of marked differences between the support for HSCs and AML cells were described, to identify potential therapeutic targets.

Critical for the support of LSCs are several molecular niche components such as CXCL12, TGF-β and adhesion molecules[99]. CXCL12 was demonstrated to be a key regulator for AML cell homing and retention in the bone marrow microenvironment[140–142]. While it was shown that, despite its central role in HSC maintenance, it is not essential for the retention of HSCs within all types of HSC niches[143]. The chemoattractant CXCL12 is secreted by several niche-associated cell types, including MSCs (mainly CAR cells), endothelial cells, macrophages and osteoblasts[104,113]. It binds to C-X-C Motif Chemokine Receptor 4 (CXCR4), which is expressed by most AML cells, and leads to retention of the leukemic cells, which promotes their survival and maintenance[140]. It was demonstrated that treatment with CXCR4-antagonists plerixafor (AMD3100) or AMD3465 induced the release of leukemic cells in the circulation and that the mobilization out of the niche led to chemosensitization of the AML cells[140–142]. These results have led to a number of clinical studies with plerixafor in combination with chemotherapeutic agents for the treatment of AML[144–146]. Adhesion molecules are also of great importance for the infiltration of leukemic cells into the niche. AML cells express several of the same adhesion molecules as HSCs, including CD44 and VLA-4, which interact with cells of the bone marrow microenvironment[115]. CD44 binds to E-selectin, which is presented by endothelial cells, to

OPN, which is expressed by osteoblasts, and to hyaluronan within the extracellular matrix[115]. For LSCs, CD44 is important for homing within the microenvironment, while it is not absolutely mandatory for normal HSC[147]. Winkler *et al*. demonstrated a chemoprotective role of E-selectin for LSCs and that E-selectin blockage led to mobilization and chemosensitization of LSCs[148]. Furthermore, they showed in a previous study that E-selectin regulates HSC proliferation and that blockage of E-selectin increased HSC quiescence, self-renewal and chemoresistance[149]. These findings suggest an opposite effect of E-selectin blockage on HSCs and LSCs, with a protective impact for HSCs and a sensitization to chemotherapeutic treatment for LSCs. VLA-4 is a ligand for VCAM-1, which is expressed by MSCs as well as by endothelial cells, and for fibronectin on stromal cells[106,115]. As demonstrated by Jacamo *et al*. binding of VLA-4 to VCAM-1 induces activation of NF-κB pathway within AML cells as well as within MSCs, which leads to an induced resistance to chemotherapy and inhibition of NF-κB pathway leads to a sensitization to chemotherapy[150]. Similarly, Matsunaga *et al*. reported that AML cells acquire chemoresistance through interaction of VLA-4 with stromal fibronectin, due to antiapoptotic signaling[151].

LSCs have an influence on the different cellular components within the bone marrow microenvironment and alteration of their physiological state causes the remodeling into a malignant niche. Studies revealed that endothelial cells are important interaction partners for leukemic cells, not only for the regulation of adhesion and migration, but also for promoting survival, proliferation and chemoresistance[103]. Cogle *et al*. demonstrated that AML cells are able to integrate into the vasculature and that they can gain endothelial-like characteristics upon fusion with endothelial cells[152]. Furthermore, a reduced proliferation rate of the integrated endothelial-like AML cells could be shown[152]. Important factor for the interaction between AML cells and vascular endothelial cells, which leads to alteration of endothelial cell proliferation, is VEGF. The proangiogenic factor VEGF is broadly expressed by AML cells, as reported by Fiedler *et al*[153]. Adhesion of AML cells and activation of VEGF signaling induces proliferation of endothelial cells, which results in enhanced angiogenesis[154]. Furthermore, it is thought that VEGF induces proliferation and survival of AML cells by autocrine as well as paracrine signaling[153,155]. Altered differentiation of MSCs by AML cells contributes to the remodeling of the bone marrow microenvironment. Hanoun *et al*. demonstrated that sympathetic neuropathy develops upon AML progression, which leads to a disrupted quiescence of nestin$^+$ cells, resulting in an expansion of MSCs, primed for the osteoblastic

lineage, and a reduction in mature osteoblasts[156]. This altered differentiation of MSCs leads to an impaired HSC niche function with a decreased ability for HSC maintenance[156]. Similarly, Kumar *et al*. reported that AML cells can remodel the microenvironment through exosome secretion into a leukemia promoting microenvironment at the expense of normal hematopoiesis[157]. AML-derived exosomes can increase mesenchymal stromal progenitors, but inhibit the differentiation into mature osteoblasts[157]. As demonstrated by Battula *et al*., AML cells not only promote osteogenic differentiation of MSCs, they also inhibit adipogenic differentiation[158]. This alteration creates a niche of osteoblastic-primed MSCs, which enhances leukemic cell expansion[158]. Additionally, Boyd *et al*. reported that AML impairs adipogenic maturation, leading to a compromised formation of bone marrow adipose tissue and an altered regulation of HSCs[159]. Furthermore, they could demonstrate that induced bone marrow adipogenesis leads to a rebalanced hematopoiesis and suppressed leukemic proliferation[159]. On the contrary, Shafat *et al*. reported a leukemic supporting function of bone marrow adipocytes within the malignant niche[160]. AML cells induce adipocyte lipolysis and therefore the transfer of free fatty acids from adipocytes to AML cells, which is used as an energy source and promote cell proliferation and survival[160].

Important for AML progression and chemoresistance are several members of the immune system within the bone marrow microenvironment. AML cells are able to generate an immunosuppressive microenvironment, with altered innate as well as adaptive immune responses[161]. Several mechanisms such as increased expression of immunosuppressive cytokines, attraction of regulatory T cells (Tregs) and altered expression of immune checkpoint molecules contribute to the generation[161].

In addition to the molecular alterations, it was demonstrated that AML cells also induce remodeling of the vascular system within the bone marrow[99]. Physiologically the bone marrow vasculature consists of arteries, veins and capillaries[162]. Arteries, which enter the bone via the cortical region, branch into arterioles, which terminate into type H capillaries[162]. Type H capillaries, which are localized near the endosteum and in the metaphysis, merge into highly interconnected type L capillaries, which are sinusoidal vessels within the bone cavity, and which terminate into the central vein[162]. Sinusoids are the side of cell trafficking and they show a higher permeability as well as a lower blood flow speed compared to arterial vessels[163,164]. Duarte *et al*. could demonstrate that AML can remodel endosteal as well as central bone marrow vasculature, which leads to a decreased ability for HSC maintenance

within the endosteal niche[165]. Furthermore, they showed that prevention of endosteal blood vessel loss can increase the efficiency of chemotherapy[165].

AML cells are able to infiltrate and remodel the HSC niche and reside as LSCs within the microenvironment[102]. Retention of LSCs induces chemotherapy resistance and leads to persistence of minimal residual disease, which eventually leads to AML relapse[102]. Therefore, it is of great interest to therapeutically target this specific AML cell population as well as its microenvironment.

## 1.4 Guanine nucleotide exchange factor DOCK1

Dedicator of cytokinesis 1 (DOCK1), also known as DOCK180, was the first member identified of the DOCK180 superfamily. It belongs to the class of guanine nucleotide exchange factors (GEFs) for the small G-protein Rac and is therefore influencing several biological processes such as cell migration and invasion[166,167].

### 1.4.1 Guanine nucleotide exchange factors (GEFs)

Guanine nucleotide exchange factors (GEFs) mediate the activation of Rho GTPases through catalyzing the exchange of the nucleotides guanosine diphosphate (GDP) to guanosine triphosphate (GTP)[168]. Rho GTPases are a subfamily of Ras-related small GTPases with 22 proteins, which activation is regulated by three distinct classes of proteins: GEFs promote the activation, whereas GTPase-activating proteins (GAPs) enhance the hydrolyzation of bound GTP to GDP by the GTPase and guanine nucleotide-dissociation inhibitors (GDIs) sequester the Rho GTPases in a GDP-bound state in the cytosol[168] (Figure 2).

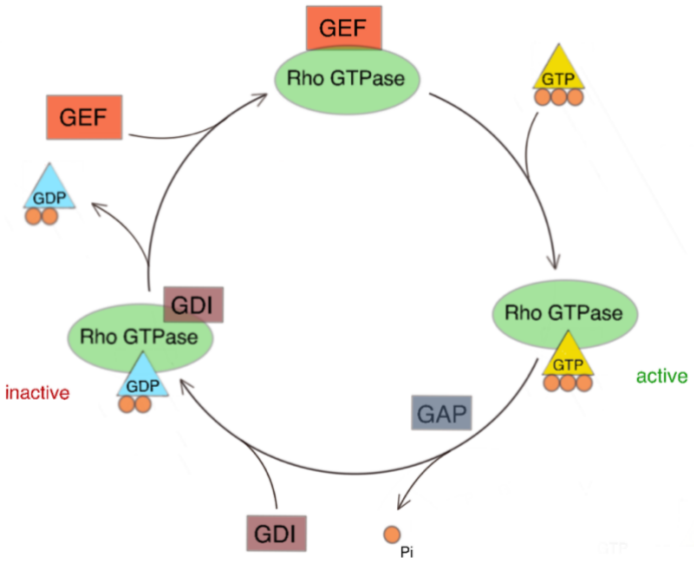


**Figure 2: Regulation of Rho GTPases.** Rho GTPases are regulated by three distinct types of proteins. guanine nucleotide exchange factors (GEF) promote the activation of Rho GTPases by binding and stabilizing the nucleotide-free form. Rapid GTP loading is promoted and leads to a dissociation of the complex into GTP-bound Rho GTPase and GEF. When Rho GTPases are GTP-bound, they are active and regulate several downstream processes. GTPase-activating proteins (GAP) enhance the intrinsic hydrolyzation of bound GTP into GDP by the Rho GTPase. GDP-bound Rho GTPases are inactive. Guanine nucleotide-dissociation inhibitors (GDI) bind to the inactive GDP-bound form to sequester GTPases in the cytosol. The release of the nucleotide-free GTPase is not yet completely understood. GDP, guanosine diphosphate; GTP, guanosine triphosphate; $P_i$, inorganic phosphate (Figure and text adapted from Rossman *et al.*)[168]

GEFs can be subdivided into two main classes: the classical Dbl-related GEFs and the DOCK180 family of GEFs[168]. Dbl-related GEFs are characterized by a Dbl-homology (DH) domain and a DH-associated pleckstrin-homology (PH) domain[168]. The nucleotide exchange within the Rho GTPases is catalyzed by the DH domain of Dbl-related GEFs[168]. Proteins of the DOCK180 family function as GEFs for the Rho GTPases Rac and Cdc42[169]. They do not contain a DH domain, instead they are characterized by two evolutionarily conserved domains, DOCK homology region (DHR) 1 and DHR2[169–171]. The DHR2 domain (also known as CZH-2 or docker) determines the catalytic activity in terms of Rho GTPase activation[169–171]. Similar to the DH domain in Dbl-related GEFs, the DHR2 domain was shown to interact with the nucleotide-depleted GTPase, stabilizing the intermediate state for the rapid binding to GTP[169,170]. It was demonstrated that Rac activation can be blocked by inactivation of DHR2 domain in DOCK1 proteins[169,170]. While the DHR2 domain was shown to be responsible for the GEF activity, the DHR1 domain (also known as CZH-1) was found to be a binding site for phospholipids[172]. Côté *et al*. demonstrated that the DHR1 domain in DOCK1 interacts with phosphatidylinositol (3,4,5)-triphosphate ($PIP_3$), mediating $PIP_3$ signaling[172]. By binding to $PIP_3$, the localized Rac activation takes place at sites of $PIP_3$ accumulation, promoting directional cell movement,

which is important for cell elongation and migration[172]. Therefore, the DHR1 domain has an important role in Rac signaling, by polarizing the Rac activation to certain locations.

### 1.4.2 DOCK180 family

Proteins of the DOCK180 family are highly conserved and act as GEFs for the Rho GTPases Rac and Cdc42[169]. So far, 11 DOCK180-related proteins could be identified in mammals, named DOCK1 (also known as DOCK180) to DOCK11[169]. They are classified into four subgroups (A-D) based on their sequence homology[169] (Figure 3). DOCK proteins of group A (DOCK1, 2 and 5) and group B (DOCK3 and 4) contain an amino-terminal SH3 domain, which mediates their binding to engulfment and cell motility protein (ELMO) 1 and 2[169,173]. Furthermore, several members of both groups contain a proline-rich carboxy-terminal domain that binds Crk proteins[169,174]. DOCK proteins of group A and B act as GEFs for the GTPase Rac[167]. DOCK6-8, also called zizimin related (Zir) 1-3, respectively, belong to the subgroup C and their GEF activity is considered specific for Rac as well as for Cdc42[167,169]. Group D consists of DOCK9-11, also called zizimin (Ziz) 1-3, respectively, and they are GEFs for the GTPase Cdc42[167,169]. Proteins of the group D contain an amino-terminal PH-domain, which are generally known to bind phosphoinositides and participate in protein-protein interactions[169,175].

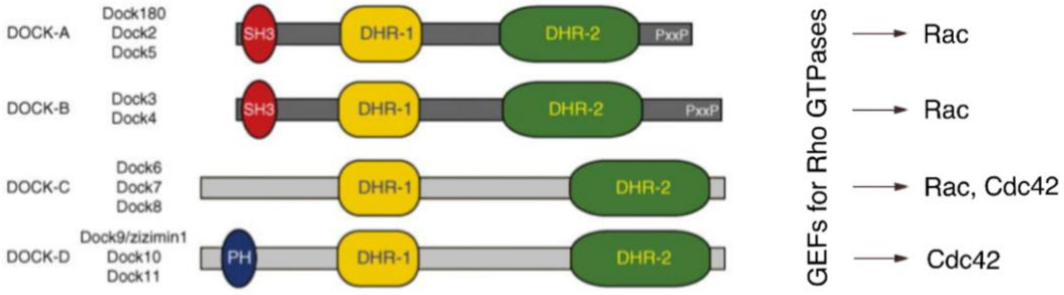


**Figure 3: Schematic structure of DOCK180 family proteins.** DOCK180 family proteins are characterized by their evolutionary conserved domains DHR1 and DHR2. The DHR1 domain mediates the binding to phospholipids, while the DHR2 domain is responsible for the GEF activity towards the respective Rho GTPases. DOCK proteins of group A and B contain a N-terminal SH3 domain, which mediates their binding to ELMO1 and 2. The proline-rich C-terminal of group A and B DOCK proteins binds to Crk proteins. DOCK proteins of group D contain a N-terminal PH domain, which is involved in binding phosphoinositides. DHR, DOCK homology region; GEF, guanine nucleotide exchange factor; P, proline; PH, pleckstrin-homology. (Figure and text modified from Côté and Vuori)[173]

### 1.4.3 Physiological function of DOCK1

DOCK1 was originally identified as a cytoplasmatic 180 kilodalton (kDa)-binding protein for the proto-oncogene product CrkII[174]. Further studies revealed that DOCK1 acts as a GEF for the GTPase Rac, through its DHR2 domain[166,169,170]. GTP-bound Rac is involved in the reorganization of the actin cytoskeleton and is therefore influencing several biological processes, such as cell migration and invasion, phagocytosis of apoptotic cells, cell spreading and adhesion[168]. Furthermore, Rac GTPases are involved in proliferation and cell survival[176,177].

The amino-terminal SH3 domain of DOCK1 was revealed as a binding site for ELMO proteins[169,173]. It is common consensus that the formation of a DOCK1-ELMO complex increases the affinity towards the nucleotide-free Rac and therefore enhances the catalytic activity of DOCK1. DOCK1 and ELMO function together as a bipartite GEF for Rac[170,178]. Lu and Ravichandran proposed three distinct mechanisms, by which ELMO modulates the DOCK1 function towards Rac[179] (see also Figure 4):

1. **ELMO helps DOCK1 to stabilize Rac in its nucleotide-depleted state.** ELMO proteins contain a conserved atypical PH domain and a carboxy-terminal proline-rich region[173]. The SH3 domain of DOCK1 mediates the binding to the proline-rich region in ELMO[180]. The atypical PH domain of ELMO was found to be the key feature for the formation of a ternary complex of DOCK1, ELMO and nucleotide-free Rac and the enhanced affinity of DOCK1 towards Rac[178]. ELMO itself is not able to interact with nucleotide-free Rac[181], therefore it is believed that the formation of a low-affinity DOCK1-Rac complex creates a binding-site in Rac for ELMO[179]. By formation of the ternary complex, the affinity of DOCK1 towards nucleotide-free Rac is increased and therefore the GTP loading[178,179].
2. **ELMO relieves the DOCK1 self-inhibition.** It could be demonstrated that the SH3 domain of DOCK1 functions as an intramolecular inhibitor for the DHR2 domain[180]. At the basal state of DOCK1, the SH3 domain interacts with the catalytical DHR2 domain and therefore inhibits the access of Rac[180]. By blocking the DHR2 domain, the GEF activity of DOCK1 is reduced. ELMO relieves this self-inhibition by binding the SH3 domain with its proline-rich region, allowing a better access of Rac to the DHR2 domain[180]. ELMO itself is also highly regulated by autoinhibitory activity[182].

3. **ELMO localizes the DOCK1-ELMO complex to the plasma membrane.** ELMO contains an amino-terminal Armadillo (ARM) repeat, which was suggested to interact with membrane-associated active GTPase RhoG[183]. By interaction of ELMO with RhoG, the DOCK1-ELMO complex is translocated to the plasma membrane, where it can activate Rac[184]. The activation of Rac in a distinct location could be shown to be important for directed cell movement in phagocytosis and cell migration[183,184]. Similar recruiting mechanisms are discussed for Arf-family GTPases Arl4A and Arf6[185,186].

Many of the mechanisms described remain model-based, as their biological relevance could not yet be fully demonstrated in mammalian systems.

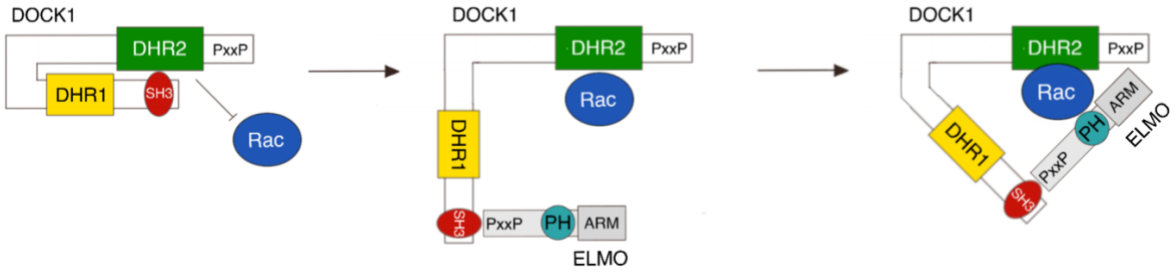


**Figure 4: Schematic mechanism of the bipartite GEF.** ELMO1 relieves DOCK1 self-inhibition by binding to the SH3 domain of DOCK1 with its proline-rich C-terminal region, which allows the access of Rac to the DHR2 domain of DOCK1. The formation of a low-affinity complex between DOCK1 and Rac creates a binding site for ELMO. A ternary complex is formed through binding of the atypical PH domain of ELMO to Rac, which increases the affinity of DOCK1 towards nucleotide-free Rac. ARM, Armadillo; DHR, DOCK homology region; P, proline; PH, pleckstrin-homology. (Figure and text adapted from Lu *et al.*)[179]

As previously described, the Rac activation at distinct sites of the cell can also be mediated by the binding of DOCK1 DHR1 domain to $PIP_3$[172]. $PIP_3$ is a second messenger molecule and was found to be a key regulator for cell polarization and establishment of the leading edge[187]. DOCK1 is therefore localized to sites of accumulated $PIP_3$, where it activates Rac[172]. A form of DOCK1 that lacks the DHR1 domain, was found to be unable to promote cell migration, even though it was able to induce Rac activation, indicating that the localization towards the leading edge is essential for directed cell movement[172]. For the formation of membrane protrusions and directed cell movement, the stabilization of microtubules at the plasma membrane is essential[188]. The actin cross-linking family 7 (ACF7) protein has a conserved role in membrane protrusion formation by interacting with microtubules and mediating their cross-linking to the actin cytoskeleton[189,190]. Margaron *et al*. could demonstrate direct binding of ELMO to ACF7, promoting the recruitment of ACF7 to the plasma membrane, where it is involved in maintaining the membrane protrusion by microtubule stabilization[188]. Furthermore, they

could show that protrusion formation mediated by the ELMO-ACF7 complex requires Rac activation by DOCK1[188]. These mechanisms highlight the critical role of the DOCK1-ELMO complex in directed cell migration. Binding to $PIP_3$ directs the complex to sites with accumulated $PIP_3$, resulting in high Rac activity[172]. High Rac activity leads to actin cytoskeleton reorganization and formation of the leading edge and membrane protrusion[172]. By binding of ELMO to ACF7, the microtubule-stabilizing protein is recruited to the site[188]. ELMO-ACF7 complex promotes microtubule dynamics by Rac activation, stabilizing the membrane protrusion[188].

DOCK1 is involved in the targeted Rac activation not only at the leading edge, but also at sites of focal adhesion. Kiyokawa *et al*. showed that DOCK1 is involved in integrin signaling by the formation of a DOCK1-CrkII-$p130^{Cas}$ complex at sites of focal adhesion, which induces Rac activation and cellular spreading[166,191]. It was demonstrated that DOCK1 is phosphorylated on serine residues upon integrin stimulation, which correlates with the tyrosine phosphorylation of $p130^{Cas}$ in integrin stimulated cells[191]. Furthermore, the integrin stimulation induced the binding of DOCK1 to CrkII as well as the binding of CrkII to $p130^{Cas}$ [191]. They showed that only the co-expression of all three leads to an accumulation of the ternary complex at sites of focal adhesion[191]. Tachibana *et al*. could demonstrate that ankyrin domain repeat protein 28 (ANKRD28) also binds to the SH3 domain of DOCK1, competing with ELMO for the binding site[192]. In contrast to ELMO, ANKRD28 drives the Rac activation mediated by DOCK1 not to the leading edge, but instead to sites of focal adhesion (Figure 5)[192]. By localizing the DOCK1-CrkII-$p130^{Cas}$ complex to sites of focal adhesion, it stabilizes those sites[192].

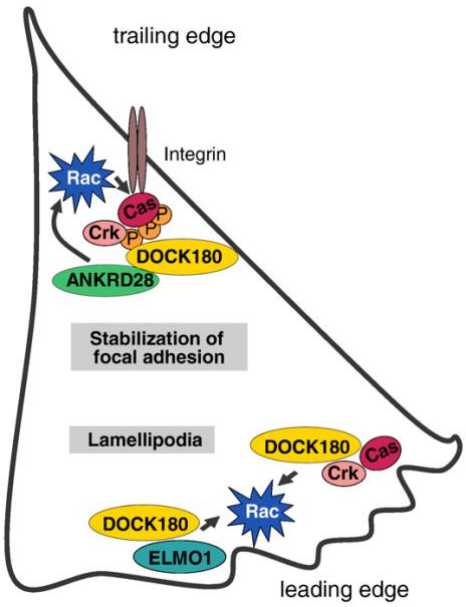


**Figure 5: Involvement of DOCK1 during directed cell movement.** Rac activation through DOCK1 is directed to distinct locations within the cell. ANKRD28 drives Rac activation by DOCK1-CrkII-$p130^{Cas}$ complex to sites of focal adhesion, whereas ELMO directs DOCK1 towards the leading edge. P, phosphate.(Figure and text modified from Tachibana *et al*.)[192]

It is under discussion, whether DOCK1 might be regulated by mechanisms such as phosphorylation and targeted degradation. As previously described, Kiyokawa *et al*. could demonstrate serine phosphorylation of DOCK1 upon integrin signaling[191]. The amount of DOCK1 can be regulated through an ubiquitin-proteasome-dependent protein degradation mechanism, as demonstrated by Makino *et al*.[193]. DOCK1 is ubiquitylated mainly on the plasma membrane and ELMO1 is inhibiting this ubiquitylation[193]. Therefore, ELMO1 stabilizes DOCK1 through inhibition of the ubiquitylation and thereby its degradation, resulting in higher DOCK1 levels[193]. Interestingly, the ubiquitylation of DOCK1 was enhanced by epidermal growth factor (EGF) and Crk proteins, which might contribute to a tight regulation of Rac activation[193].

### 1.4.4 DOCK1 in cancer entities

Several studies revealed a prognostic or pathophysiologic impact of DOCK1 in different cancer entities. In most of the studied malignancies, a direct functional association between DOCK1 activation and cancer cell migration and invasion could be demonstrated.

Laurin *et al*. reported a negative correlation between high DOCK1 expression and patient survival in $HER2^+$ and basal breast cancer subtypes[194]. Furthermore, they showed that DOCK1 is a downstream mediator of HER2 for Rac activation and cell migration, which is essential for HER2-mediated breast cancer metastasis[194]. Upon Heregulin β1 treatment or overexpression of an activated form of HER2 *in vitro*, DOCK1 was phosphorylated by Src protein kinases at amino acid residue $Y^{1811}$ within a regulatory site of DOCK1, which enhances the GEF activity towards Rac[194]. Moreover, DOCK1 was identified to be required for STAT3 phosphorylation, which is a known mediator of metastasis, downstream of HER2[194]. Li *et al*. presented Gαi2 as a novel binding partner for ELMO1 upon CXCL12 signaling, which regulates actin cytoskeleton changes during breast cancer metastasis[195]. Binding of CXCL12 to G protein-coupled receptor CXCR4 releases Gαi2, which associates with ELMO1 and locates it to the plasma membrane, where it forms the bipartite GEF complex with DOCK1 and mediates Rac dependent actin cytoskeleton reorganization[195]. As demonstrated by Liang *et al*., a downregulation of DOCK1 and ELMO1 in triple-negative breast cancer epithelial cells leads to decreased migration and invasion through the RhoA/Rac1 pathway *in vitro*[196]. Additionally, Chiang *et al*. reported a negative correlation of high DOCK1 expression and patient survival for triple-negative breast cancer patients[197]. Moreover, in claudin-low breast cancer cells, DOCK1 was associated with

growth and motility regulation of the cancer cells by downregulating Claudin 1-expression via Rac1/ribosomal RNA processing protein 1B (RRP1B)/DNA methyltransferase (DNMT) signaling pathway[197].

Zhao *et al*. identified DOCK1 as a potential prognostic marker in ovarian cancer, since high DOCK1 expression was associated with poor patient survival as well as an aggressive phenothype[198]. They could demonstrate *in vitro* that DOCK1 is involved in ovarian cancer cell migration and invasion and that downregulation of DOCK1 is associated with a reduced matrix metalloproteinase 2 (MMP-2) expression[198]. MMP-2 functions as an early regulator in ovarian cancer metastasis[199].

DOCK1 was identified to be involved in cell migration and invasion of human glioblastoma multiforme (GBM), a highly invasive brain tumor. It was demonstrated that DOCK1 and ELMO1 are co-overexpressed in invading tumor cells within the invasive areas of glioma[200]. Feng *et al*. reported an activation of Rac signaling through phosphorylation of DOCK1 upon stimulation of platelet-derived growth factor receptor α (PDGFRα) and a constitutively active epidermal growth factor receptor mutant (EGFRvIII)[201–204]. PDGFRα is a commonly amplified gene in GBM and the stimulation of PDGFRα leads to phosphorylation of DOCK1 at amino acid residue $Y^{1811}$ by Src protein kinases, which enhances the GEF activity of DOCK1 by increasing its association with CrkII and $p130^{Cas}$ [201]. A co-expression of $DOCK1^{Y1811}$, $Src^{Y418}$ and PDGFRα in GBM was associated with a poor patient prognosis[201]. Furthermore, a protein kinase A (PKA)-dependent phosphorylation of DOCK1 at amino acid residue $S^{1250}$ within the DHR2 domain, which leads to Rac activation, was demonstrated after PDGFRα stimulation[202]. In GBM, EGFRvIII is commonly co-overexpressed with EGFR and promotes tumorigenesis[203]. Feng *et al*. reported that EGFRvIII induces phosphorylation of DOCK1 at amino acid residue $Y^{722}$ within the interdomain of DHR1 and DHR2 by Scr protein kinases as well as PKA depended phosphorylation of DOCK1 at amino acid residue $S^{1250}$ [203,204]. DOCK1 phosphorylation leads to Rac activation, therefore promoting glioblastoma cell survival and migration[203,204]. Co-expression of $DOCK1^{Y722}$, $Src^{Y418}$ and EGFRvIII was associated with a poor survival of glioblastoma patients[203]. Zhang *et al*. showed that DOCK1 promotes the mesenchymal transition of glioma cells and that its expression is modulated by miR-31[205]. Rac-dependent cell migration and invasion of glioblastoma cells was demonstrated to be enhanced upon hepatocyte growth factor (HGF) stimulation[206]. HGF induced the formation of a protein complex on the cell membrane, consisting of the two receptor tyrosine kinases AXL and MET

as well as DOCK1 and ELMO2, which mediated the Rac activation[206]. This HGF-dependent formation of the AXL/MET/DOCK1/ELMO2 complex was shown to be present in various types of cancer cells[206].

Studies indicate that DOCK1 might be involved in mechanisms which promote the resistance to chemotherapy in cancer cells. Chen *et al*. report a higher resistance to cisplatin in bladder cancer cell lines with a high DOCK1 expression, while downregulation of DOCK1 sensitizes bladder cancer cells to the cisplatin treatment[207]. Moreover, they demonstrated that cisplatin treatment induces epithelial-mesenchymal transition and downregulation of DOCK1 prevents this program[207]. In non-small-cell lung cancer, Pan *et al*. could demonstrate a reduced tumor growth with the combined treatment of the tyrosine kinase inhibitor genfitinib and the low molecular weight heparin enoxaparin[208]. Enoxaparin addition led to a decreased migration compared to genfitinib alone and a lower expression of DOCK1 as well as decreased Akt activity[208]. They concluded that enoxaparin sensitizes lung cancer cells to genfitinib through downregulation of DOCK1 expression besides others[208].

### 1.4.5 DOCK1 in AML

As described above, DOCK1 has been reported to be involved in the tumorigenesis of several solid cancer entities, but until now only little is known about its role in hematological malignancies. Preliminary work of the research group Fiedler/Wellbrock revealed a potential role of DOCK1 in the pathophysiology of AML (unpublished data).

Microarray-based gene expression analysis of co-cultured primary AML blasts with primary endothelial cells as well as co-cultures with primary osteoblasts revealed DOCK1 as a possible component in the interaction between the bone marrow niche and AML cells. It was shown that *DOCK1* was directly upregulated only in co-cultured primary AML cells, but not in co-cultured healthy $CD34^+$ hematopoietic progenitor cells. Further analysis of microarray-based gene expression data of a large cohort of AML patients (n=290), published by Verhaak *et al*. (Gene Expression Omnibus GSE6891)[209], identified DOCK1 as an independent prognostic marker since high DOCK1 expression was associated with a poor overall survival as well as poor event-free survival. These findings are in line with a recently published study by Lee *et al*.[1]. Their study revealed DOCK1 as a strong independent prognostic marker through analysis of three independent datasets of AML patient cohorts[1]. Furthermore, it was demonstrated that high DOCK1 expression was associated with other clinical and biological

parameters, such as older age or higher platelet and peripheral blast counts at diagnosis[1]. Additionally, higher DOCK1 expression correlated with intermediate-risk cytogenetics and occurrence of FLT3-ITD as well as mutations in MLL, DNMT3A, NPM1, PTPN11, RUNX1 and ASXL1[1]. Zhang *et al*. recently reported a negative prognostic impact of high DOCK1 expression for AML patients undergoing allo-HSCT[210]. In contrast to the finding that DOCK1 is an adverse prognostic marker in AML, the closely related DOCK protein DOCK2, which is predominantly expressed in hematopoietic cells, was demonstrated to be an independent favorable prognostic marker, since high DOCK2 expression coincided with longer overall survival and event-free survival[211,212]. Interestingly, while DOCK2 expression is restricted to hematopoietic cells, DOCK1 is wildly expressed[212].

Preliminary *in vitro* approaches of the research group Fiedler/Wellbrock revealed DOCK1 as an inducible factor in AML cells, when co-cultured with stromal cells of the bone marrow microenvironment (unpublished data). In co-culture assays with endothelial cells, an upregulation of *DOCK1* mRNA expression in *DOCK1* non-expressing AML cell lines MV4-11 and THP-1 as well as in primary AML blasts, compared to single cultured cells, could be shown. Furthermore, the two cell lines with the inducible *DOCK1* expression showed a high endogenous CXCR4 expression and inhibition of CXCR4 with AMD3100 lead to a decreased induction of *DOCK1* expression within co-culture assays, indicating a possible upstream function of CXCR4 for DOCK1 signaling in AML.

Wang *et al*. identified the GTPase Rac1, which is the downstream target of DOCK1, as an important regulator for LSC homing in AML[213]. Activation of Rac1 signaling promotes leukemic cell migration, chemotherapy resistance, cell cycle quiescence and homing to the bone marrow niche[213].

## 1.5 Aim of the thesis

Although the prognosis of AML has steadily improved over the last decades, it remains unsatisfactory, as the majority of patients eventually relapse. An increasing understanding of the origin and progression of the disease has led to many new therapeutic approaches. Nevertheless, the prognosis remains poor[5,6,8–12]. The high incidence of relapses is believed to be due to the existence of LSCs and the common opinion is that not only the bulk of AML

blasts must be eliminated, but also the LSCs[53,62]. New therapeutic approaches that specifically target LSCs within their bone marrow niche are urgently needed.

Preliminary work of the research group Fiedler/Wellbrock indicate that DOCK1 is a potential niche-specific target in AML. The expression of *DOCK1* can be induced by microenvironmental cells in AML cells, but not in normal hematopoietic cells. The aim of this project was to evaluate the relevance of DOCK1 to the pathophysiology of AML and whether DOCK1 is a potential therapeutic target. To evaluate the role of DOCK1 in the AML pathophysiology, *in vitro* assays with small molecule DOCK inhibitors as well as targeted shRNA-based knockdown of *DOCK1* and *ELMO1* in AML cell lines were performed to evaluate a possible antileukemic effect of DOCK1-inhibition and to determine the functional consequences of a decreased DOCK1 activity. Since *in vitro* assays are not taking the whole complexity of the bone marrow microenvironment into account, xenotransplantation mouse models were performed, to investigate the influence of the shRNA-based knockdown of *DOCK1* on the AML progression *in vivo*. By generating a stable *DOCK1* overexpressing AML cell line, the findings from shRNA-based knockdown were to be confirmed. Another focus of project was the identification of the DOCK1-signaling pathway in AML, which included the characterization of direct DOCK1 interaction partners as well as the evaluation of potential upstream-mediators.

# II. MATERIAL AND METHODS

## 2.1 Material

### 2.1.1 Instruments

Laboratory equipment used in this study is listed in Table 3.

**Table 3: Equipment**

| Description | Instrument | Manufacturer |
|---|---|---|
| Agarose gel electrophoresis chamber | DNA Sub cell™ | Bio-Rad (Hercules, CA, USA) |
| Analytical scale | AT261 DeltaRange® | Mettler-Toledo GmbH (Greifensee, CH) |
| Analytical scale | Pioneer™ PA213 | Ohaus Corp. (Pine Brook, NJ, USA) |
| Benchtop centrifuge | Centrifuge 5424 | Eppendorf (Hamburg, DE) |
| Benchtop centrifuge | Centrifuge 5804 R | Eppendorf (Hamburg, DE) |
| Benchtop centrifuge | Centrifuge 5810 R | Eppendorf (Hamburg, DE) |
| Benchtop centrifuge | Labofuge 400 R | Heraeus (Hanau, DE) |
| Benchtop microcentrifuge | myFuge™ Mini | Benchmark Scientific (Edison, NJ, USA) |
| BioFlux system | BioFlux™ 200, BioFlux™ 48 well plate 0-20 dyn/cm$^2$ | Fluxion Biosciences (Alameda, CA, USA) |
| Biological safety cabinet | HeraSafe HS 9 | Heraeus (Hanau, DE) |
| Biological safety cabinet | LaminAir HB 2448 | Heraeus (Hanau, DE) |
| Cell counter | Vi-Cell™ XR Cell Viability Analyzer | Beckman Coulter (Brea, CA, USA) |
| Chemiluminescence detection system | Fusion SL 3500 WL | Vilber Lourmat (Collégien, FR) |
| $CO_2$-Incubator (cell culture) | Labotec Inkubator C200 | Labotec (Göttingen, DE) |
| Confocal microscope | Leica DMI 6000 (TCS SP5) with 20x HC PL APO CS IMM/CORR | Leica (Wetzlar, DE) |
| Cryostat | Thermo Scientific™ CryoStar™ NX70 | Thermo Fisher Scientific (Waltham, MA, USA) |
| Electrophoresis chamber + accessories | Mini-PROTEAN® Tetra Handcast Systems | Bio-Rad (Hercules, USA) |
| Electrophoresis chamber | XCell SureLock™ Electrophoresis Cell | Invitrogen, Thermo Fisher Scientific (Waltham, USA) |
| Flow cytometer | FACSCalibur™ | Becton, Dickinson & Company (Franklin Lakes, NJ, USA) |
| Flow cytometer | FACSCanto™ | Becton, Dickinson & Company (Franklin Lakes, NJ, USA) |
| Freezing container | Mr. Frosty™ | Nalgene, Thermo Scientific (Waltham, MA, USA) |
| Gel imaging system | ChemiDoc Touch Imaging System | Bio-Rad (Hercules, CA, USA) |
| Gel imaging system | EBOX VX2 | Vilber Lourmat (Collégien, FR) |
| Heating block | Thermomixer comfort | Eppendorf (Hamburg, DE) |

| | | |
|---|---|---|
| Incubation shaker | Certomat® IS | B. Braun Biotech International (Melsungen, DE) |
| Incubator (bacteria) | Heraeus® Kendro Typ B12 | Heraeus (Hanau, DE) |
| Incubator (cell culture) | Kelvitron® | Heraeus (Hanau, DE) |
| Inverted microscope with CCD camera | Axio Observer Z.1 with AxioCam MRc | Zeiss (Oberkochen, DE) |
| Inverted microscope | Axiovert 25 | Zeiss (Oberkochen, DE) |
| Magnetic stirrer | IKAMAG® RH | Janke & Kunkel, IKA (Staufen, DE) |
| MALDI-TOF/TOF Mass Spectrometer | Ultraflex III MALDI-TOF-TOF Massenspektrometer | Bruker Daltonics GmbH (Bremen, DE) |
| Microplate reader | Infinite® M200 Pro | Tecan Life Sciences (Männedorf, CH) |
| Neubauer counting chamber | Neubauer-Improved bright line | Paul Marienfeld GmbH & CO KG (Lauda-Königshofen, DE) |
| Nitrogen storage tank | CryoPlus™ | Thermo Fisher Scientific (Waltham, MA, USA) |
| pH meter | pH 192, WTW | Xylem Analytics (Weilheim) |
| Power supply | PowerPac™ 200 | Bio-Rad (Hercules, CA, USA) |
| Power supply | PowerPac™ 300 | Bio-Rad (Hercules, CA, USA) |
| Real-time PCR cycler | LightCycler® 96 | Roche (Basel, CH) |
| Rotating Mixer | Test-tube-rotator 34528 | Snijders (Tilburg, NL) |
| Shaker | KM-2 | Edmund Bühler GmbH (Bodelshausen, DE) |
| Tank blotting chamber | Mini-PROTEAN® 3 Cell | Bio-Rad (Hercules, USA) |
| Thermocycler | T1 Thermocycler | Biometra (Göttingen, DE) |
| Thermocycler | Mastercycler® personal | Eppendorf (Hamburg, DE) |
| Tube roller | Stuart® roller mixer SRT9D | Cole-Parmer (Staffordshire, UK) |
| UV-Vis Spectrophotometer | NanoDrop® Spectrophotometer ND-1000 | VWR International, PEQLAB (Erlangen, DE) |
| Vortexer | VF-2 | Janke & Kunkel, IKA (Staufen, DE) |
| Vortexer | Vortex-Genie 2 | Scientific Industries (Bohemia, NY, USA) |
| Water bath | GFL 1002 | Gesellschaft für Labortechnik mbH (Burgwedel, DE) |

### 2.1.2 Chemicals, reagents and commercial systems

If not stated otherwise, chemicals, reagents and cell culture supplements used in this study were obtained from the following companies: Carl Roth (Karlsruhe, DE), Sigma-Aldrich (Taufkirchen, DE), Merck KGaA (Darmstadt, DE), Lonza (Basel, CH), AppliChem (Darmstadt, DE), Serva (Heidelberg, DE), PeproTech (Hamburg, DE), STEMCELL Technologies (Vancouver, CA). All consumables and plastic ware were obtained from the companies Sarstedt (Nümbrecht, DE), Greiner Bio-One (Kremsmünster, AT), Falcon (Heidelberg, DE), Roche (Basel, CH), Eppendorf (Hamburg, DE) and B. Braun (Melsungen, DE). Further reagents as well as cell culture media and commercial systems used in this study are listed in Table 4.

**Table 4: Reagents, cell culture media and commercial systems**

| Description | Catalog number | Manufacturer |
|---|---|---|
| AB-Serum | 805135 | BioRad (Hercules, CA, USA) |
| Albumin Fraktion V (designated as BSA) | 8076.4 | Carl Roth (Karlsruhe, DE) |
| Amersham™ ECL™ Prime Western Blotting Detection Reagents | RPN2232 | GE Healthcare (Little Chalfont, UK) |
| Amersham™ Protran™ 0.45 µm NC | 10600002 | GE Healthcare (Little Chalfont, UK) |
| BD™ Comp Beads Anti-Mouse Ig, κ | 51-90-9001229 | Becton, Dickinson & Company (Franklin Lakes, NJ, USA) |
| BD™ Comp Beads Anti-Rat and Anti-Hamster Ig, κ | 51-90-9000949 | Becton, Dickinson & Company (Franklin Lakes, NJ, USA) |
| BD™ Comp Beads Negative Control | 51-90-9001291 | Becton, Dickinson & Company (Franklin Lakes, NJ, USA) |
| cOmplete™ Tablets, Mini (Protease Inhibitor Cocktail) | 04 693 124 001 | Roche (Mannheim, DE) |
| DMEM with Glucose and UltraGlutamine™ | 12-604F/U1 | Lonza (Basel, CH) |
| DAPI | D9542 | Sigma-Aldrich (Taufkirchen, DE) |
| DC™ Protein Assay Kit II | 5000112 | BioRad (Hercules, CA, USA) |
| DEPC-Treated Water | AM9906 | Invitrogen, Thermo Fisher Scientific (Waltham, MA, USA) |
| DNA Loading Dye (6x) | R0611 | Thermo Fisher Scientific (Waltham, MA, USA) |
| DreamTaq™ Green PCR Master Mix | K1081 | Thermo Fisher Scientific (Waltham, MA, USA) |
| EGM-2™ Endothelial Cell Growth Medium-2 BulletKit™ | CC-3162 | Lonza (Basel, CH) |
| Endothelial Cell Growth Medium MV (ready-to-use) | C-22020 | PromoCell (Heidelberg, DE) |
| Fast-Media® Amp Agar | fas-am-s | InvivoGen (San Diego, CA, USA) |
| FBS Superior | S0615 | Sigma-Aldrich (Taufkirchen, DE) |
| Formafix 4% gepuffert | F10010G | Grimm med. Logistik GmbH (Torgelow, DE) |
| 16% Formaldehyde Solution (w/v), Methanol-free | 28906 | Thermo Fisher Scientific (Waltham, MA, USA) |
| Gibco™ DPBS (1×), no calcium, no magnesium (designated as PBS) | 14190-094 | Thermo Fisher Scientific (Waltham, MA, USA) |
| Gibco™ Horse Serum, heat inactivated | 26050-088 | Thermo Fisher Scientific (Waltham, MA, USA) |
| Gibco™ IMDM (1×) + GlutaMAX™-I, HEPES | 31980-030 | Thermo Fisher Scientific (Waltham, MA, USA) |
| Gibco™ Medium 199, no phenol red | 11043-023 | Thermo Fisher Scientific (Waltham, MA, USA) |
| Gibco™ MEM α (1x) + GlutaMAX™-I, no nucleosides | 32561-029 | Thermo Fisher Scientific (Waltham, MA, USA) |
| Gibco™ RPMI Medium 1640 (1×) + GlutaMAX™-I, HEPES | 72400-021 | Thermo Fisher Scientific (Waltham, MA, USA) |
| Gibco™ Trypan Blue stain 0.4% | 15250-061 | Thermo Fisher Scientific (Waltham, MA, USA) |
| Heparin-Natrium-5000-ratiopharm | PZN 03170642 | Ratiopharm (Ulm, DE) |
| Human SDF-1α (CXCL12) | 300-28A | PeproTech (Hamburg, DE) |
| Human TNF-α | 300-01A | PeproTech (Hamburg, DE) |
| innuPREP RNA Mini Kit 2.0 | 845-KS-2040250 | Analytik Jena (Jena, DE) |
| Ketanest® S 25mg/mL | PZN 07829486 | Pfizer Pharma (Berlin, DE) |

| | | |
|---|---|---|
| Lane Marker Reducing Sample Buffer (5X) | 39000 | Thermo Fisher Scientific (Waltham, MA, USA) |
| Gibco™ Leibovitz's L-15 Medium + GlutaMAX™-I | 31415029 | Thermo Fisher Scientific (Waltham, MA, USA) |
| MethoCult™ H4230 | 04230 | STEMCELL Technologies (Vancouver, CAN) |
| MycoAlert™ Mycoplasma Detection Kit | LT07-318 | Lonza (Basel, CH) |
| NaCl 0.9% | 3570160 | B.Braun (Melsungen, DE) |
| Normal Donkey Serum | Ab7475 | Abcam (Cambridge, UK) |
| Novex® WedgeWell™ 4-12% Tris-Glycin Gel | XP04122BOX | Invitrogen, Thermo Fisher Scientific (Waltham, MA, USA) |
| NucleoBond® Xtra Midi Plus | 740412.50 | Macherey-Nagel (Düren, DE) |
| NucleoSpin® Gel and PCR Clean-up | 740609.50 | Macherey-Nagel (Düren, DE) |
| NucleoSpin® Plasmid | 740588.250 | Macherey-Nagel (Düren, DE) |
| NuPAGE™ Sample Reducing Agent (10x) | NP0009 | Invitrogen, Thermo Fisher Scientific (Waltham, MA, USA) |
| NuPAGE™ LDS Sample Buffer (4x) | NP0007 | Invitrogen, Thermo Fisher Scientific (Waltham, MA, USA) |
| PBS Tablets | 18912-014 | Thermo Fisher Scientific (Waltham, MA, USA) |
| Penicillin/Streptomycin, liquid (10,000 U/mL / 10.000 µg/mL) | A2213 | Biochrom (Berlin, DE) |
| Phusion™ High-Fidelity DNA Polymerase | F530S | Thermo Fisher Scientific (Waltham, MA, USA) |
| Pierce™ RIPA Buffer | 89900 | Thermo Fisher Scientific (Waltham, MA, USA) |
| Polybrene Transfection Reagent | TR-1003-G | Merck KGaA (Darmstadt, DE) |
| Polysucrose 400 | PS400L500 | BioClot GmbH (Aidenbach, DE) |
| PrimeScript™ RT Master Mix | RR036A | Takara Bio Inc. (Kusatsu, Shiga, JP) |
| Pro-Q™ Diamond Phosphoprotein Gel Stain | P33300 | Invitrogen, Thermo Fisher Scientific (Waltham, MA, USA) |
| Protein-G-Sepharose™ 4 Fast Flow | 17-0618-01 | GE Healthcare (Little Chalfont, UK) |
| Puromycin dihydrochloride | P8833 | Sigma-Aldrich (Taufkirchen, DE) |
| RapiClear®1.52 | RC152001 | SunJin Lab (Hsinchu City, Taiwan) |
| Recombinant Human GM-CSF | 300-03 | PeproTech (Hamburg, DE) |
| RNA*later*™ Stabilization Solution | AM7021 | Invitrogen, Thermo Fisher Scientific (Waltham, MA, USA) |
| ROTI®GelStain | 3865.2 | Carl Roth (Karlsruhe, DE) |
| S7 Fusion High-Fidelity DNA Polymerase | MD-S7-100 | Biozym Scientific (Hessisch Oldendorf, DE) |
| SeaKem® LE Agarose | 50004 | Lonza (Basel, CH) |
| Sodium Orthovanadate, 200 mM | ActVO-4 | Fivephoton Biochemicals (San Diego, CA, USA) |
| TEMED | 17-1312-01 | Amersham Biosciences (Uppsala, SE) |
| TB Green® Premix Ex Taq™ II (Tli RNaseH Plus) | RR820L | Takara Bio Inc. (Kusatsu, Shiga, JP) |
| Tissue-Tek® O.C.T.™ Compound | 4583 | Sakura Finetek (Alphen aan den Rijn, NL) |
| Trypan Blue solution 0.4% (ViCell) | 93595 | Sigma-Aldrich (Taufkirchen, DE) |
| Trypsin-EDTA Solution 10x | 59418C | Sigma-Aldrich (Taufkirchen, DE) |
| Xylazin 20 mg/mL | - | WDT (Garbsen, DE) |
| Zeocin™ (100 mg/mL) | ant-zn-1 | InvivoGen (San Diego, CA, USA) |
| Zombie NIR™ Fixable Viability Kit | 423105 | BioLegend (San Diego, CA, USA) |

### 2.1.3 Buffers and Solutions

The recipes for commonly used buffers and solutions are listed in Table 5.

**Table 5: Recipes for buffers and solutions**

| Description | Specification |
|---|---|
| 10% Ammonium persulfate (APS) | 50 mg APS + 500 µL $ddH_2O$; storage at -20°C |
| Erylysis buffer | 155 mM $NH_4Cl$, 10 mM $KHCO_3$, 0.1 mM EDTA, ad 1 L $ddH_2O$, sterile filtered |
| FACS-buffer | 10% AB-serum in PBS |
| Freezing solution | 45% RPMI, 45% fetal bovine serum (FBS), 10% dimethyl sulfoxide (DMSO) |
| 2x HEPES-buffered saline transfection buffer (2x HBS) | 8 g NaCl, 0.38 g KCl, 0.1 g $Na_2HPO_4$, 5 g HEPES, 1g Glucose, ad 500 mL $ddH_2O$, pH 7,05, sterile filtered |
| Ketanest®/Xylazin-narcotic | 24 mL Ketanest®S (esketamine hydrochloride), 4 mL Xylazin (xylazine hydrochloride), 22 mL 0,9% NaCl |
| LB-Agar | 40 g LB-Agar (Luria/Miller), ad 1 L $ddH_2O$, sterilized by autoclaving, |
| LB-Medium | 25 g LB-Medium (Luria/Miller), ad 1 L $ddH_2O$, sterilized by autoclaving |
| pAML-medium[214] | 85% IMDM, 15% BIT 9500, 0.1 mM β-mercaptoethanol, 100 ng/mL SCF, 50 ng/mL FLT3-Ligand, 20 ng/mL G-CSF, 20 ng/mL IL-3, 1 µM UM729, 500 nM SR1 |
| 0.1 M Phosphate buffer | 30 mL 0.1 M $Na_2HPO_4$, 10 mL 0.1 M $NaH_2PO_4$ |
| Periodate-lysine-paraformaldehyde (PLP)-fixative | 0.223 g L-Lysine, 5.92 mL $ddH_2O$, 1 mL 16% formaldehyde, pH 7-7.2 (with 640 µL 0.1 M $Na_2HPO_4$), ad 16 mL with 0.1 M phosphate buffer, 0.034 g sodium periodate |
| 10x Running buffer | 29 g Tris base, 144 g Glycine, 10 g SDS, ad 1 L $ddH_2O$ |
| 20% (w/v) Sodium dodecyl sulfate (SDS) | 20.0 g SDS, ad 100 mL $ddH_2O$ |
| 50x Tris-acetate- EDTA (TAE) buffer | 40 mM Tris-HCl, 20 mM Sodium acetate, 1 mM EDTA, pH 8.2 |
| 10x Tris-buffered saline (TBS) buffer | 24,2 g Tris base, 80,1 g NaCl, ad 1 L $ddH_2O$, pH 7.6 |
| 1x TBS with Tween® 20 (TBS-T) buffer | 100 mL 10x TBS, 1 mL Tween® 20, ad 1 L $ddH_2O$ |
| 10x Transfer buffer | 121.14 g Tris base, 144.89 g Glycine, ad 1 L $ddH_2O$ |
| 0.5 M Tris-HCl, pH 6.8 | 15.0 g Tris base, ad 250 mL $ddH_2O$; pH adjustment with 6M HCl to 6.8; storage at 4°C |
| 1.5 M Tris-HCl, pH 8.8 | 90.8 g Tris base, ad 500 mL $ddH_2O$; pH adjustment with 6M HCl to 8.8; storage at 4°C |

### 2.1.4 Laboratory Animals

For *in vivo* murine xenograft models the following mouse strains from The Jackson Laboratory (Bar Harbor, ME, UAS), bred in the UKE animal facility, were used in this thesis (Table 6).

**Table 6: Mouse strains**

| Branded or common name | Mouse strain | Stock number |
|---|---|---|
| NSG™, NOD *scid* gamma | NOD.*Cg-Prkdc*$^{scid}$ *Il2rg*$^{tm1Wjl}$/SzJ | 005557 |
| NSGS, NOD *scid* gamma Il3- GM-SF (NSG-SGM3) | NOD.*Cg-Prkdc*$^{scid}$*Il2rg*$^{tm1Wjl}$Tg(CMV-IL3,CSF2,KITLG)1Eav/MloySzJ | 013062 |

### 2.1.5 Mammalian and bacterial cells

Bacterial cells used in this study are listed in Table 7. All used mammalian cell lines and primary endothelial cells with their origin and the respective culture medium are listed in Table 8.

**Table 7: Bacterial cells**

| Bacterial cells | Description | Catalog number | Manufacturer |
|---|---|---|---|
| MGC premier cDNA clone for DOCK1 | Human DOCK1 in pCR-XL-TOPO in *E. coli* DH10B (Gene ID: 1793, Genebank accession: BC146857) | TCHS1003 | Transomic Technologies (Huntsville, AL, USA) |
| DH10B | Chemically competent *E. coli* for transformation | - | Kindly provided by the Institute of Human Genetics, UKE |
| Library Efficiency™ DH5α™ Competent Cells | Chemically competent *E. coli* for transformation | 18263012 | Invitrogen, Thermo Fisher Scientific (Waltham, MA, USA) |

**Table 8: Cell lines and primary endothelial cells**

| Cell line / primary cells | Origin | Cultivation medium | Reference / source |
|---|---|---|---|
| HEK 293T | Human embryonic kidney | DMEM + 10% FBS | Kindly provided by the Department of Stem Cell Transplantation, UKE |
| HDBEC-c adult | Human adult skin (catalog number C-12225) | Endothelial Cell Growth Medium MV | PromoCell (Heidelberg, DE) |
| HL-60 | 36-year-old Caucasian female with acute promyelocytic leukemia (1976) | RPMI + 10% FBS | ACC 3 |
| HUVEC | Human umbilical vein | 63 mL Medium 199 + 30 mL EGM-2 + 7 mL FCS + 1mL Penicillin / Streptomycin | Kindly provided by the Department of Dermatology and Venereology, UKE |
| Kasumi-1 | 7-year-old Japanese male with AML (1989) | RPMI + 20% FBS | ACC 220 |
| Molm13 | 20-year-old male with AML FAB M5a at relapse (1995) | RPMI + 10% FBS | ACC 554 |
| Mono Mac 1 | 64-year-old male with AML FAB M5 at relapse (1985) | RPMI + 10 % FBS + 1% sodiumpyruvat + 1% non-essential amino acids | ACC 252 |
| MV4-11 | 10-year-old male with biphenotypic B-myelomonocytic leukemia (1987) | RPMI + 10% FBS | ATCC® CRL-9591 |
| OCI-AML3 | 57-year-old male with AML FAB M4 (1987) | α-MEM + 20% FBS | ACC 582 |
| OCI-AML5 | 77-year-old male with AML M4 in relapse (1990) | α-MEM + 20% FBS + 2.5 ng/mL GM-CSF | ACC 247 |
| OCI-M1 | 62-year-old patient with AML M2 (1988) | RPMI + 10 %FBS | ACC 529 |

| | | | |
|---|---|---|---|
| TF-1 | 35-year-old Japanese male with severe pancytopenia (1987) | RPMI + 10% FBS + 2.5 ng/mL GM-CSF | ACC 334 |
| THP-1 | 1-year-old male with AML at relapse (1978) | RPMI + 10% FBS | ACC 16 |
| UKE-1 | 59-year-old female with secondary AML (1997) | IMDM + 10% FBS + 10% HS + 1 µM Hydrocortison | Established by Fiedler *et al*.[215] |

### 2.1.6 Enzymes

Enzymes used in this study are listed in Table 9.

**Table 9: Enzymes**

| Description | Catalog number | Manufacturer |
|---|---|---|
| FastDigest AscI (SgsI) | FD1894 | Thermo Fisher Scientific (Waltham, MA, USA) |
| Fast Digest DpnI | FD1703 | Thermo Fisher Scientific (Waltham, MA, USA) |
| FastDigest NotI | FD0593 | Thermo Fisher Scientific (Waltham, MA, USA) |
| FastDigest SalI | FD0644 | Thermo Fisher Scientific (Waltham, MA, USA) |
| FastDigest XbaI | FD0684 | Thermo Fisher Scientific (Waltham, MA, USA) |
| FastDigest XhoI | FD0694 | Thermo Fisher Scientific (Waltham, MA, USA) |
| T4 DNA Ligase | EL0011 | Thermo Fisher Scientific (Waltham, MA, USA) |

### 2.1.7 Antibodies

Primary and secondary antibodies, used for Western blot, co-immunoprecipitation, 3D-immunohistochemical staining and flow cytometry, are listed in Table 10.

**Table 10: Primary and secondary antibodies**

| Antibody | Host | Clone, Isotype | Catalog number | Manufacturer | Application |
|---|---|---|---|---|---|
| Anti-DOCK180 antibody | Rabbit | Polyclonal, IgG | ab76927 | Abcam (Cambridge, UK) | Western blot (1:500 v/v), co-immuno-precipitation |
| Mouse IgG HRP Linked Whole Ab | Sheep | - | NXA931 | GE Healthcare (Little Chalfont, UK) | Western blot (1:10 000 v/v) |
| Anti-rabbit IgG, HRP-linked Antibody | Goat | - | 7074S | Cell Signaling Technology (Danvers, MA, USA) | Western blot (1:10 000 v/v) |
| β-Actin Antibody (C4) | Mouse | C4, IgG1 | sc-47778 | Santa Cruz Biotechnology (Dallas, TX, USA) | Western blot (1:1000 v/v) |
| β-Actin (13E5) Rabbit mAb (HRP Conjugate) | Rabbit | 13E5, IgG | 5125S | Cell Signaling (Danvers, MA, USA) | Western blot (1:1000 v/v) |
| Alexa Fluor™ 488 donkey anti-rabbit IgG (H+L) | Donkey | Polyclonal, IgG | A21206 | Invitrogen, Thermo Fisher Scientific (Waltham, MA, USA) | 3D-immuno-histochemical staining (1:400 v/v) |

| | | | | | |
|---|---|---|---|---|---|
| Alexa Fluor™ 568 donkey anti-mouse IgG (H+L) | Donkey | Polyclonal, IgG | A10037 | Invitrogen, Thermo Fisher Scientific (Waltham, MA, USA) | 3D-immuno-histochemical staining (1:400 v/v) |
| Alexa Fluor™ 647 donkey anti-goat IgG (H+L) | Donkey | Polyclonal, IgG | A21447 | Invitrogen, Thermo Fisher Scientific (Waltham, MA, USA) | 3D-immuno-histochemical staining (1:400 v/v) |
| GFP antibody | Rabbit | Polyclonal, IgG | GTX113617 | GeneTex (Irvine, CA, USA) | 3D-immuno-histochemical staining (1:100 v/v) |
| mCherry antibody | Mouse | GT844, IgG2a | GTX630195 | GeneTex (Irvine, CA, USA) | 3D-immuno-histochemical staining (1:200 v/v) |
| Mouse/Rat CD31/PECAM-1 antibody | Goat | Polyclonal, IgG | AF3628 | R&D Systems (Minneapolis, MN, USA) | 3D-immuno-histochemical staining (1:100 v/v) |
| APC anti-human CD45 Antibody | Mouse | HI30, IgG1, κ | 304012 | BioLegend (San Diego, CA, USA) | Flow cytometry |
| APC Mouse IgG1, κ Isotype Ctrl (FC) Antibody | Mouse | MOPC-21, IgG1, κ | 400122 | BioLegend (San Diego, CA, USA) | Flow cytometry |
| APC anti-mouse CD117 (c-kit) Antibody | Rat | ACK2, IgG2b, κ | 135108 | BioLegend (San Diego, CA, USA) | Flow cytometry |
| FITC Mouse Anti-Human CD45 | Mouse | HI30, IgG1, κ | 555482 | Becton, Dickinson & Company (Franklin Lakes, NJ, USA) | Flow cytometry |
| PerCP-Cy™5.5 Mouse Lineage Antibody Cocktail | - | 145-2C11, M1/70, RA3-6B2, TER-119, RB6-8C5 | 561317 | Becton, Dickinson & Company (Franklin Lakes, NJ, USA) | Flow cytometry |
| PE/Cy7 anti-mouse Ly-6A/E (Sca-1) Antibody | Rat | D7, IgG2a, κ | 108114 | BioLegend (San Diego, CA, USA) | Flow cytometry |

### 2.1.8 Size standards

DNA and protein ladders used for electrophoresis to determine the size of DNA fragments or proteins are listed in Table 11.

**Table 11: Size standards**

| Description | Catalog number | Manufacturer |
|---|---|---|
| GeneRuler 1 kb Plus DNA Ladder, ready- to-use | SM1331 | Thermo Fisher Scientific (Waltham, MA, USA) |
| GeneRuler 100 bp Plus DNA Ladder | SM0321 | Thermo Fisher Scientific (Waltham, MA, USA) |
| PageRuler™ Plus Prestained Protein Ladder, 10 to 250 kDa | 26619 | Thermo Fisher Scientific (Waltham, MA, USA) |

## 2.1.9 Nucleic Acids

### *2.1.9.1 Oligonucleotides*

All oligonucleotides used in this study were synthesized by Eurofins Genomics (Ebersberg, DE) and diluted with diethyl pyrocarbonate (DEPC)-treated water in accordance with the manufacturer's instructions. Primers for cloning approaches as well as sequencing reactions are listed in Table 12 and primers for reverse transcription quantitative real-time polymerase chain reaction (RT-qPCR) are listed in Table 13.

**Table 12: Primers for cloning approaches and sequencing**

| Name | Sequence (5´→ 3´) | Application |
|---|---|---|
| LeGO C/G Vektor fw | TCCCTTGGAGAAAAGCCTTG | Colony-PCR shRNA-LeGO constructs |
| LeGO G/C shRNA fw | AAGAAGAAGGTGGAGAGAGAG | Colony-PCR shRNA-LeGO constructs |
| LeGO G/C rv | TACCCGCCCTTGATCTGAAC | Colony-PCR shRNA-LeGO constructs |
| CoPCR2-DOCK1 f | CTTCTGCTTCCCGAGCTCTA | Colony-PCR and sequencing of hDOCK1-LeGO iG2/puro$^+$ |
| CoPCR2-DOCK1 r | TCATGTTGCCCTTTTCCTTC | Colony-PCR hDOCK1-LeGO iG2/puro$^+$ |
| CoPCR2-L-iG2 r | AGGAACTGCTTCCTTCACGA | Colony-PCR hDOCK1-LeGO iG2/puro$^+$ |
| p43 | GGGGAAAGAATAGTAGACATAATA GCA | Sequencing shRNA in LeGO-vector |
| hDOCK1-LeGO fw 769 | CCCTTCTCTGGCCTTGTTTGTG | Sequencing hDOCK1-LeGO iG2/puro$^+$ |
| hDOCK1-LeGO fw 1755 | ACGATCTTATCGTCTATAAGGCCG | Sequencing hDOCK1-LeGO iG2/puro$^+$ |
| hDOCK1-LeGO fw 2598 | TGGGCTTGCTGACCATCCAGAAAC | Sequencing hDOCK1-LeGO iG2/puro$^+$ |
| hDOCK1-LeGO fw 3422 | CCCATCTTCTTTGATATGATGCAG | Sequencing hDOCK1-LeGO iG2/puro$^+$ |
| hDOCK1-LeGO fw 4217 | TTTGAGGCTCGGCTCTTAACTC | Sequencing hDOCK1-LeGO iG2/puro$^+$ |
| hDOCK1-LeGO fw 5041 | TCTGTCTGTGGCCTCTGTCTCTTC | Sequencing hDOCK1-LeGO iG2/puro$^+$ |
| hDOCK1-LeGO rv 3868 | CACATCCTCCGACCACTTAAGAAG | Sequencing hDOCK1-LeGO iG2/puro$^+$ |
| shRNA XbaI FW | ATATTCTAGACCGAGGGCCTATTTCCC ATG | Subcloning shRNA, insertion of XbaI restriction site |
| shRNA SalI RV | TACTGCCATTTGTGTCGACGTCGAGAA TTC | Subcloning shRNA, insertion of SalI restriction site |
| fw-QuikChange hDOCK1 6782 | TTCAATTTCTTTGTAGAAATTCAGCACA TTGACGGTGCAGC | Site-directed mutagenesis |
| rv-QuikChange hDOCK1 6782 | GCTGCACCGTCAATGTGCTGAATTTCT ACAAAGAAATTGAA | Site-directed mutagenesis |
| DOCK1-FL-AscI-f | GATCGGCGCGCCGCCACCATGACGCG CTGGGTGCCCACCAAG | Subcloning *hDOCK1*, insertion of AscI restriction site |
| DOCK1-FL-NotI-r | GATCGCGGCCGCTCACTGCACGATCCC GGAGT | Subcloning *hDOCK1*, insertion of NotI restriction site |

**Table 13: RT-qPCR primer**

| Gene | Location, (PrimerBank ID[216–218]) | Sequence forward primer (5´→ 3´) | Sequence reverse primer (5´→ 3´) | $T_A$ | Size [bp] | cDNA standard |
|---|---|---|---|---|---|---|
| ASS1 | f 16; r 141 (113204625c1) | TCCGTGGTTCTG GCCTACA | GGCTTCCTCGAA GTCTTCCTT | 63 | 126 | - |
| ATF3 | f 89; r 199 (346223459c1) | CCTCTGCGCTGG AATCAGTC | TTCTTTCTCGTCG CCTCTTTTT | 63 | 111 | - |
| CHAC1 | f 435; r 533 (218563699c1) | GAACCCTGGTTA CCTGGGC | CGCAGCAAGTAT TCAAGGTTGT | 63 | 99 | - |
| CMYA5 | f 312; r 446 (62241002c1) | TGGTGTGTGTAG TCGGGAAG | CCTTTCCGGCGT AATGATGG | 61 | 135 | - |
| CSNK1A1L | f 19; r 105 (269846833c1) | TCCAAAGCCGAA CTCGTTGT | GATGCCCAGATA AACGTCTCC | 63 | 87 | - |
| CTH | f 898; r 1021 (299473757c3) | CATGAGTTGGTG AAGCGTCAG | AGCTCTCGGCCA GAGTAAATA | 63 | 124 | - |
| CXCR4 | f 32, r 164 (56790928c1) | ACTACACCGAGG AAATGGGCT | CCCACAATGCCA GTTAAGAAGA | 54 | 133 | OCI AML3 |
| DOCK2 | f 600; r 759 (205277317c2) | AGAAATGTCAAA AGACCAGCCA | TATGACCGTTTG CTTGTTGGG | 51 | 160 | OCI AML3 |
| DOCK5 | f 274; r 376 (117553585c2) | ACGTCCACTCTG CGAGAATG | CGATCAGGCTGT ACGTCATCT | 51 | 103 | OCI AML3 |
| DOCK1 | f 940; r 1102 | TTTGCGAGCCGT GTTTACTG | ATCCATCACAGC CACTCCAA | 53 | 162 | *hDOCK1-pCR-XL-TOPO* |
| ECM1 | f 362; r 442 (221316613c2) | AGCACCCCAATG AACAGAAGG | CTGCATTCCAGG ACTCAGGTT | 63 | 81 | - |
| ELMO1 | f 1911; r 2054 | CGAGAGGATGAA CCAGGAAG | CGGGCATTGAGT TTCCTAAA | 55 | 143 | OCI AML3 |
| GAPDH | f 822; r 1066 | TGATGACATCAA GAAGGTGG | TTTCTTACTCCTT GGAGGCC | 60 | 244 | OCI AML3 |
| GDF15 | f 125; r 199 (153792494c1) | GACCCTCAGAGT TGCACTCC | GCCTGGTTAGCA GGTCCTC | 63 | 75 | - |
| GLCE | f 13; r 128 (51317379c1) | GCAGCTCGGGTC AACTATAAG | GAACGCCGTGGA AACTGGA | 63 | 116 | - |
| GTF2H3 | f 222; r 397 (28376643c1) | GAATGGCAGACT TGGAGACTTC | GCAAAGTTTCTG TATGTTGACCC | 63 | 176 | - |
| HSD17B10 | f 314; r 396 (91823617c2) | AGGGCCAGACCC ATACCTT | CACCAGGCGGAT CACATTGA | 63 | 83 | - |
| INHBE | f 424; r 518 (37622353c1) | ATCTTCCGATGG GGACCAAG | AGAGTTAAGGTA TGCCAGCCC | 62 | 95 | - |
| MRPL20 | f 105; r 204 (169403972c1) | AAATCGCTGCTA CAGGTTGG | CCAGAGGGTCCT CATGTTCTTTT | 63 | 100 | - |
| NXPH4 | f 414; r 489 (219879831c2) | GTATTTCCGCCAC AACTCGTC | GAACTCGACACG CTTGGAG | 63 | 76 | - |
| RPS26 | f 72; r 171 (71559137c1) | TAACTGTGCCCG ATGCGTG | GCTCGCTTCAGA AATGTCCC | 63 | 100 | - |
| TRIP6 | f 904; r 990 (91208422c3) | GTGGGCTGCTTT GTATGTTCT | GCCCTCGCAATA TGCCCTC | 63 | 87 | - |
| ULBP1 | f 123; r 296 (56181385c1) | TAAGTCCAGACC TGAACCACA | TCCACCACGTCTC TTAGTGTT | 62 | 174 | - |

bp = base pair; f = forward; r = reverse; TA = Annealing Temperature

### *2.1.9.2 short-hairpin RNA (shRNA)*

The following shRNA-sequences were used for lentiviral transfection and transduction approaches (Table 14).

**Table 14: shRNA**

| shRNA | Source | Sequence (5´→ 3´) |
|---|---|---|
| *DOCK1*-shRNA 1 in pLKO.1-puro | TRCN0000029074 MISSION® shRNA, Sigma-Aldrich (Taufkirchen, DE) | CCGGCCGAGCAGTATGAGAACGAAACTCG AGTTTCGTTCTCATACTGCTCGGTTTTT |
| *DOCK1*-shRNA 5 in pLKO.1-puro | TRCN0000029078 MISSION® shRNA, Sigma-Aldrich (Taufkirchen, DE) | CCGGCCAGACAATGAATTTGCGAATCTCGA GATTCGCAAATTCATTGTCTGGTTTTT |
| *ELMO1*-shRNA 2 in pLKO.1-puro | TRCN0000029071 MISSION® shRNA, Sigma-Aldrich (Taufkirchen, DE) | CCGGCCCAAACTCATGGAAATTGATCTCGA GATCAATTTCCATGAGTTTGGGTTTTT |
| *ELMO1*-shRNA 5 in pLKO.1-puro | TRCN0000029069 MISSION® shRNA, Sigma-Aldrich (Taufkirchen, DE) | CCGGCCGATAGTTCAAACTTCTATACTCGAG TATAGAAGTTTGAACTATCGGTTTTT |
| scrambled-shRNA in LeGO-G/puro$^+$ or LeGO-C/zeo$^+$ | #1864 Addgene (Watertown, MA, USA), subcloned | CCTAAGGTTAAGTCGCCCTCGCTCGAGCGA GGGCGACTTAACCTTAGG |

### *2.1.9.3 Vectors and Plasmids*

Vectors used for subcloning approaches as well as plasmids for lentiviral transfection are listed in Table 15.

**Table 15: Vectors and plasmids**

| Vector /plasmid | Application | Source |
|---|---|---|
| LeGO-C/zeo$^+$ | Subcloning shRNA;<br>Reporter gene: mCherry<br>Selection antibiotic: Zeocin™ | Kindly provided by PD Dr. K. Riecken and Prof. Dr. B. Fehse, UKE[219,220] (www.lentigo-vectors.de) |
| LeGO-G/puro$^+$ | Subcloning shRNA<br>Reporter gene: eGFP<br>Selection antibiotic: puromycin | Kindly provided by PD Dr. K. Riecken and Prof. Dr. B. Fehse, UKE[219,220] (www.lentigo-vectors.de) |
| LeGO-iG2/puro$^+$ | Subcloning hDOCK1-cDNA<br>Reporter gene: eGFP<br>Selection antibiotic: puromycin | Kindly provided by PD Dr. K. Riecken and Prof. Dr. B. Fehse, UKE[219,220] (www.lentigo-vectors.de) |
| pCMV-VSV-G | Envelope plasmid for transfection | Addgene (Watertown, MA, USA) |
| pMD2.G | Envelope plasmid for transfection | Addgene (Watertown, MA, USA) |
| pMDLg/pRRE | Packaging plasmid for transfection | Addgene (Watertown, MA, USA) |
| pRSV-Rev | Packaging plasmid for transfection | Addgene (Watertown, MA, USA) |
| psPAX2 | Packaging plasmid for transfection | Addgene (Watertown, MA, USA) |

### 2.1.10 Small molecule Inhibitors

Small molecule inhibitors used in this study are listed in Table 16.

**Table 16: Small molecule inhibitors**

| Inhibitor | MW [g/mol] | Stock solution | Function | Source |
|---|---|---|---|---|
| Ruxolitinib<br>IUPAC name: (3*R*)-3-cyclopentyl-3-[4-(7*H*-pyrrolo[2,3-d]pyrimidin-4-yl)pyrazol-1-yl]propanenitrile | 306.4 | 20 mM in DMSO | Kinase inhibitor for JAK1 and JAK2 | InvivoGen (San Diego, CA, USA)<br>Cat. No. tlrl-rux |
| CPYPP[221]<br>IUPAC name: 4-[3´-(2´´-chloro-phenyl)-2´-propen-1´-ylidene]-1-phenyl-3,5-pyrazoli-dinedione | 324.5 | 50 mM in DMSO | Unselective inhibitor for DOCK2, DOCK1, DOCK5 | Kindly provided by Prof. Fukui (Division of Immunogenetics, University of Tokyo) |
| TBOPP[222]<br>IUPAC name: 1-(2-(3´-(trifluoromethyl)-[1,1´-biphenyl]-4-yl)-2-oxoethyl)-5-pyrrolidinylsulfonyl-2(1*H*)-pyridone | 490.5 | 50 mM in DMSO | Selective inhibitor for DOCK1 | Kindly provided by Prof. Fukui (Division of Immunogenetics, University of Tokyo) |

MW = molecular weight

### 2.1.11 Software

Software as well as online tools used in this study are listed in Table 17.

**Table 17: Software**

| Software | Version | Manufacturer / Reference |
|---|---|---|
| Autodesk SketchBook | 5.1.7 | Autodesk Inc. |
| BioFlux™ 200 | 2.4.0.0 | Fluxion Biosciences (Alameda, CA, USA) |
| CellQuest Pro | 5.2.1 | Becton, Dickinson & Company (Franklin Lakes, NJ, USA) |
| FACS Diva™ | v6.1.1 | Becton, Dickinson & Company (Franklin Lakes, NJ, USA) |
| Flowing Software | 2.5.1 | Perttu Terho, University of Turku (Turku, FI) |
| FlowJo™ | 10.6.1 | Becton, Dickinson & Company (Franklin Lakes, NJ, USA) |
| GrapPad PRISM | 7.0a | GraphPad Software Inc. (La Jolla, CA, USA) |
| ImageJ (Fiji) | 2.0.0-rc-69/1.52p | ImageJ (http://imagej.net/Contributors) |
| LAS AF | 2.7.3.9723 | Leica (Wetzlar, DE) |
| LightCycler® 96 | SW 1.1 | Roche (Basel, CH) |
| MASCOT Server | - | Matrix Science (http://www.matrixscience.com/) |
| Mendeley Desktop | 1.19.4 | Mendeley Ltd. (London, UK) |
| mMass | - | Strohalm *et al.* 2008[223] (http://www.mmass.org/) |
| NCBI databases and tools | - | National Center for Biotechnology Information (https://www.ncbi.nlm.nih.gov) |
| Office 365 | 16.35 | Microsoft (Redmond, WA, USA) |
| PrimerBank | - | The Massachusetts General Hospital[216–218] (https://pga.mgh.harvard.edu/primerbank/index.html) |
| Quest Graph™ IC50 Calculator | - | ATT Bioquest, Inc. (https://www.aatbio.com/tools/ic50-calculator) |
| QuikChange Primer Design | - | Agilent[224] (https://www.agilent.com/store/primerDesignPprimer.jsp) |
| SnapGene® Viewer | 5.1.2 | GSL Biotech LLC (San Diego, CA, USA) |
| ZEN software | V. 2012 blue edition; ZEN 2.6 lite | Carl Zeiss Microscopy GmbH (Jena, DE) |

## 2.2 Methods

### 2.2.1 Mammalian Cell Culture

#### *2.2.1.1 Cultivation of cells, cryopreservation and storage*

All cells were cultured in a $CO_2$-incubator at 37°C, 95% relative humidity (RH) and 5% $CO_2$. Primary endothelial cells growing in a flow cell of a *BioFlux 48 well plates 0-20 dyn/cm²* in Leibovitz's L-15 Medium (L-15) + 10% FBS were cultivated without $CO_2$ equilibration at 37°C. In general, all centrifugation steps were performed at 300 xg and room temperature for 5 minutes.

All cell lines were tested for mycoplasma contamination on a regular basis using the *MycoAlert™ Mycoplasma Detection Kit* and only mycoplasma-free cells were used.

Suspension cell lines were cultivated in sterile polystyrene cell culture flasks (T25, T75) with the appropriate cell culture medium according to Table 8. They were passaged three times a week and the minimal and maximal cell density recommended by ATCC and DSMZ was maintained. Adherent cells grown in monolayers were generally passaged 2-3 times a week at a confluency of 80-90%. In order to split the cells, the medium was removed and the cell layer was washed once with sterile PBS + 0.2% ethylenediaminetetraacetic acid (EDTA). To detach the cells, they were incubated with 1x Trypsin for 2-5 minutes at room temperature or 37°C. The reaction was stopped by adding cell culture medium supplemented with 10% FBS in a ratio of 1:2 v/v and the desired cell suspension volume was centrifuged at 300 xg for 5 minutes. The supernatant was removed and the cells were resuspended in the appropriate medium and transferred back into a cell culture flask.

For long-term storage of eukaryotic cells, cryopreservation was performed. Approximately 2.5 x $10^6$ cells were centrifuged as described before, the cell pellet was resuspended in 1 mL freezing solution and transferred into a cryopreservation tube, which was slowly frozen in steps of -1°C/hr to -80°C using a freezing container (*Mr. Frosty*). Frozen cells were transferred in liquid nitrogen for long-term storage. For re-cultivation, cells were quickly thawed for 1 minute in a 37°C water bath and transferred in 9 mL pre-warmed medium in a T25-cell culture flask. After incubation overnight, the medium was renewed.

### *2.2.1.2 Primary cell acquisition*

In order to obtain primary AML blasts from newly diagnosed patients (pAML), polysucrose-density gradient centrifugation of bone marrow samples was performed.

Bone marrow samples were diluted with sterile PBS and transferred on polysucrose 400 layers. Density gradient centrifugation was performed at 400 xg for 30 minutes without the break. The mononuclear cells remain as a white layer on top of the polysucrose. The so-called buffy coat was transferred into a fresh tube and washed once with sterile PBS, followed by an erylysis step for 5 minutes at room temperature with a hypotonic erylysis buffer. The reaction was stopped by adding PBS (1:2 v/v). The cells were harvested by centrifugation at 300 xg for 5 minutes and resuspended in an appropriate volume of PBS, followed by determination of cell number and cell viability (refer 2.2.1.3).

The sample processing and subsequent *in vitro* experiments were carried out with the consent of the patients and the ethics committee of the Medical Chamber Hamburg (Ethics vote PV3469).

Primary human umbilical vein endothelial cells (HUVEC) were kindly provided by the Department of Dermatology and Venereology, UKE.

### *2.2.1.3 Cell counting*

To determine the cell concentration and cell viability of a cell suspension, a manual or automated hemocytometer was used, and trypan blue exclusion was performed.

For the manual counting, the cell suspension was mixed with trypan blue solution (1:1 v/v) and add to a Neubauer counting chamber. The trypan blue staining allows to distinguish between live and dead cells, since the dye can only penetrate through non-intact cell membranes. The mean number of cells in a large corner square was determined using the 10x objective of the microscope. To calculate the number of viable cells the following formula was used:

*Viable cells / mL = counted viable cells * 2 (dilution factor) * $10^4$*

The viability of the cell solution was calculated by using the following formula:

*Viability [%] = viable cells / (viable + dead cells) * 100%*

The automated hemocytometer *Vi-Cell™ XR* is using the same trypan blue exclusion method to determine the viable cell number and viability of a cell solution. The sample volume must be at least 500 µL.

## 2.2.2 Production of lentiviral particles and generation of knockdown- and overexpression-cell lines

### *2.2.2.1 Transfection of lentiviral vectors*

Lentiviral systems of the 3rd- and 2nd-generation were used for the production of transgenic lentiviruses, to increase the safety. To transfect the target cells HEK 293T with the three (2nd-generation) or four (3rd-generation) plasmids of the lentiviral system, calcium phosphate co-precipitation technique was used. The plasmids were mixed with 2 M $CaCl_2$ (final concentration 0.25 M) and HEPES-buffered saline transfection buffer (HBS buffer) to form calcium-phosphate-DNA co-precipitates, which can be taken up by the target cells through endocytosis.

To test a set of five ELMO1-MISSION® shRNA plasmids for their knockdown capacity, the isolated plasmids were used to produce lentiviral particles. The pLKO.1-puro backbone allows the direct use as a transfer plasmid in a 2nd-generation lentiviral system. To generate lentiviral particles with the lentiviral gene ontology (LeGO)-plasmids *hDOCK1-LeGO iG2/puro⁺* and *LeGO iG2/puro⁺* (refer 2.2.3.7 and Table 15) for *in vitro* and *in vivo* experiments, as well as with the subcloned shRNA-plasmids *hDOCK1 sh1-LeGO G/puro⁺*, *hDOCK1 sh5-LeGO G/puro⁺*, *hDOCK1-sh5-LeGO C/zeo⁺, hELMO1 sh2-LeGO C/zeo⁺, hELMO1 sh5-LeGO C/zeo⁺, scrambled-sh-LeGO G/puro⁺* and *scrambled-sh-LeGO G/zeo⁺* (refer 2.2.3.5, Table 14 and 15), a 3rd-generation lentiviral system was used. The general procedure for both lentiviral systems was the same. HEK293T cells were seeded in DMEM + 10% FBS with a cell density of 0.5 x $10^6$ cells per 1 mL. After a minimum of 6 hours incubation, the medium was replaced with fresh DMEM + 10% FBS supplemented with 25 µM chloroquine and the prepared calcium-phosphate-DNA co-precipitate (see below) was added dropwise. After incubation overnight, the supernatant was replaced with fresh DMEM + 10% FBS. The virus-containing supernatant harvested after 24 hours, was filtered through a 0.45 µm filter and was either stored at -80°C or used directly for the transduction of AML cell lines (refer 2.2.2.2).

For safety reasons the work was carried out under the conditions of biological safety level S2.

**Calcium-phosphate-DNA co-precipitate**

| | **pLKO.1-plasmids** | **LeGO-plasmids** |
|---|---|---|
| pLKO.1- / LeGO-plasmid | 1 µg | 10 µg |
| Packaging plasmid psPAX2 | 750 ng | - |
| Packaging plasmid pMDLg/pRRE | - | 10 µg |
| Packaging plasmid pRSV-Rev | - | 5 µg |
| Envelope plasmid pMD2.G | 250 ng | - |
| Envelope plasmid pCMV-VSV-G | - | 2 µg |
| 2 M $CaCl_2$ | 12.5 µL | 62.5 µL |
| Sterile dd$H_2O$ | ad 100 µL | ad 500 µL |
| DNA-$CaCl_2$ mix was added drop by drop under air bubbles to 2x HBS buffer. | | |
| 2x HBS buffer | 100 µL | 500 µL |
| Incubation for 20 minutes at room temperature. | | |

### *2.2.2.2 Transduction of AML cell lines*

To stably integrate transgene sequences of lentiviral vectors into the genome of host cells, transduction was used to transfer the vectors into the cells. To minimize the incidence of multiple insertions, and therefore the risk for mutations, the maximum transduction efficiency of 50% should not be exceeded. Virus supernatants produced in 2.2.2.1 were used for the various transductions.

To test the five ELMO1-MISSION® shRNA plasmids for their knockdown capacity, the harvested virus supernatants were used directly to transduce OCI AML3 cells. In a 24 well-plate 0.1 x $10^6$ cells in 1 mL cell culture medium supplemented with 10 µg/mL polybrene each were seeded and treated with 100 µL and 400 µL virus supernatant in duplicates. After centrifugation for 1 hour at 2000 rpm and 30°C the cells were incubated overnight. After the medium was replaced with 2 mL fresh cell medium, the cells were further incubated for two days. The duplicates were pooled and the cells were treated with 2 µg/mL puromycin for one week, to select the transduced cells. Cells were collected for RNA isolation and cDNA (complementary DNA) synthesis before and after puromycin selection, to evaluate the knockdown capacity by RT-qPCR analysis (refer 2.2.3.1 - 2.2.3.3). To verify the success of the transduction and puromycin selection, a wildtype control of the respective cell line was included throughout the experiment.

For *DOCK1*-overexpression in Molm13, 0.25 x $10^6$ cells/mL were transduced accordingly with different amounts of virus supernatant (*hDOCK1-LeGO iG2/puro*$^+$ and *LeGO iG2/puro*$^+$). The centrifugation step was performed at 22°C. The transduction efficiency was determined by

flow cytometry based on the percentage of eGFP$^+$ (enhanced green fluorescent protein) cells (refer 2.2.7). All approaches with the desired transduction efficiency were combined and a selection of the transduced cells was started with 2 µg/mL puromycin and maintained throughout the entire duration of cultivation. The transduced and selected cells were sorted for eGFP$^+$ cells with a *FACS Aria IIIu* by the UKE FACS sorting core unit (refer 2.2.7.2). To verify the success of the transduction, a wildtype control of the respective cell line was included throughout the experiment. After cell sorting, the overexpression was evaluated by RT-qPCR analysis (refer 2.2.3.1 - 2.2.3.3).

All approaches for single and double shRNA-based knockdown of *DOCK1* and *ELMO1* in TF-1 and UKE-1 cells were performed accordingly with 50 000 cells in duplicates. The selection was performed with 2 µg/mL puromycin and 0.5 mg/mL Zeocin™ depending on the used construct. Transduction efficiency and selection were evaluated by flow cytometry based on the amount of eGFP$^+$ and mCherry$^+$ cells (refer 2.2.7). After one week of antibiotic selection, cells were collected for RNA isolation and cDNA synthesis, to evaluate the knockdown capacity by RT-qPCR analysis (refer 2.2.3.1 - 2.2.3.3).

The following transductions for a *DOCK1*-overexpression were performed twice:

| | |
|---|---|
| Molm13_*LeGO iG2/puro$^+$* | → Molm13_ctrl |
| Molm13_*hDOCK1-LeGO iG2/puro$^+$* | → Molm13_dock1 |

The single transductions for a shRNA-based knockdown of *DOCK1* with eGFP-expression in TF-1 cells were performed three times and the remaining transductions of *DOCK1*-knockdown with mCherry-expression as well as the ELMO1-knockdown were performed twice, with the following approaches:

| | |
|---|---|
| TF-1 / UKE-1_*scrambled-sh-LeGO G/puro$^+$* | → TF-1_scr/eGFP, UKE-1_scr/eGFP |
| TF-1 / UKE-1_*scrambled-sh-LeGO G/zeo$^+$* | → TF-1_scr/mCherry, UKE-1_scr/mCherry |
| TF-1 / UKE-1_*hDOCK1 sh1-LeGO G/puro$^+$* | → TF-1_dock1-kd1, UKE-1_dock1-kd1 |
| TF-1 / UKE-1_*hDOCK1 sh5-LeGO G/puro$^+$* | → TF-1_dock1-kd2, UKE-1_dock1-kd2 |
| TF-1 / UKE-1_*hELMO1 sh2-LeGO C/zeo$^+$* | → TF-1_elmo1-kd1, UKE-1_elmo1-kd1 |
| TF-1 / UKE-1_*hELMO1 sh5-LeGO C/zeo$^+$* | → TF-1_elmo1-kd2, UKE-1_elmo1-kd2 |

The following double transductions with *DOCK1*- and *ELMO1*-shRNA were performed once:

TF-1 / UKE-1_ *scrambled-sh-LeGO G/puro⁺_ scrambled-sh-LeGO C/zeo⁺*
→ TF-1_scr, UKE-1_scr
TF-1 / UKE-1_*hDOCK1 sh1-LeGO G/puro⁺_ hDOCK1-sh5-LeGO C/zeo⁺*
→ TF-1_dock1-dkd, UKE-1_dock1-dkd
TF-1 / UKE-1_*hDOCK1 sh1-LeGO G/puro⁺_ hELMO1 sh5-LeGO C/zeo⁺*
→ TF-1_dock1/elmo1-kd1, UKE-1_dock1/elmo1-kd1
TF-1 / UKE-1_*hDOCK1 sh5-LeGO G/puro⁺_ hELMO1 sh2-LeGO C/zeo⁺*
→ TF-1_dock1/elmo1-kd2, UKE-1_dock1/elmo1-kd2

All work was carried out under the conditions of biological safety level S2. Transduced cells were handled under the conditions of biological safety level S2 until one week after transduction (at least three splittings or medium changes) and later on under conditions of biological safety level S1.

## 2.2.3 Molecular biological methods

### *2.2.3.1 RNA isolation*

To extract total RNA from eukaryotic cells, the *innuPREP RNA Mini Kit 2.0* was used according to the manufacturer´s instructions. Prior to isolation, up to 5 x $10^6$ cells were washed once with PBS and either used immediately for the extraction or stored in *RNAlater Stabilization Solution* at -20°C to -80°C. In case the cells were stored for later processing, *RNAlater* buffered cells were thawed and centrifuged at 20.000 xg for 10 minutes prior the RNA isolation. Isolated RNA was eluted with RNase free water and the concentration was determined photometrically with the *NanoDrop™.* RNA extracts were stored at -80°C.

All materials and reagents that have been used were RNase-free.

### *2.2.3.2 cDNA synthesis*

To transcribe 1 µg of isolated RNA into cDNA the commercial kit *PrimeScript™ RT Master Mix* was used according to the manufacturer's instructions. The transcribed cDNA was diluted 1:5 v/v with DEPC-treated water and stored at -20°C.

All materials and reagents that have been used were RNase-free.

### *2.2.3.3 Reverse transcription quantitative real-time polymerase chain reaction*

Relative quantification of mRNA expression in a total cDNA samples was performed using the reverse transcription quantitative real-time polymerase chain reaction (RT-qPCR) method. Based on the fluorescence intensity of an intercalating fluorescent dye, the number of gene copies produced in the PCR can be directly correlated.

The Kit *TB Green® Premix Ex Taq™ II* and the plate-based real-time PCR system *LightCycler® 96* were used for all RT-qPCR analyses according to manufacturer´s instructions. Samples, standards and controls were measured in triplicates. Primers listed in Table 13 were used in a concentration of 2 µM with the following PCR program (Table 18):

**Table 18: Cycler conditions for RT-qPCR.**

| Step | Temperature [°C] | Time [s] | Number of cycles |
|---|---|---|---|
| Preincubation | 95 | 45 | 1 |
| 3 Step Amplification | 95 | 5 | 40 |
| | variable | 5 | |
| | 72 | 26 | |
| Melting | 95 | 5 | 1 |
| | 65 | 60 | |
| | 95 | 1 | |
| Cooling | 37 | 30 | 1 |

The fluorescent dye SYBR Green I, which is contained in the kit, is intercalating in the double-stranded PCR products. The fluorescence intensity is proportional to the amount of PCR product. To estimate the relative amount of mRNA copies within a sample and to calculate the efficiency of the PCR, a logarithmic serial dilution of a standard cDNA listed in Table 13 was used.

For relative quantification of the gene expression according to Pfaffl[225], all RT-qPCR data were normalized to the expression data of the housekeeping gene *GAPDH* (Glyceraldehyde 3-phosphate dehydrogenase), taking the efficiency of the PCR into account. Additionally, without the need of a standard curve, ΔCT-method (2^(-ΔCt) * 1000) was used for calculation of relative gene expression, with normalization to the expression data of the reference gene *GAPDH*.

### *2.2.3.4 RNA-Sequencing*

To investigate the transcriptome of *DOCK1*-knockdown cells compared to the control cells, to reveal possible differences in the gene expression pattern, RNA-sequencing was performed by the Core Facility Genomics of the Medical Faculty Münster (CFG MFM).

Transduced TF-1 cells (refer 2.2.2.2) from three different transductions were used as biological replicates. The scrambled control was compared against the single *DOCK1*-knockdown of two different shRNAs (*hDOCK1 sh1-LeGO G/puro⁺, hDOCK1 sh5-LeGO G/puro⁺*). Per sample, 1 µg total RNA was analyzed. After data analysis by Dr. Jan Hennigs, the hits of interest (p-value < 0.05) from the control versus knockdown comparison were verified by RT-qPCR (refer 2.2.3.3). Primers for the corresponding genes are shown in Table 13.

For data analysis of the RNA-Seq results, the samples were demultiplexed (bcl2fastq2), quality controlled (FastQC) and groomed (FastQ groomer) by using the Stanford Genetics Bioinformatics Service Center Galaxy platform. After aligning the resulting reads to the human genome by using the built-in hg19 reference genome utilizing STAR aligner, the aligned reads were transferred into SeqMonk 1.45 (Babraham Institue). For quantification of the aligned reads, the built-in RNA quantification pipeline on merged transcripts of two different *DOCK1*-shRNAs combined versus control shRNA was used. By LIMMA analysis, differentially expressed genes were defined as significantly regulated merged transcripts (FDR < 0.05, Benjamin-Hochberg correction). Data analysis was performed by Dr. Jan Hennigs.

### *2.2.3.5 shRNA-cloning*

For lentiviral transduction of AML cell lines, the shRNAs listed in Table 14 were cloned into lentiviral LeGO-vectors (refer Table 15), expressing the fluorescent protein mCherry or eGFP and a selection site for puromycin or Zeocin™. The shRNAs used for subcloning were chosen based on their evaluated knockdown capacity. The following constructs were cloned:

*hDOCK1 sh1-LeGO G/puro⁺*

*hDOCK1 sh5-LeGO G/puro⁺*

*hDOCK1-sh5-LeGO C/zeo⁺*

*hELMO1 sh2-LeGO C/zeo⁺*

*hELMO1 sh5-LeGO C/zeo⁺*

*Introduction of restriction sites by PCR*

The shRNA coding pLKO.1-plasmids listed in Table 14 were used to amplify the shRNA sequences. 10 ng of the plasmids were used as a template in the PCR reaction. The overhang primers *shRNA XbaI FW* and *shRNA SalI RV* (10 µM, refer Table 12) contain the desired restriction sites for the restriction enzymes SalI and XbaI. To amplify the shRNA, *S7 Fusion High-Fidelity DNA Polymerase* was used according to manufacturer´s instructions with the following PCR program (Table 19):

**Table 19: PCR conditions for shRNA-cloning PCR.**

| Step | Temperature [°C] | Time | Number of cycles |
|---|---|---|---|
| Initial denaturation | 98 | 30 s | 1 |
| Denaturation | 98 | 10 s | 30 |
| Annealing | 65 | 30 s | |
| Extension | 72 | 30 s | |
| Final extension | 72 | 5 min | 1 |

To verify the PCR products, 5 µL of the PCR reactions were loaded next to the DNA ladder *GeneRuler 100bp plus* to a 1% agarose gel (1% agarose in 1x TAE + 0.1% *ROTI®GelStain*) and separated with 120 V for 45 minutes. Ultraviolet (UV)-light was used to visualize the DNA bands.

*Clean-up of the PCR product*

The purification of the PCR products was done with the kit *NucleoSpin® Gel and PCR Clean-up* in accordance with the manufacturer´s instructions. Purified DNA was eluted with DEPC-treated water and the concentration was determined photometrically with the *NanoDrop™.*

*Digestion of PCR products and LeGO-vectors*

In a total volume of 30 µL, 400 ng of the purified PCR product was digested with 3 µL 10x FD buffer green and 1 µL of the restriction enzymes *FastDigest XbaI* and *FastDigest SalI* for 2 hours at 37°C. The LeGO vectors *LeGO G/puro*$^{+}$ and *LeGO C/zeo*$^{+}$ were digested with the restriction enzymes *FastDigest XbaI* and *FastDigest XhoI*. In a 30 µL reaction mix, 1.5 µg of the vectors were used as a template with 1 µL of each enzyme.

The restriction endonucleases XhoI and SalI are generating compatible cohesive ends that can be directly ligated in a sticky-end ligation.

*Preparative agarose gel electrophoresis and gel extraction*

To purify the digested PCR fragments and the linearized LeGO vectors a preparative agarose gel electrophoresis was performed. The DNA fragments were separated in a 0.8% agarose gel containing *ROTI®GelStain* with 120 V for 45 minutes. To avoid any DNA damage by UV-light, the desired DNA fragments were excised blindly without UV-light exposure. In order to determine the correct position of the fragments, a small portion of the digested DNA and the DNA ladders *GeneRuler 100bp plus* and *GeneRuler 1 kb Plus* were applied to one half of the gel and the rest of the digested DNA to the other side. After gel electrophoresis, only the side with the standards and the test samples was exposed to UV-light. To excise the desired fragments a clean scalpel was used.

The extraction of the PCR products from the agarose gel was done with the kit *NucleoSpin® Gel and PCR Clean-up* in accordance with the manufacturer´s instructions. Purified DNA was eluted with DEPC-treated water and the concentration was determined photometrically with the *NanoDrop™.*

*Ligation*

To ligate the purified shRNA into the linearized LeGO vectors in a 5:1 molar ratio with 100 ng of vector-DNA, *T4 DNA Ligase* was used according to manufacturer´s instructions. The ligation mix was incubated for 15 minutes at 16°C, followed by 4°C overnight and completed on the next day for 10 minutes at 22°C. The reaction was stopped at 65°C for 10 minutes.

To amplify the recombinant plasmids, the ligation-mix was transformed into *Escherichia coli* (*E. coli*) bacteria (*Library Efficiency™ DH5α™ Competent Cells*) and positive clones were selected for plasmid isolation by Colony-PCR. The bacterial work is described in section 2.2.4. For the verification of correct cloning, sequencing of the recombinant plasmids was performed (refer 2.2.3.8).

### *2.2.3.6 Site-directed mutagenesis*

The *MGC premier cDNA clone for DOCK1* (Gene ID: 1793, Genebank accession: BC146857), carrying the plasmid *hDOCK1-pCR-XL-TOPO* was used as a cDNA source for the overexpression-cloning. Since the cDNA insert sequence (BC146857) is showing several nucleotide base substitutions after alignment to the mRNA sequence of DOCK1 transcript variant 2 (NM_001380.4), with one point-mutation leading to an amino acid exchange, site-

directed mutagenesis was performed (protocol adapted to manufacturer´s instructions of *QuikChange XL Site-Directed Mutagenesis Kit* (Agilent) and *S7 Fusion High-Fidelity DNA Polymerase)*.

At position 3613 bp the cDNA sequence contains guanine whereas the mRNA sequence contains adenine instead, leading to a missense mutation (asparagine in human protein, aspartic acid resulting from cDNA sequence). To achieve the substitution of the concerning nucleotide, mutagenic primers containing the desired mutation were designed (refer Table 12), using the *QuikChange Primer Design* tool from Agilent.

To isolate the plasmid *hDOCK1-pCR-XL-TOPO* from the *MGC premier cDNA clone for DOCK1* two 5 mL LB-overnight cultures containing 50 µg/mL kanamycin were inoculated and used for the plasmid isolation with the *NucleoSpin® plasmid* kit (refer 2.2.4.3).

The isolated plasmid *hDOCK1-pCR-XL-TOPO* was used as a template for the mutant strand synthesis reaction (Table 20) resulting in nicked circular double-stranded DNA (dsDNA) strands. For each mutagenic primer a reaction mix was prepared separately. After 5 cycles of the amplification reaction in a thermocycler, the reaction mixes were combined for the remaining cycles.

**Reaction mix for thermal cycling**

| | |
|---|---|
| 5x HF-buffer | 5 µL |
| 10 mM deoxyribonucleotide (dNTP) mix | 0.5 µL |
| 10 µM mutagenic primer (fw or rev) | 2.5 µL |
| Parental DNA *hDOCK1-pCR-XL-TOPO* (1 ng/µL) | 10 µL |
| DMSO | 0.75 µL |
| S7 Fusion DNA Polymerase | 0.25 µL |
| DEPC-treated $H_2O$ | 6 µL |
| **Total volume** | **25 µL** |

**Table 20: Cycling conditions for mutant strand synthesis reaction.**

| Step | Temperature [°C] | Time | Number of cycles |
|---|---|---|---|
| Initial denaturation | 98 | 30 s | 1 |
| Denaturation | 98 | 10 s | 5 |
| Annealing and extension | 72 | 7.5 min | |
| Pooling of the fw- and rev-reaction mixes | | | |
| Initial denaturation | 98 | 30 s | 1 |
| Denaturation | 98 | 10 s | 20 |
| Annealing and extension | 72 | 7.5 min | |

The amplified product was treated with 1 µL *FastDigest DpnI* restriction enzyme, which is specific for methylated DNA, for 30 minutes at 37°C. Plasmid DNA isolated from dam$^+$ *E. coli* is methylated, whereas amplified DNA generated by *S7 Fusion High-Fidelity DNA Polymerase* is non-methylated, resulting in a selective digestion of methylated nonmutated parental dsDNA.

5 µL of DpnI treated DNA was transformed into *Library Efficiency™ DH5α™ Competent Cells* (refer 2.2.4.1) and mutated Plasmid *hDOCK1-pCR-XL-TOPO (mut.)* was isolated (refer 2.2.4.3). Successful mutagenesis was verified by sequencing (refer 2.2.3.8).

### *2.2.3.7 Overexpression-cloning*

To generate DOCK1-overexpressing AML cell lines by lentiviral transduction the mutant cDNA (refer 2.2.3.6) was cloned into the lentiviral backbone *LeGO iG2/puro$^+$*, expressing a selection site for the antibiotic puromycin and a coding region for the fluorescent protein eGFP.

#### *Introduction of restriction sites by PCR*

The mutant plasmid *hDOCK1-pCR-XL-TOPO (mut.)* was used to amplify the mutant gene of interest *DOCK1*, with 5 ng plasmid as a template in the PCR reaction with the overhang primers *DOCK1-FL-AscI-f* and *DOCK1-FL-NotI-r* (10 µM, refer Table 12). The primers contain the desired restriction sites for the endonucleases AscI and NotI. To amplify the gene of interest the *S7 Fusion High-Fidelity DNA Polymerase* was used according to manufacturer´s instructions with the following PCR program (Table 21):

**Table 21: PCR conditions for overexpression-cloning PCR.**

| Step | Temperature [°C] | Time | Number of cycles |
|---|---|---|---|
| Initial denaturation | 98 | 30 s | 1 |
| Denaturation | 98 | 10 s | 30 |
| Annealing | 68 | 30 s | |
| Extension | 72 | 3 min | |
| Final extension | 72 | 10 min | 1 |

For verification of the PCR product, 5 µL of the PCR reaction was loaded next to the DNA ladder *GeneRuler 1kb Plus* to a 1% agarose gel, containing *ROTI®GelStain*, and separated with 120 V for 45 minutes. UV-light was used to visualize the DNA bands.

*Clean-up of the PCR product*

To purify the PCR product the kit *NucleoSpin® Gel and PCR Clean-up* was used in accordance with the manufacturer´s instructions. Purified DNA was eluted with DEPC-treated water and the concentration was determined photometrically with the *NanoDrop™.*

*Digestion of PCR product and LeGO-vector*

400 ng of the purified PCR product and 1 µg of the vector *LeGO iG2/puro⁺* were each digested with 1 µL of the restriction enzymes *FastDigest AscI* and *FastDigest NotI* in a total volume of 30 µL for 2 hours at 37°C.

*Preparative agarose gel electrophoresis and gel extraction*

The preparative gel electrophoresis and the following gel extraction of digested insert and vector were performed according to the shRNA cloning (refer 2.2.3.5).

*Ligation*

The *T4 DNA Ligase* was used to ligate the purified insert into the linearized LeGO vector in a 1:1 molar ratio with 100 ng of vector-DNA according to manufacturer´s instructions. The ligation mix was incubated for 15 minutes at 16°C, followed by 4°C overnight and completed on the next day for 10 minutes at 22°C. The reaction was stopped at 65°C for 10 minutes.

To amplify the recombinant Plasmid *hDOCK1-LeGO iG2/puro⁺*, the ligation-mix was transformed into competent DH10B *E. coli* and positive clones were selected for plasmid isolation by Colony-PCR. The bacterial work is described in section 2.2.4. For the verification of correct cloning, sequencing of the recombinant plasmid was performed (refer 2.2.3.8).

### *2.2.3.8 Sequencing*

The sequencing of the cloned plasmids *hDOCK1-pCR-XL-TOPO (mut.)*, *hDOCK1-LeGO iG2/puro⁺*, *hDOCK1 sh1-LeGO G/puro⁺*, *hDOCK1 sh5-LeGO G/puro⁺*, *hDOCK1 sh5-LeGO C/zeo⁺*, *hELMO1 sh2-LeGO C/zeo⁺* and *hELMO1 sh5-LeGO C/zeo⁺* was performed by the company Eurofins Genomics GmbH (Ebersberg, DE).

Sequencing of the shRNA constructs was run under special conditions, adapted to the secondary structure of the shRNA. The primers listed in Table 12 were used for the sequencing reaction.

## 2.2.4 Bacterial work

### *2.2.4.1 Transformation of E. coli*

Competent *E. coli* bacteria (*Library Efficiency™ DH5α™ Competent Cells*, competent DH10B) were used to replicate foreign plasmid DNA. To transform bacteria, the heat shock method was used.

An aliquot of 50 µL competent DH5α (100 µL for DH10B) was thawed on ice and 10 ng of plasmid DNA (up to 1 µg for DH10B) or 5 µL of a 1:5 diluted ligation-mix was slowly added and carefully mixed. After 30 minutes incubation on ice, the heat shock took place for 55 seconds (90 seconds for DH10B) in a 42°C water bath, followed by 2 minutes (5 minutes for DH10B) incubation on ice. 500 µL SOC medium (700 µL for DH10B) was added and the transformation-mix was incubated in a heating block for 1 hour at 37°C and 300 rpm. The transformation-mix was plated pure and concentrated on LB agar plates containing the appropriate selection antibiotic (100 µg/mL Ampicillin, 50 µg/mL Kanamycin). The plates were incubated overnight at 37°C.

### *2.2.4.2 Qualitative Colony-PCR*

Qualitative colony-PCR was used to analyze whether bacterial clones carry the desired recombinant plasmid.

With a sterile pipette tip, a single colony from the LB agar plate was picked and transferred to 20 µL sterile water. To inoculate 6 mL LB medium containing Ampicillin (100 µg/mL), 10 µL of the suspension was used. The remaining suspension was used as a template in the following PCR reaction, using the *DreamTaq™ Green PCR Master Mix* according to manufacturer´s instructions.

For the verification of shRNA constructs in LeGO vectors, the primer pairs *LeGO C/G Vektor fw* + *LeGO G/C rv* and *LeGO G/C shRNA fw* + *LeGO G/C rv* were used in two separate PCR reactions, with the first pair leading to a PCR product only in the presence of empty vectors and the second one leading to PCR products for either empty vectors or recombinant plasmids. For amplification the following PCR program was used (Table 22):

**Table 22: PCR conditions for shRNA Colony-PCR.**

| Step | Temperature [°C] | Time | Number of cycles |
|---|---|---|---|
| Initial denaturation | 95 | 3 min | 1 |
| Denaturation | 95 | 30 s | 30 |
| Annealing | 52 | 30 s | |
| Extension | 72 | 1 min | |
| Final extension | 72 | 5 min | 1 |

To verify positive clones expressing the *DOCK1*-overexpression plasmid *hDOCK1-LeGO iG2/puro*$^{+}$, the primer pairs *CoPCR2-DOCK1 f* + *CoPCR2-DOCK1 r* and *CoPCR2-DOCK1 f* + *CoPCR2-L-iG2 r* were used in two PCR reactions. The first primer pair leading to a PCR product only for recombinant plasmids with the gene of interest present, whereas the second pair leads to PCR products only in the presence of empty vectors. The following PCR program was used for both PCR reactions (Table 23):

**Table 23: PCR conditions for overexpression Colony-PCR.**

| Step | Temperature [°C] | Time | Number of cycles |
|---|---|---|---|
| Initial denaturation | 95 | 3 min | 1 |
| Denaturation | 95 | 30 s | 30 |
| Annealing | 50 | 30 s | |
| Extension | 72 | 45 s | |
| Final extension | 72 | 5 min | 1 |

To analyze the PCR products, the samples and the DNA ladder *GeneRuler 100bp plus* were loaded to a 1% agarose gel containing *ROTI®GelStain* and separated with 120 V for 45 minutes. UV-light was used to visualize the DNA bands.

For the shRNA-plasmid verification, clones that were only positive for the second PCR were selected for plasmid preparation. In the colony-PCR for overexpression verification, positive clones showed PCR products only with the first primer pair.

The prepared inoculated cultures of all positive clones were incubated overnight at 37°C and 180 rpm in a bacterial shaker. To prepare glycerol stocks, 1 mL of bacterial suspension was mixed carefully with 500 µL glycerol and stored in a cryopreservation tube at -80°C.

### *2.2.4.3 Preparation of plasmid DNA from E. coli*

To replicate transformed bacteria, LB-medium containing the appropriate antibiotic (100 µg/mL Ampicillin, 50 µg/mL Kanamycin) were inoculated with the desired clone, taken from a LB agar plate or from a glycerol stock and incubated overnight at 37°C and 180 rpm in a bacterial shaker.

For the plasmid preparation the *NucleoSpin® plasmid* kit or *the NucleoBond® Xtra Midi Plus* kit was used according to the manufacturer's instructions and the DNA concentration was determined on the *NanoDrop™*.

## 2.2.5 Protein biochemical Methods

### *2.2.5.1 Preparation of whole cell lysate and quantitative determination of protein concentration*

*RIPA buffer* was used to prepare whole cell lysates. The ready-to-use lysis buffer RIPA allows the extraction of proteins of the cytoplasm and the nucleus as well as membrane proteins.

Approximately 3-5 x $10^6$ suspension cells were washed with 1x PBS and resuspended in 100-200 µL *RIPA buffer*. To prevent proteolysis and to maintain the protein phosphorylation, protease inhibitor cocktail (1x) and sodium orthovanadate (1 mM) were freshly added to the *RIPA buffer*. After 30-minute incubation on ice, the cell suspension was centrifuged at 10 000 rpm and 4°C for 10 minutes. The supernatant containing the proteins was obtained and stored at -80°C.

For the isolation of phosphorylated proteins all steps were performed on ice or 4°C and with precooled reagents.

Protein concentration was determined with the *DC Protein Assay* according to manufacturer's instructions. A bovine serum albumin (BSA) serial dilution served as a standard.

### *2.2.5.2 Co-Immunoprecipitation*

#### *Identification of potential DOCK1 interaction partners*

To analyze protein-protein interactions of DOCK1, co-immunoprecipitation with cell lysates of *DOCK1*-double-knockdown and control cells was performed. A DOCK1-specific antibody was used to pull down DOCK1 and all proteins bound to it.

Whole cell lysates of double-transduced TF-1 and UKE-1 cells (refer 2.2.2.2) were prepared with 6 x $10^6$ cells and the protein concentration was determined by *DC Protein Assay* (refer 2.2.5.1).

The anti-hDOCK1 antibody was bound to *Protein-G-Sepharose™ 4 Fast Flow*, a resin coupled recombinant protein G, which has a high binding capacity for a wide range of IgG subclasses

from a variety of mammalian species. To couple the antibody, *Protein-G-Sepharose™* was washed three times with a fivefold volume of *RIPA buffer*. For TF-1-cell lysates 1 µg antibody and 40 µL *Protein-G-Sepharose™* (50:50 slury) were added to 250 µL *RIPA buffer* per sample. For UKE-1-cell lysates 2 µg antibody was used. The mixture was incubated for 4 hours at 4°C in a rotating mixer. The antibody-containing supernatant was replaced by 300 µL cell lysate, containing 500 µg total protein. The pulldown of DOCK1 took place overnight at 4°C in a rotating mixer.

After washing the *Protein-G-Sepharose™* twice with 500 µL *RIPA buffer*, the immunoprecipitated proteins were eluted with 5 µL *NuPAGE™ Sample Reducing Agent (10x)* and 10 µL *NuPAGE™ LDS Sample Buffer (4x)* by heating at 70°C for 5 minutes at 300 rpm. The protein-containing supernatant was used directly for SDS-PAGE (refer 2.2.5.3). In all steps *RIPA buffer* was supplemented with protease inhibitor cocktail (1x) and sodium orthovanadate (1 mM).

*Analysis of potential phosphorylation patterns within the signaling cascade of DOCK1*

Co-immunoprecipitation of whole cell lysates from TF-1 cells, treated with the small molecule inhibitors TBOPP and CPYPP (refer Table 16), was performed to identify potential phosphorylated proteins within the signaling cascade of DOCK1.

TF-1 cells (5 x $10^6$ each) were treated with 10 µM TBOPP, 30 µM CPYPP and DMSO as a solvent control for 10, 30 and 60 minutes. At each timepoint the cells were harvested and whole cell lysates for phosphoproteins were prepared according to 2.2.5.1. After the determination of protein concentration by *DC Protein Assay* (refer 2.2.5.1), co-immunoprecipitation for DOCK1 was performed as described above.

### *2.2.5.3 Sodium dodecyl sulfate polyacrylamide gel electrophoresis (SDS-PAGE)*

SDS-PAGE was performed to separate denatured proteins by size. In case Western blot analysis was following, the proteins were prepared for electrophoresis by mixing whole cell lysate containing 20 µg protein (refer 2.2.5.1) with *Lane Marker Reducing Sample Buffer (5X)* to a final concentration of 1x in a total volume of 20 µL. The samples were denatured for 5 minutes at 95°C prior loading to the SDS-gel. Co-immunoprecipitated samples (refer 2.2.5.2) could be loaded without further treatment.

Pre-cast (*Novex® WedgeWell™ 4-12% Tris-Glycin Gel*) as well as hand-cast SDS-gels were used for electrophoresis with 1x running buffer inside an electrophoresis chamber. To separate the proteins the electrophoresis was run at 185 V for approximately 60 minutes, until the migration front reached the bottom of the gel. The size standard *PageRuler™ Plus Prestained Protein Ladder 10-250 kDa* was loaded next to the samples to determine the size of the proteins.

To prepare hand-cast gels the following two acrylamide/bis-acrylamide containing mixtures were prepared:

**SDS polyacrylamide gel (for one gel)**

| | **Resolving gel 12.5%** | **Stacking gel 4%** |
|---|---|---|
| $ddH_2O$ | 3.2 mL | 2.9 mL |
| 30% (w/v) Acrylamide-Bis (37.5:1) | 4.15 mL | 0.65 mL |
| 1.5 M Tris/HCl (pH 8.8) | 2.5 mL | - |
| 0.5 M Tris/HCl (pH 6.8) | - | 1.25 mL |
| 20% (w/v) SDS | 50 µL | 25 µL |
| 10% (w/v) APS | 50 µL | 25 µL |
| TEMED | 10 µL | 5 µL |
| **Total volume** | **9.96 mL** | **4.855 mL** |

The 12.5% resolving gel was poured between two glass plates in a casting stand and topped with 99.8% isopropanol (2-propanol). After complete polymerization, the isopropanol was removed and replaced by the 4% stacking gel mixture. To form sample wells, a comb was added until the gel was completely polymerized.

### *2.2.5.4 Western blot analysis*

The protein transfer from a SDS polyacrylamide gel onto a nitrocellulose membrane (*Amersham™ Protran™ 0.45 µm NC*) was performed in the tank blotting system *Mini-PROTEAN® 3 Cell* with cold 1x transfer buffer at 0.35 A for one hour.

After the protein transfer, the proteins of interest were detected by immunostaining with specific antibodies (refer Table 10). To prevent unspecific antibody binding, the nitrocellulose membrane was blocked with 5% BSA in 1x TBS-T for 1 hour at an orbital shaker at room temperature. After washing the membrane three times with 1x TBS-T for 10 minutes at 150 rpm, the membrane was cut horizontally at the 100 kDa band level. The upper half was used for the immunostaining of DOCK1 protein, with the rabbit-anti-hDOCK1 primary antibody diluted 1:5000 v/v in blocking buffer, and the lower part of the membrane was used

for staining of β-Actin as a loading control, with the either the HRP-conjugated rabbit-anti-hβ-Actin primary antibody or unconjugated mouse-anti-hβ-Actin primary antibody diluted 1:1000 v/v. The incubation with the primary antibodies was performed overnight at 4°C in a 50 mL tube at a roll shaker, followed by washing three times as indicated above. The membranes, stained with uncoupled primary antibodies, were incubated with the HRP-coupled secondary antibodies anti-rabbit-IgG or anti-mouse-IgG diluted 1:10 000 v/v in blocking buffer for one hour at room temperature at 50-100 rpm. The final washing with 1x TBS-T was performed three times for 5 at 200 rpm. To visualize the stained protein bands *Amersham™ ECL™ Prime Western Blotting Detection Reagents* were used according to manufacturer's instructions, followed by chemiluminescence detection with the *Fusion SL 3500 WL*.

### *2.2.5.5 Phosphoprotein gel staining*

To selectively stain phosphoproteins in SDS-polyacrylamide gels, the *Pro-Q™ Diamond Phosphoprotein Gel Stain* was used according to manufacturer's instructions. After co-immunoprecipitation of whole cell lysates from TBOPP and CPYPP treated TF-1 cells and protein separation by SDS-PAGE (refer 2.2.5.1 - 2.2.5.3), the SDS-gel was fixed two times for 30 minutes at 50 rpm on an orbital shaker with 100 mL fixation buffer (50% v/v Methanol, 10% v/v acetic acid) each. The gel was washed with 100 mL $ddH_2O$ for at least 1 hour.

The following steps of the staining protocol were performed by Dr. Steffen Ostendorp from the Institute of Plant Science and Microbiology (Universität Hamburg) according to the manufacturer's instructions. The gel was stained for 90 minutes in the dark at 50 rpm with 60 mL Pro-Q Diamond staining solution and destained overnight with 100 mL destain solution (20% v/v acetonitrile, 50 mM sodium acetate, pH 4.0). After a second 30-minute destain step, the gel was washed two times with 100 mL $ddH_2O$ for 5 minutes. The phosphoproteins were detected with a *ChemiDoc Touch Imager*.

### *2.2.5.6 Coomassie staining and mass spectrometry (MS)*

To identify protein bands of interest in SDS-gels for MS analysis, colloidal Coomassie G-250 staining was performed according to Dyballa N. and Metzger S.[226] by Dr. Steffen Ostendorp.

To identify potential DOCK1 interaction partners, cell lysates of *DOCK1*-double-knockdown compared to control UKE-1 and TF-1 cells (refer 2.2.2.2) were co-immunoprecipitated and

separated by SDS-PAGE (refer 2.2.5.1 - 2.2.5.3). After Coomassie staining, protein bands of the same size, but different intensities were selected for mass spectrometric analysis. For the analysis of potential phosphorylation patterns within the signaling cascade of DOCK1, *Pro-Q™ Diamond* stained SDS-gels (refer 2.2.5.5) were stained for whole protein with Coomassie staining. Proteins of interest were selected based on differences in both stains. Peptide mass fingerprinting (PMF) of the selected protein samples was performed after trypsin digestion with a MALDI-TOF/TOF Mass Spectrometer (matrix assisted laser desorption ionization - time of flight), followed by analysis with the software *mMass*[223], by Dr. Steffen Ostendorp. The resulting signals were compared against the NCBI database using the *MASCOT Server*[227], with peptide tolerance of 0.3 Da and methionine oxidation as a variable modification. The taxonomy was restricted to *Homo sapiens*. A protein was considered as identified, if at least five peptides could be matched, the total protein coverage was at least 20% and a significant score during the MASCOT search (p-value < 0.05) was achieved.

## 2.2.6 In vitro assays

### *2.2.6.1 Proliferation assays*

#### *GM-CSF-dependency of TF-1 cells*

The cell proliferation of the AML cell line TF-1 is dependent on the growth factor granulocyte-macrophage colony-stimulating factor (GM-CSF)[228]. To verify the persistence of the GM-CSF-dependency the cells were tested on a regular basis, to prevent an outgrowth of independent cell clones.

TF-1 cells were seeded in a 24-well plate with 0.2 x $10^6$ cells/mL in RPMI + 10% FBS in two triplicates with 1 mL per well. The first triplicate was treated with 2.5 ng/mL GM-CSF, the second one remained untreated. After three days of incubation at 37°C and 5% $CO_2$ the cells were counted with the *Vi-Cell™ XR.* The rest of the cell suspension was split 1:5 and re-stimulated with 2.5 ng/mL GM-CSF for another three days, followed by cell counting. As long as the proliferation rate of the untreated cells was slower compared to the treated ones, the cell line was considered to be GM-CSF dependent.

Experiments with TF-1 cells were only carried out with GM-CSF dependent cells.

*Effect of small molecule inhibitors CPYPP and TBOPP on the proliferation of AML cells*

The effect of the small molecule inhibitors CPYPP and TBOPP (refer Table 16) on the proliferation rate of the AML cell lines UKE-1, TF-1 and Molm13 as well as the proliferation rate of primary AML cells were analyzed.

The cells were seeded in triplicates with 0.5 mL (0.25 mL for pAML cells) per sample in a 24-well plate. UKE-1 and TF-1 cells were seeded with a cell density of 1 x $10^6$ cells/mL, Molm13 cells with 0.5 x $10^6$ cells/mL and pAML cells with 2 x $10^6$ cells/mL. The appropriate culture medium for each cell line was used for seeding (refer Table 8). Primary AML cells were seeded in pAML-medium. To each well, 0.5 mL (0.25 mL for pAML cells) of inhibitor-containing medium was added, leading to final cell concentrations of 0.5 x $10^6$ cells/mL for UKE-1 and TF-1 cells, 0.25 x $10^6$ cells/mL for Molm13 cells and 1x x $10^6$ cells/mL for pAML cells and final inhibitor concentrations in a range of 5-100 µM. One triplicate with DMSO as solvent control was seeded the same way. After three to four days of incubation, the cell number was determined with the *Vi-Cell™ XR*. For UKE-1 and TF-1 cells, the rest of the cell suspension was split 1:5, for pAML cells 2:5 and for TBOPP treated Molm13 1:10. The cells were re-stimulated with the appropriate inhibitor concentration for another three to four days, followed by cell counting. For all pAML samples used in the experiment, the mRNA expression of the three *DOCK*-homologs (*DOCK1*, *DOCK2* and *DOCK5*) was determined by RT-qPCR analysis (refer 2.2.3.3).

*Effect of DOCK1-, ELMO1- or combined shRNA-based knockdown or DOCK1 overexpression on the proliferation of AML cells*

To determine whether either an overexpression of the gene *DOCK1* or a shRNA-based knockdown of the genes *DOCK1* and *ELMO1* alone or in combination has an influence on the proliferation rate of AML cells, transduced cells, described in section 2.2.2.2, were used.

Single and double transduced TF-1 and UKE-1 cells were seeded with 0.3 x $10^6$ cells/mL in triplicates in a 24-well plate. *DOCK1*-overexpressing Molm13 cells were seeded with a cell concentration of 0.1 x $10^6$ cells/mL. After three days of incubation, the cell number was determined with the *Vi-Cell™ XR*. The rest of the cell suspension was split 1:5 and was further cultivated for another three days, followed by a second cell count.

To take possible differences in the cell concentration of the initial cell suspensions in account, the cell number of the initial cell suspensions were determined with the *Vi-Cell™ XR* and included in the calculations of the results.

The assay was performed in presence of the appropriate selection antibiotic (puromycin 2 µg/mL, Zeocin™ 0.5 mg/mL). Cells used in the assays were verified for the presence of knockdown or overexpression by RT-qPCR.

#### *2.2.6.2 Colony formation assays*

Hematopoietic stem and progenitor cells (HSPCs) as well as leukemic cells show the ability to proliferate and form colonies in semi-solid medium. Each colony is derived from a single cell, therefore the number of colonies is reflecting the clonal proliferation and differentiation potential of these cells.

##### *Effect of small molecule inhibitors CPYPP and TBOPP on colony formation of AML cells*

The effect of the small molecule inhibitors CPYPP and TBOPP (refer Table 16) on the colony forming abilities of the AML cell lines UKE-1, TF-1 and Molm13 were analyzed.

The cells were seeded with a cell density of 250 cells/mL in triplicates. Methylcellulose-based semi-solid medium for human cells *MethoCult™ H4230* was used to seed the cells. The inhibitors were added to final concentrations of 3-50 µM and DMSO was used as solvent control. For each sample 1.1 mL of cell suspension was plated without air bubbles into 3.5 cm-Petri dishes. The plates were incubated for 5-7 days at 37°C, 95% RH and 5% $CO_2$. Counting of the colonies was done under an inverted microscope.

##### *Effect of DOCK1-, ELMO1- or combined shRNA-based knockdown or DOCK1 overexpression on colony formation of AML cells*

The influence of either an overexpression of the gene *DOCK1* or a shRNA-based knockdown of the genes *DOCK1* and *ELMO1*, alone or in combination, on the colony forming abilities of AML cells was analyzed using transduced cells, described in section 2.2.2.2.

Based on previous experiments with wildtype-cells, single and double transduced TF-1 and UKE-1 cells were seeded in triplicates as described above. The assay was performed in presence of the appropriate selection antibiotic (puromycin 2 µg/mL, Zeocin™ 0.5 mg/mL).

Cells used in the assays were verified for the presence of knockdown or overexpression by RT-qPCR.

### *2.2.6.3 Adhesion assay in a microfluidic system (Bio Flux)*

To analyze the adhesion properties of AML cells to endothelial cells under controlled shear flow conditions within a microfluidic system the *BioFlux™ 200* device was used in accordance to the manufacturer's instructions. The BioFlux system allows to observe two microfluidic channels simultaneously in a live cell assay. *BioFlux 48 well plates 0-20 dyn/cm²* were used for the experiments.

To prepare the channels for the experiment, a coating and priming step was performed. Fibronectin in PBS (c = 50 µg/mL; kindly provided by the Department of Dermatology and Venereology, UKE) was used to coat the channels. After one hour of incubation, the channels were primed with sterile $ddH_2O$ followed by prewarmed L-15 medium + 10% FBS, each for 15 minutes at 2 dyn/cm$^2$. The BioFlux plate was incubated overnight at 37°C without $CO_2$ equilibration. Primary HUVEC cells in passage 1-4 were perfused at 1 dyn/cm$^2$ with a cell density of 12.5 x $10^6$ cells. To allow the cells to attach to the coated channels, the plate was incubated for 2 hours at 37°C without $CO_2$ equilibration. After cell attachment, the inlet well was filled with 1 mL prewarmed L-15 medium +10% FBS, to let the cells grow overnight under gravity flow. When the cell layer was confluent, the cells were activated by tumor necrosis factor-α (TNF-α) stimulation 4-5 hours prior to the experiment. TNF-α containing medium (c = 10 ng/mL) was perfused for 5 minutes at 1 dyn/cm$^2$ and the remaining stimulation period was under gravity flow at 37°C without $CO_2$ equilibration.

The experiment was performed at 37°C. Transduced AML cells (refer 2.2.2.2) at 2 x $10^6$ cells/mL in L-15 + 10% FBS were perfused at 1 dyn/cm$^2$ and the adhesion was documented with the inverted microscope Axio Observer Z.1. For image acquisition and analysis ZEN software and the open-source software ImageJ were used. Cells used in the assays were verified for the presence of knockdown or overexpression by RT-qPCR.

### *2.2.6.4 CXCR4-stimulation or -inhibition in AML cells*

To determine the effect of stimulation or inhibition of CXCR4 on the mRNA expression level of *DOCK1* and *CXCR4* in primary AML cells, RT-qPCR analysis was performed.

The cells were seeded in a 24 well-plate with a cell density of 1 x $10^6$ cells/mL in pAML-medium. Cells were treated with 50 ng/mL and 500 ng/mL of CXCR4-ligand CXCL12 as well as with 400 µL/mL 24 hour-supernatant from human dermal blood endothelial cells (HDBEC) for different time points. The cells were harvested, washed once with PBS and stored in *RNAlater Stabilization Solution* at -80°C. After RNA-isolation and cDNA-synthesis, RT-qPCR analysis was performed (refer 2.2.3.1 - 2.2.3.3).

#### *2.2.6.5 JAK2-axis modulation in AML cell lines*

The mRNA expression of *DOCK1* and *CXCR4* as well as the protein expression of DOCK1 was analyzed by RT-qPCR and Western Blot after stimulation or inhibition of JAK2.

UKE-1 cells with a cell concentration of 0.5 x $10^6$ cells/mL were treated with the JAK-inhibitor ruxolitinib for 4 hr, 8 hr, 24 hr and 48 hr. Different concentrations of the inhibitor (40-600 nM) were used and DMSO was included as a solvent control. To determine the appropriate concentrations of the inhibitor, a proliferation assay was performed with UKE-1 cells over four days. For RT-qPCR analysis, 2 mL cell suspensions were stored in *RNAlater Stabilization Solution* at -80°C until RNA-isolation (refer 2.2.3.1). After cDNA-synthesis, RT-qPCR analysis was performed (refer 2.2.3.2 and 2.2.3.3). For Western Blot analysis, 10 mL cell suspensions treated with DMSO, 100nM and 600 nM ruxolitinib for 24 hr and 48 hr were harvested and whole cell lysates were prepared (refer 2.2.5.1 and 2.2.5.4).

TF-1 cells with a cell concentration of 0.5 x $10^6$ cells/mL were treated with 2.5 ng/mL GM-CSF for 4 hr, 8 hr, 24 hr and 48 hr. For RT-qPCR and Western blot analysis, cells were harvested as described above.

### 2.2.7 Flow cytometry and cell sorting

Flow cytometry enables the characterization of single cells within a cell suspension in terms of size and granularity as well as fluorescent labeling. Fluorophore-conjugated antibodies are used to label cell surface as well as intracellular proteins, to determine their expression. Also, fluorescent protein expression, such as eGFP or mCherry expression, can be detected by flow cytometry. Hydrodynamic focusing allows the cells to enter the laser beam one by one. The laser beam is scattered when it strikes the cell and the light scattering is detected as forward scatter (FSC) and side scatter (SSC). Fluorophores or expressed fluorescent proteins are excited by the laser and their emitted light can be detected[229].

All measurements were performed on either a *FACS Calibur™* with the software *CellQuest Pro 5.2.1* or *FACS Canto™* with the software *FACS Diva v6.1.1*. Cell sorting was performed on a FACS AriaIIIu at the UKE FACS sorting core unit. Antibodies used for fluorescent labeling of the cells are shown in Table 10.

### *2.2.7.1 Flow cytometry of transduced cells*

To evaluate the transduction efficiency and selection of transduced cells (refer 2.2.2.2), the percentage of $eGFP^+$ or $mCherry^+$ cells was determined four days after transduction and again after one week of antibiotic selection. Due to their potential infection risk, freshly transduced cells were handled under biological safety level S2 conditions and had to be fixed with formaldehyde solution (*Formafix 4%*). Cells were centrifuged in a FACS-tube (round bottom) and resuspended in *Formafix 4%*. After 30-minute incubation at room temperature, the cells were washed once with PBS, resuspended in 300 µL PBS and analyzed at a flow cytometer for eGFP or mCherry fluorescence. A wildtype control was included throughout the experiment.

### *2.2.7.2 Cell sorting of transduced cells*

Fluorescence activated cell sorting (FACS) was used to separate transduced cells from possible remaining wildtype cells, since the selection with antibiotics is not completely accurate. For *in vivo* experiments as well as *Bio Flux*-assays it was essential to have a clean cell population of $eGFP^+$ or $mCherry^+$ cells. The following transduced cells (refer 2.2.2.2) were sorted at a FACS Aria IIIu for $eGFP^+$ or $mCherry^+$ cells:

> TF-1_scr/eGFP, TF-1_scr/mCherry, TF-1_dock1-kd2
> UKE-1_scr/eGFP, UKE-1_scr/mCherry, UKE-1_dock1-kd2
> Molm13_ctrl, Molm13_dock1

### *2.2.7.3 Characterization of cells by cell surface proteins*

To characterize cells by cell surface proteins with flow cytometry, fluorescently labeled antibodies against certain epitopes at the surface of the cell were used (refer Table 10). Cells were incubated with the respective antibodies and analyzed at a flow cytometer.

To determine the infiltration of human blasts within the mouse bone marrow in the *in vivo* early engraftment study (refer 2.2.8.2), the isolated bone marrow cells were stained for $CD45^+$ cells and measured for eGFP-, mCherry- and CD45-expression (refer 2.2.8.2).

For the *in vivo* engraftment study, the isolated cells from bone marrow, peripheral blood, spleen and liver were stained with a live/dead stain as well as with an antibody against CD45. The cells were analyzed by flow cytometry for $eGFP^+$ and $CD45^+$ cells, to evaluate the infiltration with human blasts. Furthermore, bone marrow and spleen cells were stained for HSPCs, using a lineage antibody cocktail and antibodies against tyrosine-protein kinase KIT (cKit) and stem cell antigen-1 (Sca1) (refer 2.2.8.3). The lineage antibody cocktail is designed to stain cells from the major hematopoietic lineages, by recognizing the lineage markers CD3e, CD11b, CD45R, Ly-76, Ly-6G and Ly-6C. HSPCs were identified as lineage marker negative, but Sca1 and cKit positive cells[230].

## 2.2.8 *In vivo* experiments

An AML-xenograft-model was established to study the effect of a *DOCK1*-overexpression and -knockdown in AML cell lines *in vivo*. The main focus of the experiments was on the survival time of the mice and the engraftment of the AML cells within the bone marrow niche.

All *in vivo* experiments were carried out with the approval of the Animal Welfare Officer of the University Medical Center Hamburg-Eppendorf, the local authority (Behörde für Gesundheit und Verbraucherschutz, Fachbereich Veterinärwesen, Hamburg) and ethics review board (Tierversuchsantrag 98/15). The guidelines of the German Animal Welfare Act (Tierschutzgesetz) and the EU Directives on the protection of animals used for scientific purposes (2010/63/EU) were observed.

Animals (refer Table 6) were bred in the UKE animal facility and housed in individually ventilated cages (IVCs) in a defined pathogen-free environment with a 12 hour light cycle at 22 ± 1°C and 55% relative humidity. Water and food were available to the animals without limit.

### *2.2.8.1 Survival studies*

To determine the effect of a *DOCK1*-overexpression or -knockdown on the progression of human AML in immunocompromised mice (NSG or NSGS), the transduced and sorted cells described in section 2.2.2.2 and 2.2.7.2 were used in AML-xenograft-models.

The AML cells were injected into the tail vein in a total volume of 100 µL per mouse, diluted in sterile PBS. For the *in vivo* experiment with transduced Molm13 cells, 0.1 x $10^6$ cells per

mouse were transplanted, for the experiments with transduced TF-1 or UKE-1 cells 1 x $10^6$ cells per mouse were used for transplantation. The mice were monitored daily with regard to their state of health. Based on a scoring list, characteristics such as body weight (measured twice a week), general condition, behavior and trial-specific criteria (*e.g.* occurrence of solid tumors, signs of paralysis) were assessed. In case of severe burden or occurrence of exclusion criteria, the animals were taken out of the experiment. The mice were sacrificed by a lethal injection of Ketanest®/Rompun®-narcotic with 10 µL/g body weight, followed by cervical dislocation. They were examined for the presence of solid tumors and other visible abnormalities (*e.g.* liver appearance). Furthermore, the dimensions and weight of the spleen were measured.

#### *2.2.8.2 Engraftment study*

To analyze the different infiltration of *DOCK1*-knockdown compared to control TF-1 cells within various organs as well as the localization of HSPCs by flow cytometry, an AML-xenograft-study with NSGS mice was performed.

Transduced and sorted TF-1 cells (refer 2.2.2.2 and 2.2.7.2) were used for the experiment. Tail vein transplantation was performed with 1 x $10^6$ cells in 100 µL per mouse. The mice were monitored daily with a scoring list (refer 2.2.8.1) and the experiment was terminated when the first mouse reached one of the exclusion criteria. They were sacrificed by a lethal injection of Ketanest®/Rompun®-narcotic, followed terminal heart puncture and cervical dislocation (refer 2.2.8.1). The tissue of interest (tibiae, femora, coxal bones, liver and spleen) were carefully removed, cleaned and rinsed in PBS. Dimensions and weight of liver and spleen were measured.

##### *Tissue preparation for flow cytometry and staining*

To evaluate the infiltration of AML cells at the time of death, the amount of human blasts (TF-1 cells expressing eGFP, $CD45^+$) in the different tissue was determined by flow cytometry. Furthermore, the amount of HSPCs in bone marrow and spleen was analyzed.

To isolate bone marrow cells, tibiae and coxal bones were crushed three times with a total of 30 mL PBS. To obtain a single cell suspension a 70 µm cell strainer was used and the cells were centrifuged at 300 xg for 5 minutes. The peripheral blood (PB) from terminal heart puncture was mixed with a drop of heparin (2 500 I.E./mL in PBS) immediately after collection to prevent

coagulation. For erylysis, 5 mL hypotonic erylysis buffer were added to the bone marrow cells as well as to peripheral blood. After incubation for 5 minutes at room temperature, the reaction was stopped by adding 10 mL PBS. The cells were harvested by centrifugation at 300 xg for 5 minutes, resuspended in 10 mL PBS and stored on ice until further processing.

To isolate primary cells from spleen and liver, 70 µm cell strainers were used. Half of the spleen and the main part of the liver were carefully homogenized through the mesh of the cell strainer. To obtain a single cell solution the strainer was washed with 10 mL PBS. The cell suspensions were stored on ice until further processing.

The cell number of spleen-, liver- and BM-cell suspensions were determined with the *Vi-Cell™ XR*. Two times 2 x $10^6$ cells were transferred into FACS-tubes and the PB-cell suspension was divided into two tubes. The cells were centrifuged at 400 xg for 5 minutes and resuspended in 100 µL FACS-buffer. Unstained samples were stored at 4°C until further processing. All washing steps of the staining protocol were performed with 3 mL PBS followed by centrifugation at 400 xg for 5 minutes. For live/dead-staining, 5 µL *Zombie NIR* (1:10 dilution) was added to the stained samples and the cells were incubated for 10 minutes at 4°C in the dark. After incubation, the cells were washed once and resuspended in 100 µL FACS-buffer. The antibodies (refer Table 10) were added according to the following scheme (Table 24):

**Table 24: Pipetting scheme for antibody-staining of tissue samples**

| Antibody | Volume [µL] | BM | Spleen | Liver | PB |
|---|---|---|---|---|---|
| CD45-FITC | 5 | + | + | + | + |
| Lin-PerCP/Cy5-5 | 5 | + | + | - | - |
| Sca1-PE/Cy7 | 0.5 | + | + | - | - |
| cKit-APC | 2 | + | + | - | - |

After 20 minute-incubation at 4°C in the dark, the cells were washed once, resuspended in 0.5% formaldehyde for fixation and incubated for 15 minutes at 4°C in the dark. After one washing step, the cells were resuspended in 300 µL PBS and stored at 4°C until flow cytometric analysis.

Fluorescent-minus-one (FMO)-controls were prepared additionally for spleen, liver and BM using exemplary material from one non-transplanted and transplanted mouse (Table 25). For compensation controls wildtype and eGFP-expressing TF-1 cells as well as compensation beads coupled with antibody were used (Table 26).

**Table 25: Pipetting scheme for FMO controls**

| Sample | Cells | CD45-FITC | Lin-PerCP/C5-5 | Sca1-PE/Cy7 | cKit-APC | Zombie NIR |
|---|---|---|---|---|---|---|
| eGFP/CD45-FMO | nt-mouse | - | 5 µL | 0.5 µL | 2 µL | 5 µL |
| Lineage-FMO | nt-mouse + t-mouse | 5 µL | - | 0.5 µL | 2 µL | 5 µL |
| Sca1-FMO | nt-mouse + t-mouse | 5 µL | 5 µL | - | 2 µL | 5 µL |
| cKit-FMO | nt-mouse + t-mouse | 5 µL | 5 µL | 0.5 µL | - | 5 µL |
| Zombie NIR-FMO | nt-mouse + t-mouse | 5 µL | 5 µL | 0.5 µL | 2 µL | - |

nt = not transplanted; t = transplanted

**Table 26: Pipetting scheme for compensation controls**

| Fluorochrome/fluorescent agent | Beads/cells | Antibody (1 µL) |
|---|---|---|
| eGFP | $eGFP^+$ TF-1 + wt TF-1 | - |
| PerCP/Cy5-5 | anti-rat/-hamster Ig beads + neg. beads | Lin-PerCP/Cy5-5 |
| PE/Cy7 | anti-rat/-hamster Ig beads + neg. beads | Sca1-PE/Cy7 |
| APC | anti-rat/-hamster Ig beads + neg. beads | cKit-APC |
| Zombie NIR | anti-mouse Ig beads + neg. beads | human APC/Cy7-coupled antibody |
| Negative control beads | anti-rat/-hamster Ig beads + anti-mouse Ig beads + neg. beads | - |
| Negative control cells | wt TF-1 | - |

wt = wildtype; pos. = positive; neg. = negative

### *2.2.8.3 Early engraftment studies*

To study the early engraftment of *DOCK1*-knockdown AML cells compared to control cells within the bone marrow niche, knockdown- and control-cells were transplanted in parallel into the same animal.

Transduced and sorted cells described in section 2.2.2.2 and 2.2.7.2 were used for transplantation of NSGS mice. The control- and knockdown-cells were mixed 1:1 v/v in sterile PBS and each mouse was receiving 100 µL of the cell mix with 10 x $10^6$ cells/mL by tail vein injection. The mice were monitored daily with a scoring list (refer 2.2.8.1). At day 14 or 15 after transplantation the mice were sacrificed by a lethal injection of Ketanest®/Rompun®-narcotic, followed by cervical dislocation (refer 2.2.8.1). Tibiae, femora and coxal bones were carefully removed, cleaned and rinsed in PBS.

*Preparation of bone marrow cells for flow cytometry and staining*

To evaluate the state of infiltration at the time of death, the amount of human blasts (UKE-1 or TF-1 cells expressing eGFP or mCherry, $CD45^+$) in the bone marrow was determined by flow cytometry.

One tibia or tibiae and coxal bones were opened at one end and centrifuged with the microcentrifuge *myFuge™ Mini* to collect the bone marrow. After adding 500 µL of erylysis buffer, the cells were incubated for 5 minutes at room temperature. The reaction was stopped by adding 500 µL PBS. The cells were harvested by centrifugation at 300 xg for 5 minutes and resuspended in PBS. To obtain a single cell suspension, a 70 µm cell strainer was used.

To stain the cells for FACS analysis the cells were resuspended in 200 µL FACS-buffer and divided into two FACS-tubes (round bottom). One half was stained with CD45-APC antibody, by adding 2.5 µL antibody to 100 µL cell suspension and incubating 20 minutes at 4°C in the dark. After incubation of the cells, both unstained and stained samples, were washed with PBS, resuspended in 300 µL PBS and analyzed at a flow cytometer. For compensation control wildtype, mCherry- and eGFP-expressing AML cells as well as single stained cells or compensation beads with CD45-APC antibody were used. APC-coupled isotype control was included in order to determine unspecific binding of the antibody.

*Cryopreservation of femora for 3D-immunohistochemical staining*

To preserve the bones for immunohistochemical staining, the femora were incubated in PLP-fixative overnight at 4°C. For rehydration of the bone the PLP-fixative was removed and replaced with 20% sucrose in PBS for 2 days. The fixed and rehydrated bones were embedded in the specimen matrix *Tissue-Tek® O.C.T.™ Compound* and stored at -80°C until further processing.

### 2.2.9 3D-immunohistochemical staining

The 3D visualization of engrafted AML cells within whole-mount mouse tissue was achieved by confocal microscopy after immunohistochemical staining and optical tissue clearing.

Cryopreserved samples of mouse tissue (refer 2.2.8.3) were sectioned at a cryostat. Bones were opened from both longitudinal sides until the bone marrow was fully visible. To clear the sections from *Tissue-Tek® O.C.T.™ Compound* the samples were washed several times with

PBS until no residues were left. After blocking overnight at 4°C with 10% donkey serum + 0.2% Triton X-100 in PBS, immunohistochemical staining was performed. Primary antibodies of the respective concentration (refer Table 10) in blocking buffer (10% donkey serum + 0.2% Triton X-100 in PBS) were added to the sample and incubated overnight at 4°C. After washing three to four times with PBS for one hour each at 4°C, the second antibodies diluted 1:400 v/v (refer Table 10) and 4',6-diamidino-2-phenylindole (DAPI) diluted 1:1000 v/v in blocking buffer were added and incubated overnight at 4°C in the dark. The samples were washed once again three to four times with PBS for 1 hour each at 4°C in the dark, followed by optical tissue clearing overnight at 4°C in the dark with *RapiClear®1.52*. After tissue clearing, the samples were embedded in *RapiClear®1.52* on a microscope slide and stored at 4°C in the dark until confocal immunofluorescent microscopy. For image acquisition and analysis LAS AF and ImageJ were used. Determination of eGFP and mCherry positive cells was based on the overlay of the channels and thus difference between the Alexa Fluor™ 488 ($eGFP^+$ cells) and Alexa Fluor™ 568 ($mCherry^+$ cells) signal. Due to a high bleed-through of the Alexa Fluor™ 568 fluorescence emission, the emission of Alexa Fluor™ 568 was also detected in the channel reserved for Alexa Fluor™ 488. Confocal immunofluorescent microscopy was performed in the UKE Microscopy Imaging Facility.

### 2.2.10 Statistics

Statistical analyses were performed using GraphPad Prism 7. For analyses of *in vitro* assays statistics were performed as paired t-test (two-tailed), repeated-measures one-way ANOVA followed by Dunnett´s multiple comparison test or repeated-measures two-way ANOVA followed by Dunnett's or Sidak's multiple comparison test. Survival analyses for the *in vivo* experiments were displayed in a Kaplan-Meier curve. The differences between the survival period within the groups were evaluated with a Log-rank test. Further statistics for analyses of *in vivo* experiments were performed as unpaired t-test with Welch´s correction, paired t-test (two-tailed), one-way ANOVA followed by Holm-Sidak´s multiple comparison test or repeated-measures one-way ANOVA followed by Dunnett´s multiple comparison test. Significance was assumed at a p-value < 0.05. The following levels of significance were defined: $p < 0.05$ = *; $p < 0.01$ = **; $p < 0.001$ = ***; $p < 0.0001$ = ****.

# III. RESULTS

## 3.1 Expression analyses in cell lines and in patient-derived samples

To investigate the expression of different genes of interest in AML cells, RT-qPCR analyses were performed. The expression of the three closely related *DOCK*-variants *DOCK1, DOCK2* and *DOCK5* as well as their cooperating partner *ELMO1* was analyzed in 11 AML cell lines. Further, the expression of the three *DOCK*-variants in 21 pAML-samples was evaluated. ΔCT-method was used for calculation of relative gene expression for the AML cell lines, with normalization to the expression data of the reference gene *GAPDH*. Relative quantification of gene expression for the pAML-samples was performed with the ΔCT-method as well as according to Pfaffl[225], taking the efficiency of the PCR into account, with *GAPDH* as a reference gene. The relative expression data for *DOCK*-genes in cell lines and pAML-samples is visualized in Figure 6 and the individual expression values are shown in Supplementary Tables 1 and 2.

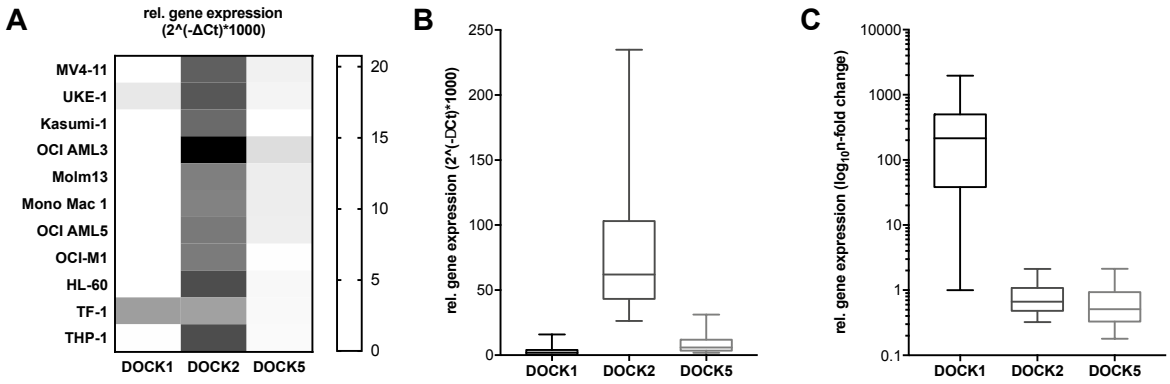


**Figure 6: Relative mRNA expression of *DOCK1, DOCK2* and *DOCK5*.** Relative gene expression was determined by RT-qPCR, with *GAPDH* as a reference gene, in 11 AML cell lines with the ΔCT-method (**A**) and 21 pAML-samples with the ΔCT-method (**B**) as well as according to Pfaffl[225] (**C**). Relative gene expression ratio of AML cell lines was expressed in a heatmap representing the mean values. Relative gene expression ratios of pAML-samples were visualized in a box-and-whiskers plot, displaying the median with whiskers from minimum to maximum.

Only two of the AML cell lines showed a low to moderate endogenous *DOCK1*-expression (UKE-1 1.81, TF-1 7.87), whereas all cell lines expressed *DOCK*2 on a high level. *DOCK5* was relatively low expressed in all cell lines, except Kasumi-1, which did not show any expression. The expression level of *ELMO1* was moderately high for all AML cell lines tested (Supplementary Table 2).

All three *DOCK*-variants were expressed in the tested pAML-samples. The relative expression ratio, resulting from ΔCT-method, is reflecting how highly expressed a gene is. Similar to the

AML cell lines, *DOCK1* (3.01 ± 3.99, n = 21) and *DOCK5* (8.21 ± 6.71, n = 21) showed a moderate expression level. *DOCK2* (76.53 ± 48.74, n = 21), however, showed again a high expression rate in all tested samples. The high standard deviations already indicate that the expression level was highly variable between the single pAML-samples. That became even more evident when the data was analyzed according to the Pfaffl-method[225], which evaluates the n-fold change in expression level relative to a calibrator. The sample with the lowest *DOCK1* expression was selected as calibrator (pAML 09) for all genes. A very variable gene expression could be seen for *DOCK1*, with more than 1000-fold change in expression level compared to the calibrator for individual samples. *DOCK2* and *DOCK5* on the contrary showed a very robust expression level in all samples (*DOCK2*: 0.80 ± 0.43-fold change; *DOCK5*: 0.66 ± 0.45, n = 21). Spearman correlation revealed a negative correlation between the relative mRNA-expression ratio (ΔCT-method) of *DOCK1* and *DOCK5*, r = -0.63, **p < 0.01. In contrast, a positive correlation was observed between the relative mRNA-expression ratio (ΔCT-method) of *DOCK2* and *DOCK5*, r = 0.55, **p < 0.01.

## 3.2 Relevance of DOCK1 in AML-pathophysiology *in vitro*

### 3.2.1 Antileukemic effect of small molecule inhibitors for DOCK1

The antileukemic effect of the small molecule inhibitors TBOPP and CPYPP, kindly provided by Professor Fukui (Division of Immunogenetics, University of Tokyo), was investigated. A reduced proliferation and colony formation of AML cells reflects the antileukemic properties of a compound. CPYPP is classified as a DOCK2 inhibitor, but also has comparable high affinity and inhibitory activity for DOCK1 and DOCK5[221]. TBOPP was identified as a DOCK1-selective inhibitor, without affecting the biological functions of DOCK2 and DOCK5[222]. Both compounds are inhibiting the catalytic activity of the DOCK proteins by reversible binding to the DHR-2 domain[221,222].

#### *3.2.1.1 Effect of small molecule inhibitors CPYPP and TBOPP on the proliferation of AML cells*

To investigate the antileukemic effect of the small molecule inhibitors CPYPP and TBOPP and to determine their $IC_{50}$ values in the respective AML cell lines, proliferation assays were performed over the duration of one week. The *DOCK1* expressing cell lines UKE1 and TF-1 as well as the non-expressing cell line Molm13 were treated with different inhibitor

concentrations (5-100 µM) and the viable cell number, normalized to the solvent control, was determined after three and six days (Figure 7). The $IC_{50}$ value was calculated based on the cell number after three days of treatment.

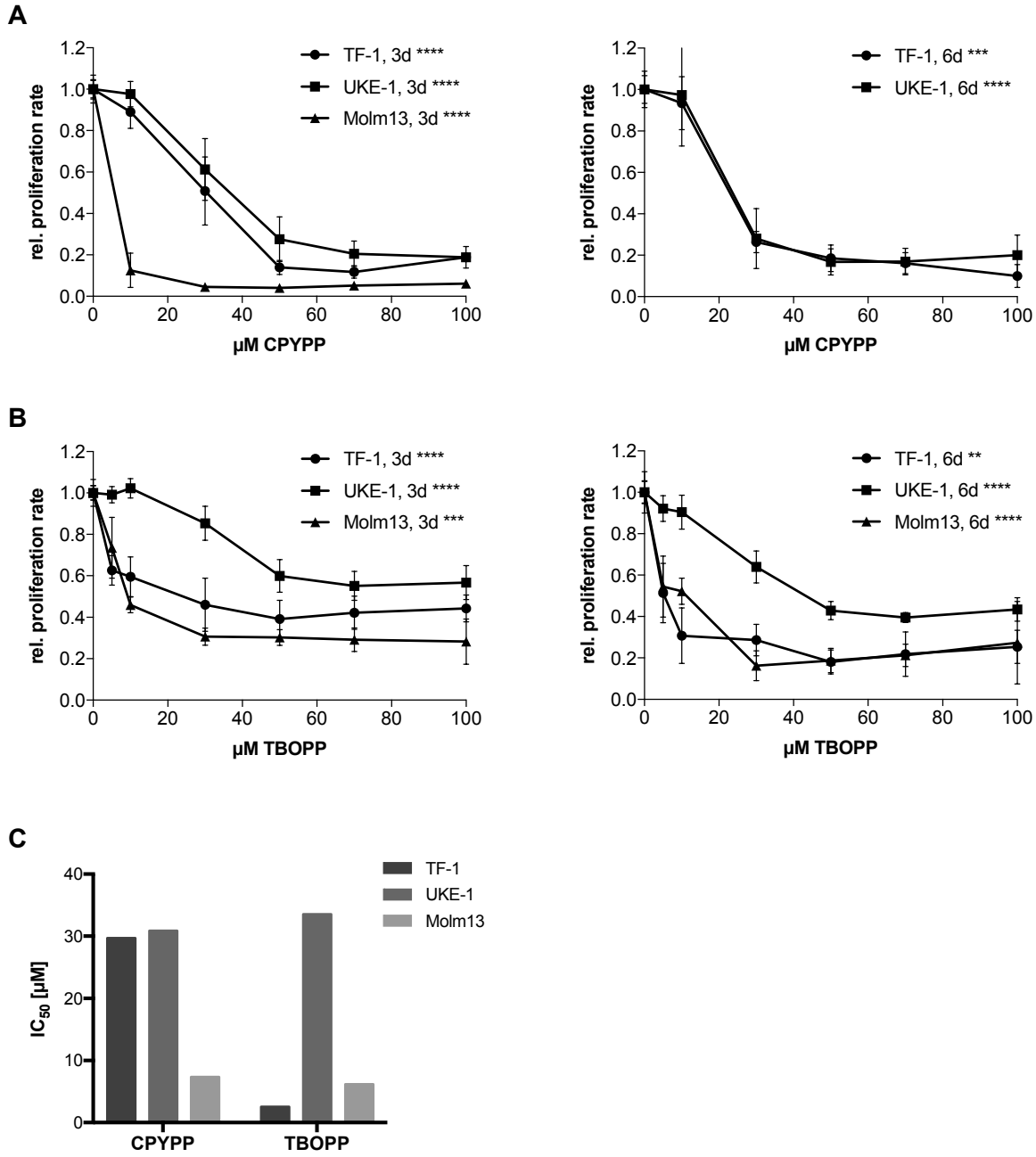


**Figure 7: Antiproliferative effect of CPYPP and TBOPP in AML cell lines.** TF-1, UKE-1 and Molm13 cells were treated with the small molecule inhibitors CPYPP (**A**) and TBOPP (**B**) in triplicates for three and six days and the number of viable cells was determined. Data are displayed as the mean ± standard deviation (SD) of three independent experiments, each normalized to the solvent control (0 µM). Statistics were performed as repeated-measures one-way ANOVA followed by Dunnett´s multiple comparison test. The $IC_{50}$ values (**C**) for all cell lines were calculated based on three independent experiments with the IC50 Calculator (ATT Bioquest). Levels of significance: $p < 0.05$ = *; $p < 0.01$ = **; $p < 0.001$ = ***; $p < 0.0001$ = ****

Both DOCK-inhibitors showed a clear antiproliferative effect in all three AML cell lines already three days after seeding. The reduction in the proliferation rate was statistically significant for

both time points and all cell lines. The unspecific DOCK-inhibitor CPYPP had the strongest effect in Molm13 cells ($IC_{50}$ = 7.35 µM). Detection of viable cells at the second time point was not possible. The dose-response relationship of CPYPP in TF-1 ($IC_{50}$ = 29.71 µM) and UKE-1 ($IC_{50}$ = 30.88 µM) was very similar, in both cell lines a dose-dependent reduction to approximately 0.2-fold, compared to the control, could be observed. The DOCK1-selective inhibitor TBOPP showed the highest effect in the *DOCK1*-expressing cell line TF-1 ($IC_{50}$ = 2.55 µM), followed by the non-expressing cell line Molm13 ($IC_{50}$ = 6.12 µM). The *DOCK1*-expressing cell line UKE-1 was the least sensitive cell line tested for TBOPP ($IC_{50}$ = 33.56 µM). The findings suggest that both inhibitors are able to reduce the proliferation rate of AML cell lines effectively, but independent of the expression of *DOCK1*.

The findings in the AML cell lines could be confirmed in primary AML samples. pAML cells were treated accordingly to the cell lines and the viable cell number, normalized to the solvent control, was determined after three to four days as well as after six to seven days (Figure 8). Both inhibitors showed a clear dose-dependent inhibitory effect on the cell proliferation in most of the pAML samples. Only two samples did not show a high sensitivity to TBOPP. The examination for the expression of the *DOCK*-variants from the corresponding samples (refer Figure 6, Supplementary Tables 1) showed no direct correlation between the response to the inhibitors and the expression pattern, even though both samples, which were insensitive to TBOPP, had a low *DOCK1* expression. This underlines the assumption that the antiproliferative properties of both inhibitors are independent of *DOCK1* expression.

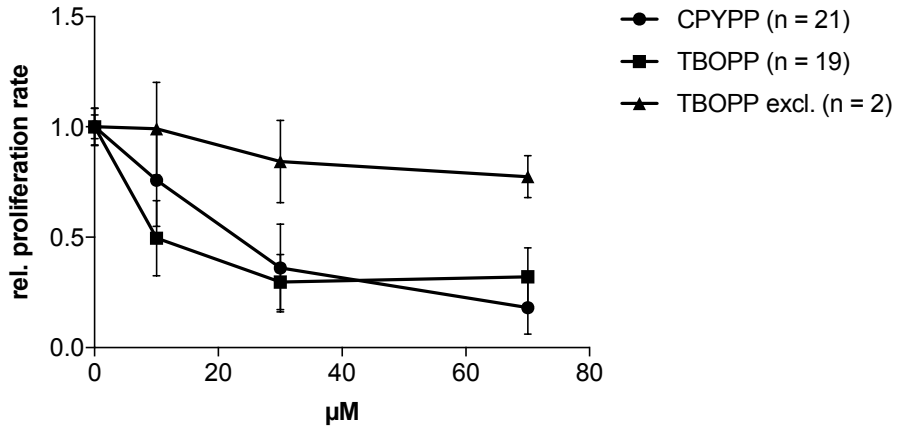


**Figure 8: Antiproliferative effect of CPYPP and TBOPP in pAML samples after three to four days.** pAML cells were treated with the small molecule inhibitors CPYPP and TBOPP in triplicates for three to four days. The number of viable cells was determined and normalized to the solvent control (0 µM). Data for the first timepoint (3-4 days) are displayed as the mean ± SD of 21 samples.

*3.2.1.2 Effect of small molecule inhibitors CPYPP and TBOPP on colony formation of AML cells*

Hematopoietic stem and progenitor cells (HSPCs) as well as leukemic cells show the ability to proliferate and form colonies in semi-solid medium. Each colony is derived from a single cell; therefore, the number of colonies is reflecting the clonal proliferation and differentiation potential of these cells. The ability of cancer cells to proliferate independently of external growth factors and their immortality are two hallmarks of cancer[231,232]. The colony formation assay allows to investigate these abilities *in vitro*, also in response to various treatments and genetic knockdown or overexpression. Therefore, the antileukemic effect of the small molecule inhibitors CPYPP and TBOPP was investigated in the three AML cell lines, used in the previous proliferation assays. The results of two independent experiments are shown in Figure 9.

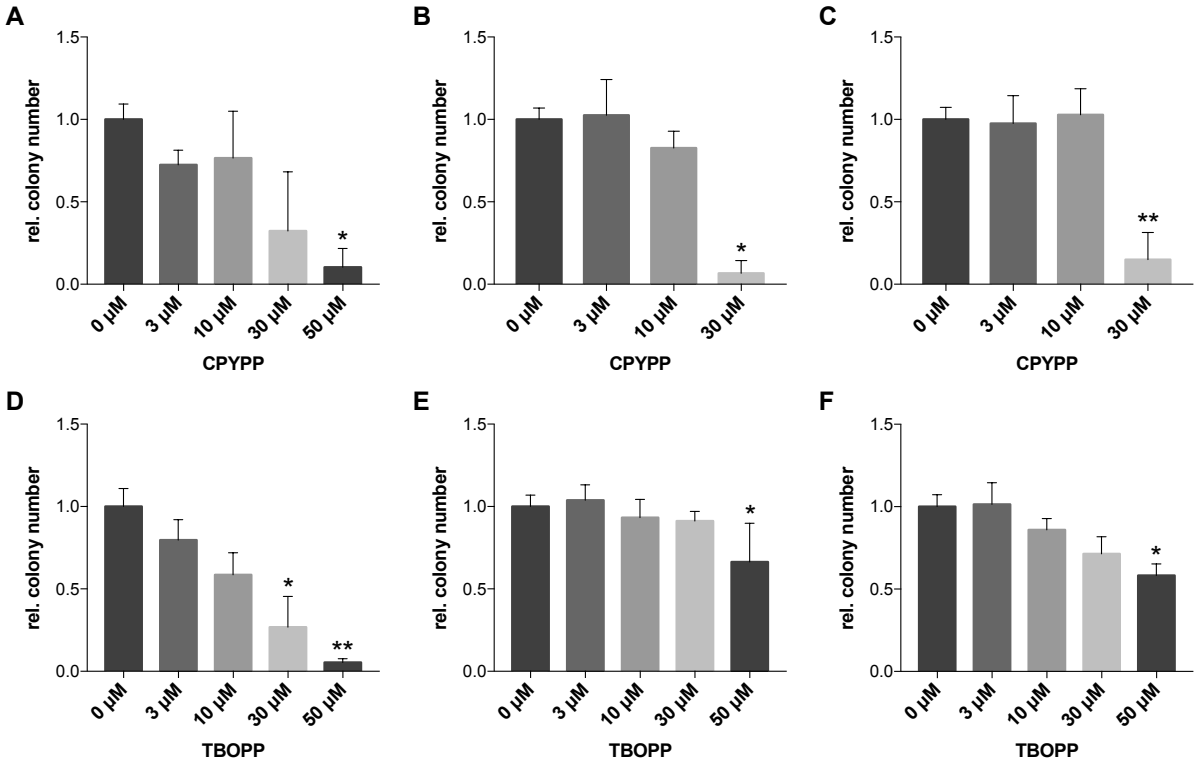


**Figure 9: Effect of CPYPP and TBOPP on colony forming abilities in AML cell lines.** TF-1 (**A**, **D**), UKE-1 (**B**, **E**) and Molm13 (**C**, **F**) cells were treated with the small molecule inhibitors CPYPP and TBOPP in triplicates for one week. The number of colonies was determined and normalized to the solvent control (0 µM). Data are displayed as the mean ± SD of two independent experiments. Statistics were performed as repeated-measures one-way ANOVA followed by Dunnett's multiple comparison test. Levels of significance: $p < 0.05$ = *; $p < 0.01$ = **; $p < 0.001$ = ***; $p < 0.0001$ = ****

Both DOCK-inhibitors displayed a dose-dependent effect on the colony forming abilities of AML cells. Due to high standard deviation, the dose-dependent decrease in relative colony number by CPYPP in TF-1 cells (Figure 9 A) was statistically significant only for the highest

concentration tested. For the two other cell lines, UKE-1 and Molm13, the unspecific DOCK-inhibitor was showing a significant effect with regard to the inhibitor concentration. Both cell lines were insensitive to low inhibitor concentrations, but showed strong sensitivity at higher concentrations. The highest concentration tested (50 µM) inhibited the colony formation completely. Similar to the effect on the proliferation rate, the DOCK1-selective inhibitor TBOPP had the strongest effect in *DOCK1*-expressing TF-1 cells. The non-expressing cell line Molm13 showed a significant, but not so strong sensitivity to the DOCK1-selective TBOPP, compared to TF-1 cells. UKE-1 cells had once again the least sensitivity to TBOPP. The results support the hypothesis that the effects of the inhibitors are independent of the DOCK homologs.

### 3.2.2 Effect of DOCK1-, ELMO1- or combined shRNA-based knockdown or DOCK1 overexpression

To verify the antileukemic effect of the small molecule inhibitors for DOCK proteins, CPYPP and TBOPP, a stable shRNA-based knockdown of *DOCK1* and *ELMO1* alone or in combination in AML cell lines UKE-1 and TF-1 as well as a stable overexpression of *DOCK1* in AML cell line Molm13 was generated (refer 2.2.2.2). Functional *in vitro* and *in vivo* analyses were performed, to investigate the influence of DOCK1 to the pathophysiology of AML.

#### *3.2.2.1 Lentiviral cloning approaches*

For functional *in vitro* and *in vivo* experiments, a stable downregulation or overexpression of *DOCK1* as well as a stable downregulation of its binding partner *ELMO1* was to be achieved through lentiviral transduction of AML cell lines. For the virus production the regarding shRNA or cDNA had to be cloned into LeGO-vectors[219,220]. The vectors integrate into the host genome and allow expression of one shRNA or transgene in addition to a fluorescent marker protein and selection site.

*shRNA-plasmids*

For the knockdown of *DOCK1* and *ELMO1*, two distinct shRNAs that are directed against the respective gene were each selected from a set of five MISSION® shRNA plasmids. For *DOCK1*, the respective set of MISSION® shRNA plasmids were previously evaluated regarding the knockdown capacity. Based on the preliminary data two shRNAs were chosen for the cloning

approach. The knockdown capacity of the five MISSION® shRNA plasmids directed against *ELMO1* was evaluated as part of this thesis (refer 2.2.2.1 and 2.2.2.2; data not shown). Both selected shRNAs against *DOCK1* were subcloned into *LeGO G/puro*$^+$ and both *ELMO1*-shRNAs into *LeGO C/zeo*$^+$ (refer 2.2.3.5). The successful cloning was verified by sequencing (data not shown).

*DOCK1 transgene-plasmid*

The *MGC premier cDNA clone for DOCK1* (Gene ID: 1793, Genebank accession: BC146857), carrying the plasmid *hDOCK1-pCR-XL-TOPO* was used as a cDNA source for the overexpression-cloning. After alignment to the mRNA sequence of *DOCK1* transcript variant 2 (NM_001380.4), the sequence of the cDNA insert (BC146857) showed several nucleotide base substitutions. One of the point-mutations causes an amino acid exchange, while all others represent silent mutations (Figure 10). At position 3613 bp the cDNA sequence contains guanine whereas the mRNA sequence contains adenine instead, leading to a missense mutation (asparagine in human protein, aspartic acid resulting from cDNA sequence). Site-directed mutagenesis was performed to achieve the substitution of the concerning nucleotide (refer 2.2.3.6). The successful mutagenesis was confirmed by sequencing. The mutant cDNA was further subcloned into the lentiviral backbone *LeGO iG2/puro*$^+$ and the successful cloning was once again confirmed by sequencing (data not shown).


**Figure 10: Missense mutation in *DOCK1* cDNA clone at position 3613 bp.** Single nucleotide exchange at position 3613 bp leads to an amino acid exchange. *DOCK1* transcript variant 2 translates into asparagine (Asn), whereas the cDNA clone translates to aspartic acid (Asp).

### *3.2.2.2 Evaluation of transduction efficiency and antibiotic selection*

To evaluate the transduction efficiency and selection of transduced cells, the percentages of eGFP$^+$ or mCherry$^+$ cells were determined by flow cytometry four days after transduction and for shRNA-based knockdown again after one week of antibiotic selection (refer 2.2.7.1). For

*DOCK1*-overexpressing cells, the efficiency of antibiotic selection was evaluated before cell sorting.

The efficiency for single transduced cells was determined by the percentage of corresponding marker protein expressing cells. For double transduced cells, only double positive cells were taken in account. The results for transduction and selection efficiency are listed in Table 27.

**Table 27: Transduction and selection efficiencies of independent transduction approaches in UKE-1, TF-1 and Molm13 cells**

| Approach | Transduced cells | $E_T$ T1 [%] | $E_T$ T2 [%] | $E_T$ T3 [%] | $E_S$ T1 [%] | $E_S$ T2 [%] | $E_S$ T3 [%] |
|---|---|---|---|---|---|---|---|
| shRNA-based single knockdown | TF-1_scr/eGFP | 17.21 | 37.08 | 75.01 | 98.24 | 98.20 | 99.11 |
| | TF-1_scr/mCherry | 21.82 | 44.12 | - | 70.79 | 64.79 | - |
| | TF-1_dock1-kd1 | 12.39 | 14.45 | 61.78 | 88.55 | 88.60 | 94.02 |
| | TF-1_dock1-kd2 | 16.77 | 26.50 | 78.45 | 98.18 | 98.01 | 98.96 |
| | TF-1_elmo1-kd1 | 27.39 | 17.17 | - | 72.60 | 64.67 | - |
| | TF-1_elmo1-kd2 | 16.14 | 33.47 | - | 69.54 | 57.94 | - |
| | UKE-1_scr/eGFP | 20.68 | 26.47 | - | 98.35 | 98.00 | - |
| | UKE-1_scr/mCherry | 31.83 | 20.65 | - | 90.70 | 78.11 | - |
| | UKE-1_dock1-kd1 | 23.24 | 20.33 | - | 88.79 | 89.28 | - |
| | UKE-1_dock1-kd2 | 19.72 | 37.55 | - | 97.84 | 98.32 | - |
| | UKE-1_elmo1-kd1 | 13.17 | 28.92 | - | 90.69 | 76.78 | - |
| | UKE-1_elmo1-kd2 | 23.11 | 16.39 | - | 89.95 | 79.95 | - |
| shRNA-based double-knockdown | TF-1_scr | 1.09 | - | - | 80.17 | - | - |
| | TF-1_dock1-dkd | 4.62 | - | - | 68.97 | - | - |
| | TF-1_dock1/elmo1-kd1 | 7.26 | - | - | 67.57 | - | - |
| | TF-1_dock1/elmo1-kd2 | 9.96 | - | - | 81.07 | - | - |
| | UKE-1_scr | 3.32 | - | - | 80.5 | - | - |
| | UKE-1_dock1-dkd | 3.73 | - | - | 83.1 | - | - |
| | UKE-1_dock1/elmo1-kd1 | 4.40 | - | - | 76.3 | - | - |
| | UKE-1_dock1/elmo1-kd2 | 4.32 | - | - | 78.2 | - | - |
| Overexpression | Molm13_ctrl | 7.7 | 21.2 | - | 97.1 | 98.3 | - |
| | Molm13_dock1 | 0.3 | 0.1 | - | 1.4 | 12.3 | - |

$E_T$ = Transduction efficiency; $E_S$ = Selection efficiency; T = Transduction Number; kd = knockdown; dkd = double-knockdown; scr = scrambled

### *3.2.2.3 Verification of shRNA-based knockdown and overexpression in transduced AML cells on mRNA and protein level*

Cells, transduced with shRNA, were verified for their knockdown capacity by RT-qPCR after one week of antibiotic selection and on a regular basis throughout the cultivation period, to ensure the maintenance of the knockdown (refer 2.2.3.3). *DOCK1*-overexpressing Molm13 cells were tested for their *DOCK1* mRNA expression regularly after cell sorting. *In vitro* and *in vivo* experiments were carried out with cells verified for the presence of knockdown or overexpression.

The relative mRNA expression for *DOCK1* and *ELMO1* normalized to the reference gene *GAPDH* in transduced cells is shown in Figure 11. The knockdown in *DOCK1*- or *ELMO1*-shRNA transduced cells was determined in comparison to scrambled-shRNA transduced cells, which served as controls. Overexpression in transduced Molm13 cells was compared to cells transduced with the empty LeGO-vector, which did not show any *DOCK1*-expression.

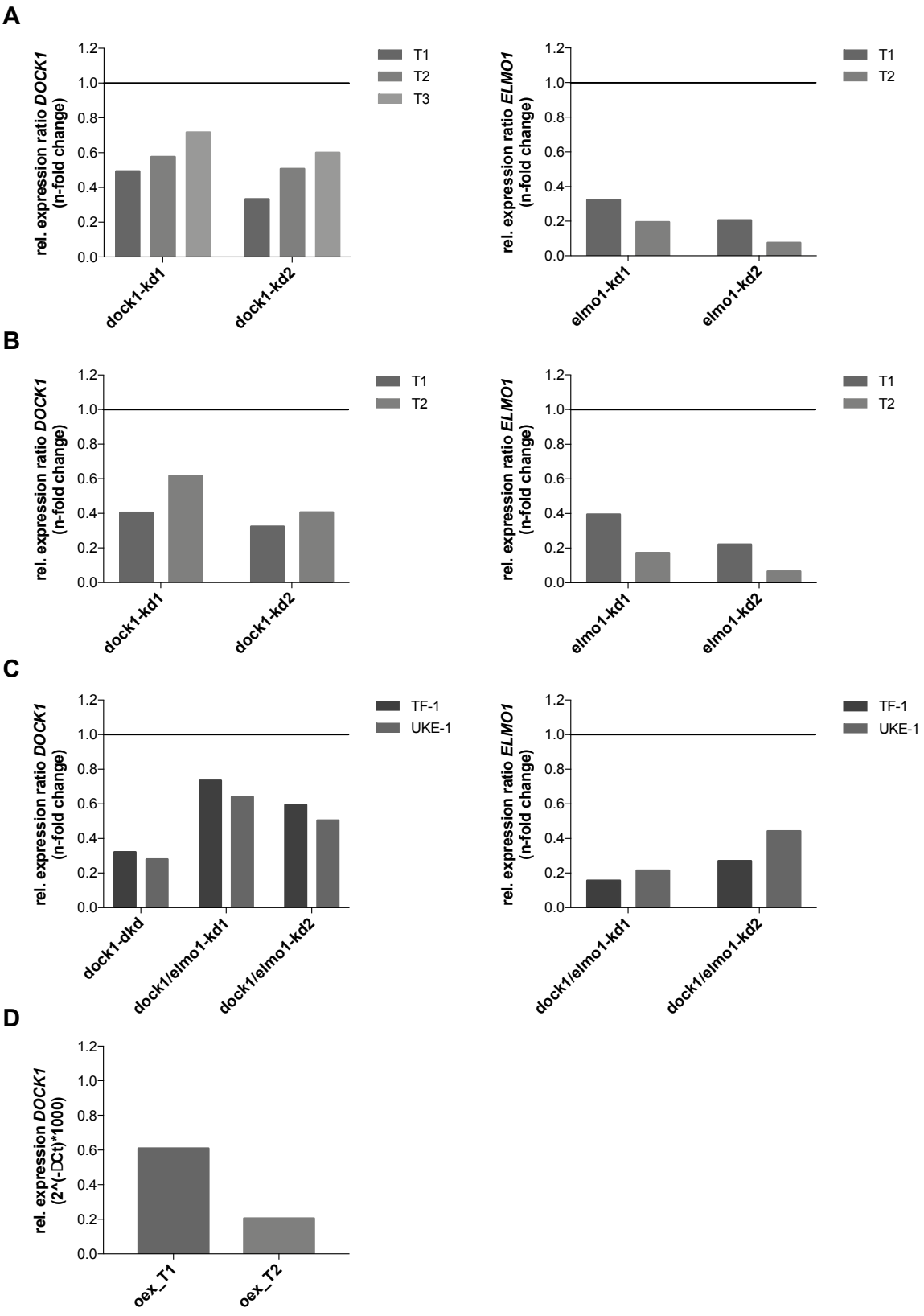


**Figure 11: Relative *DOCK1*- and *ELMO1*-mRNA expression in transduced cell lines.** RT-qPCR analyses were performed after one week of antibiotic selection for all single transduction approaches with *DOCK1*- and *ELMO1*-shRNA in TF-1 (**A**) and UKE-1 (**B**) as well as for the double transduction (**C**). Relative gene expression was determined according to Pfaffl[225] with the respective scrambled-shRNA transduced cells serving as calibrator (represented as a black line). *DOCK1* overexpression in Molm13 (**D**) was verified after cell sorting. The relative *DOCK1*-expression was evaluated using the ΔCT-method.

In all cells transduced with *DOCK1*- or *ELMO1*-shRNA, a successful downregulation of the genes *DOCK1* or *ELMO1* could be achieved (Figure 11 A-C). Stable *DOCK1* mRNA expression could be shown in Molm13 cells transduced with the overexpression-plasmid (Figure 11 D). The knockdown and overexpression were stable throughout the cultivation period of the cells (data of the follow-up verification is not shown).

Furthermore, the knockdown of DOCK1 could be verified on protein level by Western Blot analyses (refer 2.2.5.1, 2.2.5.3, 2.2.5.4). Samples were collected during the cultivation period of the cells. Figure 12 shows representative Western Blot results for the first and second single knockdown approach for DOCK1 in TF-1 and UKE-1 cells.

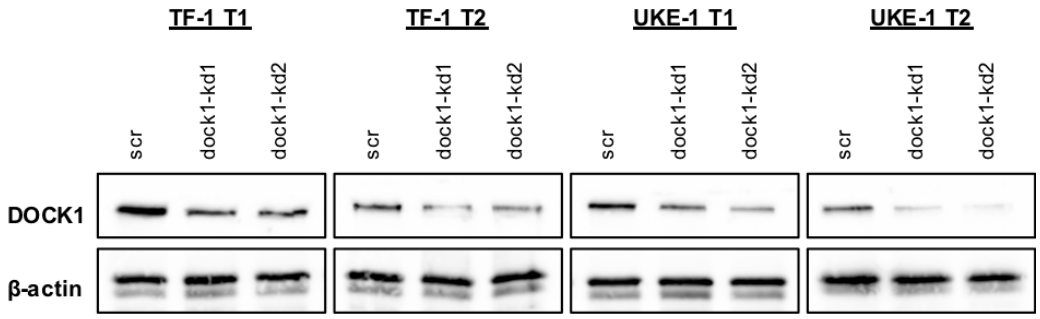


**Figure 12: DOCK1-knockdown on protein level.** Western blot analysis of single DOCK1-knockdown in TF-1 and UKE-1, after first (T1) and second (T2) transduction. DOCK1 protein expression is displayed, with β-actin as reference protein.

A successful downregulation of DOCK1 on protein level could be achieved for all single and double transduction approaches. This downregulation was stable throughout the cultivation period (data not shown).

### *3.2.2.4 Effect of DOCK1-, ELMO1- or combined shRNA-based knockdown or DOCK1 overexpression on the proliferation of AML cells*

The effect of a targeted shRNA-based knockdown of *DOCK1* and *ELMO1* alone or in combination on the proliferative capacity of the AML cell lines UKE-1 and TF-1 over a duration of one week was investigated (refer 2.2.6.1). The number of viable cells was determined three (data not shown) and six days after cell seeding. The influence of *DOCK1*-overexpression on the proliferation in the AML cell line Molm13 was analyzed accordingly (Figure 13).

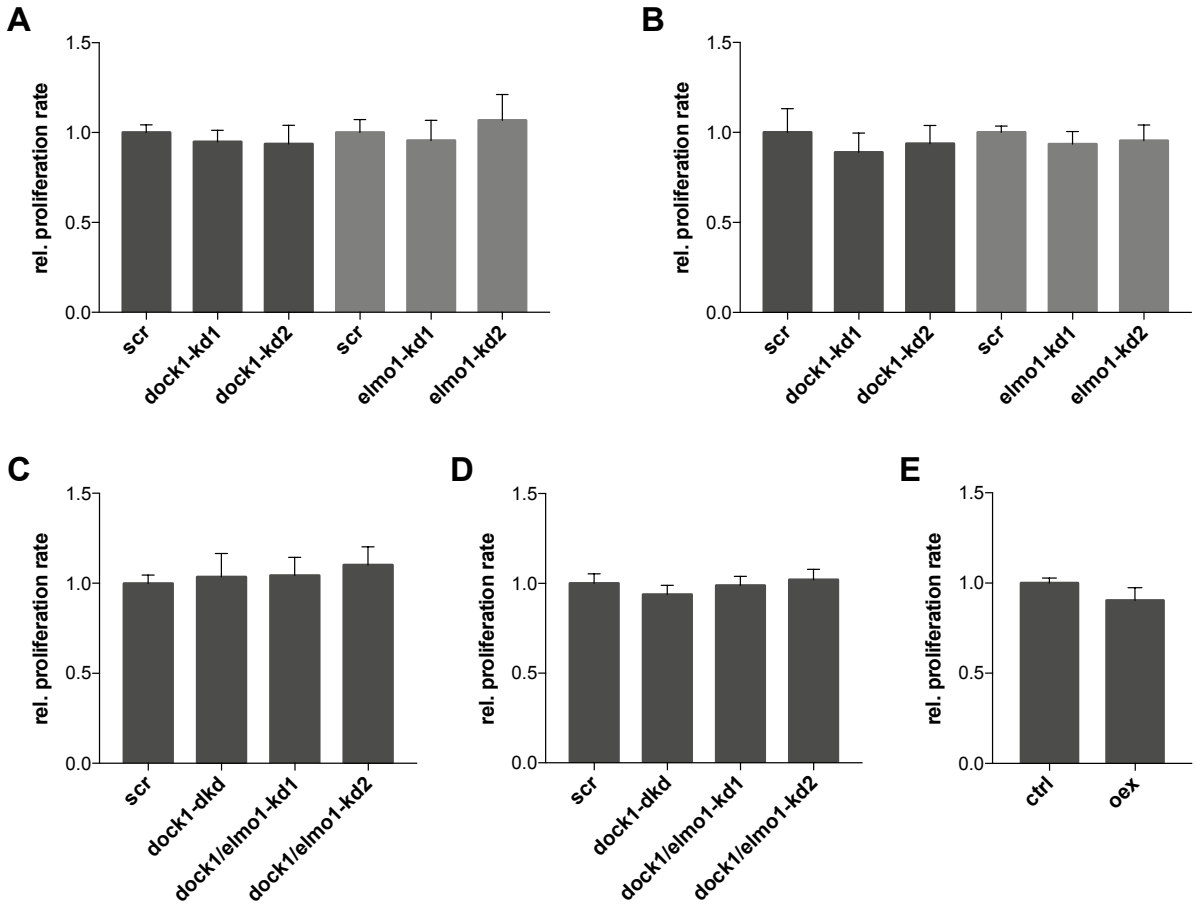


**Figure 13: Effect of a *DOCK1* or *ELMO1* shRNA-based knockdown or *DOCK1* overexpression on the proliferation of AML cells.** Transduced cells and their respective controls were seeded in triplicates in the same cell density and the number of viable cells was determined after six days. The cell number was normalized to the respective control and is expressed as mean ± SD of at least three independent experiments. Statistics were performed as repeated-measures one-way ANOVA followed by Dunnett's multiple comparison test for shRNA-based knockdown cells and paired t-test (two-tailed) was performed for *DOCK1*-overexpressing cells. No significant differences could be seen. Single transduced TF-1 with shRNA (**A**). Single transduced UKE-1 with shRNA (**B**). shRNA-double transduced TF-1 (**C**). shRNA-double transduced UKE-1 (**D**). *DOCK1*-overexpression in Molm13 (**E**).

Both, the targeted knockdown of *DOCK1* and of its cooperating partner *ELMO1* alone or in combination, could not reproduce the antiproliferative effect of the small molecule DOCK-inhibitors (refer 3.2.1). Overall the proliferation of the knockdown cells remained unaffected in comparison to the control cells. Furthermore, a *DOCK1*-overexpression in the highly proliferating Molm13 cells did not have any significant influence on the proliferation capacity.

### *3.2.2.5 Effect of DOCK1-, ELMO1- or combined shRNA-based knockdown or DOCK1 overexpression on colony formation of AML cells*

The colony forming abilities of TF-1 and UKE-1 cells after a *DOCK1*- or *ELMO1*-knockdown alone or in combination were investigated compared to the respective scrambled control. The

effect of *DOCK1*-overexpression on the clonogenic properties in the AML cell line Molm13 was analyzed accordingly (refer 2.2.6.2).

Cells with a verified knockdown or overexpression were seeded with the same cell density in a semi-solid medium. After a growth period of 5-7 days, the number of colonies was determined.

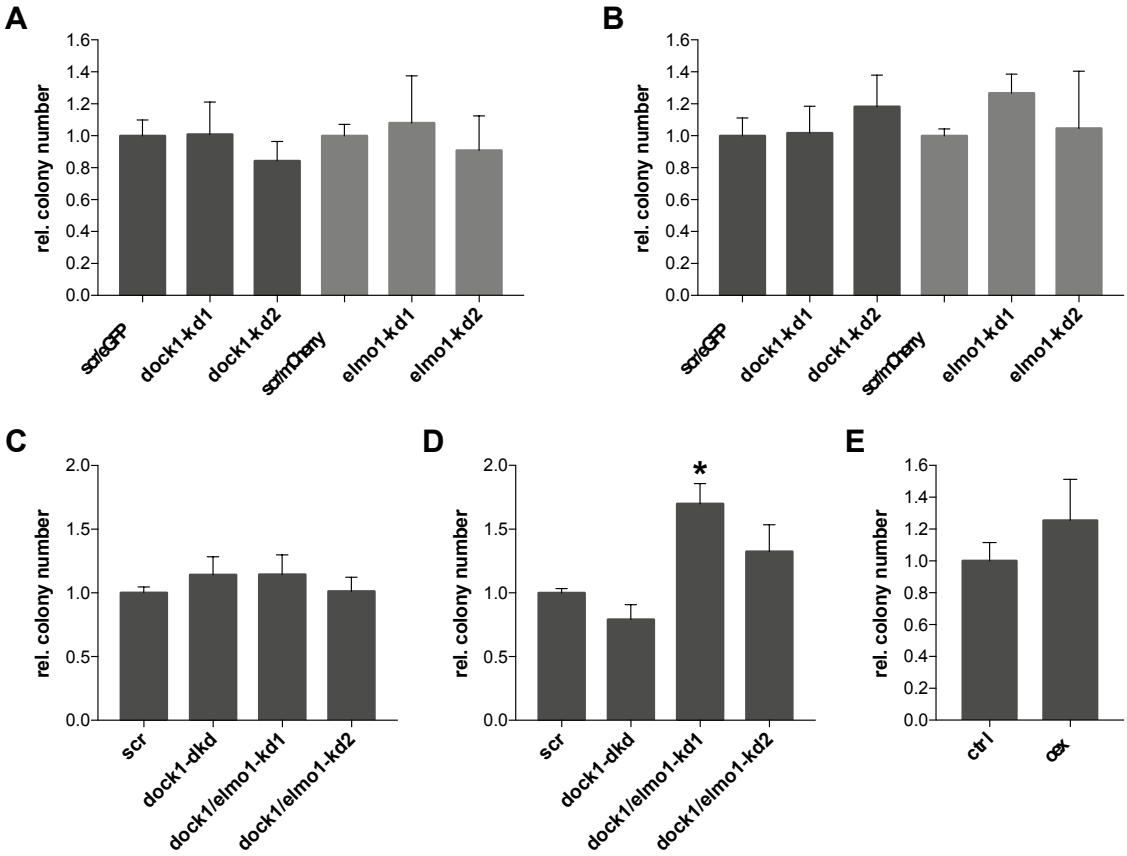


**Figure 14: Effect of a *DOCK1* or *ELMO1* shRNA-based knockdown or *DOCK1* overexpression on the colony forming abilities of AML cells.** With *DOCK1*- or *ELMO1*-shRNA single transduced TF-1 (**A**) and UKE-1 (**B**) as well as their respective scrambled-transduced control cells were seeded in the same cell density in a semisolid medium and the number of colonies was determined after 5-7 days with an inverted microscope. The colony number was normalized to the respective control and is expressed as the mean ± SD of three independent experiments. Double transduced TF-1 (**C**) and UKE-1 (**D**) cells were examined the same way in two independent experiments. Statistics were performed as repeated-measures one-way ANOVA followed by Dunnett's multiple comparison test. For *DOCK1*-overexpressing Molm13 (**E**) compared to their respective control cells, three independent experiments were performed. Paired t-test (two-tailed) was performed for statistical analysis. Levels of significance: $p < 0.05$ = *; $p < 0.01$ = **; $p < 0.001$ = ***; $p < 0.0001$ = ****

Overall, neither the knockdown nor the overexpression of *DOCK1* showed any significant effect on the colony forming abilities. Only the combined *DOCK1*- and *ELMO1*-knockdown in UKE-1 cells showed an increased number of colonies compared to the respective control, with a significant increase in relative colony number to 1.70 ± 0.12-fold ($p = 0.0107$, $n = 3$) for dock1/elmo1-kd1 and a non-significant increase to 1.33 ± 0.23-fold ($p = 0.1014$, $n = 3$) for dock1/elmo1-kd2.

### *3.2.2.6 Effect of DOCK1 shRNA-based knockdown or DOCK1 overexpression on adhesion properties of AML cells in a microfluidic system*

Sinusoidal endothelial cells are the key regulators for the trafficking of HSPCs as well as leukemic cells within the perivascular niche[103,122]. Upon adhesion to endothelial cells, AML cells are able to migrate or even integrate into the endothelium[103,152]. Since Rac-dependent signaling is important for migration and invasion[168], *DOCK1* modification might influence the adhesion properties of AML cells. BioFlux™ 200 device was used to analyze the adhesion properties of AML cells to endothelial cells under controlled shear flow conditions within a microfluidic system. Live cell assays with transduced and sorted *DOCK1* knockdown or overexpression cells (refer 3.2.2.2 and 3.2.2.3) were performed in HUVEC-coated flow channels (70 µm tall x 350 µm wide) mimicking the vascular environment. Adhesion and cell rolling of AML cells could be observed (Figure 15). The number of attached AML cells was determined after five minutes of controlled shear flow with 1 dyn/cm$^2$ (Figure 16). Within the bone marrow microvasculature, cellular trafficking takes place exclusively in sinusoids, with hematopoietic cell rolling and adhesion events as well as transendothelial migration of mature leukocytes and immature HSC[163]. Sinusoids show a higher permeability and a lower blood flow speed as well as shear stress compared to arterial vessels[163,164]. Bixel *et al*. showed that shear stress in sinusoidal capillaries is approximately 2.9 ± 2.7 dyn/cm$^2$, but can be even below 1 dyn/cm$^2$, whereas in arterial vessels it is much higher (65.5 ± 16.0 dyn/cm$^2$)[164]. The rolling behavior of different cell types on the endothelium is markedly influenced by shear stress, with a reduced rolling cell fraction with shear stress over 2-3 dyn/cm$^2$ [164,233,234]. Therefore, 1 dyn/cm$^2$ was chosen for the experimental setup.

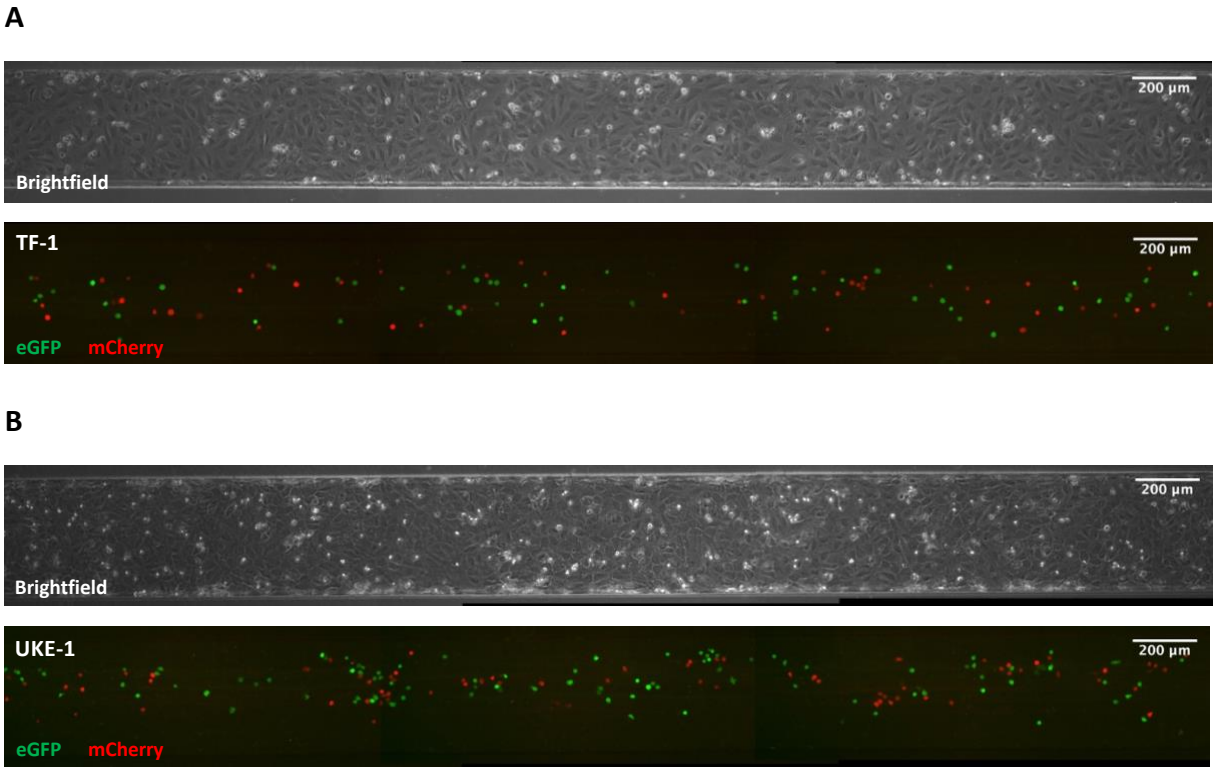


**Figure 15: Cell adhesion at HUVEC-coated microfluidic channels.** (**A**) Top: TNF-α stimulated endothelial cell layer, formed under gravity flow, before applying the shear flow. Bottom: Attached leukemic cells (TF-1_scr/mCherry and TF-1_dock1-kd2/eGFP) after 5 minutes of controlled shear flow (1 dyn/cm$^2$). (**B**) Top: TNF-α stimulated endothelial cell layer, formed under gravity flow, before applying the shear flow. Bottom: Attached leukemic cells (UKE-1_scr/mCherry and UKE-1_dock1-kd2/eGFP) after 5 minutes of controlled shear flow (1 dyn/cm$^2$).

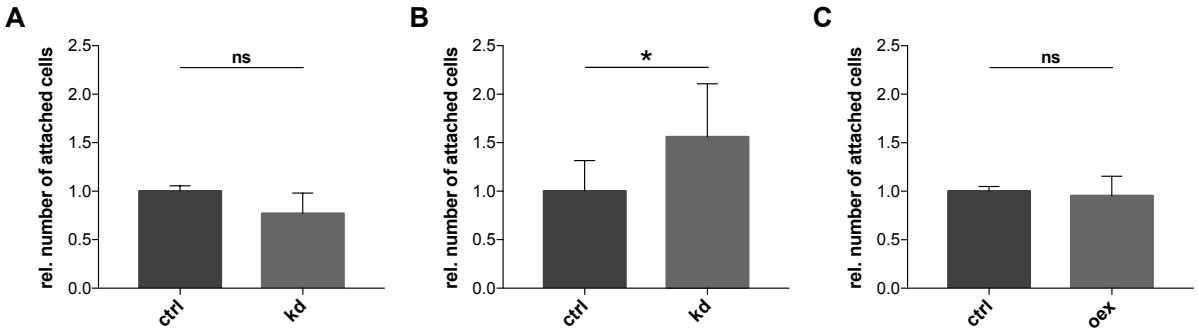


**Figure 16: Effect of *DOCK1* knockdown or overexpression on the adhesion properties in AML cell lines.** Single transduced cells in $CO_2$-independent medium (c = 2 x 10$^6$ cells/mL) were perfused with 1 dyn/cm$^2$ in a HUVEC-coated microfluidic channel (minimum 80% confluency). Prior the experiment, HUVEC cells were stimulated with 10 ng/mL TNF-α for 4-5 hours. Number of cells attached to the HUVEC layer was determined after 5 minutes of controlled shear flow in duplicates. For TF-1 (**A**) and UKE-1 (**B**), mCherry-labeled control cells and eGFP-labeled knockdown cells were perfused as a 1:1-cell mix into the same channel. For Molm13 (**C**), eGFP-labeled control and overexpression cells were perfused simultaneously in separate channels. The cell number was normalized to the respective control and is expressed as the mean ± SD of at least three independent experiments. Statistics were performed as paired t-test (two-tailed). Levels of significance: $p < 0.05$ = *; $p < 0.01$ = **; $p < 0.001$ = ***; $p < 0.0001$ = ****

The knockdown of *DOCK1* in TF-1 cells did not show any significant effect on the adhesion properties of the cells. A light reduction in the number of attached cells could be observed for the knockdown cells compared to control cells (0.77 ± 0.22-fold, n = 4), but due to high variability between the assays, the observed difference was statistically not significant (p = 0.0678). Contrary to our hypothesis, in UKE-1 cells the knockdown of *DOCK1* resulted in a statistically significant increase of attached cells (1.53 ± 0.42-fold, p = 0.0374, n = 4). The overexpression of *DOCK1* in Molm13 cells did not show any influence on the adhesion properties of the cells.

## 3.3 Relevance of DOCK1 in AML-pathophysiology *in vivo*

### 3.3.1 Survival studies

To determine the effect of a *DOCK1*-overexpression or -knockdown on the progression of human AML in immunocompromised mice (NSG or NSGS), the transduced and sorted cells described in section 3.2.2.2 and 3.2.2.3 were used in AML-xenograft-models, after verification of knockdown or overexpression. Xenotransplantation models with NSG and NSGS mice are well described for promoting engraftment of human AML cells[235,236].

The following xenograft studies were performed:

> TF-1_dock1-kd2 vs. TF-1_scr/eGFP in NSGS mice
>
> UKE-1_dock1-kd2 vs. UKE-1_scr/eGFP in NSG mice
>
> Molm13_dock1 vs. Molm13_ctrl in NSG mice

#### *3.3.1.1 Progression of a TF-1 xenograft-model*

Two independent experiments in NSGS mice were performed. For xenotransplantation of TF-1 cells, NSGS mice, which are characterized by the expression of human IL3, GM-CSF and SCF, were used due to the GM-CSF dependency of the TF-1 cells. For the first experiment, 5-6-week-old female mice were transplanted with 1 x $10^6$ cells per mouse intravenously, with five animals for the control group (TF-1_scr/eGFP) and six animals for the experimental group (TF-1_dock1-kd2). The second experiment was carried out accordingly with 4-week-old male mice, with eight mice for the control group and nine mice for the experimental group. The mice were monitored daily with regard to their state of health and in case of severe burden or occurrence of exclusion criteria, the animals were taken out of the experiment. The main

focus of the experiment was the survival period. No significant survival benefit for either group could be observed (Figure 17 A, B). The mean survival for the control group was 24.6 ± 0.6 days (n = 5) in the first experiment and 25.5 ± 1.2 days (n = 8) in the second experiment. For the experimental group, the mean survival was 24.3 ± 0.5 days (n = 6) in the first experiment and 25.2 ± 1.7 days (n = 9) in the second experiment. Next to the survival period, the dimensions of the spleen were measured after exitus (Figure 17 C-F). Significant differences in spleen size as well as spleen weight between control and experimental group could be demonstrated. The spleen was significantly enlarged in terms of size and weight within the control cohort (first experiment (n =5): 1.26 ± 0.05 cm ($p = 0.0017$), 61.8 ± 7.9 mg ($p = 0.0024$); second experiment (n = 8): 1.23 ± 0.07 cm ($p = 0.0005$), 50.5 ± 13.7 mg ($p = 0.0605$)) compared to the experimental group (first experiment (n = 6): 1.12 ± 0.04 cm, 42.5 ± 6.1 mg; second experiment (n = 9): 1.06 ± 0.09 cm, 39.0 ± 7.8 mg).

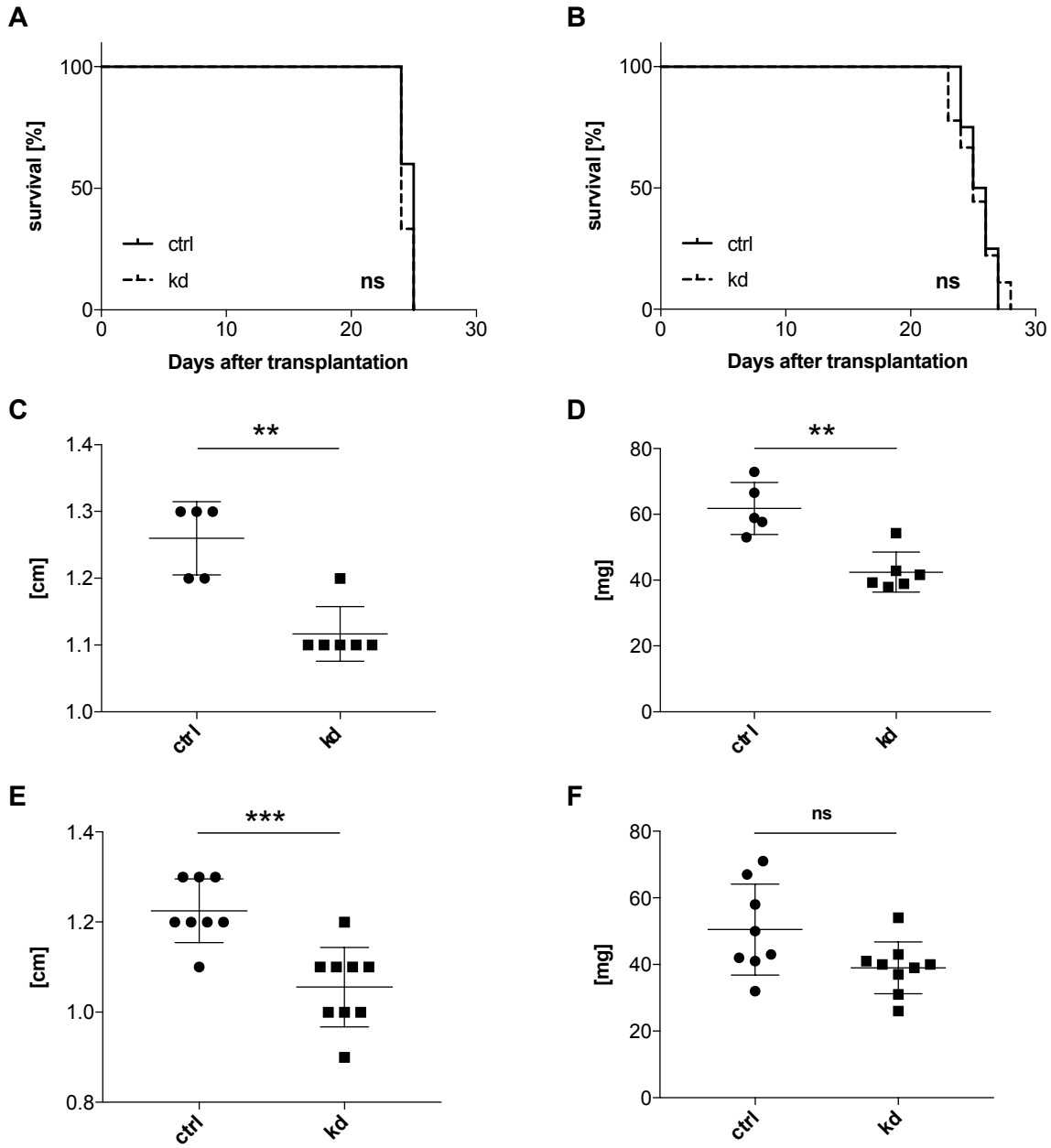


**Figure 17: Progression of a TF-1 xenograft mouse-model, with *DOCK1*-knockdown versus scrambled-control.** Two independent experiments with five to nine NSGS mice per cohort transplanted with 1 x $10^6$ cells were performed. Kaplan-Meier survival curves showed no significant effect with Log-rank test for both experiments (**A**, **B**). The span and weight of the spleen were measured for the first (**C**, **D**) and second (**E**, **F**) experiment. Data are displayed as mean ± SD. Statistics were performed as unpaired t-test with Welch´s correction. Levels of significance: $p < 0.05$ = *; $p < 0.01$ = **; $p < 0.001$ = ***; $p < 0.0001$ = ****

### *3.3.1.2 Progression of a UKE-1 xenograft-model*

One survival study with *DOCK1*-knockdown versus control UKE-1 cells in NSG mice was performed. For each cohort ten 18-22-week-old female mice were transplanted with 1 x $10^6$ cells intravenously. In accordance to the TF-1 xenograft-model, the mice were monitored daily and taken out of the experiment, when they reached one of the exclusion criteria. The survival period was determined. Similar to the previous experiments with TF-1

cells, no significant difference in survival could be observed (Figure 18 A). Mean survival for the control group (UKE-1_scr/eGFP) was 80.2 ± 21.8 days (n = 10) and in the experimental group (UKE-1_dock1-kd2) 73.0 ± 14.4 days (n = 10). The dimensions and weights of the spleens were measured and similar to the TF-1 xenograft-model, the spleen was significantly enlarged within the control group (Figure 18 C, D). The mean span of the spleen was 1.45 ± 0.16 cm (p = 0.0181) in the control group (n = 10) compared to 1.25 ± 0.18 cm in the experimental group (n = 10). The mean spleen weight was in the control group 80.75 ± 24.23 mg (p = 0.0104) and 48.24 ± 26.49 mg in the experimental group. In the progression of the UKE-1 induced AML, most mice developed various kinds of solid tumors (*e.g.* ovarian, tubal, subcutaneous). The overall tumor mass was measured, to determine the tumor burden, but no significant difference could be found between the groups (Figure 18 B). The mean tumor burden in the control group was 726.3 ± 619.0 mg and in the experimental group 409.7 ± 332.4 mg.

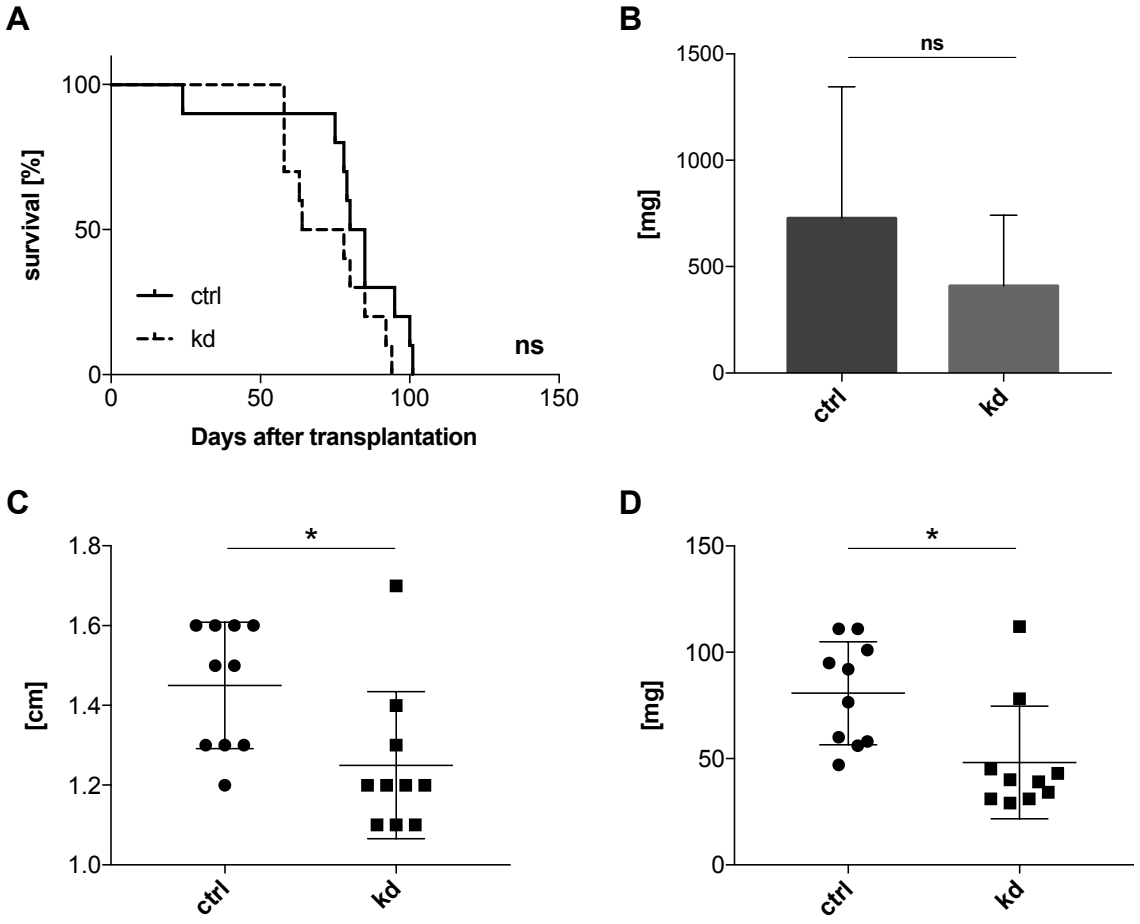


**Figure 18: Progression of a UKE-1 xenograft mouse-model, with *DOCK1*-knockdown versus scrambled-control.** Ten NSG mice per cohort were transplanted with 1 x $10^6$ cells. The Kaplan-Meier survival curve showed no significant effect with Log-rank test (**A**). The tumor burden was determined by the overall tumor mass per mouse and is expressed as the mean ± SD from 10 mice per cohort (**B**). The span and weight of the spleen showed a significant difference in an unpaired t-test with Welch´s correction (**C**, **D**). Data are displayed as mean ± SD. Levels of significance: p < 0.05 = *; p < 0.01 = **; p < 0.001 = ***; p < 0.0001 = ****

### *3.3.1.3 Progression of a Molm13 xenograft-model*

To verify the findings from the previous experiments with the *DOCK1*-knockdown AML cells, an experiment with *DOCK1*-overexpressing Molm13 compared to the control Molm13 cells in 9-10-week-old female NSG mice was performed. Ten mice per cohort were transplanted intravenously with 0.1 x $10^6$ cells per mouse. The mice were monitored daily in accordance to the previous xenograft-models with knockdown cells and taken out of the experiment, when they reached one of the exclusion criteria. A small but significant survival benefit could be observed for the experimental group (Molm13_dock1) compared to the control group (Molm13_ctrl), with a mean survival time for the control group of 13.3 ± 0.7 days (n = 10) and 14.5 ± 1.3 days (n = 10) for the experimental (Figure 19 A). For the span and weight of the spleen, the opposite effect to the previous experiments with the knockdown cells could be observed. The spleen was significantly enlarged within the experimental group (Figure 19 B, C). The mean span of the spleen was 1.76 ± 0.14 cm (p = 0.0049) in the control group (n = 10), whereas in the experimental group (n = 10) the mean span was 1.93 ± 0.09 cm. In the control group, the mean spleen weight was 139.0 ± 36.8 mg (p = 0.0016) and in the experimental group 191.3 ± 22.2 mg.

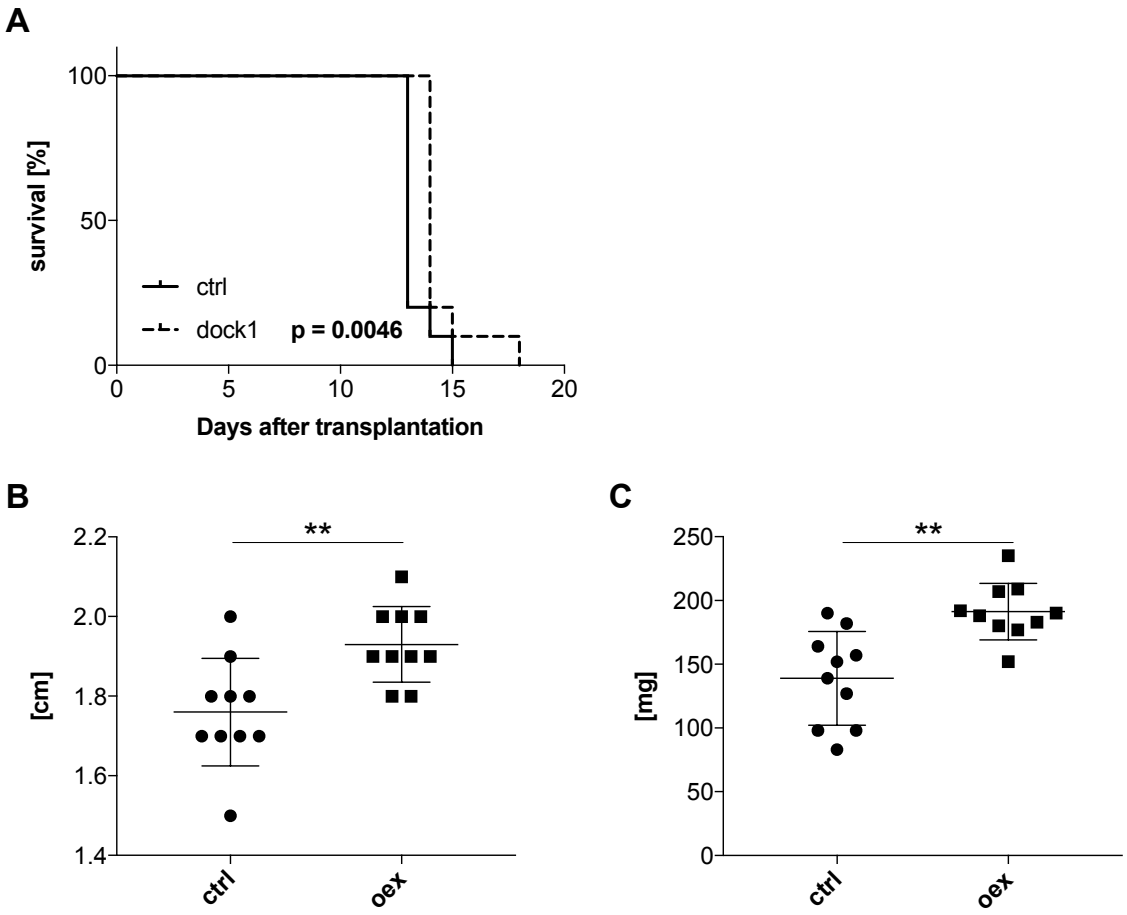


**Figure 19: Progression of a Molm13 xenograft mouse-model, with *DOCK1*-overexpression versus control.** Ten NSG mice per cohort were transplanted with 0.1 x $10^6$ cells. The Kaplan-Meier survival curve showed a significant survival benefit for the overexpression group with a Log-rank test (**A**). The span and weight of the spleen showed a significant difference in an unpaired t-test with Welch´s correction (**B**, **C**). Data are displayed as mean ± SD. Levels of significance: $p < 0.05$ = *; $p < 0.01$ = **; $p < 0.001$ = ***; $p < 0.0001$ = ****

The data of all performed survival studies indicate that the progression of human AML in immunocompromised mice with regard to the overall survival is independent of DOCK1 expression. The weight and span of the spleen, however, differ significantly depending on the *DOCK1*-expression of the transplanted AML cells. *DOCK1*-expressing AML cells cause greater enlargement of the spleen in immunocompromised mice than AML cells with no or reduced *DOCK1*-expression. Splenomegaly, due to extramedullary infiltration, is a well described characteristic in human AML that is occurring in some patients[237,238]. The mechanism when and why extramedullary infiltration occurs is still unclear. The findings of the survival studies indicate that DOCK1 might be involved in the extramedullary infiltration of the spleen.

### 3.3.2 Engraftment study

Duarte *et al*. could show in AML mouse models that the infiltration of leukemic blasts in the spleen was delayed compared to the bone marrow infiltration and that there is a negative correlation between HSPC numbers in spleen and BM[165]. With increasing AML infiltration in the BM, the number of HSPCs is progressively decreasing. In the spleen, however, the number of HSPCs is increasing during AML progression[165]. To study the effect of a *DOCK1*-knockdown on leukemic infiltration of bone marrow, peripheral blood, spleen and liver as well as the localization of HSPCs by flow cytometry, an AML-xenograft-model with 4-week-old female NSGS mice was performed. Transduced and sorted TF-1 knockdown and control cells, described in section 3.2.2.2 and 3.2.2.3, were used after knockdown-verification, for intravenous transplantation with 1 x $10^6$ cells per mouse. Three groups were included in the study:

1. Healthy control group (n = 3)
2. Wt control group (n = 6): TF-1_scr/eGFP
3. Knockdown group (n = 6): TF-1_dock1-kd2

The mice were monitored daily and the experiment was terminated, when the first mouse reached one of the exclusion criteria. In accordance to the survival analyses, the dimensions of spleen as well as the weight of liver were measured (Figure 20). By including a healthy control group, splenomegaly could be confirmed in the AML xenograft model. Both, the wt control group and the knockdown group showed a significantly enlarged spleen compared to the healthy control. The mean weight of the spleen in the healthy control group was 20.0 ± 1.0 mg (n = 3), in the wt control group 46.3 ± 8.9 mg (n = 6) and in the knockdown group 48.5 ± 10.0 mg (n = 6). The mean spleen span was 0.9 ± 0.0 cm in the healthy control group, 1.22 ± 0.08 cm in the wt control group and 1.07 ± 0.10 cm in the knockdown group. Interestingly, the two AML xenotransplanted groups compared to each other, showed a significant difference just in spleen span, but not in the spleen weight, indicating that the greater enlargement in the *DOCK1*-expressing group observed in the survival studies (refer 3.4.1) is taking place at a very late stage of AML progression. The measurement of the liver weight showed a light but due to small sample size and high standard deviation non-significant hepatomegaly in the two AML groups compared to the healthy control group. The mean weight of the liver was 1.06 ± 0.08 g in the healthy control group, 1.17 ± 0.15 g in the wt control group and 1.29 ± 0.14 g in the knockdown group.

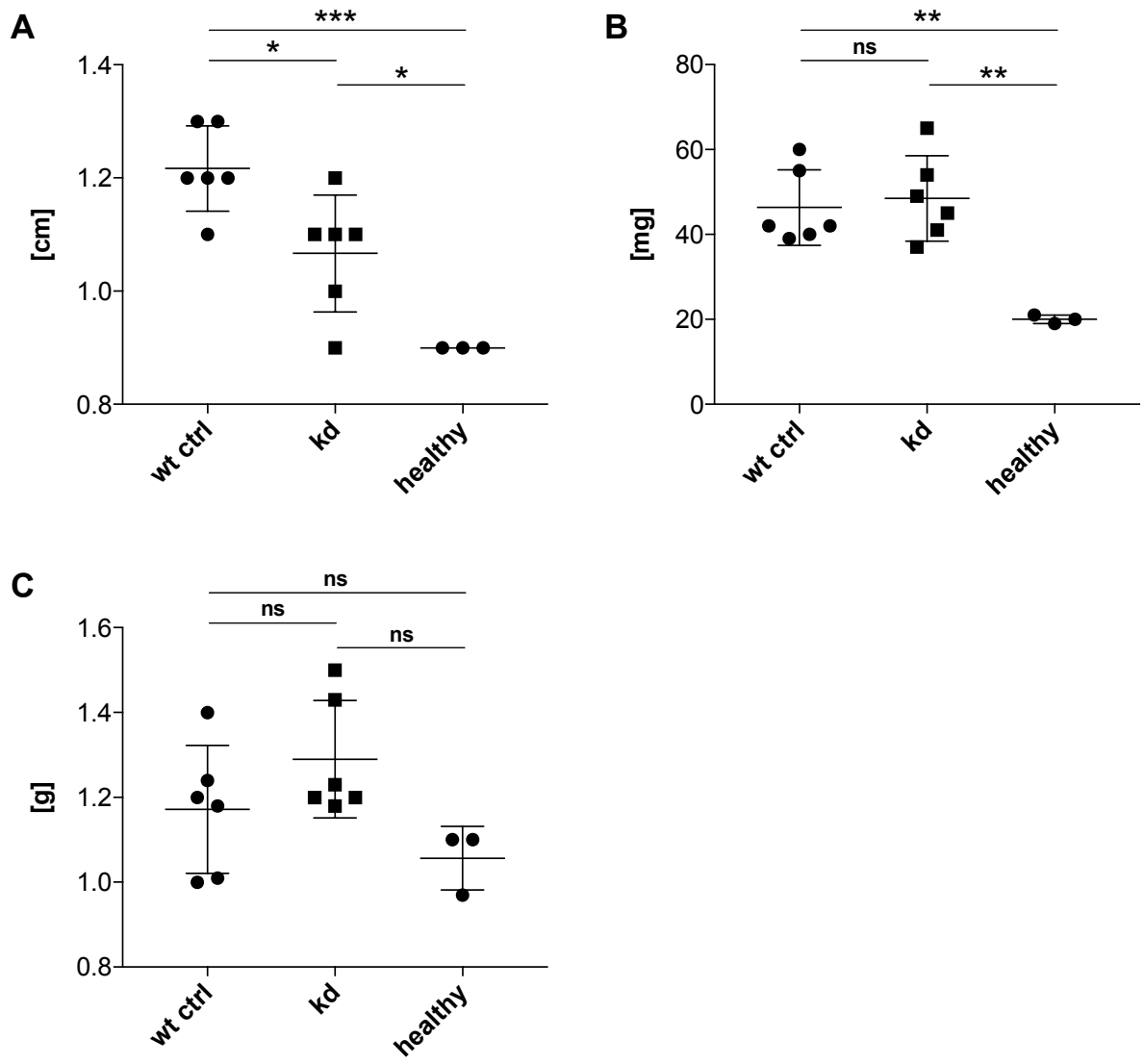


**Figure 20: Comparison of organ dimensions of a TF-1 xenograft mouse-model including a healthy control with *DOCK1*-knockdown versus scrambled-control.** Six NSGS mice per AML cohort were transplanted with 1 x $10^6$ cells, a non-transplanted group of three NSGS mice was included. Measurement of the organ dimensions after 22 days, including spleen span (**A**) and spleen weight (**B**) as well as liver weight (**C**). Significant splenomegaly in the AML xenotransplant groups compared to the healthy control could be observed. Statistics were performed as one-way ANOVA followed by Holm-Sidak´s multiple comparison test. Data are displayed as mean ± SD. Levels of significance: $p < 0.05$ = *; $p < 0.01$ = **; $p < 0.001$ = ***; $p < 0.0001$ = ****

Flow cytometric analysis showed no significant differences between the two xenotransplanted groups in infiltration of the various organs at the moment of experiment termination (Figure 22 A, C, E, F). The bone marrow infiltration was approximately 30% in both AML xenotransplant groups (wt control group: 30.52 ± 4.72%; knockdown group: 28.38 ± 7.27%). Extramedullary infiltration was much lower in both groups. Approximately 0.2% leukemic blasts could be found in the spleen (wt control group: 0.275 ± 0.145%; knockdown group: 0.189 ± 0.115%), 0.05-0.1% in the peripheral blood (wt control group: 0.097 ± 0.097%; knockdown group: 0.049 ± 0.018%) and approximately 2-4% in the liver

(wt control group: 4.07 ± 2.75%; knockdown group: 2.11 ± 2.15%). The distribution of HSPCs between bone marrow and spleen was evaluated (Figure 22 B, D). A significant decrease in the number of HSPCs in the bone marrow and a significant increase in the spleen was observed after AML infiltration. Between the both AML xenotransplant groups a significant difference could be observed only within the bone marrow. The *DOCK1*-expressing control TF-1 cells were displacing the HSPCs more strongly than the knockdown cells. These findings indicate an involvement of DOCK1 in the egress of HSPCs from the bone marrow, but not in the relocation to the spleen. The mean number of HSPCs within the bone marrow of healthy mice (n = 3) was 4.43 ± 0.81% and within the spleen only 0.46 ± 0.12%. In the wt control group (n = 6), the mean number of HSPCs was decreased to 1.45 ± 0.27% within the bone marrow and increased to 1.51 ± 0.46% within the spleen. For the knockdown group (n = 6), the mean number of HSPCs within the bone marrow was decreased to 2.22 ± 0.58% and increased to 1.28 ± 0.34% within the spleen. The gating strategy for the experiment is shown in Figure 21. HSPCs were defined as Lin$^-$ Sca1$^+$ cKit$^+$ cells[230] and leukemic blasts were defined as eGFP$^+$/CD45$^+$ cells.

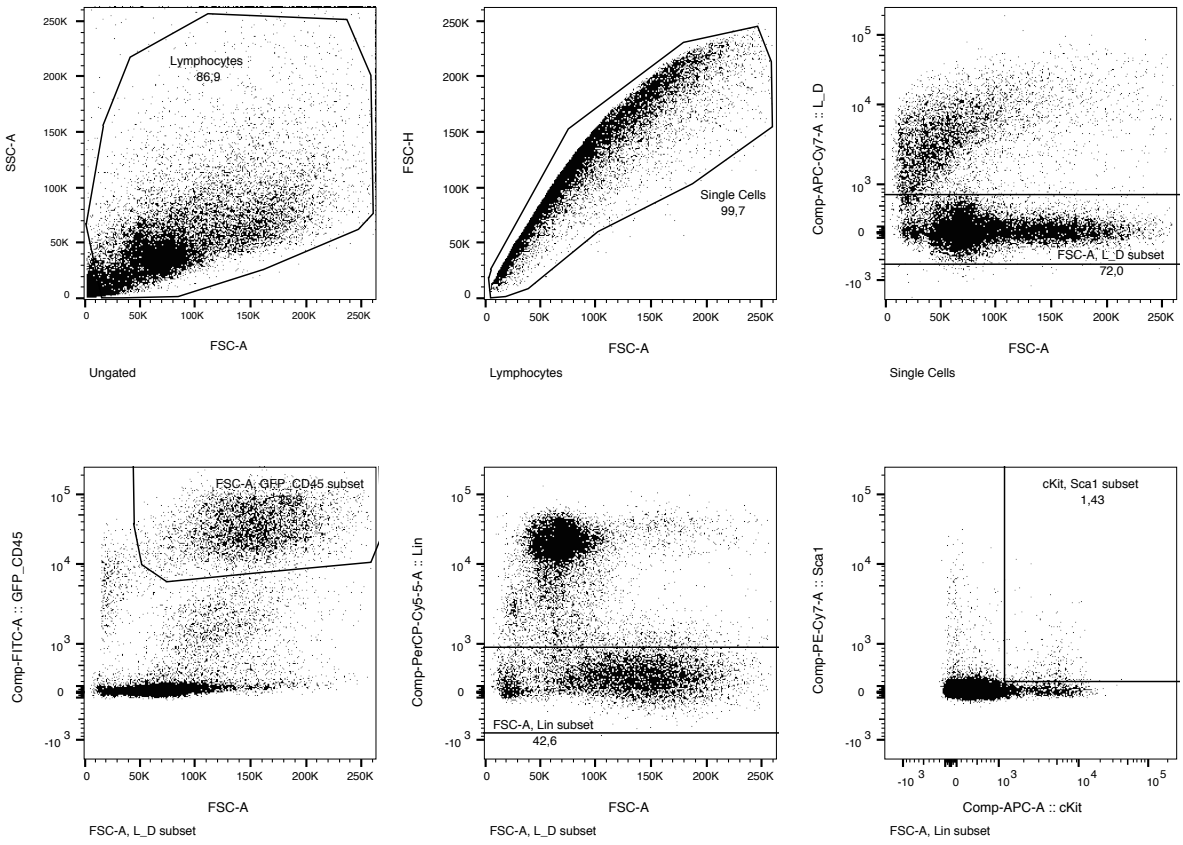


**Figure 21: Gating strategy for flow cytometric analysis of TF-1 xenograft study.** Gating strategy for HSPC (Lin$^-$ cKit$^+$ Sca$^+$ after live / dead exclusion) and AML blasts (eGFP/CD45$^+$ after live / dead exclusion) is displayed exemplary with a bone marrow sample from the wt control group.

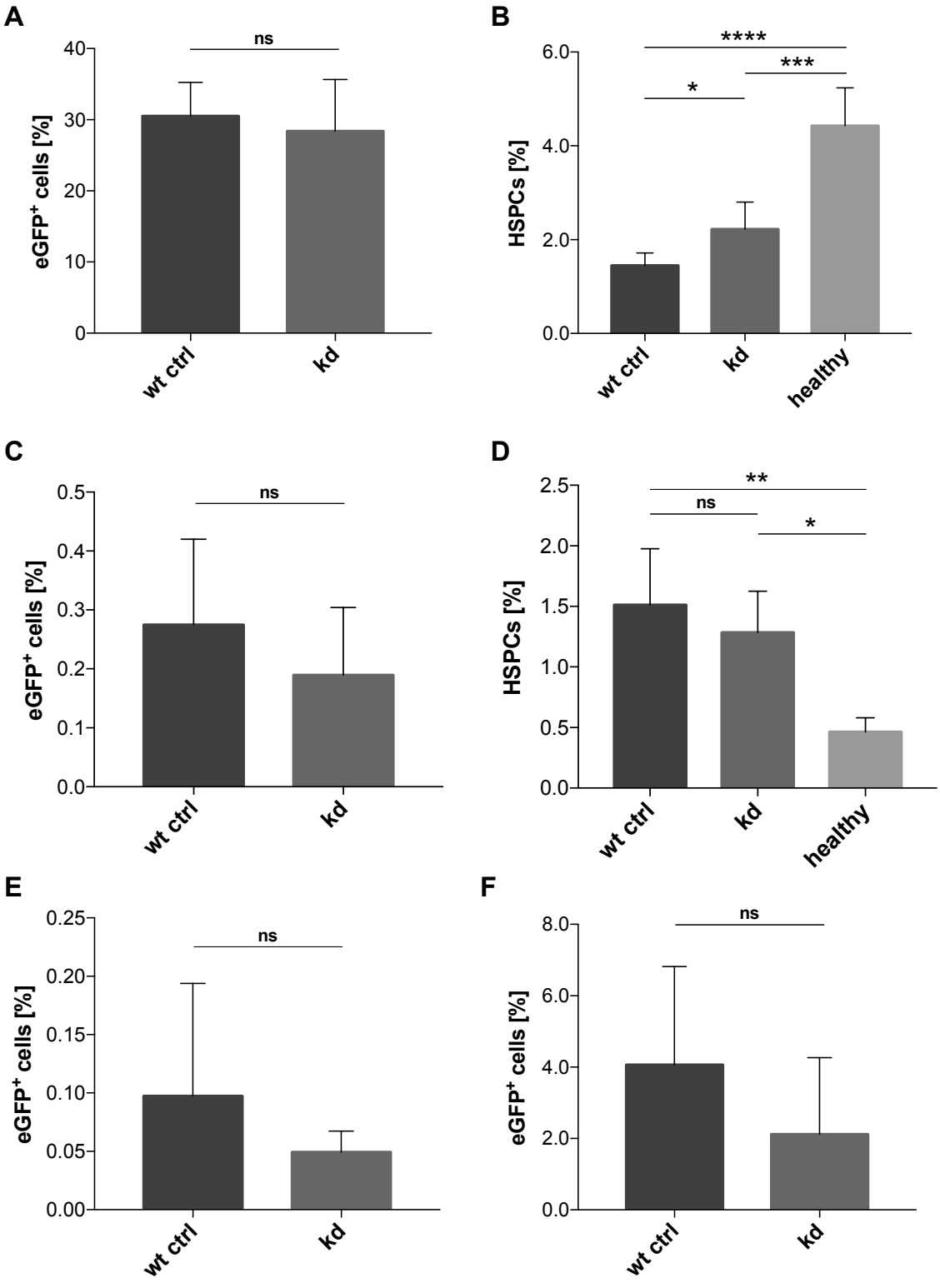


**Figure 22: Infiltration of *DOCK1*-knockdown versus scrambled-control and localization of HSPCs in a TF-1 xenograft mouse-model including a healthy control.** Six NSGS mice per AML cohort were transplanted with 1 x $10^6$ cells, a non-transplanted group of three NSGS mice was included. Measurement of the leukemic infiltration in BM (**A**), spleen (**C**), PB (**E**) and liver (**F**) after 22 days. Statistics were performed as unpaired t-test with Welch´s correction. The localization of HSPCs in BM (**B**) and spleen (**D**) was determined. With AML infiltration, the number of HSPCs within BM is significantly decreasing, but significantly increasing within the spleen. *DOCK1*-expressing cells cause a significantly higher egress of HSPCs from the BM than *DOCK1*-knockdown cells. Statistics were performed as one-way ANOVA followed by Holm-Sidak´s multiple comparison test. Data are displayed as mean ± SD. Levels of significance: $p < 0.05$ = *; $p < 0.01$ = **; $p < 0.001$ = ***; $p < 0.0001$ = ****

### 3.3.3 Early engraftment studies

To study the early engraftment of *DOCK1*-knockdown AML cells compared to control cells within the bone marrow, two AML-xenograft-models with 7-14-week-old female NSGS mice were performed:

> TF-1_dock1-kd2 + TF-1_scr/mCherry in NSGS mice
>
> UKE-1_dock1-kd2 + UKE-1_scr/mCherry in NSGS mice

Transduced and sorted cells described in section 3.2.2.2 and 3.2.2.3 were used after knockdown-verification, for intravenous transplantation with 1 x $10^6$ cells per mouse. Knockdown and control cells were transplanted in parallel into the same animal with a ratio of 1:1. The mice were monitored daily and the experiments were terminated at day 14 or 15. Two separate experiments, each with three NSGS mice per cell line, were performed.

Flow cytometric analysis confirmed an early engraftment for both AML cell lines. The bone marrow infiltration rate, defined by $CD45^+$ cells, at the moment of experiment termination was very low (Figure 23 A). The UKE-1 xenotransplant group showed an infiltration rate of 0.18 ± 0.10% (n = 6), whereas the infiltration within the TF-1 xenotransplant group was 1.46 ± 0.68% (n = 6). In both xenograft-models, the control cells ($mCherry^+$ cells) formed the dominant cell population within the $CD45^+$ cells (Figure 23 B). Compared to the *DOCK1*-knockdown cells ($eGFP^+$), the control cells showed a significantly higher engraftment. In the UKE-1 xenotransplant group, 59.5 ± 23.3% (n = 6) of the $CD45^+$ cells were control cells, while only 13.5 ± 14.4% (n = 6) were *DOCK1*-knockdown cells. In the slightly higher engrafted TF-1 xenotransplant model, the difference between control and knockdown cell engraftment was not so prominent, but still significantly present. Of the $CD45^+$ cells, 55.1 ± 13.8% (n = 6) were control cells and 24.5 ± 13.0% were *DOCK1*-knockdown cells.

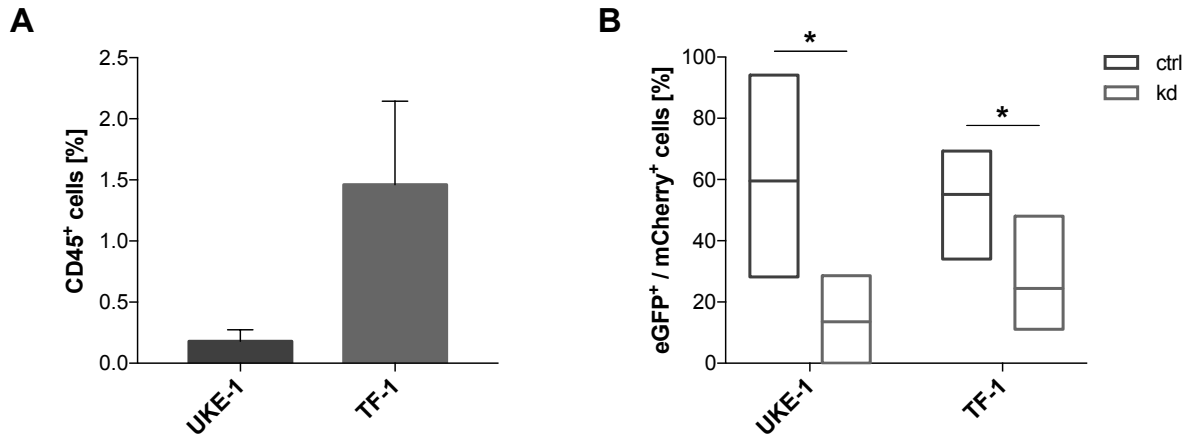


**Figure 23: Infiltration of *DOCK1*-knockdown versus scrambled-control in an UKE-1 and TF-1 xenograft mouse-model.** Six NSGS mice per AML cell line were transplanted with 1 x $10^6$ cells (*DOCK1*-knockdown (eGFP-labeled) and scrambled-control cells (mCherry-labeled) in a 1:1-ratio). Flow cytometric measurement of leukemic infiltration after 14-15 days. Total BM infiltration of UKE-1 and TF-1 cells, defined as $CD45^+$ cells, was measured and displayed as mean ± SD (**A**). Determination of the population size of control ($mCherry^+$) and *DOCK1*-knockdown ($eGFP^+$) cells within the $CD45^+$ cell population for both AML xenograft models, displayed as floating bars showing the minimum and maximum with a line at the mean (**B**). Control cells were significantly higher engrafted compared to *DOCK1*-knockdown cells. Statistics were performed as paired t-test (two-tailed). Levels of significance: $p < 0.05$ = *; $p < 0.01$ = **; $p < 0.001$ = ***; $p < 0.0001$ = ****

3D confocal visualization of the leukemic cells within the bone marrow after immunohistochemical staining of eGFP, mCherry, CD31, which serves as an endothelial cell marker, and nuclear counterstain with DAPI, revealed a perivascular location for knockdown as well as control cells in both cell lines (Figure 24). In general, TF-1 transplanted specimen displayed a much higher engraftment of leukemic cells compared to UKE-1 transplanted. In the majority of UKE-1 transplanted samples a higher engraftment of control cells ($mCherry^+$) compared to *DOCK1*-knockdown cells ($eGFP^+$) could be observed. Mainly single leukemic cells were detectable in UKE-1 transplanted samples, whereas in TF-1 transplanted samples very large cell islets were visible (Figures 25 and 26). In UKE-1 transplanted samples, however, only some small cell islets could be detected. Most of the detected cell islets were restricted to one fluorophore (eGFP or mCherry). Only in some cases the islets were not clearly distinguishable from each other.

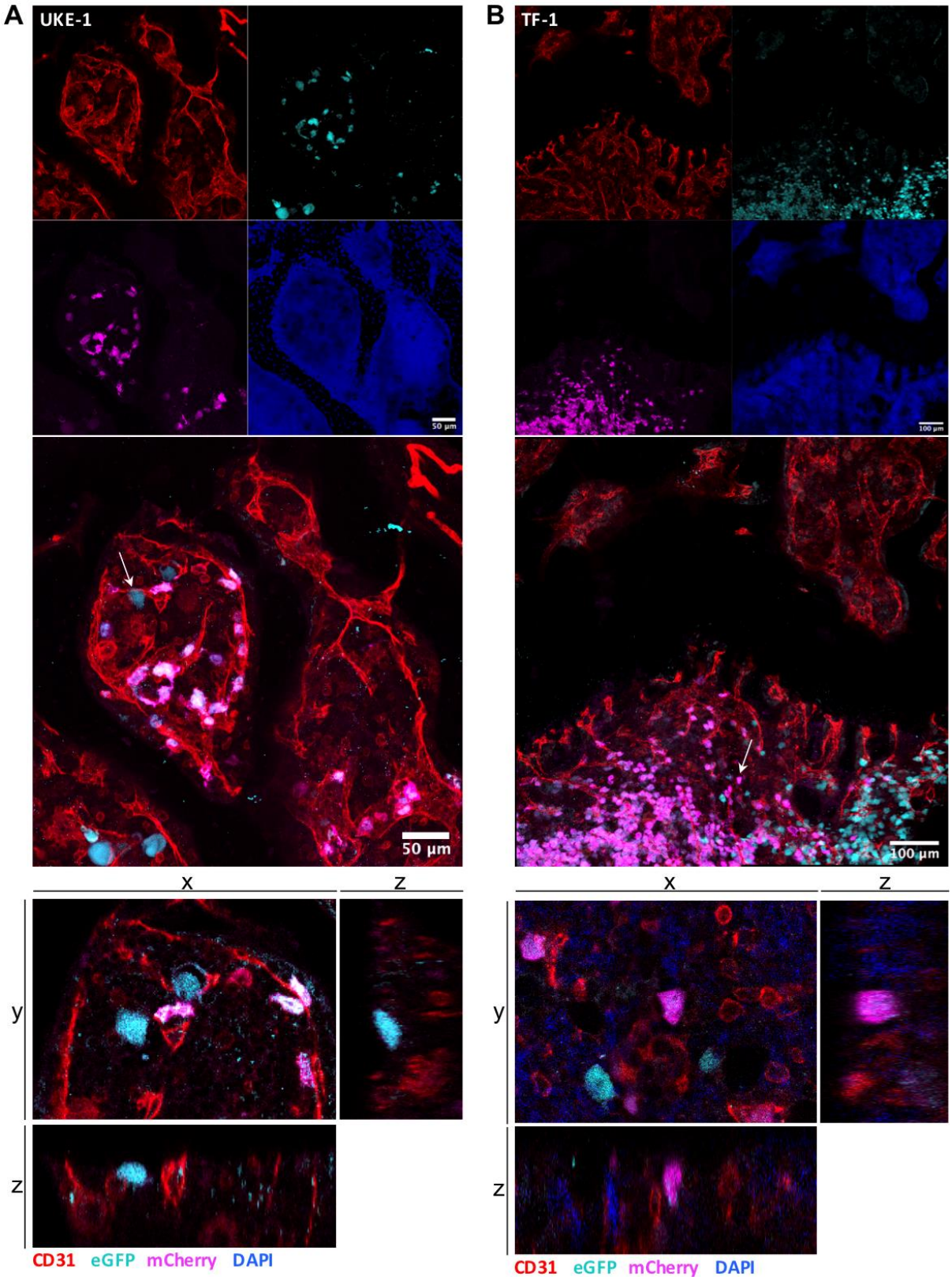


**Figure 24: Perivascular location of leukemic cells.** 3D confocal visualization of leukemic cells within the bone marrow revealed a location in close proximity to blood vessels (CD31$^+$, red) for knockdown cells (eGFP$^+$, cyan) as well as control cells (mCherry$^+$, magenta) in UKE1 (**A**) and TF-1 (**B**) cells. Orthogonal sections of the z-stack confirmed the perivascular location by revealing direct contact sites of AML cells to blood vessels, although no direct contact is visible in the 2D plane. Cells from orthogonal sections are marked with an arrow in the corresponding 3D z-stack. Areas of the bone are unstained. For each image, single channels (left) are shown next to the merged image without nuclear counterstain (right). Brightness and contrast of each color was individually adjusted for each image using ImageJ after applying standard deviation Z Project.

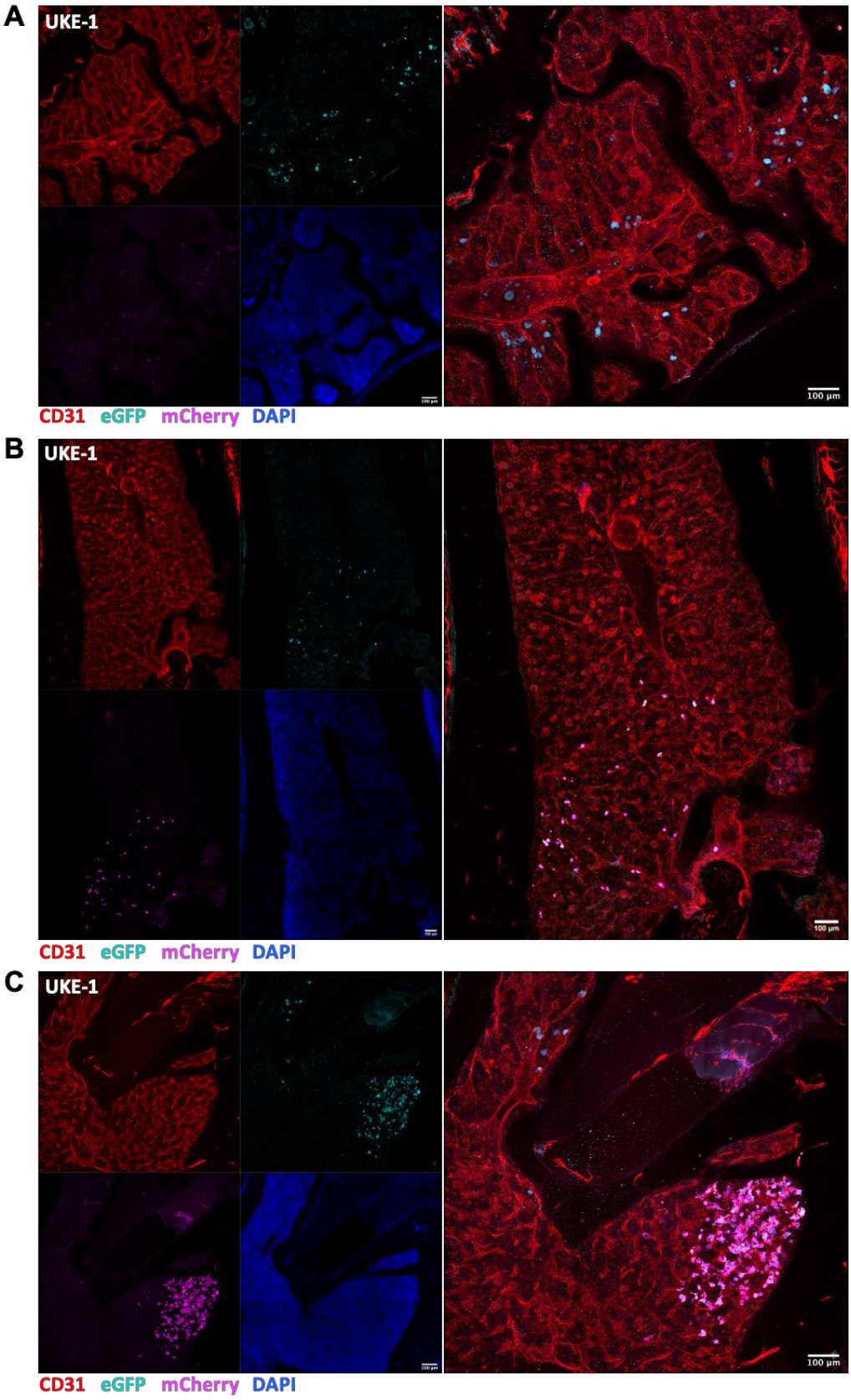


**Figure 25: Early engraftment of UKE-1 cells.** In UKE-1 transplanted samples mainly single leukemic cells were detectable for both, knockdown cells (eGFP$^+$, cyan) (**A**) as well as control cells (mCherry$^+$, magenta) (**B**). Some small cell islets were detectable for UKE-1 transplanted samples. Cell islet of control cells and single knockdown cells (**C**). For each image, single channels (left) are shown next to the merged image without nuclear counterstain (right). Brightness and contrast of each color was individually adjusted for each image using ImageJ after applying standard deviation Z Project.

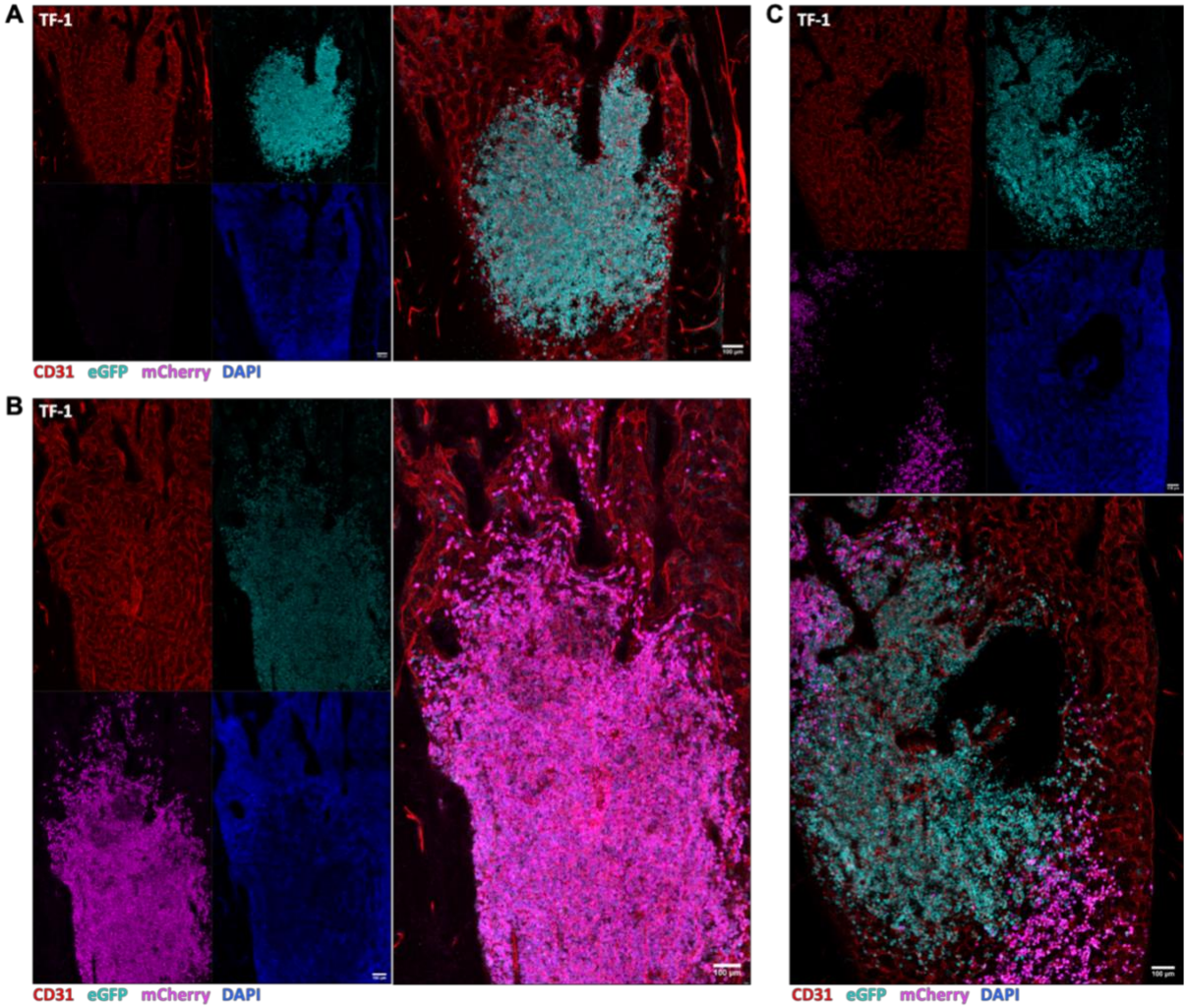


**Figure 26: Early engraftment of TF-1 cells.** In TF-1 transplanted samples large cell islets were detectable for both, knockdown cells (eGFP$^+$, cyan) (**A**) as well as control cells (mCherry$^+$, magenta) (**B**). Cell islet of knockdown cells next to two cell islets of control cells (**C**). For each image, single channels (left) are shown next to the merged image without nuclear counterstain (right). Brightness and contrast of each color was individually adjusted for each image using ImageJ after applying standard deviation Z Project.

## 3.4 Characterization of the DOCK1-signaling pathway

For solid cancer entities several upstream mediators of DOCK1 were described[194,195,201–206], but until today it is not known, through which mechanisms DOCK1 is regulated in AML. Therefore, potential upstream regulators for DOCK1 in AML cells were evaluated. Furthermore, to reveal potential unknown members of the DOCK1 signaling pathway, different approaches were pursued, including transcriptome analysis by RNA-sequencing as well as mass spectrometric analysis of protein-protein interactions and changes in protein phosphorylation.

### 3.4.1 CXCR4-stimulation in AML cells

CXCL12 was demonstrated to be a key regulator within the bone marrow environment for the homing and retention of AML cells[140–142]. Furthermore, upon CXCL12 stimulation a direct connection of the CXCR4 signaling and DOCK1 activation in breast cancer cells was revealed[195]. To investigate whether CXCR4 is a potential upstream regulator of DOCK1 in AML, primary AML samples were stimulated with the CXCR4 ligand CXCL12 (also known as SDF-1α) or supernatant of endothelial cells (HDBEC), since it is known that endothelial cells of the bone marrow microenvironment express CXCL12[123]. The relative mRNA expression of *DOCK1* and *CXCR4* according to Pfaffl[225] was determined after 24 hours and 48 hours (Figure 27). Furthermore, the relative mRNA expression of *DOCK1* and *CXCR4* according to the ΔCT-method for the untreated control samples was determined for each timepoint and the mean value was calculated (Supplementary Table 3). For six of the nine tested pAML samples, data of the surface expression of CXCR4 were available (Supplementary Table 3). As part of the normal working routine of the research group, flow cytometric analysis of the freshly isolated pAML samples were performed, to determine different surface marker expressions.

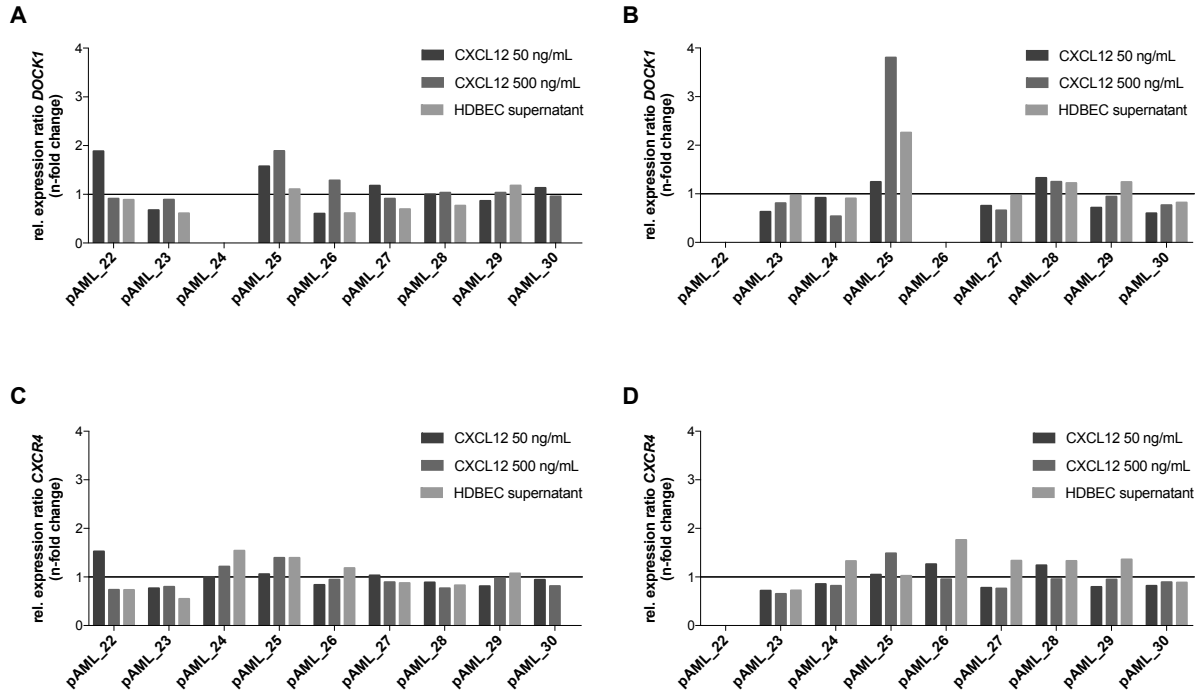


**Figure 27: Effect of CXCR4 stimulation in primary AML samples.** Freshly isolated pAML cells were treated with 50 ng/mL and 500 ng/mL CXCL12 as well as with 400 µL/mL HDBEC supernatant. Samples for RT-qPCR were obtained after 24 hr (**A**, **C**) and 48 hr (**B**, **D**). The relative mRNA expression of *DOCK1* (**A**, **B**) and *CXCR4* (**C**, **D**) was determined according to Pfaffl[225] with *GAPDH* as reference gene and untreated cells serving as calibrator. The relative expression ratio is expressed compared to the untreated control (represented as a black line).

Only the *DOCK1* expression from pAML_25 stood out. The stimulation of CXCR4 with its ligand CXCL12 increased the *DOCK1* expression already after 24 hours, while the stimulation with the endothelial supernatant unfolds its effect after 48 hours. The comparison of the CXCR4 surface expression revealed the highest CXCR4 expression for pAML_25. Furthermore, the *CXCR4* mRNA expression according to the ΔCT-method for pAML_25 was the highest among all tested samples. The *CXCR4* mRNA expression remained unaffected by the stimulation of the receptor.

### 3.4.2 JAK2-axis modulation in AML cell lines

*DOCK1* mRNA-expression analysis of AML cell lines revealed that only TF-1 and UKE-1 cells had an endogenous *DOCK1* expression (refer 3.1). UKE-1 cells contain a JAK2 V617F tyrosine kinase mutation, which is an activating point mutation, leading to a constitutively active JAK2, and which is one of the main somatic driver mutations for myeloproliferative neoplasms (MPN)[239,240]. The proliferation of TF-1 cells is dependent on GM-CSF[228] and it is known that the downstream signaling of GM-CSF can activate JAK2[241]. The potential higher JAK2 activity and the endogenous *DOCK1* expression are the common characteristics in both cell lines. It was investigated whether a causal relationship exists. Furthermore, recent findings suggest that JAK2 activation can activate the CXCR4 pathway[242]. Therefore, the JAK2 modulation was also evaluated with respect to the *CXCR4* expression.

#### *3.4.2.1 JAK2 inhibition in UKE1 cells*

To study the effect of an inhibition of JAK2 *in vitro*, UKE-1 cells were treated with the compound ruxolitinib. Ruxolitinib is an FDA approved drug for the treatment of intermediate or high-risk myelofibrosis. It is a kinase inhibitor specific for JAK1 and JAK2 and is therefore inhibiting the JAK-STAT pathway[243]. The effective concentration range for treating UKE-1 cells was determined in a proliferation assay over four days (data not shown). To evaluate the effect of an JAK2 inhibition on the mRNA expression level of *DOCK1* and *CXCR4*, UKE-1 cells were treated with 40-600 nM ruxolitinib and DMSO as solvent control for 4 hr, 8 hr, 24 hr and 48 hr. RT-qPCR analyses for *DOCK1* and *CXCR4* expression were performed. The relative expression level was determined according to Pfaffl[225] with *GAPDH* as a reference gene and DMSO control as calibrator (Figure 28 A, B). Furthermore, the DOCK1 protein level after

ruxolitinib treatment for 24 hr and 48 hr was investigated by western blot analyses (Figure 28, C, D).

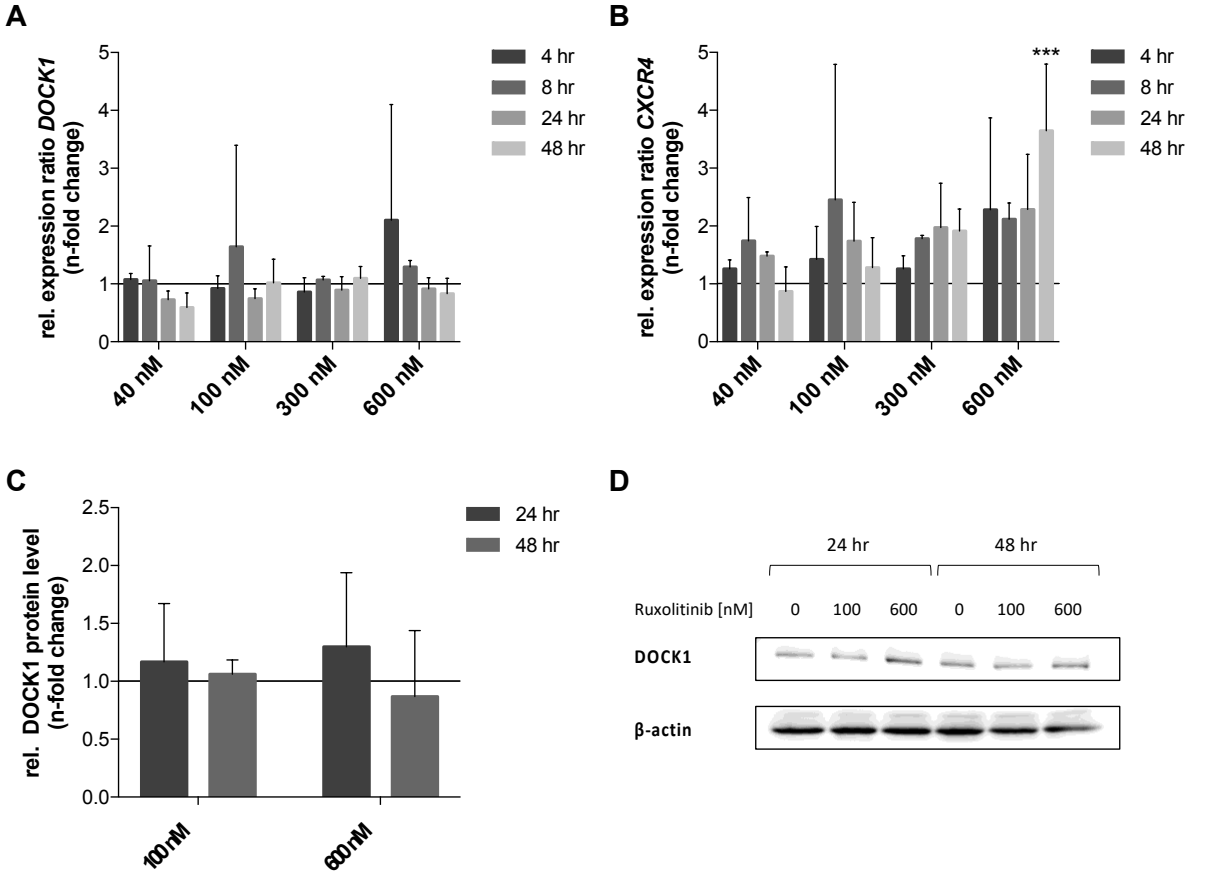


**Figure 28: Effect of JAK2 inhibition in UKE-1 cells.** UKE-1 cells were treated with 40-600 nM ruxolitinib. Samples for RT-qPCR were obtained after 4 hr, 8 hr, 24 hr and 48 hr and for western blot after 24 hr and 48 hr. The relative mRNA expression of *DOCK1* (**A**) and *CXCR4* (**B**) was determined according to Pfaffl[225] with *GAPDH* as reference gene and the untreated cells serving as calibrator (represented as a black line). The relative expression ratio is expressed as mean ± SD of three independent experiments. Relative DOCK1 protein expression (**C**) was determined with β-actin as reference protein and was normalized to the untreated cells (represented as a black line). Data are expressed as mean ± SD of three independent experiments. Representative western blot (**D**). Statistics were performed as repeated-measures two-way ANOVA followed by Dunnett's multiple comparison test. Levels of significance: $p < 0.05$ = *; $p < 0.01$ = **; $p < 0.001$ = ***; $p < 0.0001$ = ****

The pharmacological inhibition of JAK2 with ruxolitinib did not show any significant effect in *DOCK1* mRNA expression or DOCK1 protein level. Changes in the mRNA expression could not be correlated to inhibitor concentration or time. Two-way ANOVA analysis of the *CXCR4* expression after ruxolitinib treatment revealed that there is a statistically significant difference regarding the inhibitor concentration. Overall a dose-dependent increase in expression level could be observed, but independent of treatment time.

### *3.4.2.2 Downstream-signaling of GM-CSF in TF-1 cells*

To investigate whether DOCK1 is involved in the downstream-signaling of GM-CSF, RT-qPCR and western blot analyses of TF-1 cells after withdrawal of GM-CSF were performed. The proliferation of TF-1 cells is dependent on GM-CSF[228]. To verify the GM-CSF-dependency in the used TF-1 cells, proliferation assays were performed over the duration of 1 week (Figure 29).

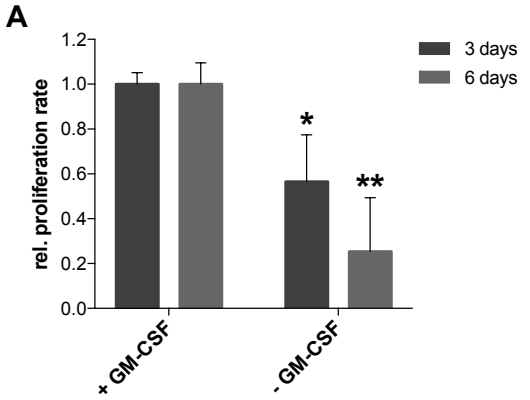


**Figure 29: Relative proliferation rate of TF-1 cells in the presence and absence of GM-CSF.** TF-1 cells were cultured with or without 2.5 ng/mL GM-CSF. After three and six days, the number of viable cells was determined and normalized to the GM-CSF treatment and is expressed as the mean ± SD of three independent experiments. Statistics were performed as repeated-measures two-way ANOVA followed by Sidak's multiple comparison test. Levels of significance: $p < 0.05$ = *; $p < 0.01$ = **; $p < 0.001$ = ***; $p < 0.0001$ = ****

The proliferation rate was significantly reduced after three (0.57 ± 0.22-fold, $p = 0.0464$, $n = 3$) and six days (0.25 ± 0.27-fold, $p = 0.0074$, $n = 3$). Therefore, the withdrawal of GM-CSF had a significant effect on the proliferation capacity of TF-1 cells.

The influence of a GM-CSF withdrawal in TF-1 cells on the transcription of *DOCK1* and *CXCR4* was investigated by RT-qPCR at different time points (Figure 30 A, B). GM-CSF can activate JAK2[241], which activation is known to collaborate with CXCR4-signaling[242]. Therefore, an influence on the *CXCR4* expression via JAK2 signaling is possible. Furthermore, the effect of GM-CSF withdrawal on DOCK1 protein expression was determined by western blot analyses (Figure 30 C, D).

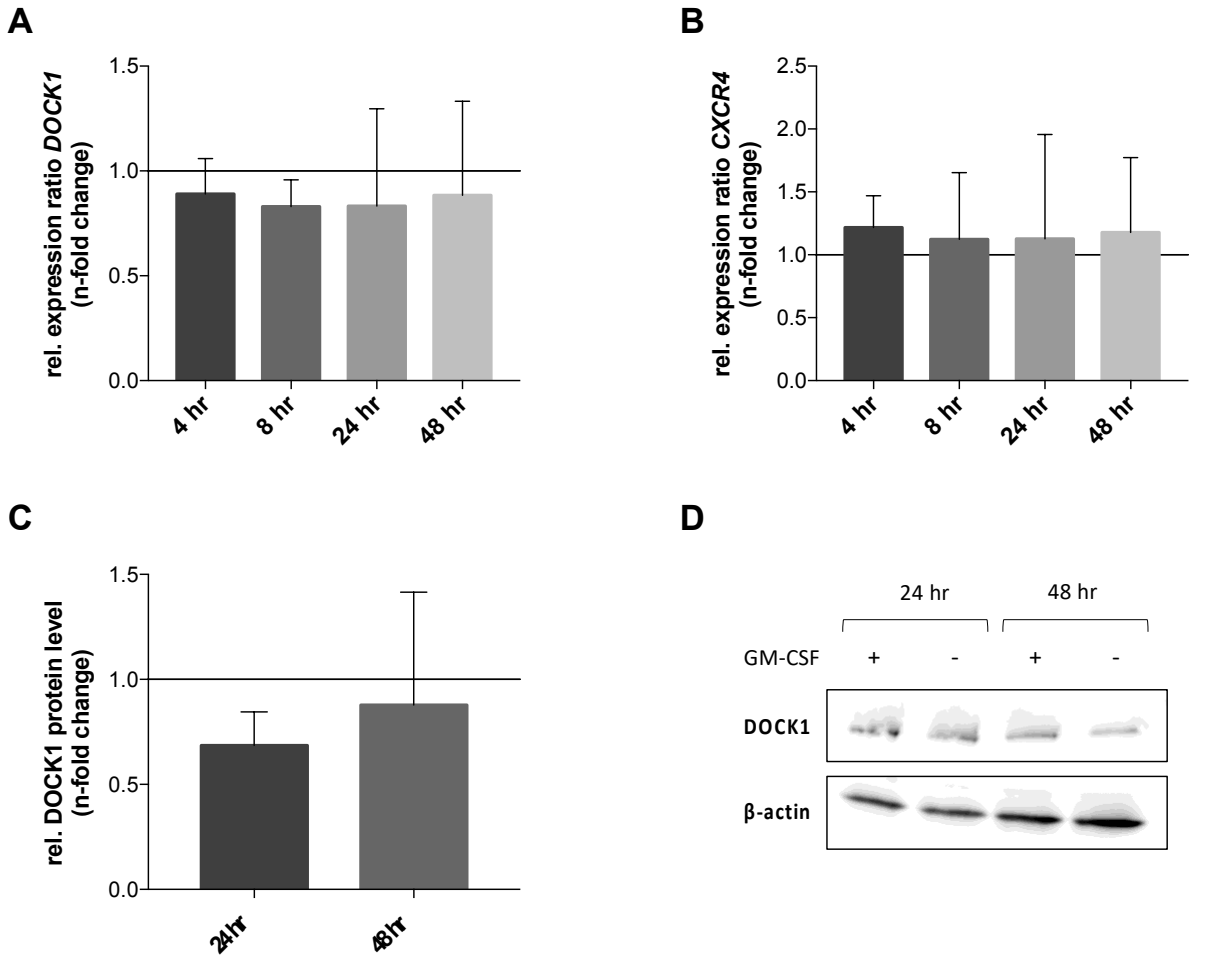


**Figure 30: Effect of GM-CSF withdrawal in TF-1 cells.** TF-1 cells were treated with or without 2.5 ng/mL GM-CSF. Samples for RT-qPCR were obtained after 4 hr, 8 hr, 24 hr and 48 hr and for western blot after 24 hr and 48 hr. The relative mRNA expression of *DOCK1* (**A**) and *CXCR4* (**B**) was determined according to Pfaffl[225] with *GAPDH* as reference gene and the GM-CSF-treated cells serving as calibrator (represented as a black line). The relative expression ratio is expressed as mean ± SD of three independent experiments. Relative DOCK1 protein expression (**C**) was determined with β-actin as reference protein and was normalized to the GM-CSF-treated cells (represented as a black line). Data are expressed as mean ± SD of three independent experiments. Representative western blot (**D**). Statistics were performed as repeated-measures two-way ANOVA followed by Sidak's multiple comparison test.

The *DOCK1* mRNA and protein expression was slightly reduced in the absence of GM-CSF. After 4 hours the relative mRNA expression was reduced to 0.89 ± 0.17, after 8 hours to 0.83 ± 0.13, after 24 hours to 0.83 ± 0.46 and after 48 hours to 0.88 ± 0.45. However, due to high standard deviation, the reduction was statistically not significant. The relative protein expression was reduced statistically not significant to 0.69 ± 0.16 after 24 hours and after 48 hours to 0.88 ± 0.54. The relative *CXCR4* mRNA expression level was showing a minimal, but not significant increase after withdrawal of GM-CSF. The expression was increased to 1.22 ± 0.25 after 4 hours, after 8 hours to 1.13 ± 0.53, after 24 hours to 1.13 ± 0.83 and after 48h to 1.18 ± 0.60.

The withdrawal of GM-CSF and therefore a reduced JAK2 signaling, did not show a significant influence on the expression level of *DOCK1* or *CXCR4*.

## 3.4.3 Identification of potential DOCK1 interaction partners

### *3.4.3.1 RNA-Sequencing (RNA-Seq) of DOCK1-knockdown TF-1 cells*

To investigate the transcriptome of *DOCK1*-knockdown cells compared to control cells with the aim to reveal possible differences in the gene expression pattern, RNA-sequencing was performed on *DOCK1*-knockdown TF-1 cells from three different transduction approaches (refer 3.2.2.2, 3.2.2.3). RNA-Seq was carried out by the Core Facility Genomics of the Medical Faculty Münster (CFG MFM) and data analysis was performed by Dr. Jan Hennigs. The scrambled control (TF-1_scr/eGFP) was compared against single *DOCK1*-knockdown of two different shRNAs (TF-1_dock1-kd1, TF-1_dock1-kd2). The relevant hits ($p < 0.05$) from the control versus combined knockdown comparison are listed in Table 28.

**Table 28: Relevant hits in control versus combined knockdown comparison of RNA-Seq analysis.**

| Gene | Encoder protein | Ensemble number | FC 1 | FC 2 | F | p-value | FDR |
|---|---|---|---|---|---|---|---|
| *DOCK1* | Dedicator of cytokinesis protein 1 | ENSG0000 0150760 | 0.404 | 0.312 | 35.43 | 0.00005 | 0.75 |
| *CMYA5* | Cardiomyopathy-associated protein 5 | ENSG0000 0164309 | 1.796 | 3.117 | 8.62 | 0.008 | 1.00 |
| *ECM1* | Extracellular matrix protein 1 | ENSG0000 0143369 | 2.110 | 1.263 | 7.35 | 0.012 | 1.00 |
| *INHBE* | Inhibin beta E chain | ENSG0000 0139269 | 0.066 | 0.053 | 6.57 | 0.017 | 1.00 |
| *MRPL20* | Mitochondrial ribosomal protein L20 | ENSG0000 0242485 | 1.143 | 0.767 | 6.45 | 0.018 | 1.00 |
| *CHAC1* | ChaC Glutathione-specific gamma-glutamylcyclotransferase 1 | ENSG0000 0128965 | 0.133 | 0.127 | 6.27 | 0.019 | 1.00 |
| *GTF2H3* | General transcription factor IIH subunit 3 | ENSG0000 0111358 | 0.645 | 0.782 | 6.10 | 0.021 | 1.00 |
| *GLCE* | Glucuronic acid epimerase | ENSG0000 0138604 | 0.743 | 0.958 | 6.01 | 0.021 | 1.00 |
| *ULBP1* | UL16-binding protein 1 | ENSG0000 0111981 | 0.143 | 0.217 | 5.84 | 0.023 | 1.00 |
| *RPS26* | Ribosomal protein S26 | ENSG0000 0197728 | 1.546 | 1.274 | 5.79 | 0.024 | 1.00 |

| | | | | | | | |
|---|---|---|---|---|---|---|---|
| *NXPH4* | Neurexophilin 4 | ENSG0000 0182379 | 0.322 | 0.708 | 5.59 | 0.026 | 1.00 |
| *ATF3* | Cyclic AMP-dependent transcription factor ATF-3 | ENSG0000 0162772 | 0.320 | 0.275 | 5.12 | 0.032 | 1.00 |
| *CTH* | Cystathionine gamma-lyase | ENSG0000 0116761 | 0.249 | 0.229 | 5.05 | 0.033 | 1.00 |
| *GDF15* | Growth/differentiation factor 15 | ENSG0000 0130513 | 0.365 | 0.388 | 4.91 | 0.036 | 1.00 |
| *CSNK1A 1L* | Casein kinase 1 alpha 1 like | ENSG0000 0180138 | 0.434 | 1.221 | 4.85 | 0.037 | 1.00 |
| *HSD17B 10* | Hydroxysteroid 17-beta dehydrogenase 10 | ENSG0000 0072506 | 1.345 | 1.295 | 4.57 | 0.042 | 1.00 |
| *ASS1* | Argininosuccinate synthetase | ENSG0000 0130707 | 0.157 | 0.163 | 4.42 | 0.045 | 1.00 |
| *KCNE3* | Potassium voltage-gated channel subfamily E member 3 | ENSG0000 0175538 | 0.542 | 0.646 | 4.35 | 0.047 | 1.00 |
| *TRIP6* | Thyroid hormone receptor interactor 6 | ENSG0000 0087077 | 2.721 | 1.973 | 4.30 | 0.048 | 1.00 |
| *CFAP58* | Cilia and flagella associated protein 58 | ENSG0000 0120051 | 0.491 | 0.481 | 4.24 | 0.050 | 1.00 |

FC = fold change; F = F-value; FDR = false discovery rate

The RNA-Seq results verified a *DOCK1*-knockdown in the shRNA-transduced TF-1 cells. Furthermore, 19 differentially expressed genes with a p-value < 0.05 could be identified in the combined analysis of both knockdown variants. The false discovery rate (FDR) for all hits was very high, therefore the hits cannot be considered significant.

Nevertheless, of the 19 hits of interest, 17 were screened for their divergent expression by RT-qPCR. TRIP6 and ATF3 could not be detected by RT-qPCR. ASS1, ULBP1 and CSNK1A1L showed an expression level close to the detection limit and therefore were not reliably evaluable. Only four of the screened hits (NXPH4, INHBE, CHAC1, GDF15) revealed the same approximate tendency in the RT-qPCR as in the RNA-Seq comparison and therefore represent potential candidates for further validation (Figure 31). All other analyses provided inconsistent results for the different transduction approaches (Supplementary Figure 1).

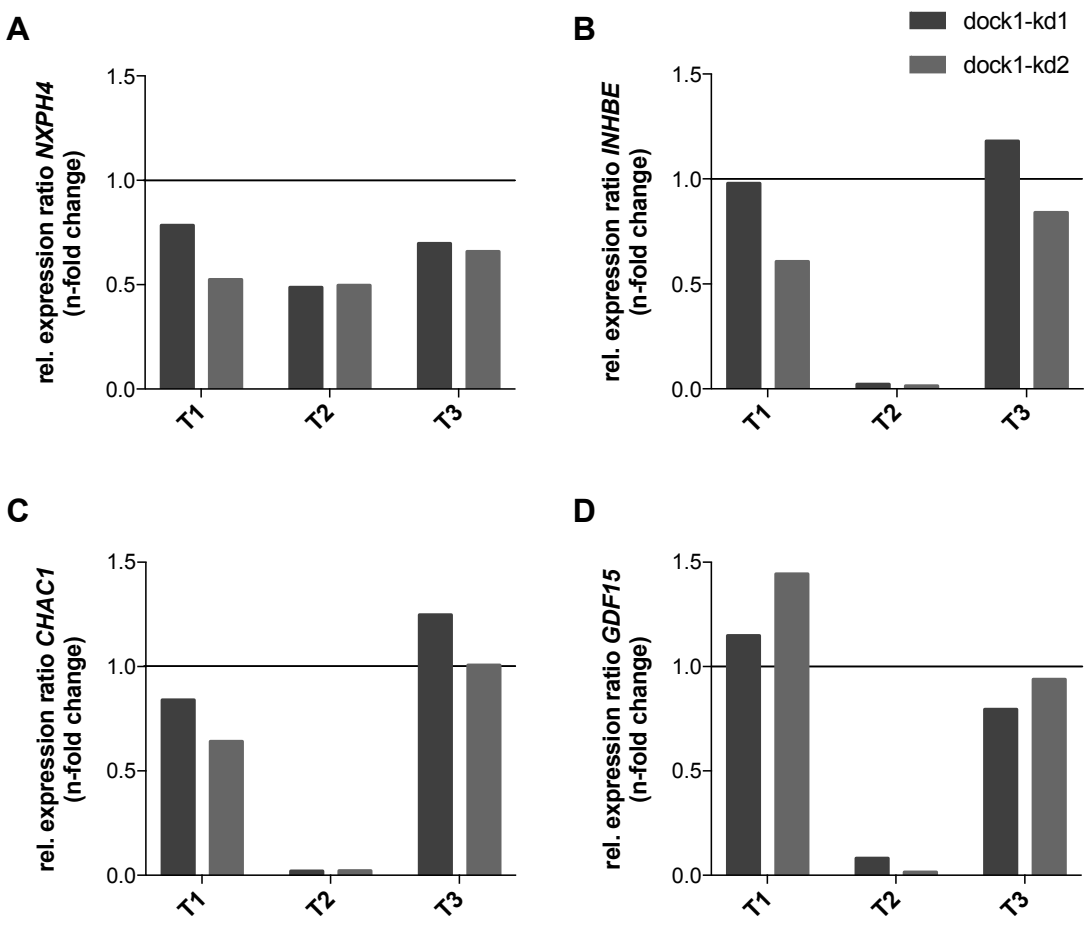


**Figure 31: Verification of relevant hits of the RNA-Seq comparison with RT-qPCR.** RNA samples from three independent transductions (T), which were included in the RNA-Seq analysis, were used for RT-qPCR. TF-1-scrambled control was compared against single *DOCK1*-knockdown of two different shRNAs in TF-1. The relative mRNA expression of *NXPH4* (**A**), *INHBE* (**B**), *CHAC1* (**C**) and *GDF15* (**D**) was determined according to Pfaffl[225] with *GAPDH* as reference gene and scrambled-shRNA transduced cells serving as calibrator. The relative expression ratio is expressed compared to the scrambled-shRNA transduced control cells (represented as a black line).

### *3.4.3.2 Mass spectrometric analysis of DOCK1-knockdown AML cells*

To analyze protein-protein interactions of DOCK1, co-immunoprecipitation for DOCK1 with cell lysates of *DOCK1*-double-knockdown and control UKE-1 and TF-1 cells was performed. Electrophoretically separated proteins were stained for whole protein in a polyacrylamide gel. Based on visible differences in protein band intensity or band absence between knockdown and control cells, spots were chosen for MALDI-TOF/TOF mass spectrometric analysis. Well visible bands that appeared in all lanes irrespective of *DOCK1*-knockdown were analyzed as well. Samples were analyzed by PMF and the resulting signals were compared against the NCBI database with the *MASCOT Server*[227]. A protein was considered as identified, if the Mascot score was significant (> 68), five peptides or more could be matched, the protein coverage

was at least 20% and the identified protein had a similar molecular weight as the sample in the Coomassie gel. Reliable and not reliable identified proteins are displayed in Table 29.

**Table 29: Proteins identified by PMF after DOCK1-pulldown.** Samples for mass spectrometric analysis were chosen from a Coomassie gel of co-immunoprecipitated cell lysates of TF-1 or UKE-1 *DOCK1*-double-knockdown and control cells. Samples marked as "all lanes" were well visible bands in all lanes independent of cell type. For all additional samples, the cell type, where the band was visible, is named.

| Sample | Identified Protein<br>reliable, *not reliable* | Accession Number | Mass [kDa] | Mascot Score | Coverage [%] |
|---|---|---|---|---|---|
| TF-1_scr | Dedicator of cytokinesis protein 1 isoform 2 | NP_001371 | 215 | 135 | 21 |
| All lanes | Stress-70 protein, mitochondrial | NP_004125 | 73 | 187 | 45 |
| All lanes | Membrane protein, palmitoylated 4 (MAGUK p55 subfamily member 4) | EAW70288 | 67 | 72 | 21 |
| All lanes | Tubulin beta chain | BAH14636 | 46.5 | 132 | 39 |
| All lanes | *Actin-related protein 2/3 complex subunit 1A isoform 2* | NP_001177925 | 39.8 | 68 | 29 |
| All lanes | Heterogeneous nuclear ribonucleoproteins A2/B1 isoform A2 | NP_002128 | 35.9 | 218 | 57 |
| TF-1_ dock1-dkd | Fer-1 like protein 3 | AAG23737 | 233 | 226 | 17 |
| UKE-1_ dock1-dkd | Ankyrin repeat domain-containing protein 26 isoform 1 | NP_055730 | 196 | 111 | 11 |

dkd = double-knockdown; scr = scrambled

Even though the proteins Fer-1 like protein 3 and Ankyrin repeat domain-containing protein 26 did not reach the required sequence coverage of at least 20%, the proteins could be considered as reliable identified, based on the high Mascot score and since both proteins have a high protein mass.

To verify the identified proteins, the experiment was repeated once. The proteins could be detected again, but not with a significant score. Since a clear identification was not possible in the second attempt, the results can only be considered as a tendency that the identified proteins might be relevant. Further validation is mandatory.

### 3.4.4 Identification of phosphorylation patterns by mass spectrometry

To identify potential kinase targets within the DOCK1 signaling cascade, changes in phosphorylation pattern were analyzed after DOCK1 inhibition. *DOCK1*-expressing TF-1 cells were treated with the small molecule DOCK-inhibitors CPYPP and TBOPP for up to one hour and after protein isolation co-immunoprecipitation for DOCK1 was performed.

Phosphoproteins were selectively stained in a polyacrylamide gel followed by a whole protein stain. Based on phosphoprotein and whole protein staining, spots were chosen for MALDI-TOF/TOF mass spectrometric analysis (Figure 32).

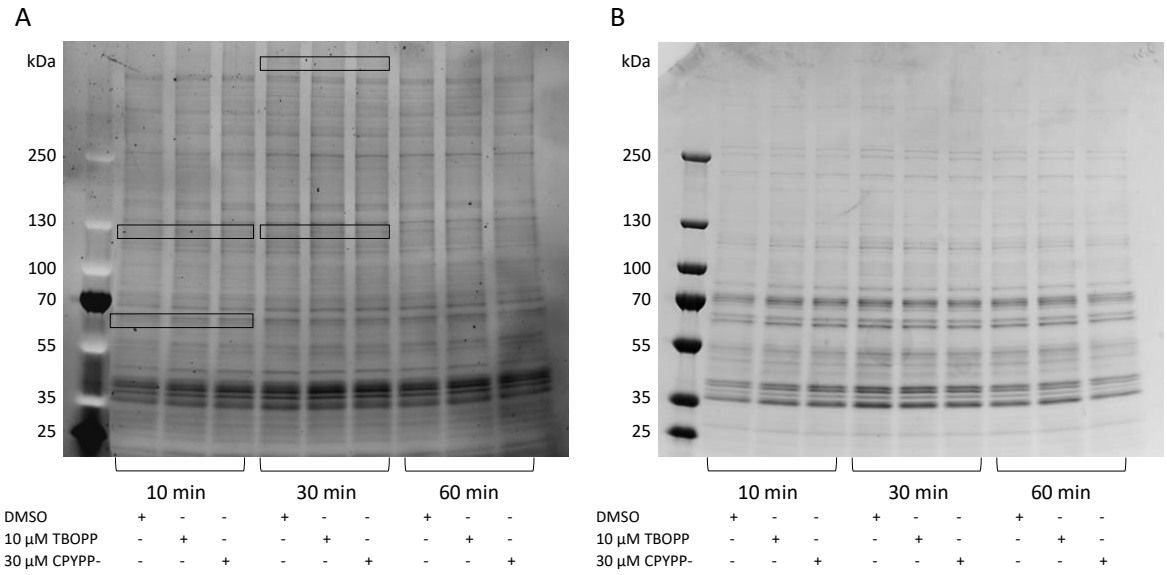


**Figure 32: Identification of protein bands of interest for mass spectrometric analysis.** Based on differences in phosphoprotein staining with Pro-Q™ Diamond (**A**) and whole protein staining with colloidal Coomassie G-250 (**B**) in a polyacrylamide gel with protein lysates of DOCK-inhibitor treated TF-1 cells after co-immunoprecipitation for DOCK1, three protein bands of interest could be identified, with approximate protein molecular mass of > 250 kDa, 130 kDa and 65 kDa.

Peptide mass fingerprinting (PMF) revealed a protein mixture for the > 250 kDa protein band as well as the 130 kDa band, consisting of proteins of similar size, respectively. The top score for the > 250 kDa band was found as WD repeat and FYVE domain-containing protein 3 (WDFY3, XP_011530068.1). The mascot score was 90 ($p < 0.05$) and a 7% protein sequence coverage could be observed. WDFY3, also known as ALFY, is a phosphatidylinositol-3-phosphate (PI3P)-binding protein that acts as an autophagy scaffold protein[244]. The top score for the 130 kDa protein band was found as synaptojanin-1 (SYNJ1, AAI36604.1), with a mascot score of 116 ($p < 0.05$) and 12% sequence coverage. SYNJ1 is a polyphosphoinositide phosphatase and is involved in synaptic vesicle traffic[245]. The 65 kDa protein band could not be identified with PMF. Since the criteria for protein identification (refer 3.4.3.2) were not fulfilled, a more precise analysis using a high-resolution gel in order to achieve higher separation of the protein mixture is necessary.

# IV. DISCUSSION

The prognosis and treatment of AML has steadily improved over the last decades, but despite the increasing understanding of origin and progression of the disease, patient outcome remains poor[5,6,8–12]. The majority of patients eventually relapse, even though several new therapeutic approaches emerged over the last years. The high incidence of relapses is believed to be due to the existence of LSCs, therefore, the common opinion is that not only the bulk of AML blasts must be eliminated to cure the disease, but also the LSCs[53,62]. Targets, which are specific for the LSC bone marrow microenvironment, have come into focus of research.

DOCK1 has been reported to be involved in the tumorigenesis of several solid cancer entities, but until now only little is known about its role in hematological malignancies. Preliminary work of the research group Fiedler/Wellbrock revealed a potential role of DOCK1 in the pathophysiology of AML (unpublished data). Moreover, it was demonstrated that DOCK1 expression in AML cells was inducible when co-cultured with stromal cells of the microenvironment, leading to the assumption that DOCK1 might be a niche-specific target in AML (unpublished data). Since DOCK1 was exclusively upregulated only in co-cultured AML cells, but not in normal hematopoietic cells, it could be an attractive candidate to selectively target malignant cells, while keeping healthy cells unaffected.

In the present work, the relevance of DOCK1 for the pathophysiology of AML was investigated. Initially, the antileukemic effect and functional consequences of DOCK1-downregulation were investigated in *in vitro* assays. To further evaluate the effect of DOCK1 on AML progression, *in vivo* xenotransplantation mouse models were performed. Furthermore, the DOCK1 signaling pathway in AML was investigated. Different approaches were chosen to identify possible interaction partners of DOCK1 in AML. *In vitro* assays were performed to evaluate possible upstream mediators. In the following, the results of this thesis are discussed and assessed in terms of the relevance of DOCK1 for the pathophysiology of AML.

## 4.1 Relevance of DOCK1 in AML-pathophysiology

### 4.1.1 Treatment with small molecule DOCK-inhibitors show an antileukemic effect in functional *in vitro*-assays

The small molecule inhibitors CPYPP and TBOPP were used to investigate the antileukemic potential of a pharmacological inhibition of DOCK1. Both compounds are inhibiting the catalytic activity of DOCK proteins by reversible binding to the DHR-2 domain[221,222]. CPYPP is classified as a DOCK2 inhibitor, but displays comparable high affinity and inhibitory activity for DOCK1 and DOCK5[221]. TBOPP was identified as a DOCK1-selective inhibitor, without affecting the biological functions of DOCK2 and DOCK5[222]. To determine the antileukemic properties of a compound, proliferative and colony forming abilities of AML cells, treated with various concentrations of the inhibitors, were observed. The compounds inhibit the catalytic activity of DOCK proteins, including DOCK1, therefore the Rac activation is reduced[221,222]. Since Rac activation can promote cell proliferation[176,177], a decreased proliferation rate indicates a reduced activation of Rac. Wang *et al*. revealed that Rac1 is often overexpressed in primary AML samples and that *in vitro* siRNA-based downregulation or inhibition of Rac1 in AML cell lines leads to a reduced cell migration, proliferation and colony formation[246].

For proliferation and colony formation assays with the small molecule inhibitors, the two *DOCK1*-expressing cell lines UKE-1 and TF-1 as well as the *DOCK1*-non-expressing cell line Molm13 were used. Both inhibitors showed significant antiproliferative effects in all three AML cell lines tested. The unspecific DOCK-inhibitor CPYPP had the strongest effect in Molm13 cells. For UKE-1 and TF-1 cells, a similar dose-response relationship for CPYPP was observed. Since CPYPP inhibits DOCK1, DOCK2 and DOCK5 equally, an antileukemic effect for all three cell lines was anticipated. The DOCK1-selective inhibitor TBOPP showed the highest effect in the *DOCK1*-expressing cell line TF-1, followed by the non-expressing cell line Molm13. The *DOCK1*-expressing cell line UKE-1 was the least sensitive cell line tested for TBOPP.

All three cell lines displayed a relatively high *DOCK2*-expression, but only a very low *DOCK5*-expression. TF-1 cells showed a similar high expression of *DOCK1* as of *DOCK2*, while UKE-cells expressed *DOCK1* on a much lower level. Molm13 cells, which are not expressing *DOCK1*, were used to validate the DOCK1-selective effect of TBOPP. Interestingly, the DOCK1-selective inhibitor had a strong effect in the *DOCK1*-non-expressing cell line Molm13.

According to the published data, the selectivity of TBOPP for DOCK1 is 8.7-fold and 5.4-fold higher than for DOCK2 and DOCK5, respectively[222]. Furthermore, TBOPP is not affecting the biological functions of DOCK2 and DOCK5, only DOCK1-dependent mechanisms such as invasion and macropinocytosis[222]. Based on the published data, a higher sensitivity and thus a stronger antiproliferative effect of TBOPP in *DOCK1*-expressing cells was anticipated. However, the present data cannot confirm this assumption. The results suggest that even though both inhibitors are able to reduce the proliferation rate of AML cell lines effectively, their functional effect is independent of the *DOCK1*-expression.

Moreover, the dose-dependent antiproliferative effect of both inhibitors could be confirmed in primary AML blasts. Of 21 pAML samples tested, only two were relatively insensitive to TBOPP. Even though both samples, which were insensitive to TBOPP, had a low *DOCK1*-expression, no direct correlation between the response to the inhibitors and the expression pattern of the three *DOCK* variants could be detected. This underlines the assumption that the antiproliferative properties of both inhibitors are independent of *DOCK1* expression.

To further characterize the antileukemic effect of the small molecule inhibitors, colony formation assays in the presence of various inhibitor concentrations were performed, using the three AML cell lines UKE-1, TF-1 and Molm13. The colony formation assay allows the *in vitro* investigation of the clonal proliferation and differentiation potential of leukemic cells. The ability of cancer cells to proliferate independently of external growth factors and their immortality are two hallmarks of cancer[231,232]. A decreased colony formation indicates an antileukemic effect of the respective inhibitor, due to reduced self-renewal properties of the cells. Both DOCK-inhibitors displayed a dose-dependent effect on the colony forming abilities of AML cells. Low concentrations of the unselective inhibitor CPYPP showed an inhibitory effect only in TF-1 cells. UKE-1 and Molm13 cells were insensitive to low inhibitor concentrations, but showed strong sensitivity at higher concentrations. Similar to the effect on the proliferation rate, the DOCK1-selective inhibitor TBOPP had the strongest effect in TF-1 cells. In comparison, the non-expressing cell line Molm13 showed a significant, but not so strong sensitivity to TBOPP. UKE-1 cells demonstrated once again the least sensitivity to TBOPP. These results support the hypothesis that the effects of the inhibitors are independent of the *DOCK* variants.

These findings suggest that the antileukemic effect of CPYPP is based on the inhibition of all three different DOCK variants as described by the authors[221]. Contrary to the published

data[222], the DOCK1-specific inhibitor TBOPP also appears to inhibit the biological functions of the DOCK proteins in AML cells in an unspecific manner. Further detailed investigation of Rac activation after inhibitor treatment, using Rac activation assay, would be necessary to detect any differences between the antagonistic effect of the inhibitor on the DOCK variants in AML cells.

### 4.1.2 Targeted *DOCK1*- or *ELMO1*-knockdown cannot reproduce the antileukemic effect of the pharmacological inhibition

To validate the antileukemic effect of the small molecule inhibitors and to determine the functional consequences of a downregulation of *DOCK1*-expression, shRNA-based knockdown approaches in the *DOCK1*-expressing cell lines TF-1 and UKE-1 were performed. Two distinct shRNAs for *DOCK1* were used to transduce the AML cells. Since the single knockdown did not reach a high knockdown-capacity, a double-knockdown was performed, to further decrease the *DOCK1*-expression. Unexpectedly, the double-knockdown approach did not exceed the knockdown-capacity substantially. Nevertheless, neither single nor double-knockdown of *DOCK1* had any influence on the proliferation or colony formation abilities of the transduced AML cells. To verify the findings of the *DOCK1*-knockdown, an overexpression of *DOCK1* in the *DOCK1*-non-expressing cell line Molm13 was performed. Similar to the knockdown, the overexpression did not have any effect on the proliferation or colony formation rate.

To determine whether a downregulation of the complete bipartite GEF complex is necessary to achieve an antileukemic effect in AML cells, a combined shRNA-based knockdown of *DOCK1* and *ELMO1* was performed. To ensure that observed effects were based on the combined knockdown, single knockdown approaches of *ELMO1* with two different shRNAs were performed. Similar to the *DOCK1*-knockdown, the single *ELMO1*-knockdown had no influence on the proliferation or colony formation abilities of UKE-1 or TF-1 cells. While the proliferation of the transduced cells was unaffected by the combined knockdown of *DOCK1* and *ELMO1*, the colony forming ability in UKE-1 cells was altered. Interestingly, the colony formation was enhanced contrary to expectations. However, due to high internal variability of the assay and the low number of repeats, this result must be considered with caution. In summary, the results indicate that neither a downregulation of *DOCK1* nor of *ELMO1* shows an antileukemic effect. These findings underline the assumption that the antileukemic effect of the small molecule inhibitors is independent of DOCK1, but rather depends on the more dominant

DOCK-homologs. It is likely that the other DOCK variants, especially DOCK2, which has a similar function to DOCK1, can compensate for the knockdown of *DOCK1*. As reviewed by Gadea and Blangy, DOCK2, mainly expressed on hematopoietic cells, acts as a bipartite GEF for Rac GTPases together with ELMO and thereby regulates especially immunological functions, such as chemokine-induced lymphocyte migration, adhesion of lymphocytes to the endothelium and formation of immunological synapses by T cells and natural killer (NK) cells[167,247–251]. DOCK5, however, is highly expressed in osteoclasts and plays a critical role in their function by promoting osteoclast adhesion[167,252]. To determine the effect of DOCK2 and DOCK5 on the pathophysiology of AML, a project outline for a medical doctoral thesis was drawn. The medical doctoral candidate Nader Attar was assigned to the project, which he subsequently carried out and continued to develop. Preliminary results could so far only indicate antileukemic effects for the shRNA-based knockdown of *DOCK2* in Molm13 cells, but not in UKE-1 or TF-1 cells (data unpublished, kindly provided by Nadar Attar). Possibly the opposite effect occurred, where the expression of *DOCK1* compensated the downregulation of *DOCK2*. Therefore, a combined knockdown of *DOCK1* and *DOCK2* could be considered for further investigations.

To further determine the influence of DOCK1 to biological functions, adhesion assays in a microfluidic system were performed. Rac activation is critical for cell adhesion, migration and invasion[168]. Due to its key regulatory function, it was hypothesized that a decreased Rac activation through downregulation of the expression of its GEF DOCK1 would lead to a reduced adhesion rate and an upregulation through overexpression would result in enhanced adhesion to endothelial cells. Unexpectedly, apart from the UKE-1 knockdown cells, no significant differences in the adhesion properties between control cells and *DOCK1*-knockdown or -overexpression cells were found. In TF-1 cells, the *DOCK1*-knockdown resulted in an insignificant light reduction of attached cells, compared to the control cells. Even though a high number of cell bonding was observed with the Molm13 cells, no differences between control and overexpression cells could be detected. Since the expression rate of *DOCK1* in the transgenic cells was very low at the time of the experiment, it is likely that no functional differences were noticeable. Interestingly, contrary to expectations, the *DOCK1*-knockdown in UKE-1 cells showed an increased number of attached cells compared to the control cells. One limitation of the adhesion assay was the non-optimal type of endothelial cells. HUVEC cells represent macrovascular endothelial cells[253], which display a low permeability due to

tight junctions between the cells in a confluent monolayer[254]. However, the site of cellular trafficking within the bone marrow microvasculature, the sinusoids, are characterized by a high permeability[163]. The adhesion of different cell types differs distinctly between the two types of endothelial cells[122,255]. Despite the fact that TNF-α stimulation increases the permeability of HUVEC cells[254], they are not the optimal cell type to represent the bone marrow microvasculature. Nevertheless, the use of this cell type was inevitable, since it was not possible to establish a reproducible protocol with microvascular cells. The performed assays focused on the initial adhesion process, which allows no indication of the migratory and invasive properties of the leukemic cells. To gain more information about the migratory properties of the transduced AML cells, the next step would be to expand the experiment to a transmigration assay. After the initial attachment of the leukemic cells to the endothelial cell layer, transmigration would be observed at low shear stress over a longer period of time.

The reason why the combined *DOCK1*- and *ELMO1*-knockdown in UKE-1 cells led to an elevated clonogenic activity and the single *DOCK1*-knockdown in UKE-1 cells resulted in an enhanced cell attachment to endothelial cells in a microfluidic system, has to be further investigated. A determination of the Rac activation may provide information regarding possible feedback mechanisms.

Overall, the performed *in vitro* assays with the transduced cells indicate that DOCK1 is not essential for the functional properties of malignant cells in AML, in contrast to other cancer entities such as breast cancer. With a targeted siRNA-based knockdown Liang *et al*. demonstrated that a downregulation of *DOCK1* or *ELMO1* led to a reduced viability and colony formation in breast cancer cell lines[196]. Furthermore, the migration and invasion was decreased upon a *DOCK1* or *ELMO1* knockdown[196]. Similarly, Chiang *et al*. performed a shRNA-based knockdown of *DOCK1* in breast cancer cell lines and observed a decreased viability and colony formation as well as a suppressed migration and invasion after *DOCK1*-downregulation[197]. The data presented here indicate that the regulatory function of DOCK1 for biological functions demonstrated in breast cancer cell lines, is not present in AML cells. It is likely that due to the high *DOCK2* expression in AML cells, the downregulated DOCK1-functionality is compensated by DOCK2. Since DOCK2 is predominantly expressed on hematopoietic cells[212], it can be assumed that its expression on breast cancer cell lines is much lower, compared to AML cells.

### 4.1.3 DOCK1-expression promotes splenomegaly and HSPC egress from the bone marrow *in vivo*

Rac GTPases are described as critical regulators for HSPC homing, maintenance and trafficking to the bone marrow niches[256]. The localization of HSCs is tightly regulated and actin cytoskeleton rearrangements are involved in several processes. Furthermore, Rac GTPases are important for cell survival and proliferation[176,177]. In hematopoietic cells, three distinct Rac GTPases Rac1, Rac2 and Rac3 are co-expressed, with Rac2 being exclusively expressed by hematopoietic cells[256]. Different studies indicate that Rac1 has a key function in regulating HSPC trafficking and homing, since Rac1 deficiency in HSCs led to impaired engraftment during hematopoietic reconstitution[257,258]. The combined deficiency of Rac1 and Rac2 led to a massive egress of HSPCs from the bone marrow[257,258]. It was demonstrated that Rac1 is overexpressed in most primary AML samples and its aberrant activation is involved in migration and proliferation of leukemic cells[246]. Reduced Rac1 activation resulted in decreased proliferation, colony formation and cell migration of leukemic cells[246]. In another study, Wang *et al*. described Rac activation as a critical regulatory function in LSC homing and maintenance[213]. They demonstrated that activation of Rac1 promotes leukemic cell quiescence, chemotherapy resistance and homing to the bone marrow microenvironment[213]. Furthermore, gene expression analysis revealed an association of Rac1 expression and the expression of cell cycle inhibitors as well as extrinsic mediators, which are important for the interaction of LSCs with the osteoblastic niche[213]. Rac activation is tightly controlled by their GEFs[256]. Therefore, DOCK1 is an interesting target based on its GEF activity for Rac.

Moreover, a niche-specific function of DOCK1 in AML was anticipated based on preliminary data of the research group Fiedler/Wellbrock (unpublished data). *In vitro* approaches revealed an inducible expression of *DOCK1* within AML cells in the presence of bone marrow microenvironment cells. Nevertheless, further *in vitro* assays, performed in the presented work, revealed no direct impact of DOCK1 to biological functions of AML cells such as proliferation, clonogenic activity or cell adhesion. Rather, a function of DOCK1 within the interplay between niche cells and AML cells was assumed. Therefore, xenotransplantation mouse models were performed, to investigate the influence of shRNA-based knockdown or overexpression of *DOCK1* on the AML progression *in vivo*. That way, the whole complexity of the bone marrow microenvironment was taken into account.

DOCK1 was identified as an independent prognostic marker in AML since high *DOCK1* expression has been associated with a poor overall survival as well as poor event-free survival[1]. Therefore, the main focus of the first *in vivo* experiments was to determine whether an up- or downregulation of *DOCK1* expression in AML cells has an influence on the survival period of xenotransplanted mice. *DOCK1*-knockdown in TF-1 or UKE-1 cells had no impact on the survival period. Interestingly, contrary to expectations, the *DOCK1*-overexpression in Molm13 had a small but significant survival benefit compared to the control cohort. Mice, transplanted with *DOCK1*-overexpressing Molm13 cells, survived an average of one day longer than mice, transplanted with the control Molm13 cells. Since the group size was limited and the Molm13-xenotransplantation model is very aggressive, this finding has to be further validated in order to preclude a random effect. Overall, the data of all performed survival studies indicate that the progression of human AML in immunocompromised mice with regard to the overall survival is possibly independent of *DOCK1* expression.

In the process of the survival studies, significant differences in weight and span of the spleen were detected in all performed xenotransplantation experiments. Both parameters differ significantly depending on the *DOCK1*-expression of the transplanted AML cells. *DOCK1*-expressing AML cells caused greater enlargement of the spleen in immunocompromised mice compared to AML cells with no or reduced *DOCK1*-expression. In human AML, an enlargement of the spleen due to extramedullary infiltration of AML cells, called splenomegaly, is described for some patients[237,238]. The underlying mechanism of the reason for splenomegaly occurrence is still unclear. The findings of the survival studies indicate that DOCK1 might be involved in the extramedullary infiltration of the spleen. As demonstrated with a murine model by Duarte *et al*., the extramedullary infiltration of AML blasts into the spleen is delayed compared to the bone marrow infiltration[165]. Furthermore, they described a negative correlation between HSPC numbers in spleen and bone marrow during AML progression. The number of HSPCs within the bone marrow is progressively decreasing with increasing AML infiltration, whereas the HSPC number within the spleen is increasing during AML progression[165]. The underlying mechanism of the HSPC loss was identified to be an extensive endosteal remodeling of the vasculature and HSC niche[165]. To evaluate whether DOCK1 might be involved in the progress of leukemic infiltration or HSPC loss in AML, a xenotransplantation model with *DOCK1*-knockdown TF-1 cells was performed. The bone marrow infiltration as well as the extramedullary infiltration of spleen, liver and peripheral blood were determined.

Furthermore, the distribution of HSPCs between bone marrow and spleen was investigated. By including a healthy control group, splenomegaly could be confirmed in the TF-1 xenograft model. Both, the wildtype control group and the knockdown group showed a significantly enlarged spleen compared to the healthy control. Interestingly, compared to each other, only a significant difference in spleen span, but not in the spleen weight was detected. That leads to the assumption that the greater enlargement in the *DOCK1*-expressing group observed in the previous survival studies is taking place at a very late stage of AML progression. Additionally, a non-significant light enlargement of the liver in the xenotransplanted groups compared to the healthy control group was detected. Since the sample size was very small and the measurement displayed a high standard deviation, further validation is necessary to confirm hepatomegaly. The comparison of leukemic infiltration between *DOCK1*-knockdown and wildtype control group revealed no significant differences for all tested organs. However, an insignificant tendency to a lower infiltration rate within the *DOCK1*-knockdown group could be observed within the spleen, liver and peripheral blood. Since the sample size per cohort was fairly small, further validation is mandatory. In general, extramedullary infiltration was much lower than bone marrow infiltration in both experimental groups. The evaluation of the distribution of HSPCs between bone marrow and spleen revealed a significant decrease in the number of HSPCs in the bone marrow and a significant increase in the spleen after AML infiltration compared to the healthy control cohort. The two xenotransplant groups compared to each other showed a significant difference only within the bone marrow. The *DOCK1*-expressing control TF-1 cells were displacing the HSPCs more strongly than the *DOCK1*-knockdown cells. These findings indicate an involvement of DOCK1 in the egress of HSPCs from the bone marrow, but not in the relocation to the spleen. Downregulation of *DOCK1* within AML cells can mitigate the loss of HSPCs from the bone marrow.

To investigate the influence of *DOCK1*-knockdown on the early engraftment of AML cells into the bone marrow, an additional xenograft mouse model was performed. Knockdown- and control-cells were transplanted in parallel into the same animal. The experiment was terminated two weeks after transplantation to ensure an infiltration of the bone marrow at an early timepoint. Flow cytometric analysis confirmed an early engraftment for both AML cell lines, TF-1 and UKE-1. Interestingly, for both cell lines, the control cells formed the dominant cell population compared to *DOCK1*-knockdown cells, indicating that the *DOCK1* expression might be beneficial for initiating leukemic infiltration and engraftment into the bone marrow

niche. Due to the parallel transplantation of knockdown and control cells, both cell types were in direct competition. Further investigations whether the dominance of the control cells over the knockdown cells is balanced out at an advanced stage of disease would be interesting, since the previous engraftment study revealed no difference in bone marrow engraftment between knockdown or control cells at a late timepoint. However, both models cannot be directly compared to each other, due to different experimental conditions. While in the previous xenograft model, transplantation was performed with a single cell type per animal, due to a different research aim, in this model both cell types were transplanted in parallel. Therefore, the previous model lacks the direct competition between knockdown and control cells.

The 3D confocal visualization of the leukemic cells within the bone marrow in the early engraftment study revealed no differences in the localization of *DOCK1*-knockdown and control cells in both AML cell lines. Both cell types displayed a perivascular localization and the formation of cell-islets of the same color, which spread throughout the bone marrow. In accordance with the flow cytometric data, the majority of UKE-1 transplanted samples showed a higher engraftment of control cells compared to knockdown cells. In the UKE-1 transplanted samples, mainly single leukemic cells were detectable, indicating that the early engraftment might be caused by infiltration of single leukemic cells. In TF-1 transplanted samples, however, very large cell islets were visible, whereas in UKE-1 transplanted specimen only small cell islets could be detected. This leads to the assumption that in the course of the engraftment, clonal expansion of leukemic cells might lead to the formation of cell islets, since most of the detected islets were restricted to one fluorophore. In general, TF-1 transplanted samples displayed a much higher engraftment of leukemic cells compared to UKE-1 transplanted samples. Therefore, a visual evaluation of the cell proportions was not possible without bioinformatic analysis.

## 4.2 Characterization of the DOCK1-signaling pathway

### 4.2.1 *DOCK1*-expression is independent of CXCR4- or JAK2-signaling

Even though several upstream mediators of DOCK1 are described for solid cancer entities[194,195,201–206], until today it is not known, how DOCK1 is regulated in AML. In breast cancer cells it was demonstrated that CXCR4 stimulation with CXCL12 (also known as SDF-1α)

leads to a DOCK1 activation by the released Gαi2, which forms a complex with ELMO1 and locates the GEF complex to the plasma membrane[195]. Furthermore, CXCL12 was demonstrated to be a key regulator within the bone marrow niche for the homing and retention of AML cells[140–142].

In the present thesis, CXCR4 was investigated as a potential upstream mediator of *DOCK1*-expression in AML cells. The mRNA expression level of *DOCK1 and CXCR4* was evaluated after stimulation of primary AML samples with the CXCR4 ligand CXCL12 or supernatant of endothelial cells. The *CXCR4* expression level was unaffected by the stimulation of the receptor. Therefore, the concentrations applied and the duration of stimulation did not activate any negative or positive feedback mechanisms. The *DOCK1* expression level however, remained unaffected as well, except of one pAML sample tested. Interestingly, the exceptional sample displayed not only the highest *CXCR4* mRNA-expression among all tested samples, but also by far the highest surface expression level of CXCR4. It can be concluded that the *DOCK1*-expression level in AML cells with a low to moderate CXCR4-surface expression is independent of CXCR4-signaling. Whether a high CXCR4-surface expression can amplify the CXCR4 signaling to such an extent that the *DOCK1* transcription rate is amplified has to be evaluated with additional samples. Further evaluation of the influence of CXCR4 signaling to the functionality of DOCK1 such as Rac activation or cell migration with respect to the CXCR4-surface expression might be interesting to investigate.

In addition to the CXCR4 signaling, JAK2 was evaluated as a possible upstream mediator, since both *DOCK1*-expressing cell lines, UKE-1 and TF-1, can be associated with an aberrant JAK2 signaling. One of the main somatic driver mutations for myeloproliferative neoplasms, the JAK2 V617F tyrosine kinase mutation, which leads to a constitutively active JAK2, is present in UKE-1 cells[239,240]. In TF-1 cells, the proliferation is dependent on the presence of GM-CSF[228]. The downstream signaling of GM-CSF can promote JAK2 activation[241]. Therefore, it was investigated whether a causal relationship between JAK2 signaling and *DOCK1*-expression exists. Since it was demonstrated that JAK2 activation can activate the CXCR4 pathway[242], the *CXCR4* expression was evaluated accordingly.

In UKE-1 cells, treatment of the cells with the JAK-inhibitor ruxolitinib did not show any significant effect in *DOCK1*-mRNA expression or DOCK1-protein level. Interestingly, the treatment with ruxolitinib resulted in a dose-dependent increase in *CXCR4*-expression level, contrary to expectations. This leads to the assumption that this increase might be a form of

feedback mechanism due to JAK2 inhibition, where the JAK2 inhibition may inhibit the CXCR4 signaling, which is compensated by an increased *CXCR4*-transcription rate. In TF-1 cells however, the withdrawal of GM-CSF did not lead to a significant decrease in *DOCK1*-mRNA expression or protein level, even though the proliferation was significantly reduced.

In general, it can be concluded that both signaling pathways, CXCR4 and JAK2, are not relevant for the regulation of *DOCK1* transcription in AML. Whether they influence the functional properties in AML cells has to be further analyzed.

### 4.2.2 Several potential members of the DOCK1 signaling pathway are revealed

To reveal potential unknown members of the DOCK1 signaling pathway, different approaches were pursued. The transcriptome of *DOCK1*-knockdown TF-1 cells compared to control cells was analyzed by RNA-sequencing. Several genes with an aberrant gene expression resulting from a *DOCK1*-knockdown were revealed. Since the FDR for all dysregulated genes with a p-value < 0.05 was very high, the hits can only be considered as a tendency that the identified genes might be relevant. Of the 19 hits of interest, four genes (*NXPH4, INHBE, CHAC1, GDF15*) showed the same approximate tendency in RT-qPCR analysis as in the RNA-Seq comparison and therefore represent potential candidates for further validation. All four genes displayed a simultaneous downregulation with *DOCK1* in RNA-Seq analysis and RT-qPCR.

*NXPH4* encodes for an α-neurexin ligand, which interacts with α-neurexin and $GABA_A$ receptors within the cerebellum[259]. Until today, no involvement of NXPH4 in cancer entities has been described.

RefSeq information describes *INHBE* (NM_031479.5) as a member of the TGF-β superfamily, which encodes for an inhibin beta subunit[260]. Inhibins are involved in several cellular processes such as proliferation, apoptosis, hormone secretion and immune response[260]. INHBE is predominantly expressed in the liver[261], but could be detected in normal as well as malignant cervical, placental and endometrial tissue[262–264]. Mechanistically, INHBE is described as a hedgehog target gene for stem cell signaling regulation[265]. Interestingly, high expression levels of the family member inhibin subunit beta A (INHBA) was identified to be a negative prognostic marker in *de novo* AML[266].

The gene *CHAC1* (NM_001142776.4) encodes for a member of the gamma-glutamylcyclotransferase family[260]. High expression of the encoded protein was reported to

be associated with poor patient outcomes in breast and ovarian cancer as well as in uveal melanoma[267,268]. Liu *et al*. demonstrated for uveal melanoma cells that a downregulation of *CHAC1* decreased the cell proliferation and migration[268]. Furthermore, the PI3K pathway was suppressed after downregulation of *CHAC1* in uveal melanoma cells[268]. As previously presented, the PI3K/AKT signaling pathway has been described to be aberrantly regulated in LSCs[62,83] (refer 1.2.2). Moreover, Rac GTPases are known PI3K downstream effectors[269,270]. Thereby, CHAC1 might be a potential upstream regulator for DOCK1-dependent Rac activation through PI3K signaling.

*GDF15* (NM_004864.4) is encoding a secreted ligand for TGF-β receptors, which acts as a cytokine and leads to activation of SMAD family transcription factors[260]. In tumor progression, opposing functions for GDF15 have been described, as it is associated with tumor promoting and tumor suppressive properties[271]. GDF15 is of particular interest as a potential member of the DOCK1 signaling pathway, since it was reported to be a critical component for the interaction between AML cells and stromal cells of the bone marrow microenvironment. Zhai *et al*. revealed an involvement of GDF15 in the chemo-protective function of cancer-associated fibroblasts (CAF) for AML cells within the bone marrow[272]. Reduction of CAF-derived GDF15 led to chemosensitization of AML cells[272]. GDF15 is not only expressed in stromal cells, Lu *et al*. demonstrated that it is also highly expressed by AML cells[273]. Furthermore, it was shown that GDF15, derived from leukemic cells, contribute to the remodeling of bone marrow adipocytes, which promote AML cell proliferation[273]. In a recently published study, the PI3K/AKT signaling pathway was identified as a downstream pathway of GDF15 upon binding to its receptor TGFβRII in bone marrow adipocytes[274]. An inhibition of adipocyte remodeling led to a prolonged survival in an AML *in vivo* mouse model[274]. In response to chemotherapy, however, an overexpression of GDF15 by bone marrow mononuclear cells, which promoted inhibitory effects on adipogenesis, was demonstrated[275]. A reduced bone marrow adipocyte volume during complete remission was shown to be beneficial for AML patients[275]. These findings indicate that GDF15 plays a divergent role for cancer progression in different cellular constellations. For several cancer entities GDF15-involvement in migratory and invasive processes is described[276–279].

Of the remaining 15 hits revealed by the RNA-sequencing analysis, eight genes (*CYMA5*, *MRPL20*, *GTF2H3*, *RPS26*, *CSNK1A1L*, *HSD17B10*, *KCNE3*, *CFAP58*) could not be directly associated with tumor progression in any malignant entity by literature research. The last

seven of the identified genes (*GLCE*, *ULBP1*, *ATF3*, *CTH*, *ASS1*, *ECM1*, *TRIP6*) could be associated with tumorigenesis. Most of them are involved in cancer cell migration and invasion.

*GLCE* encodes for the D-glucuronyl C5-epimerase, a key enzyme for the biosynthesis of proteoglycans, and it was identified as a potential tumor suppressor in breast cancer and lung cancer[280,281]. Whereas for prostate cancer cells, a tumor promoting effect of GLCE through activation of angiogenesis, is discussed[282]. The RNA-Seq analysis for *GLCE*, however, showed the first fold change (FC) value above the cutoff of 0.75 and the second one near 0.75. Furthermore, the RT-qPCR could not verify the divergent expression. Therefore, it seems unlikely that GLCE is a potential member of the DOCK1 signaling in AML.

The gene *ULBP1* encodes for an activating NK receptor ligand, which is frequently expressed by AML blasts next to other activating and inhibitory ligands[283]. It was demonstrated that *ULBP1* expression in AML cells is regulated by c-Myc[284]. Literature research could not identify any involvement of ULBP1 in DOCK1-related signaling and RT-qPCR analysis could not verify a dysregulation after DOCK1-knockdown in TF-1 cells. Therefore, further investigations seem unlikely to reveal a connection.

The role of the transcription factor ATF3, which is encoded by the gene *ATF3*, in tumorigenesis is controversially discussed. In colorectal cancer, glioblastoma and bladder cancer, ATF3 was identified as a tumor-suppressor by reducing the migratory ability of the malignant cells[285–287]. In lung cancer and colon cancer metastasis, however, an oncogenic effect of ATF3 was described[288,289]. Interestingly, in gastric cancer cells, a simultaneous downregulation of *DOCK1* and upregulation of *AFT3* among other divergent regulated genes were observed after treatment with mycophenolic acid, an inosine monophosphate dehydrogenase inhibitor[290]. Whether there is a causal relationship between both molecules, is not yet known. Contrary to the study in gastric cancer cells, RNA-sequencing for *DOCK1*-knockdown AML cells indicated a simultaneous downregulation for both genes. Since *ATF3* was not detectable in TF-1 cells by RT-qPCR, this tendency could not be verified.

Only little is known about the role of *CTH* in tumorigenesis. In prostate cancer cells, elevated expression of the encoded $H_2S$-producing enzyme cystathionine γ-lyase was reported to promote cancer progression and metastasis through NF-κB signaling[291]. RNA-Seq analysis showed that a downregulation of *CTH* was obtained after *DOCK1*-knockdown. This tendency

could not be verified by RT-qPCR. Therefore, a possible link between the signaling pathways of both molecules is unlikely.

*ASS1* encodes for a key enzyme for arginine synthesis and is associated with cancer cell migration and invasion[292–294]. In gastric cancer cells ASS1 expression is commonly increased and it is reported to promote migration and invasion[293,294]. Whereas in hepatocellular cancer cells, the opposite effect was described. The ASS1 expression was often low and it was demonstrated that ASS1 suppresses cancer cell invasion and metastasis[292]. In AML patients, however, leukemic blasts are mostly deficient for ASS1, while normal HSPCs express ASS1 on a higher level[295]. Further it was shown that arginine deprivation is a possible therapeutic strategy in addition to chemotherapy in AML[295]. Until today, it is not known whether ASS1 is involved in migratory or invasive processes in AML and no common signaling pathway for ASS1 and DOCK1 was identified so far.

The encoded glycoprotein of the gene *ECM1* was reported to promote migratory and invasive processes in several solid cancer entities and a number of different mechanisms have been discussed[296–301]. In cholangiocarcinoma cells, an overexpression of ECM1, which contributed to cancer cell migration and invasion, was associated with an activation of AKT/NF-κB signaling[296]. AKT was identified as a downstream molecule of DOCK1 in cardiomyocytes and lung adenocarcinoma cells, which led to a pro-survival effect[208,302]. In glioma and breast cancer cells, an activation of the NF-κB/Snail signaling pathway by DOCK1 was demonstrated, which induced epithelial-mesenchymal transition (EMT), a process that promote cancer cell migration and invasion[205,303,304]. In hepatocellular carcinoma cells it was demonstrated that ECM1 is also involved in EMT promotion[297]. Furthermore, in breast cancer cells, it was demonstrated that ECM1 is involved in the regulation of actin cytoskeleton changes possibly by altering expression of the pro-metastatic molecule S100A4 and Rho-family GTPases[298]. Even though the divergent expression of *ECM1* which was revealed by RNA-Seq analysis could not be verified by RT-qPCR analysis, the literature research revealed several common features for ECM1 and DOCK1 signaling. Therefore, further investigation of possible connections between signaling pathways in AML would be interesting.

Although the upregulation of *TRIP6* upon *DOCK1*-knockdown could not be validated by RT-qPCR, the encoded adaptor protein TRIP6 might be of great interest. TRIP6 was identified to have a dual role as a cytoskeletal and a signaling protein[305]. It is involved in a variety of cellular processes such as actin cytoskeleton organization, cell adhesion, migration, invasion,

proliferation and survival[305,306]. The main location is at sites of focal adhesion and the cytosol, where TRIP6 interacts with several different proteins[305,306]. Additionally, it is capable to translocate into the nucleus, where it acts as a transcriptional coregulator[305,306]. Of particular interest is the involvement of TRIP6 in focal adhesion, actin cytoskeleton reorganization and cell motility, since DOCK1 was also reported to be involved in these cellular processes as reviewed in section 1.4.3. TRIP6 was associated with several direct binding partners, including $p130^{Cas}$ and Crk[307,308]. Both were identified to be involved in Rac-mediated actin cytoskeleton remodeling upon integrin signaling by forming an DOCK1-CrkII-$p130^{Cas}$ complex at sites of focal adhesion[166,191]. Furthermore, it was demonstrated in HeLa cells that TRIP6 is important for Rho GTPase-mediated actin cytoskeleton reorganization during cell-matrix and cell-cell adhesion[309]. Interestingly, an increased Rac1 activation was observed in TRIP6-depleted cells, resulting in abnormal level of actin polymerization. It was demonstrated that this enhanced Rac1 activation was not mediated through the DOCK1-CrkII-$p130^{Cas}$ complex, rather it was suggested that the DOCK1-CrkII-$p130^{Cas}$ complex was suppressed by TRIP6-depletion[309]. The published studies indicate that there might be a closer relationship between TRIP6 and DOCK1 signaling pathways. Until today, it is not known whether TRIP6 is involved in the cancer progression of AML. For several other cancer entities, an aberrant regulation of TRIP6 has been reported and an overexpression was mainly associated with enhanced cell motility[310–312].

Literature research revealed *ECM1* and *TRIP6* as interesting candidates for further investigations, even though RT-qPCR analysis could not verify the divergent expression, which was revealed by RNA-sequencing. Although the genes *GLCE*, *ULBP1*, *ATF3*, *CTH*, *ASS1* could be associated with tumorigenesis, no obvious connection to DOCK1 could be revealed. Therefore, a relevance of the respective gene products for DOCK1 signaling seems unlikely.

Next to the transcriptome of *DOCK1*-knockdown TF-1 cells, protein-protein interactions were analyzed by mass spectrometry using *DOCK1*-double-knockdown TF-1 and UKE-1 cells. Since the quality of the samples in the second attempt was not high enough to reliably identify protein bands matching the criteria for significant identification, further validation is mandatory and the revealed proteins can only be considered as a tendency. Of the identified seven protein bands, only two had a visibly different protein amount between knockdown and control cells (Fer-1 like protein 3, Ankyrin repeat domain-containing protein 26). The remaining five were well visible bands in all lanes (Stress-70 protein, MAGUK p55 subfamily

member 4, Tubulin beta chain, Actin-related protein 2/3 complex subunit 1A, Heterogeneous nuclear ribonucleoprotein A2/B1).

The Fer-1 like protein 3, also known as Myoferlin, was only visible in TF-1 double-knockdown cells. Myoferlin is a membrane-anchored protein, which is involved in a variety of membrane trafficking processes such as membrane fusion and repair[313]. It was reported to be involved in cancer progression by promoting cellular processes such as cancer cell proliferation, migration and invasion in several cancer entities[313,314]. In AML however, the encoder gene *MYOF* was identified as a possible biomarker[315].

Ankyrin repeat domain-containing protein 26 (ANKRD26), could only be detected in UKE-1 double-knockdown cells. Point mutations in the *ANKRD26* gene were associated with the development of thrombocytopenia and increased risk for developing AML[316].

The encoder gene for Stress-70 protein, also known as HSPA9 or mortalin, was identified to be highly conserved and to present a potential myeloid leukemia tumor suppressor gene on chromosome 5q31, which is frequently deleted in myeloid leukemias[317]. The mortalin protein however, had been reported to be overexpressed in different cancer entities, which contributes to tumorigenesis[318]. In breast cancer cells it was demonstrated that mortalin overexpression promoted EMT as well as cell motility and was associated with an upregulation of proteins involved in focal adhesion, PI3K/AKT, and JAK/STAT signaling pathways[319]. Furthermore, Yun *et al*. reported that an overexpression of mortalin contributes to cancer cell stemness[320].

Ibrahim *et al.* reported that MAGUK p55 subfamily member 4 (MPP4) was downregulated in breast cancer cells after downregulation of syndecan-1[321]. Decreased Syndecan-1 led to increased cell motility by Rho GTPase activation and E-cadherin downregulation[321]. Further investigations about the role of MPP4 were not pursued by the authors.

Tubulin beta chain, encoded by the gene *TUBB* (Gene ID: 203068), is a structural component of microtubules[260]. It had been reported to be involved in the chemoresistance of non-small cell lung cancer cells[322].

Actin-related protein 2/3 complex subunit 1A (ARPC1A) is a subunit of the Arp2/3 complex, which is a key regulator of actin polymerization by generating branched actin networks and is therefore important for cell motility[323]. In pancreatic cancer an elevated expression of the

encoder gene *ARPC1A* was demonstrated and associated with the regulation of cell migration and invasion[324].

Heterogeneous nuclear ribonucleoprotein A2/B1 (hnRNP A2/B1), a RNA-binding protein, which is involved in mRNA processing, was reported to be involved in the migration and invasion of different cancer cells types such as lung cancer cells, glioblastoma cells and cervical cancer cells[325–327]. Mechanistically, different signaling pathways, like PI3K/AKT and NF-κB, were discussed to be involved[327,328].

Even though most of the identified proteins were reported to be involved in cell motility or in cancer progression, potential connections between the identified proteins and DOCK1 signaling pathway could not be revealed by literature research. Therefore, further investigations are needed.

In addition to the analysis of protein-protein interactions by mass spectrometry, changes in the phosphorylation pattern were analyzed after DOCK1 inhibition in TF-1 cells, to identify potential kinase targets within the signaling cascade. Phosphoprotein staining of the polyacrylamide gel revealed only three spots, which were visibly different. From those three spots, only two could be recognized by peptide mass fingerprinting. Both spots consisted of a protein mixture. For each spot a top score protein was revealed, but both did not fulfill the criteria for significant protein identification. Therefore, further validation is mandatory and the revealed proteins can only be considered as a tendency.

One of the revealed proteins was WD repeat and FYVE domain-containing protein 3 (WDFY3), also known as ALFY, which is a PI3P-binding protein, that acts as an autophagy scaffold protein[244]. In AML, ALFY was reported to have a critical role in granulocytic differentiation of leukemic cells, which is of great importance for ATRA-treated cells[329]. The second revealed protein was synaptojanin-1 (SYNJ1), which is a polyphosphoinositide phosphatase, involved in synaptic vesicle traffic[245]. The closely related family member synaptojanin-2 was identified as a downstream effector of Rac1 and possibly contributes to the Rac1-mediated regulation of cell proliferation by inhibiting endocytosis of growth factor receptors[330]. It can be assumed that the related synaptojanin-1 might fulfill a similar function in AML cells. Further investigations are necessary to confirm this assumption.

In summary, the different approaches to reveal potential unknown members of the DOCK1 signaling pathway in combination with a profound literature research identified several

interesting molecules, which might be directly or indirectly involved in DOCK1 signaling. Since the performed approaches did not provide reliable results, the corresponding hits could only be regarded as a tendency and a suitable validation is mandatory.

## 4.3 Conclusion and Outlook

The bone marrow and its microenvironment are highly complex and numerous different signaling pathways are involved. The thesis presented here demonstrates that the transfer from a complex biological system of an organism to simplified *in vitro* approaches is not always achievable. Most of the *in vitro* assays performed did not fulfill the expectations. Although the small molecule inhibitors CPYPP and TBOPP showed a clear antileukemic effect, this could not be deduced as a function of DOCK1. Downregulation or overexpression of *DOCK1* in AML cell lines did not show any effect *in vitro*, but it could be clearly demonstrated that there is a relevance *in vivo*. The data presented here indicate that DOCK1 does not have any influence on the survival of leukemic cells. Rather a function in leukemic cell infiltration and signaling within the bone marrow niche can be assumed. Prior to this project, *DOCK1* was revealed as an inducible factor within the bone marrow microenvironment. A distinct difference between *DOCK1*-expressing AML cells and *DOCK1*-deficient cells could be demonstrated in *in vivo* experiments, performed as part of this thesis. *DOCK1* expression led to a higher early leukemic infiltration and a greater promotion of splenomegaly as well as HSPC egress from the bone marrow. The underlying mechanisms and the consequences for the course of the disease still remain unknown. Possibly certain genes or proteins which have been identified by RNA-sequencing or mass spectrometric analysis might be involved in the DOCK1-mediated effects.

Further detailed investigations are necessary to understand the impact and relevance of the DOCK1-induced phenomena. Validation of a causal relationship between DOCK1 and the identified genes or proteins in AML cell lines and primary AML samples could be carried out with different *in vitro* approaches. Furthermore, additional *in vivo* investigation about the pathophysiological role of the manipulation of *DOCK1*-expression in AML cell lines would be interesting. Especially the different level of leukemic engraftment in bone marrow and extramedullary infiltration as well as the localization of HSPCs at different stages of the disease (early, intermediate, advanced engraftment) between *DOCK1*-expressing and *DOCK1*-deficient AML cells would be a promising next approach.

# SUPPLEMENT

**Supplementary Table 1: Relative mRNA-expression data of *DOCK1*, *DOCK2* and *DOCK5* in pAML-samples.** Relative mRNA expression was determined by RT-qPCR, with *GAPDH* as a reference gene, in 21 pAML-samples with the ΔCT-method as well as according to Pfaffl[225].

| pAML-sample ID | DOCK1 (ΔCt)* | DOCK2 (ΔCt)* | DOCK5 (ΔCt)* | DOCK1 (n-fold) | DOCK2 (n-fold) | DOCK5 (n-fold) |
|---|---|---|---|---|---|---|
| 01 | 10.31 | 234.88 | 1.78 | 1010.73 | 2.12 | 0.18 |
| 02 | 0.04 | 125.87 | 31.25 | 3.94 | 1.21 | 2.13 |
| 03 | 0.61 | 136.79 | 15.73 | 64.50 | 1.36 | 1.19 |
| 04 | 0.04 | 48.36 | 8.79 | 3.92 | 0.55 | 0.73 |
| 05 | 0.28 | 116.63 | 10.67 | 32.87 | 1.23 | 0.86 |
| 06 | 15.84 | 62.07 | 3.67 | 1972.55 | 0.69 | 0.34 |
| 07 | 1.98 | 33.49 | 1.85 | 217.55 | 0.38 | 0.19 |
| 08 | 1.82 | 34.67 | 3.42 | 202.97 | 0.39 | 0.32 |
| 09 | 0.01 | 97.40 | 12.87 | 1.00 | 1.00 | 1.00 |
| 10 | 4.10 | 45.75 | 5.80 | 492.95 | 0.52 | 0.51 |
| 11 | 2.56 | 87.17 | 13.32 | 281.00 | 0.90 | 1.03 |
| 12 | 8.09 | 63.81 | 3.31 | 859.19 | 0.66 | 0.31 |
| 13 | 1.93 | 87.17 | 7.65 | 215.84 | 0.91 | 0.64 |
| 14 | 0.02 | 108.82 | 11.60 | 2.58 | 1.16 | 0.92 |
| 15 | 2.23 | 26.28 | 3.33 | 293.87 | 0.32 | 0.32 |
| 16 | 4.68 | 46.39 | 3.67 | 686.04 | 0.57 | 0.35 |
| 17 | 3.80 | 64.26 | 6.30 | 506.30 | 0.74 | 0.55 |
| 18 | 0.76 | 40.67 | 4.98 | 78.71 | 0.44 | 0.44 |
| 19 | 0.39 | 39.28 | 4.61 | 43.66 | 0.45 | 0.42 |
| 20 | 0.95 | 58.72 | 12.01 | 105.46 | 0.64 | 0.94 |
| 21 | 2.84 | 48.70 | 5.88 | 344.46 | 0.55 | 0.51 |

** ΔCt = 2^(- ΔCt)*1000*

**Supplementary Table 2: Relative mRNA-expression data of *DOCK1*, *DOCK2*, *DOCK5* and *ELMO1* in AML cell lines.** Relative mRNA expression was determined by RT-qPCR, with *GAPDH* as a reference gene, in 11 AML cell lines with the ΔCT-method.

| Cell line | DOCK1 (ΔCt)* | DOCK2 (ΔCt)* | DOCK5 (ΔCt)* | ELMO1 (ΔCt)* |
|---|---|---|---|---|
| MV4-11 | 0 | 12.96 | 1.08 | 2.80 |
| UKE-1 | 1.81 | 13.60 | 0.86 | 5.56 |
| Kasumi-1 | 0 | 12.09 | 0 | 7.70 |
| OCI AML3 | 0 | 20.76 | 2.71 | 1.18 |
| Molm13 | 0 | 10.38 | 1.45 | 4.58 |
| Mono Mac | 0 | 10.17 | 1.40 | 2.34 |
| OCI AML5 | 0 | 10.90 | 1.38 | 8.67 |
| OCI-M1 | 0 | 10.67 | 0.07 | 4.81 |
| HL-60 | 0 | 14.48 | 0.50 | 6.43 |
| TF-1 | 7.87 | 7.65 | 0.46 | 11.05 |
| THP-1 | 0.008 | 14.48 | 0.36 | 10.31 |

** ΔCt = 2^(- ΔCt)*1000*

**Supplementary Table 3: Relative surface expression of CXCR4 as well as relative mRNA expression of *CXCR4* and *DOCK1* in pAML samples.** Relative mRNA expression was determined by RT-qPCR, with *GAPDH* as a reference gene, in 9 pAML-samples with the ΔCT-method. Relative surface expression of CD33, CD34 and CXCR4 was determined by flow cytometric analysis as part of a routine FACS-panel of the research group for primary AML samples. CXCR4 expression was assessed on CD33- or CD34-positive cells, since these markers are usually found on AML blasts.

| pAML-sample ID | CD33 total [%] | CD33/CXCR4 double-pos. [%] | CD34 total [%] | CD34/CXCR4 double-pos. [%] | CXCR4 (ΔCt)* | DOCK1 (ΔCt)* |
|---|---|---|---|---|---|---|
| 22 | 5.73 | 1.41 | - | - | 29.24 ± 3.15 | 1.26 ± 0.27 |
| 23 | 87.30 | 15.35 | 2.28 | 0.49 | 62.80 ± 4.61 | 2.54 ± 0.15 |
| 24 | 2.16 | 0.42 | 35.85 | 2.14 | 8.24 ± 4.20 | < 0.001 |
| 25 | 94.09 | 70.88 | 3.44 | 2.54 | 88.44 ± 21.81 | 0.013 ± 0.006 |
| 26 | 74.17 | 0.74 | 73.24 | 0.17 | 25.80 ± 25.61 | 0.01 ± 0.01 |
| 27 | - | - | - | - | 80.83 ± 16.91 | 1.37 ± 0.09 |
| 28 | - | - | - | - | 14.69 ± 0.72 | 0.81 ± 0.02 |
| 29 | - | - | - | - | 44.44 ± 4.13 | 0.78 ± 0.29 |
| 30 | 98.07 | 43.60 | 21.46 | 4.06 | 24.01 ± 3.53 | 1.24 ± 0.15 |

** ΔCt = 2^(- ΔCt)*1000*

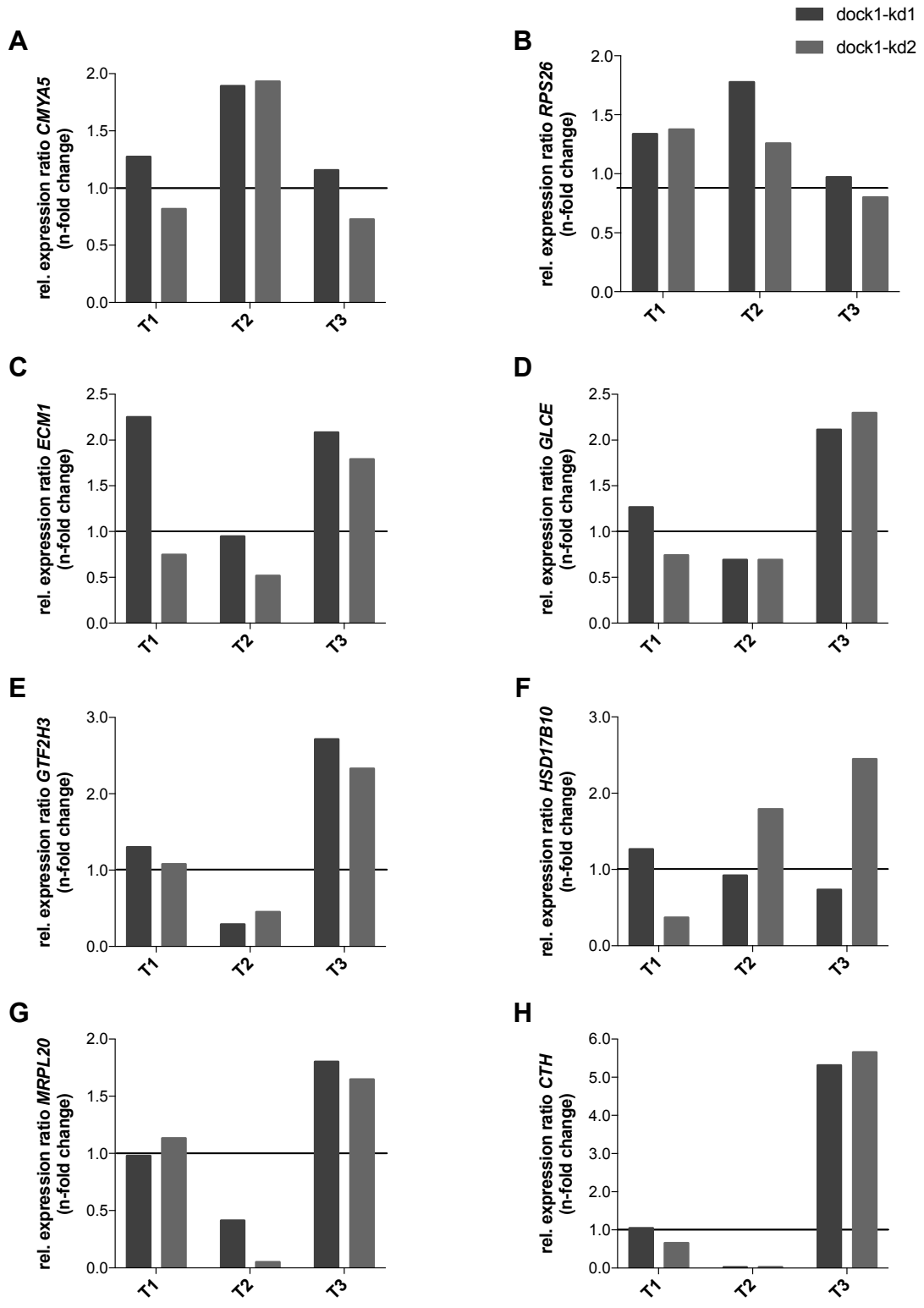


**Supplementary Figure 1: Verification of hits of the RNA-Seq comparison with RT-qPCR.** RNA samples from three independent transductions (T), which were included in the RNA-Seq analysis, were used for RT-qPCR. TF-1-scrambled control was compared against single TF-1-*DOCK1*-knockdown of two different shRNAs. The relative mRNA expression of *CMYA5* (**A**), *RPS26* (**B**), *ECM11* (**C**), *GLCE* (**D**), *GTF2H3* (**E**), *HSD17B10* (**F**), *MRPL20* (**G**) and *CTH* (**H**) was determined according to Pfaffl[225] with *GAPDH* as reference gene and scrambled-shRNA transduced cells serving as calibrator. The relative expression ratio is expressed compared to the scrambled-shRNA transduced control cells (represented as a black line).

# LITERATURE


1. Lee, S. *et al.* High expression of dedicator of cytokinesis 1 (DOCK1) confers Poor Prognosis in Acute Myeloid Leukemia. *Oncotarget* **8**, 72250–72259 (2017).
2. Prada-Arismendy, J., Arroyave, J. C. & Röthlisberger, S. Molecular biomarkers in acute myeloid leukemia. *Blood Rev.* **31**, 63–76 (2017).
3. Döhner, H., Weisdorf, D. J. & Bloomfield, C. D. Acute Myeloid Leukemia. *New England Journal of Medicine* **373**, 1136–1152 (2015).
4. De Kouchkovsky, I. & Abdul-Hay, M. 'Acute myeloid leukemia: A comprehensive review and 2016 update'. *Blood Cancer Journal* **6**, e441 (2016).
5. Nennecke, A., Wienecke, A. & Kraywinkel, K. Inzidenz und Überleben bei Leukämien in Deutschland nach aktuellen standardisierten Kategorien. *Bundesgesundheitsbl.* **57**, 93–102 (2014).
6. Kraywinkel, K. & Spix, C. Epidemiologie akuter Leukämien in Deutschland. *Onkologe* **23**, 499–503 (2017).
7. Yamamoto, J. F. & Goodman, M. T. Patterns of leukemia incidence in the United States by subtype and demographic characteristics, 1997–2002. *Cancer Causes Control* **19**, 379–390 (2008).
8. Shah, A., Andersson, T. M.-L., Rachet, B., Björkholm, M. & Lambert, P. C. Survival and cure of acute myeloid leukaemia in England, 1971-2006: a population-based study. *Br. J. Haematol.* **162**, 509–516 (2013).
9. Bertoli, S. *et al.* Improved outcome for AML patients over the years 2000-2014. *Blood Cancer J.* **7**, 635 (2017).
10. Derolf, Å. R. *et al.* Improved patient survival for acute myeloid leukemia: a population-based study of 9729 patients diagnosed in Sweden between 1973 and 2005. *Blood* **113**, 3666–3672 (2009).
11. Thein, M. S., Ershler, W. B., Jemal, A., Yates, J. W. & Baer, M. R. Outcome of older patients with acute myeloid leukemia. *Cancer* **119**, 2720–2727 (2013).
12. Pulte, D. *et al.* Survival in patients with acute myeloblastic leukemia in Germany and the United States: Major differences in survival in young adults. *Int. J. Cancer* **139**, 1289–1296 (2016).
13. Sill, H., Olipitz, W., Zebisch, A., Schulz, E. & Wölfler, A. Therapy-related myeloid neoplasms: pathobiology and clinical characteristics. *Br. J. Pharmacol.* **162**, 792–805 (2011).
14. Leone, G., Mele, L., Pulsoni, A., Equitani, F. & Pagano, L. The incidence of secondary leukemias. *Haematologica* **84**, 937–945 (1999).
15. Granfeldt Østgård, L. S. *et al.* Epidemiology and Clinical Significance of Secondary and Therapy-Related Acute Myeloid Leukemia: A National Population-Based Cohort Study. *J. Clin. Oncol.* **33**, 3641–3649 (2015).
16. Patel, J. P. *et al.* Prognostic Relevance of Integrated Genetic Profiling in Acute Myeloid Leukemia. *N. Engl. J. Med.* **366**, 1079–1089 (2012).
17. Greenman, C. *et al.* Patterns of somatic mutation in human cancer genomes. *Nature* **446**, 153–158 (2007).
18. Cancer Genome Atlas Research Network *et al.* Genomic and epigenomic landscapes of adult

de novo acute myeloid leukemia. *N. Engl. J. Med.* **368**, 2059–2074 (2013).

19. Vosberg, S. & Greif, P. A. Clonal evolution of acute myeloid leukemia from diagnosis to relapse. *Genes, Chromosom. Cancer* **58**, 839–849 (2019).
20. Ferrara, F. & Schiffer, C. A. Acute myeloid leukaemia in adults. *Lancet* **381**, 484–495 (2013).
21. Döhner, H. *et al.* Diagnosis and management of AML in adults: 2017 ELN recommendations from an international expert panel. *Blood* **129**, 424–447 (2017).
22. Béné, M. C. *et al.* Immunophenotyping of acute leukemia and lymphoproliferative disorders: a consensus proposal of the European LeukemiaNet Work Package 10. *Leukemia* **25**, 567–574 (2011).
23. Bennett, J. M. *et al.* Proposals for the Classification of the Acute Leukaemias French-American-British (FAB) Co-operative Group. *Br. J. Haematol.* **33**, 451–458 (1976).
24. Bennett, J. M. *et al.* Proposed Revised Criteria for the Classification of Acute Myeloid Leukemia : A Report of the French-American-British Cooperative Group. *Ann. Intern. Med.* **103**, 620–625 (1985).
25. Bennett, J. M. *et al.* Criteria for the Diagnosis of Acute Leukemia of Megakaryocyte Lineage (M7): A Report of the French-American-British Cooperative Group. *Ann. Intern. Med.* **103**, 460–462 (1985).
26. Bloomfield, C. D. & Brunning, R. D. FAB M7: Acute Megakaryoblastic Leukemia-Beyond Morphology. *Ann. Intern. Med.* **103**, 450–452 (1985).
27. Bennett, J. M. *et al.* Proposal for the recognition of minimally differentiated acute myeloid leukaemia (AML-MO). *Br. J. Haematol.* **78**, 325–329 (1991).
28. Vardiman, J. W. *et al.* The 2008 revision of the World Health Organization (WHO) classification of myeloid neoplasms and acute leukemia: rationale and important changes. *Blood* **114**, 937–951 (2009).
29. Arber, D. A. *et al.* The 2016 revision to the World Health Organization classification of myeloid neoplasms and acute leukemia. *Blood* **127**, 2391–2405 (2016).
30. Canaani, J. *et al.* Impact of FAB classification on predicting outcome in acute myeloid leukemia, not otherwise specified, patients undergoing allogeneic stem cell transplantation in CR1: An analysis of 1690 patients from the acute leukemia working party of EBMT. *Am. J. Hematol.* **92**, 344–350 (2017).
31. Kantarjian, H. *et al.* Results of intensive chemotherapy in 998 patients age 65 years or older with acute myeloid leukemia or high-risk myelodysplastic syndrome: *Cancer* **106**, 1090–1098 (2006).
32. Hulegårdh, E. *et al.* Characterization and prognostic features of secondary acute myeloid leukemia in a population-based setting: A report from the Swedish Acute Leukemia Registry. *Am. J. Hematol.* **90**, 208–214 (2015).
33. Byrd, J. C. *et al.* Pretreatment cytogenetic abnormalities are predictive of induction success, cumulative incidence of relapse, and overall survival in adult patients with de novo acute myeloid leukemia: results from Cancer and Leukemia Group B (CALGB 8461). *Blood* **100**, 4325–4336 (2002).
34. Papaemmanuil, E. *et al.* Genomic Classification and Prognosis in Acute Myeloid Leukemia. *N. Engl. J. Med.* **374**, 2209–2221 (2016).
35. Gupta, V., Tallman, M. S. & Weisdorf, D. J. Allogeneic hematopoietic cell transplantation for adults with acute myeloid leukemia: myths, controversies, and unknowns. *Blood* **117**, 2307–2318 (2011).

36. Gurnari, C., Voso, M. T., Maciejewski, J. P. & Visconte, V. From Bench to Bedside and Beyond: Therapeutic Scenario in Acute Myeloid Leukemia. *Cancers* **12**, 357 (2020).

37. Larrosa-Garcia, M. & Baer, M. R. FLT3 Inhibitors in Acute Myeloid Leukemia: Current Status and Future Directions. *Mol. Cancer Ther.* **16**, 991–1001 (2017).

38. Daver, N., Schlenk, R. F., Russell, N. H. & Levis, M. J. Targeting FLT3 mutations in AML: review of current knowledge and evidence. *Leukemia* **33**, 299–312 (2019).

39. U.S. Food and Drug Administration. Midostaurin. *28.04.2017* (2017). Available at: https://www.fda.gov/drugs/resources-information-approved-drugs/midostaurin.

40. Stone, R. M. *et al.* Midostaurin plus Chemotherapy for Acute Myeloid Leukemia with a FLT3 Mutation. *N. Engl. J. Med.* **377**, 454–464 (2017).

41. U.S. Food and Drug Administration. FDA approves addition of survival data to gilteritinib label for refractory AML with a FLT3 mutation. *29.05.2019* (2019). Available at: https://www.fda.gov/drugs/resources-information-approved-drugs/fda-approves-addition-survival-data-gilteritinib-label-refractory-aml-flt3-mutation.

42. Perl, A. E. *et al.* Gilteritinib or Chemotherapy for Relapsed or Refractory FLT3-Mutated AML. *N. Engl. J. Med.* **381**, 1728–1740 (2019).

43. Im, A. *et al.* DNMT3A and IDH mutations in acute myeloid leukemia and other myeloid malignancies: associations with prognosis and potential treatment strategies. *Leukemia* **28**, 1774–1783 (2014).

44. Dhillon, S. Ivosidenib: First Global Approval. *Drugs* **78**, 1509–1516 (2018).

45. DiNardo, C. D. *et al.* Durable Remissions with Ivosidenib in IDH1-Mutated Relapsed or Refractory AML. *N. Engl. J. Med.* **378**, 2386–2398 (2018).

46. Kim, E. S. Enasidenib: First Global Approval. *Drugs* **77**, 1705–1711 (2017).

47. Stein, E. M. *et al.* Enasidenib in mutant IDH2 relapsed or refractory acute myeloid leukemia. *Blood* **130**, 722–731 (2017).

48. Popovici-Muller, J. *et al.* Discovery of AG-120 (Ivosidenib): A First-in-Class Mutant IDH1 Inhibitor for the Treatment of IDH1 Mutant Cancers. *ACS Med. Chem. Lett.* **9**, 300–305 (2018).

49. Shih, A. H. *et al.* AG-221, a Small Molecule Mutant IDH2 Inhibitor, Remodels the Epigenetic State of IDH2-Mutant Cells and Induces Alterations in Self-Renewal/Differentiation in IDH2-Mutant AML Model in Vivo. *Blood* **124**, 437 (2014).

50. Harding, J. J. *et al.* Isoform Switching as a Mechanism of Acquired Resistance to Mutant Isocitrate Dehydrogenase Inhibition. *Cancer Discov.* **8**, 1540–1547 (2018).

51. Zhou, J. *et al.* BCL2 overexpression: clinical implication and biological insights in acute myeloid leukemia. *Diagn. Pathol.* **14**, 68 (2019).

52. Lagadinou, E. D. *et al.* BCL-2 Inhibition Targets Oxidative Phosphorylation and Selectively Eradicates Quiescent Human Leukemia Stem Cells. *Cell Stem Cell* **12**, 329–341 (2013).

53. Thomas, D. & Majeti, R. Biology and relevance of human acute myeloid leukemia stem cells. *Blood* **129**, 1577–1585 (2017).

54. U.S. Food and Drug Administration. FDA approves venetoclax in combination for AML in adults. *21.11.2018* (2018). Available at: https://www.fda.gov/drugs/fda-approves-venetoclax-combination-aml-adults.

55. DiNardo, C. D. *et al.* Venetoclax combined with decitabine or azacitidine in treatment-naive, elderly patients with acute myeloid leukemia. *Blood* **133**, 7–17 (2019).

56. Irvine, D. A. & Copland, M. Targeting hedgehog in hematologic malignancy. *Blood* **119**, 2196–

2204 (2012).

57. Wellbrock, J. *et al.* Expression of Hedgehog Pathway Mediator GLI Represents a Negative Prognostic Marker in Human Acute Myeloid Leukemia and Its Inhibition Exerts Antileukemic Effects. *Clin. Cancer Res.* **21**, 2388–2398 (2015).

58. Fukushima, N. *et al.* Small-molecule Hedgehog inhibitor attenuates the leukemia-initiation potential of acute myeloid leukemia cells. *Cancer Sci.* **107**, 1422–1429 (2016).

59. Norsworthy, K. J. *et al.* FDA Approval Summary: Glasdegib for Newly Diagnosed Acute Myeloid Leukemia. *Clin. Cancer Res.* **25**, 6021–6025 (2019).

60. Cortes, J. E. *et al.* Randomized comparison of low dose cytarabine with or without glasdegib in patients with newly diagnosed acute myeloid leukemia or high-risk myelodysplastic syndrome. *Leukemia* **33**, 379–389 (2019).

61. Stresemann, C. & Lyko, F. Modes of action of the DNA methyltransferase inhibitors azacytidine and decitabine. *Int. J. Cancer* **123**, 8–13 (2008).

62. Wang, X., Huang, S. & Chen, J.-L. Understanding of leukemic stem cells and their clinical implications. *Mol. Cancer* **16**, 2 (2017).

63. Lapidot, T. *et al.* A cell initiating human acute myeloid leukaemia after transplantation into SCID mice. *Nature* **367**, 645–648 (1994).

64. Bonnet, D. & Dick, J. E. Human acute myeloid leukemia is organized as a hierarchy that originates from a primitive hematopoietic cell. *Nat. Med.* **3**, 730–737 (1997).

65. Corces-Zimmerman, M. R., Hong, W.-J., Weissman, I. L., Medeiros, B. C. & Majeti, R. Preleukemic mutations in human acute myeloid leukemia affect epigenetic regulators and persist in remission. *Proc. Natl. Acad. Sci. U. S. A.* **111**, 2548–2553 (2014).

66. Shlush, L. I. *et al.* Identification of pre-leukaemic haematopoietic stem cells in acute leukaemia. *Nature* **506**, 328–333 (2014).

67. Goardon, N. *et al.* Coexistence of LMPP-like and GMP-like Leukemia Stem Cells in Acute Myeloid Leukemia. *Cancer Cell* **19**, 138–152 (2011).

68. Jan, M. *et al.* Clonal Evolution of Preleukemic Hematopoietic Stem Cells Precedes Human Acute Myeloid Leukemia. *Sci. Transl. Med.* **4**, 149ra118 (2012).

69. Quek, L. *et al.* Genetically distinct leukemic stem cells in human CD34- acute myeloid leukemia are arrested at a hemopoietic precursor-like stage. *J. Exp. Med.* **213**, 1513–1535 (2016).

70. Taussig, D. C. *et al.* Anti-CD38 antibody–mediated clearance of human repopulating cells masks the heterogeneity of leukemia-initiating cells. *Blood* **112**, 568–575 (2008).

71. Ng, S. W. K. *et al.* A 17-gene stemness score for rapid determination of risk in acute leukaemia. *Nature* **540**, 433–437 (2016).

72. Ishikawa, F. *et al.* Chemotherapy-resistant human AML stem cells home to and engraft within the bone-marrow endosteal region. *Nat. Biotechnol.* **25**, 1315–1321 (2007).

73. Jin, L. *et al.* Monoclonal Antibody-Mediated Targeting of CD123, IL-3 Receptor α Chain, Eliminates Human Acute Myeloid Leukemic Stem Cells. *Cell Stem Cell* **5**, 31–42 (2009).

74. Jaiswal, S. *et al.* CD47 Is Upregulated on Circulating Hematopoietic Stem Cells and Leukemia Cells to Avoid Phagocytosis. *Cell* **138**, 271–285 (2009).

75. Majeti, R. *et al.* CD47 Is an Adverse Prognostic Factor and Therapeutic Antibody Target on Human Acute Myeloid Leukemia Stem Cells. *Cell* **138**, 286–299 (2009).

76. Askmyr, M. *et al.* Selective killing of candidate AML stem cells by antibody targeting of IL1RAP.

*Blood* **121**, 3709–3713 (2013).

77. Reya, T. *et al.* A role for Wnt signalling in self-renewal of haematopoietic stem cells. *Nature* **423**, 409–414 (2003).

78. Wang, Y. *et al.* The Wnt/β-Catenin Pathway Is Required for the Development of Leukemia Stem Cells in AML. *Science (80-. ).* **327**, 1650–1653 (2010).

79. Simon, M., Grandage, V. L., Linch, D. C. & Khwaja, A. Constitutive activation of the Wnt/β-catenin signalling pathway in acute myeloid leukaemia. *Oncogene* **24**, 2410–2420 (2005).

80. Cook, A. M. *et al.* Role of altered growth factor receptor-mediated JAK2 signaling in growth and maintenance of human acute myeloid leukemia stem cells. *Blood* **123**, 2826–2837 (2014).

81. Gurska, L. M., Ames, K. & Gritsman, K. Signaling Pathways in Leukemic Stem Cells. in *Leukemia Stem Cells in Hematologic Malignancies* (eds. Zhang, H. & Li, S.) 1–39 (Springer Singapore, 2019). doi:10.1007/978-981-13-7342-8_1

82. Hemmings, B. A. & Restuccia, D. F. PI3K-PKB/Akt Pathway. *Cold Spring Harb. Perspect. Biol.* **4**, a011189 (2012).

83. Martelli, A. M. *et al.* Phosphoinositide 3-kinase/Akt signaling pathway and its therapeutical implications for human acute myeloid leukemia. *Leukemia* **20**, 911–928 (2006).

84. Kharas, M. G. *et al.* Constitutively active AKT depletes hematopoietic stem cells and induces leukemia in mice. *Blood* **115**, 1406–1415 (2010).

85. Yilmaz, Ö. H. *et al.* Pten dependence distinguishes haematopoietic stem cells from leukaemia-initiating cells. *Nature* **441**, 475–482 (2006).

86. Varnum-Finney, B. *et al.* Pluripotent, cytokine-dependent, hematopoietic stem cells are immortalized by constitutive Notch1 signaling. *Nat. Med.* **6**, 1278–1281 (2000).

87. Chen, P. *et al.* Down-regulation of Notch-1 expression decreases PU.1-mediated myeloid differentiation signaling in acute myeloid leukemia. *Int. J. Oncol.* **32**, 1335–1341 (2008).

88. Klinakis, A. *et al.* A novel tumour-suppressor function for the Notch pathway in myeloid leukaemia. *Nature* **473**, 230–233 (2011).

89. Lobry, C. *et al.* Notch pathway activation targets AML-initiating cell homeostasis and differentiation. *J. Exp. Med.* **210**, 301–319 (2013).

90. Kannan, S. *et al.* Notch activation inhibits AML growth and survival: a potential therapeutic approach. *J. Exp. Med.* **210**, 321–337 (2013).

91. Kato, T. *et al.* Hes1 suppresses acute myeloid leukemia development through FLT3 repression. *Leukemia* **29**, 576–585 (2015).

92. Kode, A. *et al.* Leukaemogenesis induced by an activating β-catenin mutation in osteoblasts. *Nature* **506**, 240–244 (2014).

93. Liu, X. *et al.* Niche TWIST1 is critical for maintaining normal hematopoiesis and impeding leukemia progression. *Haematologica* **103**, 1969–1979 (2018).

94. Guzman, M. L. *et al.* Nuclear factor-κB is constitutively activated in primitive human acute myelogenous leukemia cells. *Blood* **98**, 2301–2307 (2001).

95. Zimmerman, A. L. & Wu, S. MicroRNAs, cancer and cancer stem cells. *Cancer Lett.* **300**, 10–19 (2011).

96. Han, Y.-C. *et al.* microRNA-29a induces aberrant self-renewal capacity in hematopoietic progenitors, biased myeloid development, and acute myeloid leukemia. *J. Exp. Med.* **207**, 475–489 (2010).

97. Khalaj, M. *et al.* miR-99 regulates normal and malignant hematopoietic stem cell self-renewal. *J. Exp. Med.* **214**, 2453–2470 (2017).

98. Lechman, E. R. *et al.* miR-126 Regulates Distinct Self-Renewal Outcomes in Normal and Malignant Hematopoietic Stem Cells. *Cancer Cell* **29**, 214–228 (2016).

99. Behrmann, L., Wellbrock, J. & Fiedler, W. Acute myeloid leukemia and the bone marrow niche - Take a closer look. *Front. Oncol.* **8**, 444 (2018).

100. Pinho, S. & Frenette, P. S. Haematopoietic stem cell activity and interactions with the niche. *Nat. Rev. Mol. Cell Biol.* **20**, 303–320 (2019).

101. Zhou, H.-S., Carter, B. Z. & Andreeff, M. Bone marrow niche-mediated survival of leukemia stem cells in acute myeloid leukemia: Yin and Yang. *Cancer Biol. Med.* **13**, 248–259 (2016).

102. Lane, S. W., Scadden, D. T. & Gilliland, D. G. The leukemic stem cell niche: current concepts and therapeutic opportunities. *Blood* **114**, 1150–1157 (2009).

103. Shafat, M. S., Gnaneswaran, B., Bowles, K. M. & Rushworth, S. A. The bone marrow microenvironment – Home of the leukemic blasts. *Blood Rev.* **31**, 277–286 (2017).

104. Goulard, M., Dosquet, C. & Bonnet, D. *Role of the microenvironment in myeloid malignancies*. *Cellular and Molecular Life Sciences* **75**, 1377–1391 (Birkhauser Verlag AG, 2018).

105. Schofield, R. The relationship between the spleen colony-forming cell and the haemopoietic stem cell. *Blood Cells* **4**, 7–25 (1978).

106. Méndez-Ferrer, S. *et al.* Mesenchymal and haematopoietic stem cells form a unique bone marrow niche. *Nature* **466**, 829–834 (2010).

107. Ding, L., Saunders, T. L., Enikolopov, G. & Morrison, S. J. Endothelial and perivascular cells maintain haematopoietic stem cells. *Nature* **481**, 457–462 (2012).

108. Calvi, L. M. *et al.* Osteoblastic cells regulate the haematopoietic stem cell niche. *Nature* **425**, 841–846 (2003).

109. Cuminetti, V. & Arranz, L. Bone Marrow Adipocytes: The Enigmatic Components of the Hematopoietic Stem Cell Niche. *J. Clin. Med.* **8**, 707 (2019).

110. Yamazaki, S. *et al.* Nonmyelinating Schwann Cells Maintain Hematopoietic Stem Cell Hibernation in the Bone Marrow Niche. *Cell* **147**, 1146–1158 (2011).

111. Katayama, Y. *et al.* Signals from the Sympathetic Nervous System Regulate Hematopoietic Stem Cell Egress from Bone Marrow. *Cell* **124**, 407–421 (2006).

112. Kiel, M. J. *et al.* SLAM Family Receptors Distinguish Hematopoietic Stem and Progenitor Cells and Reveal Endothelial Niches for Stem Cells. *Cell* **121**, 1109–1121 (2005).

113. Hira, V. V. V., Van Noorden, C. J. F., Carraway, H. E., Maciejewski, J. P. & Molenaar, R. J. Novel therapeutic strategies to target leukemic cells that hijack compartmentalized continuous hematopoietic stem cell niches. *Biochim. Biophys. Acta - Rev. Cancer* **1868**, 183–198 (2017).

114. Acar, M. *et al.* Deep imaging of bone marrow shows non-dividing stem cells are mainly perisinusoidal. *Nature* **526**, 126–130 (2015).

115. Gruszka, A., Valli, D., Restelli, C. & Alcalay, M. Adhesion Deregulation in Acute Myeloid Leukaemia. *Cells* **8**, 66 (2019).

116. Rouault-Pierre, K. *et al.* HIF-2α Protects Human Hematopoietic Stem/Progenitors and Acute Myeloid Leukemic Cells from Apoptosis Induced by Endoplasmic Reticulum Stress. *Cell Stem Cell* **13**, 549–563 (2013).

117. Dominici, M. *et al.* Minimal criteria for defining multipotent mesenchymal stromal cells. The International Society for Cellular Therapy position statement. *Cytotherapy* **8**, 315–317 (2006).

118. Tormin, A. *et al.* CD146 Expression in Primary Bone Marrow MSC Progenitor/Stem Cells Is Dependent On Their In Vivo Location. *Blood* **114**, 251 (2009).

119. Méndez-Ferrer, S., Lucas, D., Battista, M. & Frenette, P. S. Haematopoietic stem cell release is regulated by circadian oscillations. *Nature* **452**, 442–447 (2008).

120. Sugiyama, T., Kohara, H., Noda, M. & Nagasawa, T. Maintenance of the Hematopoietic Stem Cell Pool by CXCL12-CXCR4 Chemokine Signaling in Bone Marrow Stromal Cell Niches. *Immunity* **25**, 977–988 (2006).

121. Omatsu, Y. *et al.* The Essential Functions of Adipo-osteogenic Progenitors as the Hematopoietic Stem and Progenitor Cell Niche. *Immunity* **33**, 387–399 (2010).

122. Rafii, B. S. *et al.* Isolation and Characterization of Human Bone Marrow Microvascular Endothelial Cells: Hematopoietic Progenitor Cell Adhesion. *Blood* **84**, 10–19 (1994).

123. Sipkins, D. A. *et al.* In vivo imaging of specialized bone marrow endothelial microdomains for tumour engraftment. *Nature* **435**, 969–973 (2005).

124. Dimitroff, C. J., Lee, J. Y., Rafii, S., Fuhlbrigge, R. C. & Sackstein, R. CD44 is a major E-selectin ligand on human hematopoietic progenitor cells. *J. Cell Biol.* **153**, 1277–1286 (2001).

125. Nilsson, S. K. *et al.* Osteopontin, a key component of the hematopoietic stem cell niche and regulator of primitive hematopoietic progenitor cells. *Blood* **106**, 1232–1239 (2005).

126. Jung, Y. *et al.* Regulation of SDF-1 (CXCL12) production by osteoblasts; a possible mechanism for stem cell homing. *Bone* **38**, 497–508 (2006).

127. Arai, F. *et al.* Tie2/Angiopoietin-1 Signaling Regulates Hematopoietic Stem Cell Quiescence in the Bone Marrow Niche. *Cell* **118**, 149–161 (2004).

128. Yoshihara, H. *et al.* Thrombopoietin/MPL Signaling Regulates Hematopoietic Stem Cell Quiescence and Interaction with the Osteoblastic Niche. *Cell Stem Cell* **1**, 685–697 (2007).

129. Chou, F.-S. & Mulloy, J. C. The Thrombopoietin/MPL pathway in hematopoiesis and leukemogenesis. *J. Cell. Biochem.* **112**, 1491–1498 (2011).

130. Yamazaki, S. *et al.* TGF-β as a candidate bone marrow niche signal to induce hematopoietic stem cell hibernation. *Blood* **113**, 1250–1256 (2009).

131. Adams, G. B. *et al.* Stem cell engraftment at the endosteal niche is specified by the calcium-sensing receptor. *Nature* **439**, 599–603 (2006).

132. Xu, X. *et al.* Transforming growth factor-β in stem cells and tissue homeostasis. *Bone Res.* **6**, 2 (2018).

133. Kollet, O. *et al.* Osteoclasts degrade endosteal components and promote mobilization of hematopoietic progenitor cells. *Nat. Med.* **12**, 657–664 (2006).

134. Chow, A. *et al.* Bone marrow CD169+ macrophages promote the retention of hematopoietic stem and progenitor cells in the mesenchymal stem cell niche. *J. Exp. Med.* **208**, 261–271 (2011).

135. Christopher, M. J., Rao, M., Liu, F., Woloszynek, J. R. & Link, D. C. Expression of the G-CSF receptor in monocytic cells is sufficient to mediate hematopoietic progenitor mobilization by G-CSF in mice. *J. Exp. Med.* **208**, 251–260 (2011).

136. Zhao, M. *et al.* Megakaryocytes maintain homeostatic quiescence and promote post-injury regeneration of hematopoietic stem cells. *Nat. Med.* **20**, 1321–1326 (2014).

137. Bruns, I. *et al.* Megakaryocytes regulate hematopoietic stem cell quiescence through CXCL4 secretion. *Nat. Med.* **20**, 1315–1320 (2014).

138. DiMascio, L. *et al.* Identification of Adiponectin as a Novel Hemopoietic Stem Cell Growth

Factor. *J. Immunol.* **178**, 3511–3520 (2007).

139. Zhou, B. O. *et al.* Bone marrow adipocytes promote the regeneration of stem cells and haematopoiesis by secreting SCF. *Nat. Cell Biol.* **19**, 891–903 (2017).

140. Tavor, S. *et al.* CXCR4 Regulates Migration and Development of Human Acute Myelogenous Leukemia Stem Cells in Transplanted NOD/SCID Mice. *Cancer Res.* **64**, 2817–2824 (2004).

141. Zeng, Z. *et al.* Targeting the leukemia microenvironment by CXCR4 inhibition overcomes resistance to kinase inhibitors and chemotherapy in AML. *Blood* **113**, 6215–6224 (2009).

142. Nervi, B. *et al.* Chemosensitization of acute myeloid leukemia (AML) following mobilization by the CXCR4 antagonist AMD3100. *Blood* **113**, 6206–6214 (2009).

143. Ding, L. & Morrison, S. J. Haematopoietic stem cells and early lymphoid progenitors occupy distinct bone marrow niches. *Nature* **495**, 231–235 (2013).

144. Uy, G. L. *et al.* A phase 1/2 study of chemosensitization with the CXCR4 antagonist plerixafor in relapsed or refractory acute myeloid leukemia. *Blood* **119**, 3917–3924 (2012).

145. Uy, G. L. *et al.* A phase 1/2 study of chemosensitization with plerixafor plus G-CSF in relapsed or refractory acute myeloid leukemia. *Blood Cancer J.* **7**, e542 (2017).

146. Roboz, G. J. *et al.* Phase I trial of plerixafor combined with decitabine in newly diagnosed older patients with acute myeloid leukemia. *Haematologica* **103**, 1308–1316 (2018).

147. Duarte, D., Hawkins, E. D. & Lo Celso, C. The interplay of leukemia cells and the bone marrow microenvironment. *Blood* **131**, 1507–1511 (2018).

148. Winkler, I. G. *et al.* Vascular Niche E-Selectin Protects Acute Myeloid Leukaemia Stem Cells from Chemotherapy. *Blood* **124**, 620 (2014).

149. Winkler, I. G. *et al.* Vascular niche E-selectin regulates hematopoietic stem cell dormancy, self renewal and chemoresistance. *Nat. Med.* **18**, 1651–1657 (2012).

150. Jacamo, R. *et al.* Reciprocal leukemia-stroma VCAM-1/VLA-4-dependent activation of NF-κB mediates chemoresistance. *Blood* **123**, 2691–2702 (2014).

151. Matsunaga, T. *et al.* Interaction between leukemic-cell VLA-4 and stromal fibronectin is a decisive factor for minimal residual disease of acute myelogenous leukemia. *Nat. Med.* **9**, 1158–1165 (2003).

152. Cogle, C. R. *et al.* Functional integration of acute myeloid leukemia into the vascular niche. *Leukemia* **28**, 1978–1987 (2014).

153. Fiedler, W. *et al.* Vascular Endothelial Growth Factor, a Possible Paracrine Growth Factor in Human Acute Myeloid Leukemia. *Blood* **89**, 1870–1875 (1997).

154. Zhang, J. *et al.* Cross-talk between leukemic and endothelial cells promotes angiogenesis by VEGF activation of the Notch/Dll4 pathway. *Carcinogenesis* **34**, 667–677 (2013).

155. Dias, S. *et al.* Inhibition of both paracrine and autocrine VEGF/ VEGFR-2 signaling pathways is essential to induce long-term remission of xenotransplanted human leukemias. *Proc. Natl. Acad. Sci. U. S. A.* **98**, 10857–10862 (2001).

156. Hanoun, M. *et al.* Acute Myelogenous Leukemia-Induced Sympathetic Neuropathy Promotes Malignancy in an Altered Hematopoietic Stem Cell Niche. *Cell Stem Cell* **15**, 365–375 (2014).

157. Kumar, B. *et al.* Acute myeloid leukemia transforms the bone marrow niche into a leukemia-permissive microenvironment through exosome secretion. *Leukemia* **32**, 575–587 (2018).

158. Battula, V. L. *et al.* AML-induced osteogenic differentiation in mesenchymal stromal cells supports leukemia growth. *JCI Insight* **2**, e90036 (2017).

159. Boyd, A. L. *et al.* Acute myeloid leukaemia disrupts endogenous myelo-erythropoiesis by compromising the adipocyte bone marrow niche. *Nat. Cell Biol.* **19**, 1336–1347 (2017).

160. Shafat, M. S. *et al.* Leukemic blasts program bone marrow adipocytes to generate a protumoral microenvironment. *Blood* **129**, 1320–1332 (2017).

161. Isidori, A. *et al.* The role of the immunosuppressive microenvironment in acute myeloid leukemia development and treatment. *Expert Rev. Hematol.* **7**, 807–818 (2014).

162. Ramasamy, S. K. Structure and Functions of Blood Vessels and Vascular Niches in Bone. *Stem Cells Int.* **2017**, 5046953 (2017).

163. Itkin, T. *et al.* Distinct bone marrow blood vessels differentially regulate haematopoiesis. *Nature* **532**, 323–328 (2016).

164. Bixel, M. G. *et al.* Flow Dynamics and HSPC Homing in Bone Marrow Microvessels. *Cell Rep.* **18**, 1804–1816 (2017).

165. Duarte, D. *et al.* Inhibition of Endosteal Vascular Niche Remodeling Rescues Hematopoietic Stem Cell Loss in AML. *Cell Stem Cell* **22**, 64–77 (2018).

166. Kiyokawa, E. *et al.* Activation of Rac1 by a Crk SH3-binding protein, DOCK180. *Genes Dev.* **12**, 3331–3336 (1998).

167. Gadea, G. & Blangy, A. Dock-family exchange factors in cell migration and disease. *Eur. J. Cell Biol.* **93**, 466–477 (2014).

168. Rossman, K. L., Der, C. J. & Sondek, J. GEF means go: Turning on Rho GTPases with guanine nucleotide-exchange factors. *Nat. Rev. Mol. Cell Biol.* **6**, 167–180 (2005).

169. Côté, J.-F. & Vuori, K. Identification of an evolutionarily conserved superfamily of DOCK180-related proteins with guanine nucleotide exchange activity. *J. Cell Sci.* **115**, 4901–4913 (2002).

170. Brugnera, E. *et al.* Unconventional Rac-GEF activity is mediated through the Dock180-ELMO complex. *Nat. Cell Biol.* **4**, 574–582 (2002).

171. Meller, N., Irani-Tehrani, M., Kiosses, W. B., Del Pozo, M. A. & Schwartz, M. A. Zizimin1, a novel Cdc42 activator, reveals a new GEF domain for Rho proteins. *Nat. Cell Biol.* **4**, 639–647 (2002).

172. Côté, J.-F., Motoyama, A. B., Bush, J. A. & Vuori, K. A novel and evolutionarily conserved PtdIns(3,4,5)P3-binding domain is necessary for DOCK180 signalling. *Nat. Cell Biol.* **7**, 797–807 (2005).

173. Côté, J.-F. & Vuori, K. GEF what? Dock180 and related proteins help Rac to polarize cells in new ways. *Trends Cell Biol.* **17**, 383–393 (2007).

174. Hasegawa, H. *et al.* DOCK180 , a Major CRK-Binding Protein , Alters Cell Morphology upon Translocation to the Cell Membrane. *Mol. Cell. Biol.* **16**, 1770–1776 (1996).

175. Lemmon, M. A., Ferguson, K. M. & Abrams, C. S. Pleckstrin homology domains and the cytoskeleton. *FEBS Lett.* **513**, 71–76 (2002).

176. Joneson, T., McDonough, M., Bar-Sagi, D. & Van Aelst, L. RAC Regulation of Actin Polymerization and Proliferation by a Pathway Distinct from Jun Kinase. *Science (80-. ).* **274**, 1374–1376 (1996).

177. Cancelas, J. A., Jansen, M. & Williams, D. A. The role of chemokine activation of Rac GTPases in hematopoietic stem cell marrow homing, retention, and peripheral mobilization. *Exp. Hematol.* **34**, 976–985 (2006).

178. Lu, M. *et al.* PH domain of ELMO functions in trans to regulate Rac activation via Dock180. *Nat. Struct. Mol. Biol.* **11**, 756–762 (2004).

179. Lu, M. & Ravichandran, K. S. Dock180–ELMO Cooperation in Rac Activation. in *Methods in Enzymology* **406**, 388–402 (Academic Press, 2006).

180. Lu, M. *et al.* A Steric-Inhibition Model for Regulation of Nucleotide Exchange via the Dock180 Family of GEFs. *Curr. Biol.* **15**, 371–377 (2005).

181. Gumienny, T. L. *et al.* CED-12/ELMO, a Novel Member of the CrkII/Dock180/Rac Pathway, Is Required for Phagocytosis and Cell Migration. *Cell* **107**, 27–41 (2001).

182. Patel, M. *et al.* An Evolutionarily Conserved Autoinhibitory Molecular Switch in ELMO Proteins Regulates Rac Signaling. *Curr. Biol.* **20**, 2021–2027 (2010).

183. DeBakker, C. D. *et al.* Phagocytosis of Apoptotic Cells Is Regulated by a UNC-73/TRIO-MIG-2/RhoG Signaling Module and Armadillo Repeats of CED-12/ELMO. *Curr. Biol.* **14**, 2208–2216 (2004).

184. Katoh, H. & Negishi, M. RhoG activates Rac1 by direct interaction with the Dock180-binding protein Elmo. *Nature* **424**, 461–464 (2003).

185. Patel, M., Chiang, T.-C., Tran, V., Lee, F.-J. S. & Côté, J.-F. The Arf family GTPase Arl4A complexes with ELMO proteins to promote actin cytoskeleton remodeling and reveals a versatile Ras-binding domain in the ELMO proteins family. *J. Biol. Chem.* **286**, 38969–38979 (2011).

186. Santy, L. C., Ravichandran, K. S. & Casanova, J. E. The DOCK180/Elmo Complex Couples ARNO-Mediated Arf6 Activation to the Downstream Activation of Rac1. *Curr. Biol.* **15**, 1749–1754 (2005).

187. Franca-Koh, J., Kamimura, Y. & Devreotes, P. N. Leading-edge research: PtdIns(3,4,5)P3 and directed migration. *Nat. Cell Biol.* **9**, 15–17 (2007).

188. Margaron, Y., Fradet, N. & Côté, J.-F. ELMO recruits actin cross-linking family 7 (ACF7) at the cell membrane for microtubule capture and stabilization of cellular protrusions. *J. Biol. Chem.* **288**, 1184–1199 (2013).

189. Karakesisoglou, I., Yang, Y. & Fuchs, E. An epidermal plakin that integrates actin and microtubule networks at cellular junctions. *J. Cell Biol.* **149**, 195–208 (2000).

190. Kodama, A., Karakesisoglou, I., Wong, E., Vaezi, A. & Fuchs, E. ACF7: An essential integrator of microtubule dynamics. *Cell* **115**, 343–354 (2003).

191. Kiyokawa, E., Hashimoto, Y., Kurata, T., Sugimura, H. & Matsuda, M. Evidence That DOCK180 Up-regulates Signals from the CrkII-p130Cas Complex. *J. Biol. Chem.* **273**, 24479–24484 (1998).

192. Tachibana, M. *et al.* Ankyrin repeat domain 28 (ANKRD28), a novel binding partner of DOCK180, promotes cell migration by regulating focal adhesion formation. *Exp. Cell Res.* **315**, 863–876 (2009).

193. Makino, Y. *et al.* Elmo1 inhibits ubiquitylation of Dock180. *J. Cell Sci.* **119**, 923–932 (2006).

194. Laurin, M. *et al.* Rac-specific guanine nucleotide exchange factor DOCK1 is a critical regulator of HER2-mediated breast cancer metastasis. *Proc. Natl. Acad. Sci.* **110**, 7434–7439 (2013).

195. Li, H. *et al.* Association between Gαi2 and ELMO1/Dock180 connects chemokine signalling with Rac activation and metastasis. *Nat. Commun.* **4**, 1706 (2013).

196. Liang, Y., Wang, S. & Zhang, Y. Downregulation of Dock1 and Elmo1 suppresses the migration and invasion of triple-negative breast cancer epithelial cells through the RhoA/Rac1 pathway. *Oncol. Lett.* **16**, 3481–3488 (2018).

197. Chiang, S. K., Chang, W. C., Chen, S. E. & Chang, L. C. DOCK1 regulates growth and motility through the RRP1B-Claudin-1 pathway in Claudin-low breast cancer cells. *Cancers* **11**, 1762

(2019).

198. Zhao, F. *et al.* Overexpression of dedicator of cytokinesis I (Dock180) in ovarian cancer correlated with aggressive phenotype and poor patient survival. *Histopathology* **59**, 1163–1172 (2011).

199. Kenny, H. A. & Lengyel, E. MMP-2 functions as an early response protein in ovarian cancer metastasis. *Cell Cycle* **8**, 683–688 (2009).

200. Jarzynka, M. J. *et al.* ELMO1 and Dock180, a Bipartite Rac1 Guanine Nucleotide Exchange Factor, Promote Human Glioma Cell Invasion. *Cancer Res.* **67**, 7203–7211 (2007).

201. Feng, H. *et al.* Activation of Rac1 by Src-dependent phosphorylation of Dock180 Y1811 mediates PDGFRα-stimulated glioma tumorigenesis in mice and humans. *J. Clin. Invest.* **121**, 4670–4684 (2011).

202. Feng, H. *et al.* Protein kinase A-dependent phosphorylation of Dock180 at serine residue 1250 is important for glioma growth and invasion stimulated by platelet derived-growth factor receptor α. *Neuro. Oncol.* **17**, 832–842 (2015).

203. Feng, H. *et al.* Phosphorylation of dedicator of cytokinesis 1 (Dock180) at tyrosine residue Y722 by Src family kinases mediates EGFRvIII-driven glioblastoma tumorigenesis. *Proc. Natl. Acad. Sci.* **109**, 3018–3023 (2012).

204. Feng, H. *et al.* EGFRvIII stimulates glioma growth and invasion through PKA-dependent serine phosphorylation of Dock180. *Oncogene* **33**, 2504–2512 (2014).

205. Zhang, B. *et al.* Dock1 Promotes the Mesenchymal Transition of Glioma and is Modulated by MiR-31. *Neuropathol. Appl. Neurobiol.* **43**, 419– 432 (2016).

206. Li, W. *et al.* HGF-induced formation of the MET-AXL-ELMO2-DOCK180 complex promotes RAC1 activation, receptor clustering, and cancer cell migration and invasion. *J. Biol. Chem.* **293**, 15397–15418 (2018).

207. Chen, D. *et al.* Downregulation of DOCK1 sensitizes bladder cancer cells to cisplatin through preventing epithelial-mesenchymal transition. *Drug Des. Devel. Ther.* **10**, 2845–2853 (2016).

208. Pan, Y. *et al.* Enoxaparin Sensitizes Human Non-small-cell Lung Carcinomas to Gefitinib by Inhibiting DOCK1 Expression, Vimentin Phosphorylation and Akt Activation. *Mol. Pharmacol.* **87**, 378–390 (2015).

209. Verhaak, R. G. W. *et al.* Prediction of molecular subtypes in acute myeloid leukemia based on gene expression profiling. *Haematologica* **94**, 131–134 (2009).

210. Zhang, G. *et al.* High expression of dedicator of cytokinesis 1 adversely influences the prognosis of acute myeloid leukemia patients undergoing allogeneic hematopoietic stem cell transplantation. *Cancer Manag. Res.* **11**, 3053–3060 (2019).

211. Hu, N. *et al.* High expression of DOCK2 indicates good prognosis in acute myeloid leukemia. *J. Cancer* **10**, 6088–6094 (2019).

212. Nishihara, H. *et al.* Non-adherent cell-specific expression of DOCK2, a member of the human CDM-family proteins. *Biochim. Biophys. Acta - Mol. Cell Res.* **1452**, 179–187 (1999).

213. Wang, J. Y. *et al.* Activation of Rac1 GTPase promotes leukemia cell chemotherapy resistance, quiescence and niche interaction. *Mol. Oncol.* **7**, 907–916 (2013).

214. Pabst, C. *et al.* Identification of small molecules that support human leukemia stem cell activity ex vivo. *Nat. Methods* **11**, 436–442 (2014).

215. Fiedler, W. *et al.* Derivation of a new hematopoietic cell line with endothelial features from a patient with transformed myeloproliferative syndrome: A case report. *Cancer* **88**, 344–351 (2000).

216. Wang, X. & Seed, B. A PCR primer bank for quantitative gene expression analysis. *Nucleic Acids Res.* **31**, e154 (2003).

217. Spandidos, A. *et al.* A comprehensive collection of experimentally validated primers for Polymerase Chain Reaction quantitation of murine transcript abundance. *BMC Genomics* **9**, 633 (2008).

218. Spandidos, A., Wang, X., Wang, H. & Seed, B. PrimerBank: a resource of human and mouse PCR primer pairs for gene expression detection and quantification. *Nucleic Acids Res.* **38**, D792–D799 (2010).

219. Weber, K., Bartsch, U., Stocking, C. & Fehse, B. A Multicolor Panel of Novel Lentiviral "Gene Ontology" ( LeGO ) Vectors for Functional Gene Analysis. *Mol. Ther.* **16**, 698–706 (2008).

220. Weber, K., Mock, U., Petrowitz, B., Bartsch, U. & Fehse, B. Lentiviral gene ontology (LeGO) vectors equipped with novel drug-selectable fluorescent proteins: new building blocks for cell marking and multi-gene analysis. *Gene Ther.* **17**, 511–520 (2010).

221. Nishikimi, A. *et al.* Blockade of inflammatory responses by a small-molecule inhibitor of the Rac activator DOCK2. *Chem. Biol.* **19**, 488–497 (2012).

222. Tajiri, H. *et al.* Targeting Ras-Driven Cancer Cell Survival and Invasion through Selective Inhibition of DOCK1. *Cell Rep.* **19**, 969–980 (2017).

223. Strohalm, M., Hassman, M., Košata, B. & Kodíček, M. mMass data miner: an open source alternative for mass spectrometric data analysis. *Rapid Commun. Mass Spectrom.* **22**, 905–908 (2008).

224. Novoradovsky, A. *et al.* Computational principles of primer design for site directed mutagenesis. *Tech. Proc. 2005 NSTI Nanotechnol. Conf. Trade Show* **1**, 532–535 (2005).

225. Pfaffl, M. W. A new mathematical model for relative quantification in real-time RT-PCR. *Nucleic Acids Res.* **29**, e45 (2001).

226. Dyballa, N. & Metzger, S. Fast and sensitive colloidal Coomassie G-250 staining for proteins in polyacrylamide gels. *J. Vis. Exp.* **30**, 1431 (2009).

227. Perkins, D. N., Pappin, D. J. C., Creasy, D. M. & Cottrell, J. S. Probability-based protein identification by searching sequence databases using mass spectrometry data. *Electrophoresis* **20**, 3551–3567 (1999).

228. Kitamura, T. *et al.* Establishment and characterization of a unique human cell line that proliferates dependently on GM-CSF, IL-3, or erythropoietin. *J. Cell. Physiol.* **140**, 323–334 (1989).

229. Adan, A., Alizada, G., Kiraz, Y., Baran, Y. & Nalbant, A. Flow cytometry: basic principles and applications. *Crit. Rev. Biotechnol.* **37**, 163–176 (2017).

230. Mayle, A., Luo, M., Jeong, M. & Goodell, M. A. Flow cytometry analysis of murine hematopoietic stem cells. *Cytom. Part A* **83 A**, 27–37 (2013).

231. Hanahan, D. & Weinberg, R. A. The Hallmarks of Cancer. *Cell* **100**, 57–70 (2000).

232. Hanahan, D. & Weinberg, R. A. Hallmarks of Cancer : The Next Generation. *Cell* **144**, 646–674 (2011).

233. Ando, J. *et al.* Shear stress inhibits adhesion of cultured mouse endothelial cells to lymphocytes by downregulating VCAM-1 expression. *Am. J. Physiol. Physiol.* **267**, C679–C687 (1994).

234. Mueller, F.-J. *et al.* Adhesive Interactions Between Human Neural Stem Cells and Inflamed Human Vascular Endothelium Are Mediated by Integrins. *Stem Cells* **24**, 2367–2372 (2006).

235. Sanchez, P. V *et al.* A robust xenotransplantation model for acute myeloid leukemia. *Leukemia* **23**, 2109–2117 (2009).

236. Wunderlich, M. *et al.* AML xenograft efficiency is significantly improved in NOD/SCID-IL2RG mice constitutively expressing human SCF, GM-CSF and IL-3. *Leukemia* **24**, 1785–1788 (2010).

237. Chang, F., Shamsi, T. S. & Waryah, A. M. Clinical and Hematological Profile of Acute Myeloid Leukemia (AML) Patients of Sindh. *J. Hematol. Thromboembolic Dis.* **4**, 239 (2016).

238. Khan, M. Acute Myeloid Leukemia : Pattern of Clinical and Hematological Parameters in a Tertiary Care Centre. *Int. J. Pathol.* **16**, 58–63 (2018).

239. Quentmeier, H., MacLeod, R. A. F., Zaborski, M. & Drexler, H. G. JAK2 V617F tyrosine kinase mutation in cell lines derived from myeloproliferative disorders. *Leukemia* **20**, 471–476 (2006).

240. Baxter, E. J. *et al.* Acquired mutation of the tyrosine kinase JAK2 in human myeloproliferative disorders. *Lancet* **365**, 1054–1061 (2005).

241. Quelle, F. W. *et al.* JAK2 associates with the beta c chain of the receptor for granulocyte-macrophage colony-stimulating factor, and its activation requires the membrane-proximal region. *Mol. Cell. Biol.* **14**, 4335–4341 (1994).

242. Abdelouahab, H. *et al.* CXCL12/CXCR4 pathway is activated by oncogenic JAK2 in a PI3K-dependent manner. *Oncotarget* **8**, 54082–54095 (2017).

243. Kim, S. *et al.* PubChem 2019 update: improved access to chemical data. *Nucleic Acids Res.* **47**, D1102–D1109 (2019).

244. Simonsen, A. *et al.* Alfy, a novel FYVE-domain-containing protein associated with protein granules and autophagic membranes. *J. Cell Sci.* **117**, 4239–4251 (2004).

245. Cremona, O. *et al.* Essential Role of Phosphoinositide Metabolism in Synaptic Vesicle Recycling. *Cell* **99**, 179–188 (1999).

246. Wang, J. *et al.* Overexpression of Rac1 in leukemia patients and its role in leukemia cell migration and growth. *Biochem. Biophys. Res. Commun.* **386**, 769–774 (2009).

247. Sanui, T. *et al.* DOCK2 regulates Rac activation and cytoskeletal reorganization through interaction with ELMO1. *Blood* **102**, 2948–2950 (2003).

248. Fukui, Y. *et al.* Haematopoietic cell-specific CDM family protein DOCK2 is essential for lymphocyte migration. *Nature* **412**, 826–831 (2001).

249. García-Bernal, D. *et al.* DOCK2 is Required for Chemokine-Promoted Human T Lymphocyte Adhesion Under Shear Stress Mediated by the Integrin α4β1. *J. Immunol.* **177**, 5215–5225 (2006).

250. Le Floc'h, A. *et al.* Annular PIP3 accumulation controls actin architecture and modulates cytotoxicity at the immunological synapse. *J. Exp. Med.* **210**, 2721–2737 (2013).

251. Sakai, Y. *et al.* The Rac activator DOCK2 regulates natural killer cell–mediated cytotoxicity in mice through the lytic synapse formation. *Blood* **122**, 386–393 (2013).

252. Vives, V. *et al.* The Rac1 exchange factor Dock5 is essential for bone resorption by osteoclasts. *J. Bone Miner. Res.* **26**, 1099–1110 (2011).

253. Terramani, T. T. *et al.* Human macrovascular endothelial cells: Optimization of culture conditions. *In Vitro Cellular & Developmental Biology. Animal* **36**, 125–132 (2000).

254. Nooteboom, A., Hendriks, T., Ottehöller, I. & van der Linden, C. J. Permeability characteristics of human endothelial monolayers seeded on different extracellular matrix proteins. *Mediators Inflamm.* **9**, 235–241 (2000).

255. Beekhuizen, H., Corsèl-van Tilburg, A. J. & van Furth, R. Characterization of monocyte adherence to human macrovascular and microvascular endothelial cells. *J. Immunol.* **145**, 510–518 (1990).

256. Williams, D. A., Zheng, Y. & Cancelas, J. Rho GTPases and Regulation of Hematopoietic Stem Cell Localization. in *Methods in Enzymology* **439**, 365–393 (Academic Press, 2008).

257. Gu, Y. *et al.* Hematopoietic Cell Regulation by Rac1 and Rac2 Guanosine Triphosphatases. *Science (80-. ).* **302**, 445–449 (2003).

258. Cancelas, J. A. *et al.* Rac GTPases differentially integrate signals regulating hematopoietic stem cell localization. *Nat. Med.* **11**, 886–891 (2005).

259. Meng, X. *et al.* Neurexophilin4 is a selectively expressed α-neurexin ligand that modulates specific cerebellar synapses and motor functions. *eLife* **8**, e46773 (2019).

260. National Center for Biotechnology Information (US), B. (MD). The NCBI Handbook [Internet]. 2nd edition. (2013). Available at: https://www.ncbi.nlm.nih.gov/books/NBK153381/. (Accessed: 13th April 2020)

261. Hashimoto, O. *et al.* cDNA cloning and expression of human activin βE subunit. *Mol. Cell. Endocrinol.* **194**, 117–122 (2002).

262. Bergauer, F. *et al.* Inhibin/activin-betaE subunit in normal and malignant human cervical tissue and cervical cancer cell lines. *J. Mol. Histol.* **40**, 353–359 (2009).

263. Gingelmaier, A. *et al.* Inhibin/activin-betaE subunit is expressed in normal and pathological human placental tissue including chorionic carcinoma cell lines. *Arch. Gynecol. Obstet.* **283**, 223–230 (2011).

264. Mylonas, I., Matsingou, C., Käufl, S. D. & Brüning, A. Inhibin/activin betaE-subunit in uterine endometrioid adenocarcinoma and endometrial cancer cell lines: From immunohistochemistry to clinical testing? *Gynecol. Oncol.* **122**, 132–140 (2011).

265. Katoh, Y. & Katoh, M. Hedgehog signaling, epithelial-to-mesenchymal transition and miRNA (Review). *Int. J. Mol. Med.* **22**, 271–275 (2008).

266. Si, T. *et al.* High expression of INHBA is an adverse prognostic factor for de novo acute myeloid leukemia. *Leuk. Lymphoma* **59**, 114–120 (2018).

267. Goebel, G. *et al.* Elevated mRNA expression of CHAC1 splicing variants is associated with poor outcome for breast and ovarian cancer patients. *Br. J. Cancer* **106**, 189–198 (2012).

268. Liu, Y., Li, M., Shi, D. & Zhu, Y. Higher expression of cation transport regulator-like protein 1 (CHAC1) predicts of poor outcomes in uveal melanoma (UM) patients. *Int. Ophthalmol.* **39**, 2825–2832 (2019).

269. Cantley, L. C. The Phosphoinositide 3-Kinase Pathway. *Science (80-. ).* **296**, 1655–1657 (2002).

270. Fruman, D. A. *et al.* The PI3K Pathway in Human Disease. *Cell* **170**, 605–635 (2017).

271. Unsicker, K., Spittau, B. & Krieglstein, K. The multiple facets of the TGF-β family cytokine growth/differentiation factor-15/macrophage inhibitory cytokine-1. *Cytokine Growth Factor Rev.* **24**, 373–384 (2013).

272. Zhai, Y. *et al.* Growth differentiation factor 15 contributes to cancer-associated fibroblasts-mediated chemo-protection of AML cells. *J. Exp. Clin. Cancer Res.* **35**, 147 (2016).

273. Lu, W. *et al.* Growth differentiation factor 15 contributes to marrow adipocyte remodeling in response to the growth of leukemic cells. *J. Exp. Clin. Cancer Res.* **37**, 66 (2018).

274. Yang, S. *et al.* Leukemia cells remodel marrow adipocytes via TRPV4-dependent lipolysis. *Haematologica* haematol.2019.225763 (2019). doi:10.3324/haematol.2019.225763

275. Liu, H. *et al.* Consolidation Chemotherapy Prevents Relapse by Indirectly Regulating Bone Marrow Adipogenesis in Patients with Acute Myeloid Leukemia. *Cell. Physiol. Biochem.* **45**, 2389–2400 (2018).

276. Kalli, M. *et al.* Solid stress-induced migration is mediated by GDF15 through Akt pathway activation in pancreatic cancer cells. *Sci. Rep.* **9**, 978 (2019).

277. Kalli, M. *et al.* Mechanical Compression Regulates Brain Cancer Cell Migration Through MEK1/Erk1 Pathway Activation and GDF15 Expression. *Front. Oncol.* **9**, 992 (2019).

278. Louca, M., Gkretsi, V. & Stylianopoulos, T. Coordinated Expression of Ras Suppressor 1 (RSU-1) and Growth Differentiation Factor 15 (GDF15) Affects Glioma Cell Invasion. *Cancers* **11**, 1159 (2019).

279. Gkretsi, V. *et al.* Silencing of Growth Differentiation Factor-15 Promotes Breast Cancer Cell Invasion by Down-regulating Focal Adhesion Genes. *Anticancer Res.* **40**, 1375–1385 (2020).

280. Prudnikova, T. Y. *et al.* Antiproliferative effect of D-glucuronyl C5-epimerase in human breast cancer cells. *Cancer Cell Int.* **10**, 27 (2010).

281. Grigorieva, E. V *et al.* D-Glucuronyl C5-epimerase suppresses small-cell lung cancer cell proliferation in vitro and tumour growth in vivo. *Br. J. Cancer* **105**, 74–82 (2011).

282. Rosenberg, E. E., Prudnikova, T. Y., Zabarovsky, E. R., Kashuba, V. I. & Grigorieva, E. V. D-glucuronyl C5-epimerase cell type specifically affects angiogenesis pathway in different prostate cancer cells. *Tumor Biol.* **35**, 3237–3245 (2014).

283. Mastaglio, S. *et al.* Natural killer receptor ligand expression on acute myeloid leukemia impacts survival and relapse after chemotherapy. *Blood Adv.* **2**, 335–346 (2018).

284. Nanbakhsh, A. *et al.* c-Myc regulates expression of NKG2D ligands ULBP1/2/3 in AML and modulates their susceptibility to NK-mediated lysis. *Blood* **123**, 3585–3595 (2014).

285. Inoue, M. *et al.* The stress response gene ATF3 is a direct target of the Wnt/β-catenin pathway and inhibits the invasion and migration of HCT116 human colorectal cancer cells. *PLoS ONE* **13**, e0194160 (2018).

286. Guenzle, J. *et al.* ATF3 reduces migration capacity by regulation of matrix metalloproteinases via NFκB and STAT3 inhibition in glioblastoma. *Cell Death Discov.* **3**, 17006 (2017).

287. Yuan, X. *et al.* ATF3 Suppresses Metastasis of Bladder Cancer by Regulating Gelsolin-Mediated Remodeling of the Actin Cytoskeleton. *Cancer Res.* **73**, 3625–3637 (2013).

288. Li, X. *et al.* Activating transcription factor 3 promotes malignance of lung cancer cells in vitro. *Thorac. Cancer* **8**, 181–191 (2017).

289. Wu, Z.-Y., Wei, Z., Sun, S.-J., Yuan, J. & Jiao, S.-C. Activating transcription factor 3 promotes colon cancer metastasis. *Tumor Biol.* **35**, 8329–8334 (2014).

290. Dun, B. *et al.* Mycophenolic Acid Inhibits Migration and Invasion of Gastric Cancer Cells via Multiple Molecular Pathways. *PLoS ONE* **8**, e81702 (2013).

291. Wang, Y.-H. *et al.* Dysregulation of cystathionine γ-lyase promotes prostate cancer progression and metastasis. *EMBO Rep.* **20**, e45986 (2019).

292. Tao, X. *et al.* Argininosuccinate synthase 1 suppresses cancer cell invasion by inhibiting STAT3 pathway in hepatocellular carcinoma. *Acta Biochim. Biophys. Sin.* **51**, 263–276 (2019).

293. Shan, Y.-S. *et al.* Argininosuccinate synthetase 1 suppression and arginine restriction inhibit cell migration in gastric cancer cell lines. *Sci. Rep.* **5**, 9783 (2015).

294. Tsai, C.-Y. *et al.* Argininosuccinate synthetase 1 contributes to gastric cancer invasion and progression by modulating autophagy. *FASEB J.* **32**, 2601–2614 (2018).

295. Miraki-Moud, F. *et al.* Arginine deprivation using pegylated arginine deiminase has activity against primary acute myeloid leukemia cells in vivo. *Blood* **125**, 4060–4068 (2015).

296. Xiong, G. P., Zhang, J. X., Gu, S. P., Wu, Y. B. & Liu, J. F. Overexpression of ECM1 Contributes to Migration and Invasion in Cholangiocarcinoma Cell. *Neoplasma* **59**, 409–415 (2012).

297. Chen, H., Jia, W. & Li, J. ECM1 promotes migration and invasion of hepatocellular carcinoma by inducing epithelial-mesenchymal transition. *World J. Surg. Oncol.* **14**, 195 (2016).

298. Gómez-Contreras, P. *et al.* Extracellular matrix 1 (ECM1) regulates the actin cytoskeletal architecture of aggressive breast cancer cells in part via S100A4 and Rho-family GTPases. *Clin. Exp. Metastasis* **34**, 37–49 (2017).

299. Wu, H. *et al.* Downregulation of Long Non-coding RNA FALEC Inhibits Gastric Cancer Cell Migration and Invasion Through Impairing ECM1 Expression by Exerting Its Enhancer-Like Function. *Front. Genet.* **10**, 255 (2019).

300. Li, M. *et al.* miR-193a-5p promotes pancreatic cancer cell metastasis through SRSF6-mediated alternative splicing of OGDHL and ECM1. *Am. J. Cancer Res.* **10**, 38–59 (2020).

301. Steinhaeuser, S. S. *et al.* ECM1 secreted by HER2-overexpressing breast cancer cells promotes formation of a vascular niche accelerating cancer cell migration and invasion. *Lab. Investig.* (2020). doi:10.1038/s41374-020-0415-6

302. Yan, A., Li, G., Zhang, X., Zhu, B. & Linghu, H. Pro-survival effect of Dock180 overexpression on rat-derived H9C2 cardiomyocytes. *Med. Sci. Monit. Basic Res.* **19**, 12–19 (2013).

303. Li, H. *et al.* MiR-486-5p inhibits IL-22-induced epithelial-mesenchymal transition of breast cancer cell by repressing Dock1. *J. Cancer* **10**, 4695–4706 (2019).

304. Roche, J. The Epithelial-to-Mesenchymal Transition in Cancer. *Cancers* **10**, 52 (2018).

305. Willier, S., Butt, E., Richter, G. H. S., Burdach, S. & Grunewald, T. G. P. Defining the role of TRIP6 in cell physiology and cancer. *Biol. Cell* **103**, 573–591 (2011).

306. Lin, V. T. G. & Lin, F.-T. TRIP6: An adaptor protein that regulates cell motility, antiapoptotic signaling and transcriptional activity. *Cell. Signal.* **23**, 1691–1697 (2011).

307. Lai, Y.-J., Chen, C.-S., Lin, W.-C. & Lin, F.-T. c-Src-Mediated Phosphorylation of TRIP6 Regulates Its Function in Lysophosphatidic Acid-Induced Cell Migration. *Mol. Cell. Biol.* **25**, 5859–5868 (2005).

308. Yi, J. *et al.* Members of the Zyxin Family of LIM Proteins Interact with Members of the p130Cas Family of Signal Transducers. *J. Biol. Chem.* **277**, 9580–9589 (2002).

309. Bai, C.-Y., Ohsugi, M., Abe, Y. & Yamamoto, T. ZRP-1 controls Rho GTPase-mediated actin reorganization by localizing at cell-matrix and cell-cell adhesions. *J. Cell Sci.* **120**, 2828–2837 (2007).

310. Grunewald, T. G. P. *et al.* The Zyxin-related protein thyroid receptor interacting protein 6 (TRIP6) is overexpressed in Ewing's sarcoma and promotes migration, invasion and cell growth. *Biol. Cell* **105**, 535–547 (2013).

311. Zhu, L., Xu, X., Tang, Y. & Zhu, X. TRIP6 functions as a potential oncogene and facilitated proliferation and metastasis of gastric cancer. *Biologics.* **13**, 101–110 (2019).

312. Liu, W., Cheng, L., Li, Q. & Jing, J. TRIP6 regulates the proliferation, migration, invasion and apoptosis of osteosarcoma cells by activating the NF-κB signaling pathway. *Exp. Ther. Med.* **19**, 2317–2325 (2020).

313. Turtoi, A. *et al.* Myoferlin Is a Key Regulator of EGFR Activity in Breast Cancer. *Cancer Res.* **73**, 5438–5448 (2013).

314. Zhu, W. *et al.* Myoferlin, a multifunctional protein in normal cells, has novel and key roles in various cancers. *J. Cell. Mol. Med.* **23**, 7180–7189 (2019).

315. Yan, H. *et al.* Identification of prognostic genes in the acute myeloid leukemia immune microenvironment based on TCGA data analysis. *Cancer Immunol. Immunother.* **68**, 1971–1978 (2019).

316. Marconi, C. *et al.* 5'UTR point substitutions and N-terminal truncating mutations of ANKRD26 in acute myeloid leukemia. *J. Hematol. Oncol.* **10**, 18 (2017).

317. Xie, H., Hu, Z., Chyna, B., Horrigan, S. K. & Westbrook, C. A. Human mortalin (HSPA9): a candidate for the myeloid leukemia tumor suppressor gene on 5q31. *Leukemia* **14**, 2128–2134 (2000).

318. Wadhwa, R. *et al.* Upregulation of mortalin/mthsp70/Grp75 contributes to human carcinogenesis. *Int. J. Cancer* **118**, 2973–2980 (2006).

319. Na, Y. *et al.* Stress Chaperone Mortalin Contributes to Epithelial-to-Mesenchymal Transition and Cancer Metastasis. *Cancer Res.* **76**, 2754–2765 (2016).

320. Yun, C.-O. *et al.* Relevance of mortalin to cancer cell stemness and cancer therapy. *Sci. Rep.* **7**, 42016 (2017).

321. Ibrahim, S. A. *et al.* Targeting of syndecan-1 by microRNA miR-10b promotes breast cancer cell motility and invasiveness via a Rho-GTPase- and E-cadherin-dependent mechanism. *Int. J. Cancer* **131**, E884–E896 (2012).

322. Yu, X., Zhang, Y., Wu, B., Kurie, J. M. & Pertsemlidis, A. The miR-195 Axis Regulates Chemoresistance through TUBB and Lung Cancer Progression through BIRC5. *Mol. Ther. - Oncolytics* **14**, 288–298 (2019).

323. Molinie, N. & Gautreau, A. The Arp2/3 Regulatory System and Its Deregulation in Cancer. *Physiol. Rev.* **98**, 215–238 (2018).

324. Laurila, E., Savinainen, K., Kuuselo, R., Karhu, R. & Kallioniemi, A. Characterization of the 7q21-q22 amplicon identifies ARPC1A, a subunit of the Arp2/3 complex, as a regulator of cell migration and invasion in pancreatic cancer. *Genes, Chromosom. Cancer* **48**, 330–339 (2009).

325. Tauler, J., Zudaire, E., Liu, H., Shih, J. & Mulshine, J. L. hnRNP A2/B1 Modulates Epithelial-Mesenchymal Transition in Lung Cancer Cell Lines. *Cancer Res.* **70**, 7137–7147 (2010).

326. Deng, J. *et al.* Effects of hnRNP A2/B1 Knockdown on Inhibition of Glioblastoma Cell Invasion, Growth and Survival. *Mol. Neurobiol.* **53**, 1132–1144 (2016).

327. Shi, X. *et al.* Knockdown of hnRNP A2 / B1 inhibits cell proliferation, invasion and cell cycle triggering apoptosis in cervical cancer via PI3K/AKT signaling pathway. *Oncol. Rep.* **39**, 939–950 (2018).

328. Wang, H. *et al.* Long noncoding RNA miR503HG, a prognostic indicator, inhibits tumor metastasis by regulating the HNRNPA2B1/NF-κB pathway in hepatocellular carcinoma. *Theranostics* **8**, 2814–2829 (2018).

329. Schläfli, A. M., Isakson, P., Garattini, E., Simonsen, A. & Tschan, M. P. The autophagy scaffold protein ALFY is critical for the granulocytic differentiation of AML cells. *Sci. Rep.* **7**, 12980 (2017).

330. Malecz, N. *et al.* Synaptojanin 2, a novel Rac1 effector that regulates clathrin-mediated endocytosis. *Curr. Biol.* **10**, 1383–1386 (2000).

# DANKSAGUNG

Zuallererst möchte ich mich bei Professor Dr. Walter Fiedler und PD Dr. Jasmin Wellbrock für die Möglichkeit bedanken, an diesem spannenden Projekt zu arbeiten. Vielen herzlichen Dank für die tolle Unterstützung und die vielen motivierenden Worte. Auch wenn ich zwischenzeitlich schon nicht mehr an das „Das wird schon!“ geglaubt habe, hat es sich am Ende doch bewahrheitet. Mit viel fachlicher und moralischer Unterstützung hast du mich immer wieder überzeugt weiterzumachen, Jasmin. Danke, dass du jederzeit in offenes Ohr für mich hattest.

Mein herzlicher Dank gilt zudem Professor Dr. Julia Kehr, für die großartige Zweitbetreuung und die Bereitschaft die Begutachtung dieser Dissertation zu übernehmen. Vielen Dank, dass ich die massenspektrometrischen Analysen mit Ihnen in Kooperation durchführen konnte. An dieser Stelle möchte ich auch Dr. Steffen Ostendorp für die Durchführung der Analysen, Aufarbeitung der Ergebnisse sowie jegliche fachliche und technische Unterstützung danken.

Ein ganz großer Dank geht natürlich an die gesamte Arbeitsgruppe AG Fiedler/Wellbrock für die herzliche Aufnahme in die Arbeitsgruppe und viele lustige Momente im Labor. Ganz besonders möchte ich meinem „Leidensgenossen“ Zoran danken, in dem ich nicht nur einen tollen Kollegen gefunden habe, sondern auch einen sehr guten Freund. Danke, dass du mich immer wieder aufgebaut und motiviert hast und natürlich für all deine tatkräftige Unterstützung bei diversen Versuchen sowie stundenlanges Korrekturlesen. Unsere täglichen Gespräche über alles und jeden werde ich sehr vermissen. Jana, Vanessa und Gabi, ohne euch würde das Labor in einem riesigen Chaos versinken. Vielen Dank, dass ihr immer den Überblick behalten habt und mir jeder Zeit mit Rat und Tat zur Seite standet. Ein riesiges Dankeschön auch an Lena. Du hast mit deinem Optimismus und deiner Ruhe alle angesteckt. Danke, dass du mir beigebracht hast, wie man Kryoschnitte und die wunderschönen 3D-Bilder von Knochen macht.

Ein herzliches Dankeschön geht auch an die Arbeitsgruppe der Dermatologie für die Kooperation bei den BioFlux-Assays, allen voran Dr. Volker Huck. Vielen Dank für die Einführung in die Technik und die große Unterstützung bei der Etablierung der Versuche. Deine Begeisterung, für diese großartige Technik hat mich in jedem Fall angesteckt. Hier möchte ich mich auch bei Sabine, Yuanyuan, Ewa und Christian bedanken, für die viele

technische Unterstützung, Bereitstellung von HUVECs sowie ganz viel motivierenden Zuspruch und Hilfe.

Zudem möchte ich mich bei PD Dr. Sabine Hoffmeister-Ullerich nicht nur für die tolle Organisation und Begleitung der ASMB-Seminare bedanken, sondern auch dafür, dass du immer ein offenes Ohr für uns Doktoranden hattest und durch viele Tipps und Fragen uns zu neuen Ideen angeregt hast. Danke, dass du dich bereit erklärt hast, als Prüfungskommissionsmitglied für meine Promotion eingesetzt zu werden. Hier möchte ich auch Professor Dr. Thomas Oertner danken, als Prüfungskommissionsmitglied zu fungieren.

Ein großes Dankeschön an Professor Dr. Fran Platt und Dr. Nick Platt für die sprachliche Überprüfung dieser Arbeit und für die wunderbare Zeit, die ich in Oxford bei euch im Labor hatte.

Vielen Dank an die UKE Microscopy Imaging Facility, insbesondere an Dr. Antonio Virgilio Failla, für die technische Unterstützung bei den 3D-Fluoreszenzaufnahmen der Knochenschnitte sowie an die UKE FACS sorting core unit für das Sorting meiner transduzierten Zellen. Ein großer Dank geht auch an das Team der Tierhaltung für die liebevolle Unterstützung bei der Betreuung und Pflege der Mäuse. Außerdem möchte ich der *Deutschen Forschungsgemeinschaft* für die finanzielle Förderung meines Projektes danken.

Ein riesengroßer Dank gilt natürlich meiner Familie und Freunde! Ohne eure Unterstützung, Geduld und Zuspruch wäre ich nie so weit gekommen. Ein ganz besonderer Dank an meine Eltern. Ihr habt immer hinter mir gestanden, an mich geglaubt und mich bei allem, was ich mir in den Kopf gesetzt habe unterstützt. Ohne euch wäre ich nicht die, die ich heute bin. Wiebke und Maike, ihr seid die tollsten Schwestern, die man sich wünschen kann! Danke, dass ich immer mit allem zu euch kommen kann und ihr immer für mich da seid.

Ben, ohne dich wäre ich nicht, wo ich jetzt bin. Ich danke dir für die letzten 11,5 Jahre, die du mich durch alle Lebenslagen begleitet hast und immer an meiner Seite warst. Danke für deine unfassbare Unterstützung und Geduld, obwohl ich dich vermutlich so einige Male halb in den Wahnsinn getrieben habe. Dein Zuspruch und deine Motivation haben mich immer wieder angetrieben. Wir haben schon so viel zusammen erlebt und so viele gemeinsame Erinnerungen gesammelt und ich freue mich riesig auf das nächste spannende, aber wundervolle Abenteuer mit dir!

# EIDESSTATTLICHE VERSICHERUNG

Hiermit erkläre ich an Eides statt, dass ich die vorliegende Dissertationsschrift selbst verfasst und keine anderen als die angegebenen Quellen und Hilfsmittel benutzt habe.

Hamburg, den …….. ……..